Geotechnical Evaluation of Recycled Asphalt Shingles as Structural Fill

By

Ali Soleimanbeigi

A dissertation submitted in partial fulfillment
of the requirements for the degree of

Doctor of Philosophy
(Civil and Environmental Engineering)

at the

UNIVERSITY OF WISCONSIN-MADISON

2012

Date of final oral examination: 07/30/2012

The dissertation is approved by the following members of the Final Oral Committee:

Tuncer B. Edil, Professor, Civil and Environmental Engineering
Craig H. Benson, Professor, Civil and Environmental Engineering
James M. Tinjum, Assistant Professor, Civil and Environmental Engineering
Dante Fratta, Associate Professor, Civil and Environmental Engineering
Hussain Bahia, Professor, Civil and Environmental Engineering

Abstract

Geotechnical Evaluation of Recycled Asphalt Shingles as Structural Fill

Ali Soleimanbeigi

Under the Supervision of Professors Tuncer B. Edil and Craig H. Benson

at the University of Wisconsin-Madison

In this research, geotechnical properties of recycled asphalt shingles (RAS) were evaluated at constant and varying temperatures for possible use in high volume structural fill applications. Since compressibility of RAS is significantly higher than that of natural soils, addition of less compressible granular material to RAS or stabilization of RAS using self cementing fly ash were considered to reduce the compressibility. Bottom ash (BA) and foundry slag (FS) were used as granular additives to RAS. To evaluate the effect of seasonal temperature on engineering properties of RAS mixtures, a thermo-mechanical system and the related testing procedures were developed. Systematic tests to evaluate engineering properties including hydraulic conductivity, one-dimensional compression, triaxial compression and deviatoric creep tests were conducted at constant and varying temperatures (between 5 ^{o}C and 35 ^{o}C). Results show that at room temperature, RAS mixtures are favorable lightweight materials with sufficient shear strength and drainage capacity for use in structural fills. Up to 50% RAS in granular materials and between 10 to 20% fly ash content in the stabilized RAS reduced the compressibility to meet the settlement criteria for roadway design. The secondary compression index increased as a power function with stress level. As the temperature increases the shear strength decreased due to reduction in viscosity of the asphalt binder in RAS particles. However the shear strength of the mixture with RAS content up to 50% remained higher than 30^{o}. The hydraulic conductivity increased with

increasing temperature due to reduction of viscosity of permeating water. The compressibility of the compacted RAS mixtures exponentially increased with temperature. Since the viscosity of RAS particles is reduced with temperature, if the embankment containing RAS mixture is constructed during warm season of the year the majority of the compression occurs during construction and the RAS embankment settlement during the rest of the year will be negligible. RAS mixtures were also susceptible to creep rupture under the applied deviatoric stress. When designing side slopes of the embankments containing RAS, the applied stress should be reduced to 80% of the maximum deviatoric stress to ensure no creep rupture will occur. Design graphs and analytical models were developed to predict shear strength and compressibility of RAS mixtures at constant and varying temperatures under the stress levels typical to highway embankments. The results of this research contribute to testing and design procedures associated with the use of recycled materials in geotechnical applications and help provide more sustainable roadway infrastructure.

Acknowledgments

First and foremost I am deeply grateful for my family's love, encouragement and unconditional support during my graduate studies. I would like to thank Professors Tuncer Edil and Craig Benson for the invaluable guidance and experience I gained during my PhD program. I would also like to thank Professor James Tinjum, Professor Dante Fratta and Professor Hussain Bahia for serving as my committee members. I would like to thank Mr. Xiaodong Wang for his everyday help during all laboratory experiments. Support for this project was provided by the Recycled Materials Resource Center (RMRC) and Solid Waste Research Program (SWRP) at the University of Wisconsin-Madison. Their support is greatly appreciated.

I would also like to thank all my fellow graduate students, undergraduate assistants and post-docs in geological engineering that in any ways contributed to my academic life. Zhipeng Su, Dylan Kissinger, Andrew Keene, Christopher Bareither, Makhaly Ba, Jongwon Eun, Erica Hagen, Sabrina Bradshaw, Kongrat Nokkaew, Mozhdeh Rajaei, Ali Ebrahimi, Crystal Smith, Kyo-Son Kim, Abdullah Alsubhan, Tirupan Mandal, Joseph Scalia, Ryan Shedivy, Erin Hunter, Vonmarie Martinez, Kuo Tian, Jiannan Chen, Marcos Montoro, Ayse Ozdogan, Merve Bozkurt, Ozlem Bozyurt, and Jeffrey Nowgard have been great friends to me in the geological engineering program.

Table of Contents

List of Figures

List of Tables

Chapter 1 Introduction

The amount and type of generated solid waste grow as the world population increases. While landfills are the primary end place of the majority of solid waste, there have been increasing motivation and research towards feasibility and performance of reusing certain types of solid waste in highway construction. A wide variety of solid waste including coal combustion byproducts, foundry slags, tire shreds, and reclaimed paving materials have been studied and successfully used in the construction of highway embankments (RMRC 2011). In addition to promising a solution to the disposal problem and an economic alternative to natural soils, certain solid waste materials have lower dry unit weight, which makes them favorable alternative to traditional material for construction of embankments over weak grounds.

Asphalt shingle waste is produced by removing the asphalt shingles from the roofs of existing structures during renovation (called post-consumer asphalt shingle or tear-off shingle) or rejecting asphalt shingles/shingle tabs discarded in the manufacturing process of new asphalt shingles (called manufactured shingle scrap). Approximately 11 million Mg of asphalt roofing shingle waste are generated in the U.S. per year (Krivit, 2007, NERC 2011). Re-roofing jobs account for 10 million Mg, with another 1 million Mg manufacturing scrap. Different applications including as a component of hot mix asphalt (HMA), cement kiln fuel, cold patch in paved roads and dust control in gravel roads account for reuse only between 10 to 20% of the total asphalt shingle waste and therefore the remaining large amount is landfilled (Townsend, 2007; Turley, 2011). Use of the asphalt shingle waste as fill material in highway fills consuming large volume of materials will open up potentially a large reuse option for the asphalt shingle waste.

The objective of the proposed research is to evaluate the geotechnical properties of recycled asphalt shingles (RAS) as structural fill material in highway embankments or backfill material behind retaining structures and to provide relevant design guidelines. The research outlined in this proposal addresses the following hypotheses:

1- RAS as a granular material has sufficient shear strength and drainage capacity to qualify as a structural fill. Since RAS contains asphalt cement and cellulose felt, the material may exhibit higher compressibility compared to traditional fill material.

2- Addition of less compressible materials to RAS or stabilization of RAS can reduce the compressibility and increase shear strength and drainage capacity of RAS.

3- Since RAS contains viscous asphalt cement, temperature variation affects engineering properties of the compacted RAS mixtures.

4- Since RAS contains viscous asphalt cement, time-dependent shear or volumetric strain under sustained deviatoric stress may be significant.

The results of this research are presented herein as series of papers. In Chapter 2 entitled "Recycled Asphalt Shingles Mixed with Granular Byproducts as Structural Fill", physical and mechanical properties of RAS and RAS mixed with granular industrial byproducts including bottom ash (BA) and foundry slag (FS) are evaluated in a systematic manner. Results show that although pure RAS has suitable drainage capacity and shear strength as structural fill, compressibility of RAS is significant compared to natural soils. Systematic addition of BA and FS to RAS reduced the compressibility and increased shear strength and drainage capacity of RAS:BA and RAS:FS mixtures. Design graphs were developed to estimate geotechnical properties of RAS:BA and RAS:FS mixtures for a given RAS content and stress level. This chapter has been published in the Journal of ASTM International, Vol. 9, No. 1.

In Chapter 3 entitled “Evaluation of Fly Ash Stabilization of Recycled Asphalt Shingles for Use in Structural Fills”, self cementing Class C fly ash was used to stabilize RAS. Results show that stabilization remarkably reduces compressibility and increases the shear strength of RAS. However, stabilization also reduces the drainage capacity of RAS to that of silty sand or silty clay soil. Settlement of typical highway embankments were estimated based on fly ash content in stabilized RAS. This chapter has been accepted for publication in the ASCE Journal of Materials in Civil Engineering.

Chapter 4 entitled “Effect of Temperature on Geotechnical Properties of Recycled Asphalt Shingles Mixtures” evaluates the effect of temperature change on geotechnical properties of compacted RAS:BA mixture and stabilized RAS. The development of a thermo-mechanical system and test procedures at elevated temperature are described. Systematic mechanical tests at elevated temperatures (between 5 ^{o}C and 35 ^{o}C) were conducted on RAS:BA and stabilized RAS specimens. The results show that when temperature increases, the shear strength decreases but compressibility and hydraulic conductivity increases. The shear strength and hydraulic conductivity of RAS containing embankments or stabilized RAS are sufficient to provide stability and drainage capacity of road embankments at different climates in the U.S. However; to minimize long term settlement, compaction and construction of RAS embankments are recommended in warm season of the year.

Chapter 5 entitled “Shear Creep Response of Recycled Asphalt Shingles” investigates strain and strain rate of the compacted RAS:BA mixtures and stabilized RAS under different applied deviatoric stress and confining pressures. The creep behavior was also investigated at elevated temperatures. The results show that deviatoric creep strain of RAS;BA mixtures or stabilized RAS is significant and increases with applied deviatoric stress. The mixtures are also

susceptible to creep rupture and the rupture occurs at stress ratio higher than 0.80. RAS mixture has similar classical creep response to soil. The strain rate exponentially increases with increasing temperature. To reduce deviatoric creep strain of RAS containing embankments, the construction of the embankments is recommended during the warm seasons. Due to reduction of viscosity of asphalt binder in RAS particles at higher temperature, the majority of creep strain occurs during construction and the strain during the rest of the year will be compared to that of compacted sand.

Chapter 6 contains summary and conclusion from this research. Appendix I includes a paper that investigates mechanisms and practical implications associated with compressibility of RAS as the structural fill. Settlement of embankments containing RAS was found as a power function of stress level.

Chapter 2 Recycled Asphalt Shingles Mixed with Granular Byproducts as Structural Fills

Abstract: In this study, recycled asphalt shingles (RAS) were evaluated for potential use as structural fill in highway embankments or backfills behind retaining walls. Bottom ash (BA) and foundry slag (FS) were also investigated as additives to recycled asphalt shingles (RAS) to enhance its mechanical properties. The engineering properties of RAS:BA/FS mixtures including compaction characteristics, hydraulic conductivity, compressibility, shear strength, and coefficient of lateral earth pressure at rest were evaluated in a systematic manner. Results show that addition of bottom ash and foundry slag significantly reduces compressibility of RAS while increasing drainage capacity and shear strength. RAS:BA/FS mixtures are favorable light weight material for use as embankment fills or backfill behind retaining walls.

Keywords: Recycled asphalt shingle, bottom ash, foundry slag, structural fill, engineering properties.

Introduction

Approximately 11 million Mg of waste asphalt roofing shingles are generated per year in the U.S. of which 10 million Mg are tear-off roofing shingles and 1 million Mg is factory scraps (Townsend et al. 2007). Asphalt shingle waste is produced over 250,000 Mg per year in Wisconsin and is categorized as the third largest waste item by weight in the state (Recycling Connections Corporation, 2010). Reuse of recycled asphalt shingles (RAS) has been identified by the U.S. Environmental Protection Agency (EPA) as a top priory. Constituents of typical asphalt shingle include 20-35% asphalt cement, 2-15% cellulose felt, 20-38% mineral granule/aggregates, and 8-40% mineral filler/stabilizer.

The primary reuse application of RAS is in production of hot mix asphalt (HMA). Research results have shown however, that more than 5% by weight RAS in HMA will adversely affect the creep stiffness and tensile strength of HMA (Button et al. 1995, Grodinsky, 2002). Consequently, this application uses only between 10 to 20% of the total asphalt shingle waste (Turley, 2010). Another potential application, which could use large volume of asphalt shingle waste is structural fill including highway embankment fills or backfill behind retaining walls.

Preliminary compression test results showed that pure RAS is too compressible for use as structural fill (Benson et al. 2010). To reduce compressibility of RAS, addition of granular materials with verified suitability as structural fill was considered. Bottom ash (BA) is a coarse granular coal combustion product, which is collected at the bottom of the furnaces in power plants. Previous investigation has verified suitability of engineering properties and field performance of bottom ash in construction of highway embankments or working platforms (Seals et al. 1972; Moulton et al. 1973; Huang 1990; Karim 1997; Edil et al. 2002; Kim 2003; Tanyu et al. 2005; Kim et al. 2005; Yoon et al. 2009). According to American Coal Ash Association (ACAA, 2008) about 16.5 million Mg bottom ash was produced in 2009 of which 44% was reused in different applications like structural fills, embankments, road base and sub-base, soil modifications and concrete products. Of the total reused bottom ash, 42% was used as structural fills.

Foundry slag (FS) is a combination of limestone and metal impurities in metal casting industry, which is collected from top of the molten metal in the furnace. The molten slag is cooled, crushed and screened to create granular slag. According to the U.S. Geological Survey about 17 to 24 million Mg foundry slag was produced in 2008 of which about 90% were reused in a variety of engineering applications as aggregate in portland cement concrete, asphalt

concrete, aggregate base, fill material and railroad ballast. Of the total reused foundry slag 40% was used as road basement and 10% was used as fill material. The engineering properties of foundry slag are suitable for use as structural fill and working platforms (Emery 1982, Ahmed 1993; Edil et al. 2002; Tanyu et al. 2005). In this study, bottom ash and foundry slag were investigated as granular additives to improve the engineering properties of RAS.

The objective of this research is to investigate suitability of RAS:BA/FS mixtures as construction material for structural fills. For this purpose, relevant engineering properties of RAS:BA/FS mixtures including compaction characteristics, hydraulic conductivity, compressibility, shear strength and coefficient of earth pressure at rest were evaluated in a systematic manner and presented herein.

Background

While mechanical properties of recycled asphalt pavement (RAP) have been evaluated for use as structural fill (Viyanant et al. 2007; Wen and Edil 2007; Li et al. 2008), few scientific investigations have been completed on engineering properties of RAS. Most of the findings are based on field observations. Iowa Department of Transportation studied the use of ground shingles as a surface treatment on an unpaved road. Nearly 900 Mg of tear-off shingles were ground to pieces less than 25 mm to 50 mm and mixed with crushed limestone to achieve a uniform shingle/limestone mixture of about 65 mm thick. After two years of observations, the study concluded that shingles are very effective for dust control in rural roads, result in better lateral control of vehicles, reduce the loss of granular materials into the ditches, and resulted in a quieter and smoother roadway (Marks 1997).

Vermont Agency of Natural Resources (Vermont ANR) incorporated 10% by weight RAS with the maximum size (d_{max}) of 9.5 mm, 30% recycled asphalt pavement (RAP) with d_{max} of 37.5 mm and 60% of gravel with d_{max} of 37.5 mm. The material was placed and compacted on a series of municipal roadways and spread with calcium chloride solution. Over a two-year evaluation period, Vermont ANR reported that the mixture compacts very well, resists rutting and erosion, mitigates dust and in general requires less maintenance than the conventional gravel control section (Grodinsky et al. 2002).

Hooper and Marr (2004) obtained some baseline quantitative data on the physical and mechanical effects that shingles have on soils. California bearing ratio (CBR) tests on RAS samples with d_{max} of 25 mm showed that the CBR strength is 6% which categorizes RAS as a questionable to fair material for subgrade. The results showed that addition of 33% by volume of RAS to clay increased CBR of the RAS:clay mixture from 8% to 20%. However; addition of 33% by volume of RAS reduced CBR of crushed stone gravel from 92% to 23%, silty sand from 33% to 19% and clean sand from 21% to 13%. Hooper and Marr (2004) concluded that RAS behaves like granular particles in clay but may cause deterioration of inter-particle friction between sand and gravel particles. Warner (2007) evaluated beneficial use of RAS as base course and subbase layers. Compaction tests on RAS samples with the d_{max} ranging from 5 mm to 50 mm showed that the maximum dry unit weight (γ_{dmax}) of RAS varied between 8.8 kN/m^3 and 12.3 kN/m^3. The types of soil used for the mixture were Boardman silt (ML) and Grade 2 granular backfill (GP-GM). Compaction test results showed that increase in RAS content decreased dry unit weight (γ_d) of both types of soil. Resilient modulus (M_r) of pure RAS was 30 MPa, which is lower than the minimum 75 MPa recommended by NCHRP project 1-37A for

base course layer. Addition of 50% by weight of Grade 2 gravel increased the resilient modulus to 78 MPa, which made the mixture suitable for use as base course and subbase layer.

Test Materials

RAS samples used in this study were taken from Stratford Building Supply Company in Stratford, WI. Visual inspection indicated that RAS samples were free of impurities like wood chips, plastics, and nails. The Stratford Building Supply grinds the waste shingles once over and screens them through 50 mm, 25 mm and 19 mm sieve sizes. Warner (2007) concluded that RAS particles with 10 mm maximum size result in higher γ_d, higher CBR and M_r. Therefore, in this study, the RAS supply was screened to limit the d_{max} to 10 mm. Bottom ash and foundry slag samples were taken respectively from the Columbia Power Station and the Grede Foundries in Wisconsin. To compare the engineering properties of RAS:BA/FS mixtures to those of natural soil, a sample of a glacial outwash sand from Wisconsin was also used in this study.

Test Methods

Physical Property Tests

The physical property tests including grain size analysis, specific gravity, and microscopic examination were conducted on RAS, BA and FS samples. The physical properties of the glacial outwash sand sample were taken from Bareither et al. (2008).

Grain Size Analysis

The grain size distribution of RAS, BA and FS samples were determined according to ASTM D 422. The samples were first wet sieved through sieve No. 200 to separate coarse and fine particles. The coarse portions of BA and FS samples were oven dried for 24 hours prior to mechanical sieving. The coarse portion of RAS sample was air dried to prevent binding of the particles at oven temperature.

Specific Gravity

The specific gravities of RAS, BA and FS samples were measured according to ASTM D854 (Method B). To prevent clogging of RAS particles during the test and to remove any entrapped air in the slurry, the pycnometer was continuously agitated for about one hour under a constant vacuum. De-airing was accomplished by vacuuming distilled water.

Microscopic Examination

Shape, angularity and surface texture of RAS, BA, FS and outwash sand particles were examined using a light microscope to understand interaction mechanisms between the particles during different mechanical testing.

Mechanical Property Tests

The mechanical property tests including compaction, hydraulic conductivity, one-dimensional compression, and consolidated drained triaxial compression tests were performed on RAS:BA/FS mixtures with BA or FS contents of 0, 25, 50, 75 and 100%. To evaluate suitability

of RAS:BA/FS mixtures as backfill behind retaining walls, K_o-Consolidation tests were performed on the mixtures with BA or FS contents of 0, 50 and 100%.

Compaction

Standard Proctor compaction tests following ASTM D 698 (method B) were performed on RAS:BA/FS mixtures. One modified Proctor compaction test following ASTM D 1557-09 (method B) was performed on pure RAS to obtain compaction characteristics of RAS under higher compaction effort and to see if higher compaction energy will help reduce compressibility of RAS.

Hydraulic Conductivity

Flexible wall hydraulic conductivity tests were conducted on RAS:BA/FS mixtures according to ASTM D 5084-03 to evaluate the effect of confining stress (σ_c') on hydraulic conductivity of the mixtures. Each RAS:BA/FS mixture was compacted to 95% of the γ_{dmax} at optimum water content (w_{opt}) and consolidated to the desired effective stress (σ_c'=35 kPa, 70 kPa and 140 kPa) for 24 hours. After consolidation phase, the hydraulic conductivity was measured according to the falling-head rising-tail method.

One-dimensional Compression

Settlement of an embankment with large lateral extension can be considered one-dimensional and estimated from the results of one-dimensional consolidation tests. To evaluate compressibility of RAS:BA/FS mixtures, one-dimensional compression tests were performed

following ASTM D 2435-96 using a standard consolidometer ring with 64-mm diameter and 25-mm height. Each specimen was compacted at the w_{opt} and relative compaction level of 95%. The compaction in the consolidometer ring was conducted in three lifts of equal thickness by a manual hammer. RAS:BA/FS specimens were then soaked in the consolidometers for 24 hours before applying vertical loads. Pore pressure piezometers were connected to consolidometer cells to measure any generated excess pore water pressures under each stress level. The specimens were loaded incrementally from 12.5 kPa with load increment ratio (LIR) of 1.0 and load increment duration (LID) of 24 hours until the maximum vertical stress level of 1600 kPa. The one-dimensional consolidation test was also performed on a glacial outwash sand sample for comparison. The LABVIEW software (National Instruments, Austin, TX) and a data acquisition card (UPC601-U) were used for automated incremental loading and recording of vertical deformation.

Triaxial Compression Tests

To evaluate stress-strain and volumetric behavior of RAS:BA/FS mixtures under shearing and to determine the shear strength; consolidated drained (CD) triaxial compression tests were performed on compacted RAS:BA/FS mixtures. For each mixture composition three tests were performed under effective confining pressure, σ_c' of 35 kPa, 70 kPa and 140 kPa. The confining pressures were selected to represent the range of typical effective stresses in highway embankments or retaining wall backfills. Each RAS:BA/FS mixture was compacted in five layers in a split mold with 74 mm diameter and 148 mm height to achieve the compaction level of 95%. The number of tamps per layer using a standard Proctor hammer was determined such that the same compaction energy as in the standard compaction effort (592 kN.m/m^3) is applied

to each sample mixture. After assembling the cell chamber, the specimens were backpressure-saturated according to ASTM D4767 so that a B value greater than 95% was attained. The specimens were then isotropically consolidated under σ_c' of 35 kPa, 70 kPa and 140 kPa. The specimen volume change during consolidation phase was monitored in the backpressure tubing until no significant change in volume was observed. The shearing of each mixture specimen in drained condition was performed under constant strain rate. The axial deformation rate of 0.2 mm/min was selected based on the time for primary consolidation and the ultimate strain of the specimen at failure. The pore water pressure was monitored during shearing to ensure no excess pore water pressure is generated. The volume change of each specimen during shearing was recorded from the volume change of water in backpressure tubing.

K_o-Consolidation Tests

To evaluate the coefficient of lateral earth pressure at rest (K_o) of RAS:BA/FS mixtures a specifically developed K_o-Consolidation cell by Edil and Wang (2000) was used. Fig. 2.1 shows the schematic of the apparatus. The cell has the dimensions of a conventional consolidation ring (64-mm diameter and 25-mm height) and consists of a hallowed ring with a thickness of 1 mm instrumented with strain gages. The air pressure is applied into the lateral pressure chamber around the inner ring to maintain the lateral displacement of the inner ring to a minimum during application of vertical stress. A program was written in LABVIEW to automate the test and acquire the data. K_o is calculated by measuring the lateral air pressure upon application of vertical pressure on the specimen. The Poisson's ratio, ν is assessed from $\nu = K_o/(1+K_o)$.

Test Results

Grain size distribution

Fig. 2.2 shows the grain size distribution of RAS, BA, FS and outwash sand particles. More than 80% of particles of each material are sand size with fine contents less than 5%. RAS, BA and FS particles have almost similar grain size distributions; therefore, grain size distribution of different RAS:BA/FS mixtures will fall within a narrow range. According to the Unified Soil Classification System (USCS) RAS and FS are classified as well graded sand whereas BA and outwash sand are classified as poorly graded sand. Basic grain size indices and the USCS classification are included in Table 2.1.

Specific Gravity

The specific gravities of RAS, BA, FS and outwash sand samples are included in Table 2.1. The specific gravity of RAS is 1.74, which is lower than the specific gravity of outwash sand (2.71). The low specific gravity of RAS is attributed to organic cellulose felt and asphalt cement contents which together constitute about 50% by mass of RAS. The specific gravity of asphalt binder is generally between 1.0 and 1.04 (Roberts et al. 1996). The specific gravity of BA is 2.67, which is comparable to specific gravity of the outwash sand. FS has the specific gravity of 2.36 which is lower than the specific gravity of the outwash sand. The measured specific gravity of BA and FS samples fall within the range reported in the literature (RMRC 2010).

Morphological Characteristics

Fig. 2.3 shows typical particle shape of RAS and LM photomicrographs of BA, FS and outwash sand. RAS particles are plate-like, irregular in shape, highly angular and have rough surface texture. The angularity of RAS particles reduces to semi-round to round as the particle size decreases. During manufacturing, one side of the asphalt shingles is covered by sand to protect them against physical damages. The other side is covered by mineral filler to protect the shingles against adhesion during packing and shipment. Fig. 2.3(a) shows the sand and mineral surface covers on the RAS particle surfaces.

BA and FS particles are angular to highly angular, internally porous and have rough surface texture. Some pores of the particles are filled with dust. On the other hand, particles of outwash sand are solid, semi-round to round and have smooth surface texture. Particle surfaces are clean, shinny and free of dust.

Compaction Characteristics

Fig. 2.4(a) shows the variation of dry unit weight (γ_d) versus water content (w) of different RAS:BA and RAS:FS mixtures. Pure RAS has a well-defined compaction curve with the maximum dry unit weight (γ_{dmax}) of 11.3 kN/m^3 and optimum water content (w_{opt}) of 8%. The γ_d of RAS:BA mixture increases with increasing BA content. Although BA and outwash sand have comparable specific gravities, the high porosity of BA particles reduces the γ_{dmax} to 15 kN/m^3 which is lower than γ_{dmax} of typical compacted sand. As the BA content increases the γ_d of the mixture becomes less susceptible to water content. The γ_{dmax} of RAS compacted using modified Proctor test is the same as the γ_{dmax} of RAS:BA mixture with 50% BA content compacted using

standard Proctor test. The γ_d of pure RAS becomes less susceptible to water content when compacted using modified Proctor test. Although pure RAS under higher compaction energy has the same γ_{dmax} as that of RAS:BA mix with 50% BA content, the RAS:BA mixture uses less energy to produce the same γ_{dmax} thus is preferred to RAS compacted using modified Proctor test.

Systematic addition of FS to RAS only slightly reduces γ_{dmax} of the RAS:FS mixture. The γ_{dmax} of RAS:FS mixture varies between 11.3 kN/m^3 to 10.8 kN/m^3. Low specific gravity and high porosity of FS particles result in low γ_{dmax} of FS with respect to typical compacted sand. Fig. 2.4(b) shows that addition of FS to RAS does not essentially change γ_{dmax} of the RAS:FS mixture while addition of BA to RAS increases γ_{dmax} of the RAS:BA mixture from 11.3 kN/m^3 to 15.0 kN/m^3.

Hydraulic conductivity

Fig. 2.5 shows the hydraulic conductivity of RAS:BA/FS mixtures from the flexible wall hydraulic conductivity tests. Except for pure RAS under σ_c' of 140 kPa, the hydraulic conductivity of RAS:BA/FS mixture falls between 1×10^{-2} cm/s and 1×10^{-4} cm/s. The hydraulic conductivity of RAS:BA/FS generally decreases as the σ_c' increases. High compressibility of RAS particles and densification of RAS:BA/FS mixtures at higher σ_c' possibly explain the decrease in hydraulic conductivity of RAS:BA/FS mixtures with σ_c'. As the bottom ash/foundry slag content increases the hydraulic conductivity of RAS:BA/FS mixture becomes less sensitive to σ_c'. For the mixtures with bottom ash/foundry slag content more than 50%, the hydraulic

conductivity is almost constant at different σ_c'. At a particular σ_c', the hydraulic conductivity of RAS:BA/FS mixture increases with increasing BA/FS content. This is attributed to increase in void ratio. The void ratio of compacted RAS is 0.59 while the void ratios of BA and FS are 0.87 and 1.44; respectively. As the BA/FS content increases, the void ratio of the compacted mixture increases which consequently increases the hydraulic conductivity. In general, according to USBR (1987) classification for drainage capacity based on hydraulic conductivity, the RAS:BA/FS mixtures under low to moderate confining pressures have *good drainage capacity* for use as structural fill.

Compressibility

Fig. 2.6(a) shows the compression curves of RAS:BA mixtures as vertical strain, ε_v, versus logarithm of vertical effective stress, σ_v'. The compression curve of outwash sand sample is also included for comparison. Compared to outwash sand, pure RAS is highly compressible for structural fill applications. High compressibility of RAS is attributed to the asphalt cement and cellulose felt components which together constitute about 50% by weight of RAS particles. The compressibility of BA is only slightly higher than the compressibility of outwash sand which makes the BA an appropriate additive to reduce compressibility of RAS. The higher compressibility of BA than outwash sand may be attributed to angularity and rough surface texture of BA particles [Fig. 2.3(b)], which would tend to increase the stress concentration at particle contact surfaces. Increase in stress concentration at particle surface contacts is likely to result in particle damage due to abrasion or breakage of particle surface asperities or sharp particle corners which consequently increases the compressibility (Robert and de Souza 1958; Marshal 1967; Pestana and Whittle 1995; Chuhan et al. 2003). Fig. 2.6(a) shows that systematic

addition of BA to RAS reduces compressibility of RAS:BA mixtures. Under σ'_v up to 200 kPa, which is a typical overburden pressure in highway embankments, addition of 50% bottom ash to RAS significantly reduces ε_v of the RAS:BA mixture form 17% to 5%.

The compressibility curves of RAS:FS mixtures are shown in Fig. 2.6(b). Systematic addition of FS to RAS reduces compressibility of RAS:FS mixture. FS is more compressible than BA at σ'_v higher than 200 kPa. In addition to high angularity and rough surface texture that increase the possibility of particle breakage, the individual FS particles are more crushable than BA particles. Some popcorn-like slag particles were observed to break under finger pressure. Fig. 2.7 shows degradation of BA and FS particles after compaction test and after compression test under σ'_v of 1600 kPa in terms of changing grain size distribution curves. Grain size distribution of BA sample shows increased amount of finer particles after compaction and compression tests. Degradation effect on FS particles after compaction and consolidation tests is more significant than bottom ash particles due to more crushable nature of the individual slag particles.

The compression curves of the granular materials display two regions, i.e., pre-yield region at low stresses with a flatter slope designated as C_{pry} followed by increasing compression due to particle crushing at higher stresses, i.e., post-yield region with a greater slope designated as C_{psy} on the semi-logarithmic compression curves. The yield pressure (σ'_y) that separates these regions as well as the semi-logarithmic slopes, C_{pry} and C_{psy}, of the RAS:BA/FS mixtures were determined from the graphs of vertical strain versus $log\ \sigma'_v$ according to the graphical construction of Casagrande (Casagrande 1936b). Fig. 2.8 shows the variation of σ'_y of RAS:BA/FS mixtures with bottom ash/foundry slag content. The σ'_y of the mixtures increases with increase in bottom ash/foundry slag content indicating that yield pressure of RAS is

improved with BA and FS addition. Fig. 2.9 illustrates the variation of C_{pry} and C_{psy} with respect to bottom ash/foundry slag content in RAS:BA/FS mixtures determined from the compression curves. For RAS:BA mixtures, both C_{pry} and C_{psy} decrease with increasing BA content. For RAS:FS mixtures, C_{pry} decreases but C_{psy} increases with increasing FS content. The increase in C_{psy} with increasing FS content is attributed to significant particle crushing at σ'_v higher than 200 kPa during compression test as explained from Figs. 2.6(b) and 2.7(c). The settlement design of typical highway embankments with overburden pressure less than 200 kPa and constructed using RAS:BA/FS mixtures can be based on compressibility parameters in the pre-yield range. Therefore, addition of BA and FS to RAS reduces the compressibility of the mixture from moderately compressible to slightly and very slightly compressible for σ'_v in the pre-yield range according to classification criteria (Table 2.2).

Figs. 2.8 and 2.9 and Table 2.2 can be used as design tools to determine the minimum required BA and FS content in the RAS:BA/FS mixtures given a σ'_v and a desired compressibility. For example if a *very slightly compressible* mixture of RAS:BA is desired for an embankment with σ'_v of 200 kPa, the designer selects a C_{pry} between 0 and 0.05, say 0.03, from Table 2.2. Assuming that σ'_v is in the pre-yield range, from Fig. 2.9 the corresponding BA content is 50%. From Fig. 2.8, the σ'_y corresponding to the BA content of 50% is 300 kPa, which is higher than the given σ'_y of 200 kPa.

Fig. 2.10 shows the variation of ε_v with time for different RAS:BA/FS mixtures under σ'_v of 100 kPa. The time at which excess pore water pressure, Δu as measured, is dissipated marks the end of primary consolidation, t_p. The generated Δu in RAS:BA/FS mixtures dissipates in less than 2 min. The end of primary consolidation marked on the compression curves on Fig. 2.10 indicates that negligible settlement occurs due to primary consolidation in RAS:BA/FS mixtures

and the majority of settlement is due to secondary compression. The secondary compression is characterized by modified secondary compression index, which is defined as the slope of ε_v versus *log t* curve, $C_{\alpha\varepsilon} = \Delta\varepsilon_v / \Delta \log \sigma_v'$ where e_p is the void ratio at the end of primary consolidation. The secondary compression part of the compression curves shows that ε_v nonlinearly increases with time. The $C_{\alpha\varepsilon}$ increases with time for both RAS:BA and RAS:FS mixtures. A similar compression behavior was observed by Fox et al. (1992) and Mesri et al. (1997) for Middleton peat. Long term consolidation test on pure RAS under σ_v'=100 kPa (σ_v'/σ_y'=1.80) shows that $C_{\alpha\varepsilon}$ becomes constant after the standard LID of 24 h whereas in RAS:BA/FS mixtures with 50% bottom ash/foundry slag under σ_v'=100 kPa (σ_v'/σ_y'=0.33), the $C_{\alpha\varepsilon}$ increases with time after 24 h. All mechanisms of compression (including particle rearrangement through interparticle slip, rotation and particle damage; and particle deformation including bending and compression) that operate during primary compression continue into secondary compression (Robert and de Souza 1958; Lee and Farhoomand 1967; Lade et al. 1997; Mesri and Vardhanabhuti 2009). Flexible, plate-like RAS particles seem to reach a stable position after a rapid rearrangement under σ_v'/σ_y'=1.80 thus the long term compression of the specimen might be only due to particle deformation as a result of compressibility of asphalt cement and cellulose felt constituents in RAS. Addition of BA or FS to RAS may increase particle rearrangement during secondary compression. In particular, crushability of foundry slag particles may help particle damage during secondary compression resulting in higher secondary compression index over time.

To compare long term compression of different RAS:BA/FS mixtures quantitatively, $C_{\alpha\varepsilon}$ was calculated over one log cycle of time before LID of 24 hr. Fig. 2.11 shows the variation of

$C_{\alpha\varepsilon}$ with bottom ash/foundry slag content under different σ'_v. For a given σ'_v, the secondary compression of RAS:BA/FS mixtures decreases significantly as the bottom ash/foundry slag content increases. As illustrated in Fig. 2.11, for typical highway embankments with σ'_v less than 200 kPa, addition of 50% bottom ash/foundry slag to RAS reduces $C_{\alpha\varepsilon}$ from 0.023 to 0.006.

Fig. 2.12 shows the effect of secondary compression on σ'_y of pure RAS and a RAS:BA mixture. The LID under σ'_v=100 kPa was extended to 150 days for pure RAS and the RAS:BA mixture with 50% bottom ash during one-dimensional consolidation test. After the 150-day time period the consolidation test with standard LID=24 h continued until σ'_v =1600 kPa. The long-term secondary compression increased σ'_y of pure RAS from 65 kPa to 250 kPa and of the RAS:BA mixture from 300 kPa to 400 kPa. The effect of secondary compression on σ'_y is more significant on pure RAS than the RAS:BA mixture. The C_{pry} of RAS decreases from 0.07 to 0.03 as a result of preconsolidation effect. Consequently, preloading is an alternative way to reduce compressibility of RAS.

Shear Strength

Figs. 2.13 and 2.14 show respectively the stress-strain and volumetric behavior of RAS:BA and RAS:FS mixtures sheared in triaxial compression cells under CD condition at σ'_c of 140 kPa. The stress-strain and volumetric behavior of pure RAS resembles those of sandy soils in loose state. For BA or FS content up to 50%, the volumetric behavior of RAS:BA/FS mixture is contractive and the maximum deviator stress, $\sigma'_{d\max}$, remains almost unchanged. Increase in BA

or FS content beyond 50% increases $\sigma'_{d\max}$ and the volumetric behavior changes to dilative. Deviator stress at failure, σ'_{df}, was selected as the $\sigma'_{d\max}$ or the σ'_d corresponding to 10% axial strain whichever is reached earlier. Pure RAS exhibited an apparent cohesion of 7 kPa in Mohr-Coulomb failure envelop due to a slight binding of RAS particles during compaction. This apparent cohesion is neglected for practical purposes. Fig. 2.15(a) shows the variation of effective friction angle, ϕ', of RAS:BA mixtures with BA content and Fig. 2.15(b) shows the variation of ϕ' of RAS:FS mixtures with FS content for different σ'_c. Similar to $\sigma'_{d\max}$, the ϕ' remains almost unchanged with bottom ash/foundry slag content up to 50% after which the ϕ' increases. The range of ϕ' for RAS:BA mixtures is between 37^o and 53^o and for RAS:FS mixtures is between 37^o and 56^o which are higher than the ϕ' range (31^o to 45^o) for typical compacted sandy soils (US Navy 1986). Therefore, the shear strength of RAS:BA/FS mixtures are sufficient for use as structural fill material for construction of highway embankments.

Coefficient of Lateral Earth Pressure and Poisson's Ratio

Fig. 2.16 shows the results of K_o-Consolidation tests. The K_o of pure RAS nonlinearly decreases with σ'_v from about 1.0 for σ'_v less than 100 kPa to 0.36 for σ'_v higher than 500 kPa. Correspondingly, Poisson's ratio decreases from 0.5 to 0.26. On the other hand, BA has almost a constant K_o of 0.25 and Poisson's ratio of 0.2 and FS has K_o of 0.30 and Poisson's ratio of 0.25 at different σ'_v. Stronger interlock and friction between particles reduce K_o while disengagement of particle interlocks due to particle damage increases K_o (Jáky 1944; Mesri and Hayat 1993). Once the particle framework restructures at higher stress level, K_o starts to decrease. Under small

to moderate σ_v', the compressibility of RAS particles seems to help disengage the interlocks and reorient the particles. Therefore, pure RAS seems to pose lateral earth pressure almost equivalent to its overburden pressure behind retaining walls. Similarly, a typical embankment constructed using pure RAS would face relatively large lateral deformation. At higher σ_v', densification as well as apparent cohesion between RAS particles due to asphalt cement content seem to help particle interlock and engagement which consequently reduces K_o. As illustrated in Fig. 2.16, addition of 50% BA or FS to RAS significantly reduces K_o and Poisson's ratio of the RAS:BA/FS mixture close to those of bottom ash and foundry slag.

Conclusions

In this study, recycled asphalt shingles (RAS) were evaluated for potential use as structural fill in highway embankments or backfills behind retaining walls. Because of high compressibility of RAS, two byproducts, i.e., bottom ash (BA) and foundry slag (FS), were selected as granular additives to improve the mechanical properties of RAS such that to render it as an acceptable fill material. The following specific observations are made based on the test results:

1. RAS:BA/FS mixtures have lower γ_{dmax} than typical compacted soils. Low dry unit weight of RAS:BA/FS mixtures make them favorable alternatives to natural compacted soils for construction of structural fill over soft soils.
2. RAS:BA/FS mixtures have good drainage capacity as structural fills. The hydraulic conductivity of the mixture slightly decreases with increasing confining pressure due to compressibility of RAS particles. The hydraulic conductivity of the mixture increases with increase in bottom ash/foundry slag content and becomes almost insensitive to

confining pressure when the bottom ash/foundry slag content of the mixture increases to more than 50%.

3. The short-term and long-term compressibility of pure RAS are significantly higher than those of compacted sandy soils. The high compressibility is due to asphalt cement and cellulose felt contents in RAS. Systematic addition of bottom ash and foundry slag to RAS reduces compressibility of the mixture. At small to moderate stress levels typical in highway embankments, addition of more than 50% by weight bottom ash or foundry slag to RAS greatly reduces the short-term and the long-term compression and categorizes the RAS:BA/FS mixtures as slightly to very slightly compressible material.
4. Stress-strain and volumetric behavior of pure RAS is similar to those of loose sandy soils. Addition of bottom ash/foundry slag up to 50% to RAS does not have any noticeable effect on volumetric behavior and shear strength; however, the volumetric behavior tends to be dilative and shear strength starts to increase when the bottom ash/foundry slag content of the RAS:BA/FS mixture increases to more than 50%. Shear strength of different RAS:BA/FS mixtures are similar to those of compacted sandy soils and is sufficient for construction of structural fills.
5. Coefficient of lateral earth pressure of RAS:BA/FS mixtures is comparable to those of compacted sand. Good drainage capacity and lower dry unit weight of RAS:BA/FS mixtures make them favorable alternatives to sand and gravel in terms of lower lateral earth pressures behind retaining structures.

Based on the results of this research, RAS:BA/FS mixture is seen as a viable material for use in structural fills. Such an application will provide a large-volume beneficial use for RAS, which is largely disposed in landfills, as well as for BA and FS, which also are industrial byproducts not

fully recycled. Asphalt cement content in RAS may make the RAS:BA/FS mixture sensitive to temperature change and warrant further research.

Acknowledgement

Support for this study was provided by the Recycled Materials Resource Center, which is supported by the Federal Highway Administration. The opinions, findings, conclusions, or recommendations expressed herein are those of the author(s) and do not necessarily represent the views of the sponsors.

References

Ahmed, I. (1993). *Use of Waste Material in Highway Construction*. Noyes Data Corporation, Park Ridge, NJ.

American Coal Ash Association (2009). Coal Combustion Product (CCP) Production & Use Survey Results. ACAA, Aurora, CO. September 15, 2009 [online].

American Society for Testing and Materials (ASTM). (1963). "Standard test method for particle-size analysis of soils." *Designation D422-63*, PA.

American Society for Testing and Materials (ASTM). (2000). "Standard test methods for specific gravity of soil solids by water pycnometer." Designation *D854-00*, PA.

American Society for Testing and Materials (ASTM). (2000). "Standard test methods for laboratory compaction characteristics of soil using standard effort [[f12,400 ft lbf/ ft^3 (600 kN m/m^3)]." *Designation D698-00a*, PA.

American Society for Testing and Materials (ASTM). (1995). "Standard test methods for measurement of hydraulic conductivity of saturated porous materials using a flexible wall permeameter." *Designation D5084-03*, PA.

American Society for Testing and Materials (ASTM). (1996). "Standard test method for one-dimensional consolidation properties of soils." *Designation D2435-96*, PA.

Bareither, C., Edil, T., Benson, C., and Mickelson, D. (2008). "Geological and Physical Factors Affecting the Friction Angle of Compacted Sands." *Journal of Geotechnical and Geoenvironmental Engineering,* Vol. 134, No. 10, pp. 1476-1489.

Benson, C., Edil, T., and Soleimanbeigi, A. (2010). "Use of recycled asphalt shingles in highway embankments" *Proceeding of 2010 Mid-Continent Transportation Research Forum,* August 19-21, Madison, WI.

Button, J. W., Williams D., and Scherocman, J.A. (1995). "Roofing Shingles and Toner in Asphalt Pavements", Research Report 1344-2F, Texas Transportation Institute, College Station, Texas.

Casagrande, A. (1936a). "The determination of the pre-consolidation load and its practical significance." Discussion D-34, *Proc. Fist Int. Conf. Soil Mech. Found. Engr.*, Cambridge, Vol. 3, pp. 60-64.

Chuhan, F. A., Kjeldstad, A., Bjorlykke, K., and Hoeg, K. (2003). "Experimental compression of loose sands: relevance to porosity reduction during burial in sedimentary basins." Canadian Geotechnical Journal, Vol. 40, No. 5, pp. 995–1011.

Coduto, D. P. (1998). *Geotechnical Engineering Principles and Practices*. Prentice Hall.

Edil, T., Benson, C., Bin-Shafique, M., Tanyu, B., Kim, W., and Senol, A. (2002). "Field evaluation of construction alternatives for roadway over soft subgrade," *Transportation Research Record*, 1786, Transportation Research Board, National Research Council, Washington, DC, pp. 36-48.

Edil, T. B., and Wang, X. (2000). "Shear strength and K_o of peats and organic soils", *Geotechnics of High Water Content Materials, ASTM Special Technical Publication,* pp. 209-225.

Emery, J. J. (1985). "Slag utilization in pavement construction." Extending Aggregate Resources, ASTM STP No. 774, ASTM, pp. 95-118.

Fox, P. J., Edil, T. B. and Lan, L. T. (1992). "C_α/C_c concept applied to compression of peat," *Journal of Geotechnical Engineering,* ASCE, Vol. 118, No. 8, pp. 1256-1263.

Grodinsky, C., Plunkett, N., and Surwilo, J. (2002). "Performance of Recycled Asphalt Shingles for Road Applications.", *Final Report*, State of Vermont's Agency of Natural Resources.

Huang, H. W. (1990). "The use of bottom ash in highway embankments, subgrade, and subbases." Joint Highway Research Project, Final Report, FHWA/IN/JHRP-90/4, Purdue University, West Lafayette, Indiana.

Karim, A., Lovell, C., Salgado, R. (1997). Building Embankments of Fly/Bottom Ash Mixtures, FHWA/IN/JTRP-97/01, SPR-2115, Joint Transportation Research Program, Purdue University.

Kim, B. (2003). *Properties of Coal Ash Mixtures and their Use in Highway Embankments*. PhD Thesis, Purdue University, Indiana, USA.

Kim, B., Prezzi, M. and Salgado, R. (2005). "Geotechnical Properties of Fly and Bottom Ash Mixtures for Use in Highway Embankments." *Journal of Geotechnical and Geoenvironmental Engineering*, ASCE, 131(7) 914-924.

Krivit, D. (2007). Recycling of Tear-Off Shingles: Best Practices Guide. Final report prepared for the Construction Materials Recycling Association (CMRA).

Hooper, F., and Marr, W. (2004). "Effects of Reclaimed Asphalt Shingles on Engineering Properties of Soils," *Recycled Materials in Geotechnics, Geotechnical Special Publication,* 127, 137-149.

Lade, P. V., Yamamuro, J. A., and Bopp, P. A. (1997). "Influence of time effects on instability of granular materials." Computers and Geotechnics, 20, 179-193.

Lee, K. L., and Farhoomand, I. (1967). "Compressibility and crushing of granular soil in anisotropic triaxial compression." *Canadian Geotechnical Journal*, 4(1), 68-99.

Li, L., Benson, C. H., Edil, T. B., and Hatipoglu, B. (2008). "Sustainable Construction Case History: Fly Ash Stabilization of Recycled Asphalt Pavement Material." *Geotechnical and GeologicalEngineering*, 26(2), 177-188.

Marks, V. J., and Petermeier, G. (1997). "Let Me Shingle Your Roadway", *Research Project HR-2079, Iowa Department of Transportation,* Ames, Iowa

Marsal, R. J. (1967). "Large scale testing of rockfill materials." *Journal of the Soil Mechanics and Foundations Division, ASCE,* 93, 27-43.

Mesri, G., and Hayat, T. M. (1993). "The coefficient of earth pressure at rest." *Canadian Geotechnical Journal*, 30(4), 647-666.

Mesri, G., Stark, T. D., Ajlouni, M. A., and Chen, C. S. (1997). "Secondary compression of peat with or without surcharging." *Journal of Geotechnical and Geoenvironmental Engineering, ASCE*, 123(5), 411-421.

Mesri, G., and Vardhanabhuti, B. (2009). "Compression of granular materials", *Canadian Geotechnical Journal,* 46, 369-392.

Moulton, L. K., Seals, R. K., and Anderson, D. A. (1973). "Utilization of ash from coal burning power plants in highway construction." *Transportation Research Record*, 430, 26-39.

Pestana, J. M., and Whittle, A. J. (1995). "Compression model for cohesionless soils." Géotechnique, 45, 611-631.

Recycled Materials Resource Center (2010). *User Guidelines for By-products and Secondary Use Materials in Pavement Construction*, http://www.rmrc.unh.edu/tools/uguidelines/index.asp, Accessed December 2010.

Recycling Connections Corporation (2010). *Wisconsin Statewide Waste Characterization Study*. Prepared for Wisconsin Department of Natural Resources.

Roberts, J. E., and de Souza, J. M. (1958). "The compressibility of sands." *Proc., American Society for Testing and Materials*, 58, 1269-1277.

Roberts, F. L., Kandhal, P. S., Brown, E. R., Lee, D. Y. and Kennedy, T. W. (1996). *Hot Mix Asphalt Materials, Mixture Design, and Construction*. National Asphalt Paving Association Education Foundation. Lanham, MD.

Seals, R. K., Moulton, L. K., and Ruth, B. E. (1972). "Bottom ash: An engineering material." *Journal of Soil Mechanics and Foundation Division*, 98(4), 311-325.

Tanyu, B.F., Benson, C.H., Edil, T.B., and Kim, W.H. (2005), "Equivalency of crushed rock and three industrial by-products used as a working platform during pavement construction," *Transportation Research Record*, 1874, Transportation Research Board, National Research Council, Washington, DC, pp. 59-69.

Townsend, T., Powell, J., and Xu, C. (2007). Environmental issues associated with asphalt shingle recycling. *Construction Materials Recycling Association, US EPA Innovations Workgroup*.

Turley, W. (2010). Personal Communication. *Construction Materials Recycling Association*, Eola, IL.

U.S. Bureau of Reclamation. (1987). *Design of Small Dams*. U.S. Department of the Interior, Bureau of Reclamation.

U.S. Geological Survey. (2008). *Minerals Yearbook*. USGS, http://minerals.usgs.gov/minerals/pubs/commodity/iron_&_steel_slag/myb1-2008-fesla.pdf, Accessed December 2010.

U.S. Navy. (1986). "Design manual—Soil mechanics, foundations, and earth structures." *NAVFAC DM-7*, Department of the Navy, Washington, D.C.

Viyanant, C., Rathje, E. M., and Rauch, A. F. (2007). "Creep response of recycled asphalt pavement." *Canadian Geotechnical Journal*, 44, 687-697.

Warner, J. D. (2007). "The beneficial reuse of asphalt shingles in roadway construction", *MSc thesis, Department of Civil and Environmental Engineering, University of Wisconsin-Madison.*

Wen, H., and Edil, T. B. (2007). "Laboratory Study of Recycled Asphalt Pavement Materials as BaseCourse." *Proc. of 5th International Conference on Maintenance and Rehabilitation of Pavements and Technological Control*, Park City, UT, 457-462.

Yoon, S., Balunaini, U., Yildirim, I. Z., Prezzi, M. and Siddiki, N. Z. (2009). "Construction of an embankment with a fly and bottom ash mixture: Field performance study." *Journal of Materials in Civil Engineering, ASCE*, 21(6), 271-278.

Table 2.1. Grain size indices and USCS classifications of RAS, bottom ash and outwash sand

Material	d_{10} (mm)	d_{50} (mm)	C_u	C_c	% fines	G_s	USCS symbol	USCS name
RAS	0.17	1.1	7.6	1.6	3.8	1.74	SW	Well graded sand
Bottom ash	0.19	0.9	6.3	0.8	1.9	2.67	SP	Poorly graded sand
Foundry slag	0.18	1.6	11.4	2.7	4.8	2.36	SW	Well graded sand
Glacial outwash sand[a]	0.21	0.5	3.1	0.8	0.0	2.71	SP	Poorly graded sand

d_{10}: effective particle size (particle size for which 10% of the sample is finer than d_{10}); d_{50}: median particle size (particle size for which 10% of the sample is finer than d_{50}); C_u: coefficient of uniformity, d_{60}/d_{10}; C_c: coefficient of curvature, $C_{30}^2/(C_{10}\times C_{60})$; G_s: specific gravity; USCS: Unified Soil Classification System

[a] Data were taken from Bareither et al. (2008);

Table 2.2. Classification for material compressibility (after Coduto 1998)

C_{psy} or C_{pry}	Classification for compressibility
0-0.05	Very Slightly compressible
0.05-0.10	Slightly compressible
0.10-0.20	Moderately compressible
0.20-0.35	Highly compressible
> 0.35	Very Highly compressible

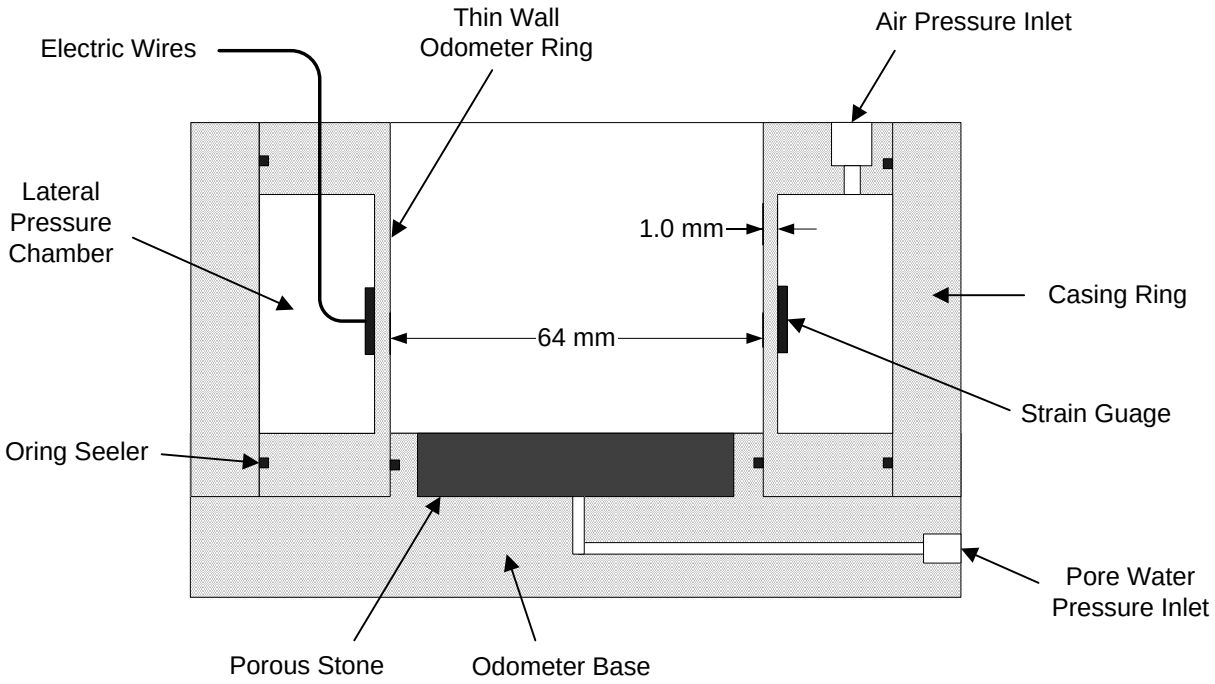

Fig. 2.1. K_o-Consolidation cell (after Edil and Wang 2000)

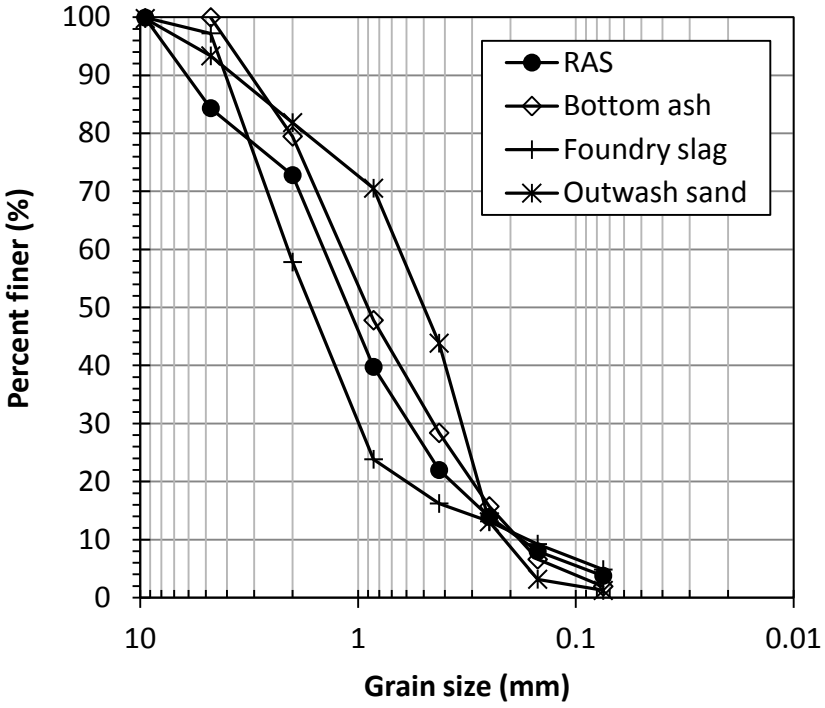

Fig. 2.2. Grain size distribution of RAS, bottom ash, foundry slag and glacial outwash sand

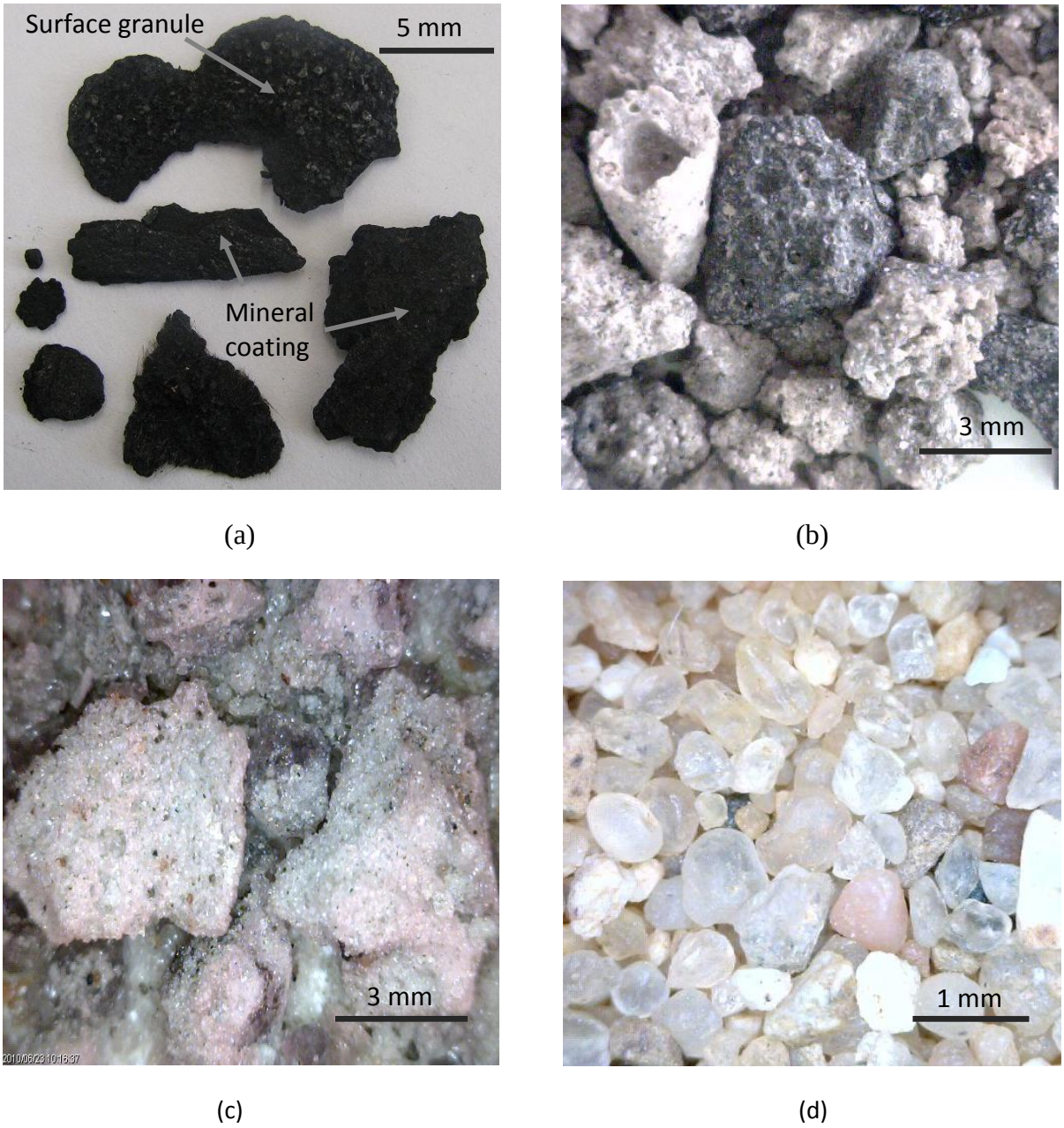

(a) (b)

(c) (d)

Fig. 2.3. Photographs of RAS (a), LM photomicrographs of bottom ash (b), foundry slag (c), and glacial outwash sand particles (d)

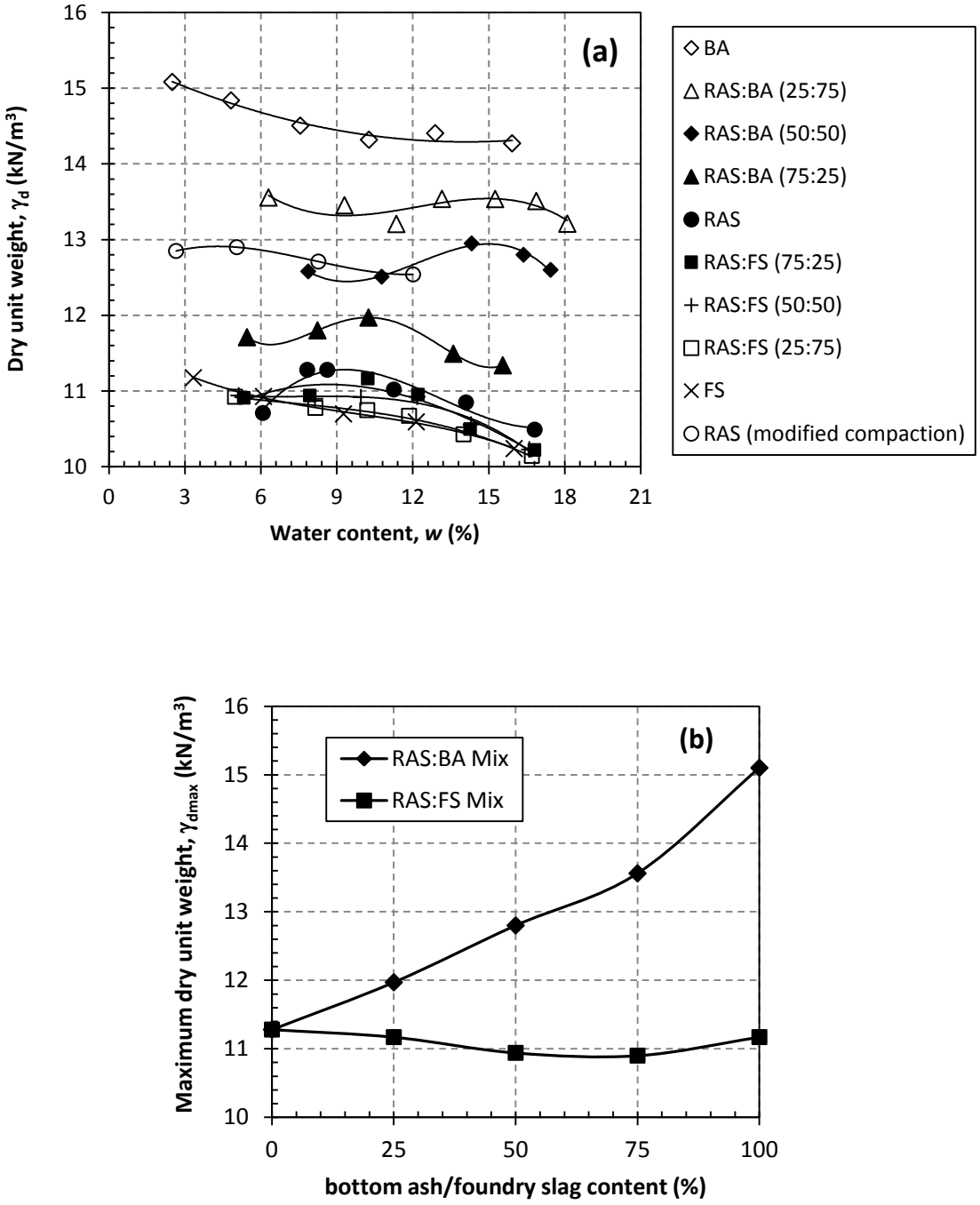

Fig. 2.4. Standard Proctor dry unit weight versus water content of RAS:BA/FS mixtures (a) maximum dry unit weight of RAS:BA/FS mixture versus bottom ash/foundry slag content (b)

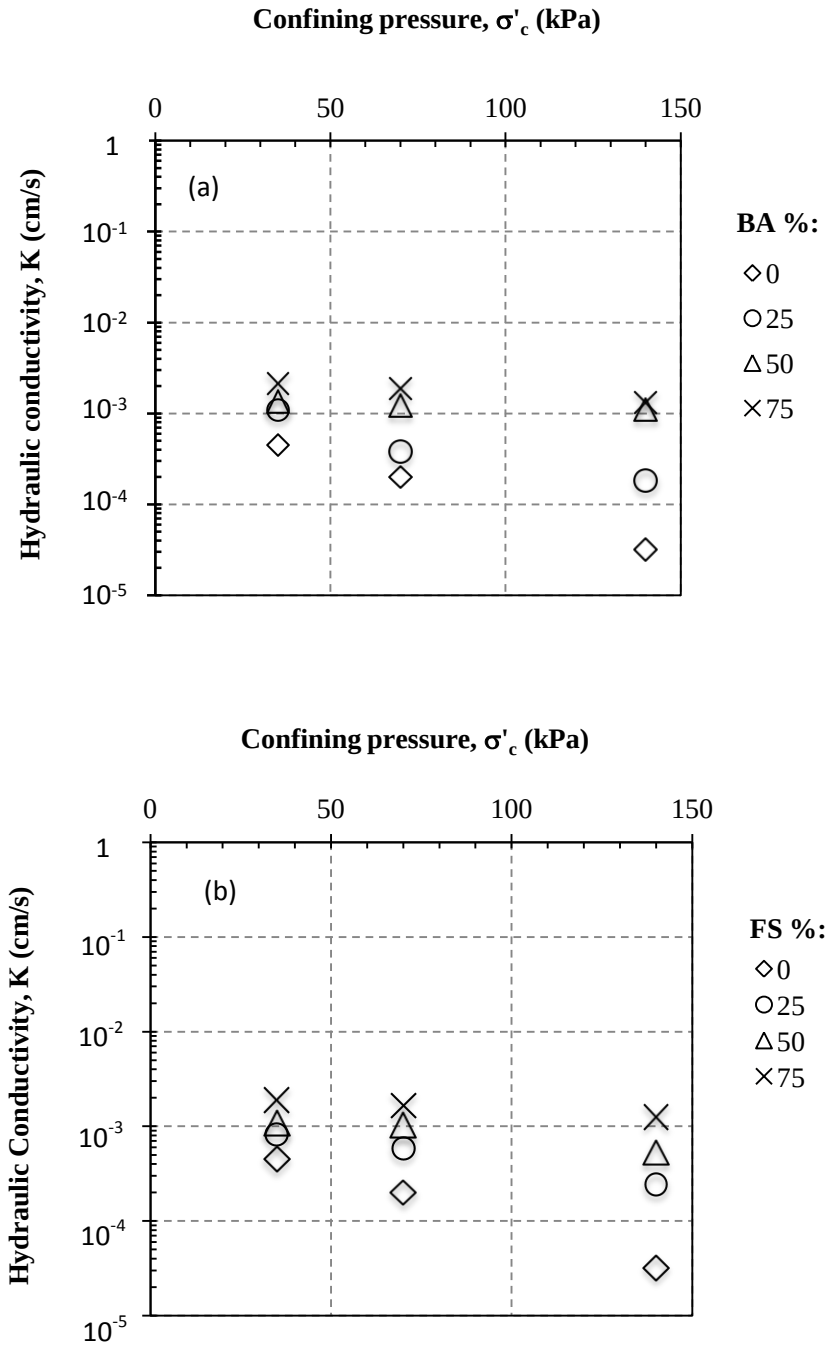

Fig. 2.5. Hydraulic conductivity of (a) RAS:BA mixtures and (b) RAS:FS mixtures versus effective confining pressure

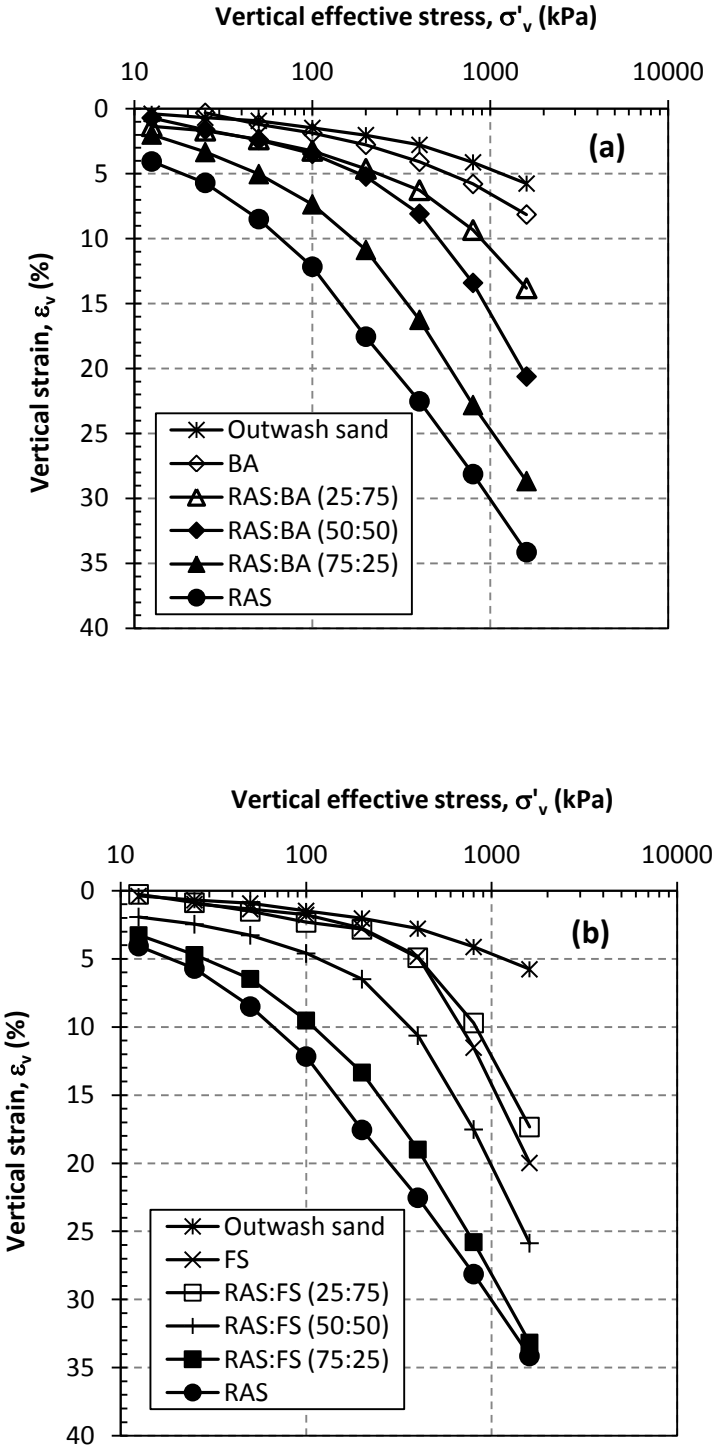

Fig. 2.6. One-dimensional compression curves of (a) RAS:BA mixtures and (b) RAS:FS mixtures

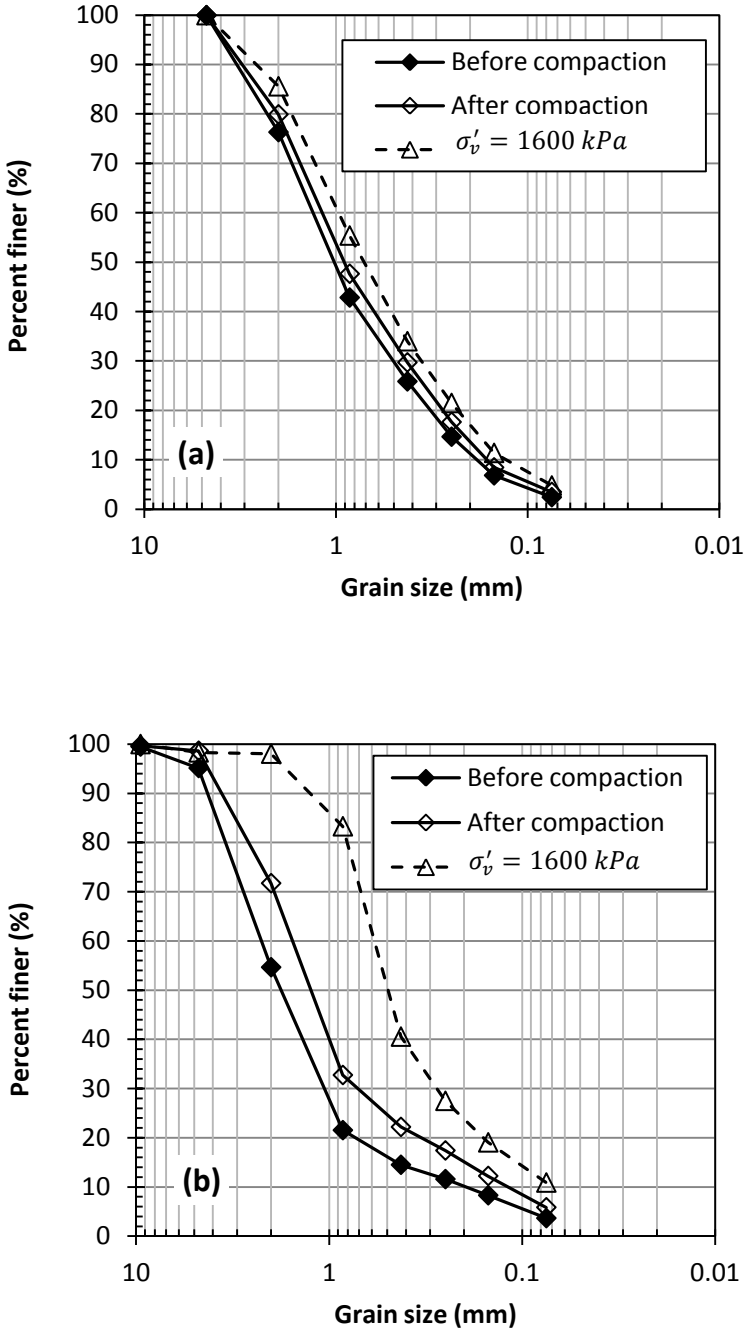

Fig. 2.7. Material degradation after compaction and compression tests (a) bottom ash and (b) foundry slag

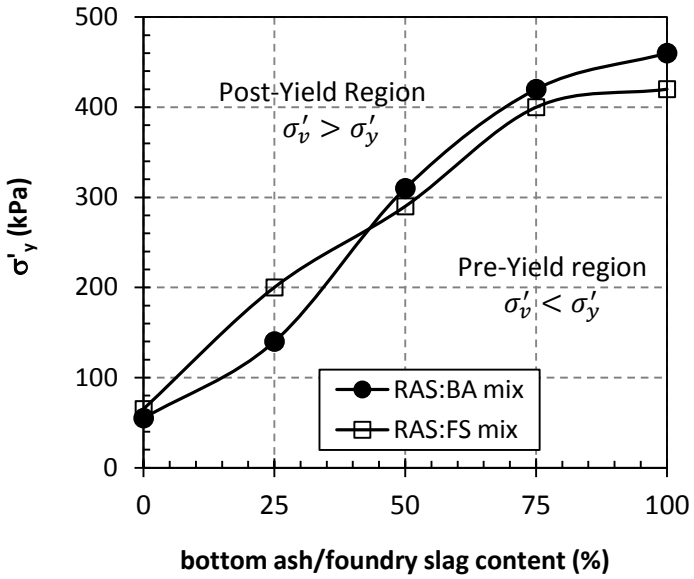

Fig. 2.8. Variation of yield pressure of RAS:BA/FS mixture with bottom ash/foundry slag contents

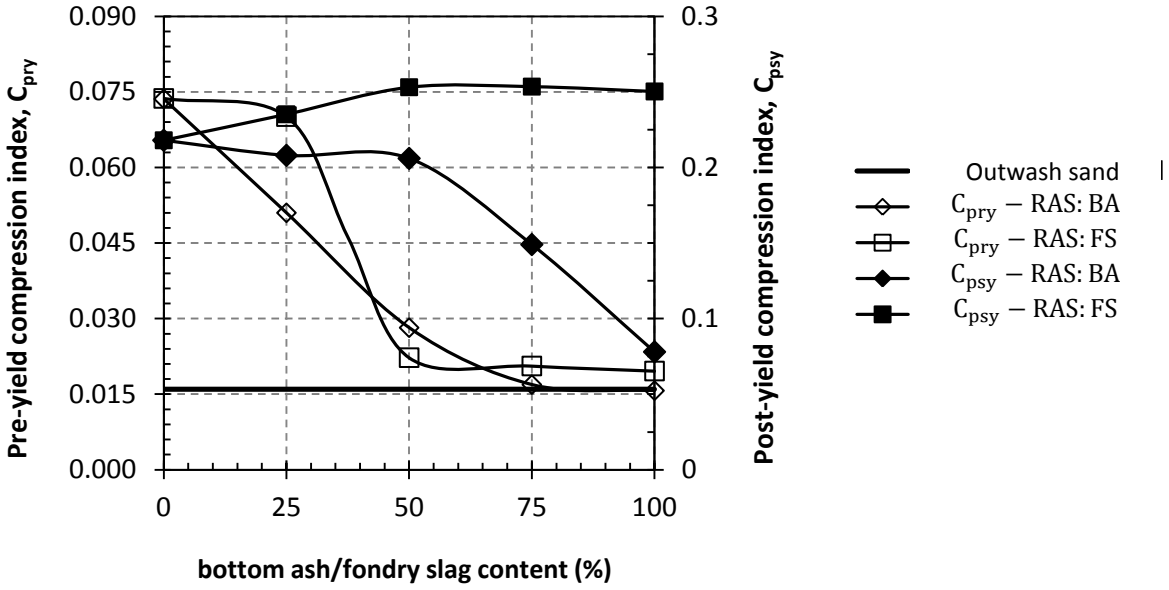

Fig. 2.9. Variation of post-yield and pre-yield compression indices of RAS:BA/FS mixtures with bottom ash/foundry slag content

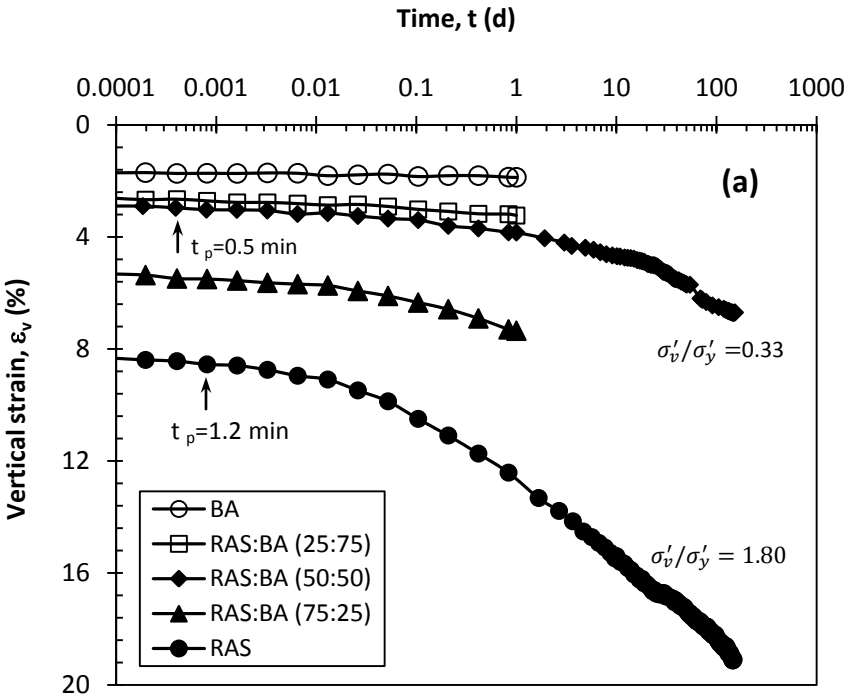

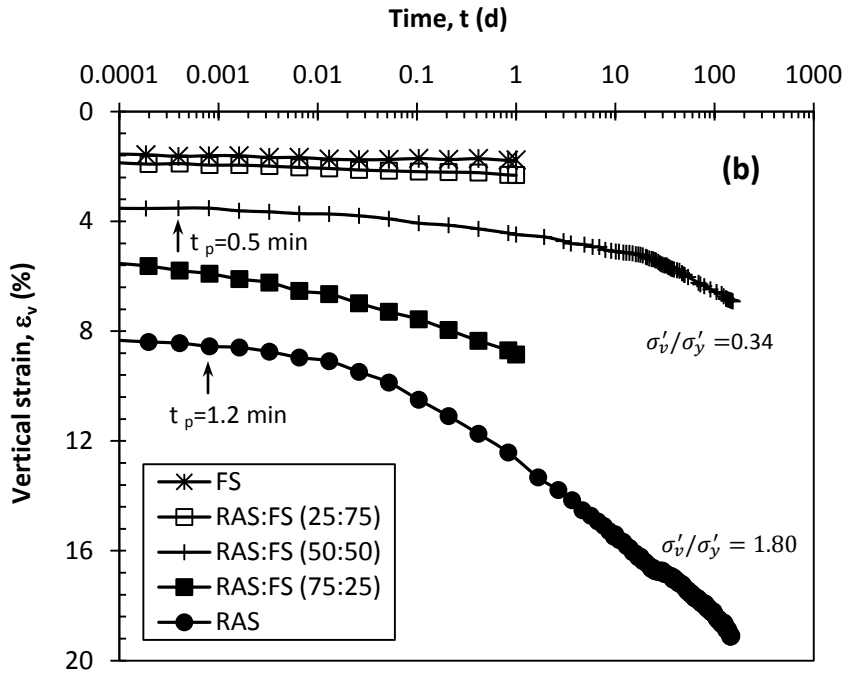

Fig. 2.10. Variation of ε_v with time for (a) RAS:BA mixtures and (b) RAS:FS mixtures

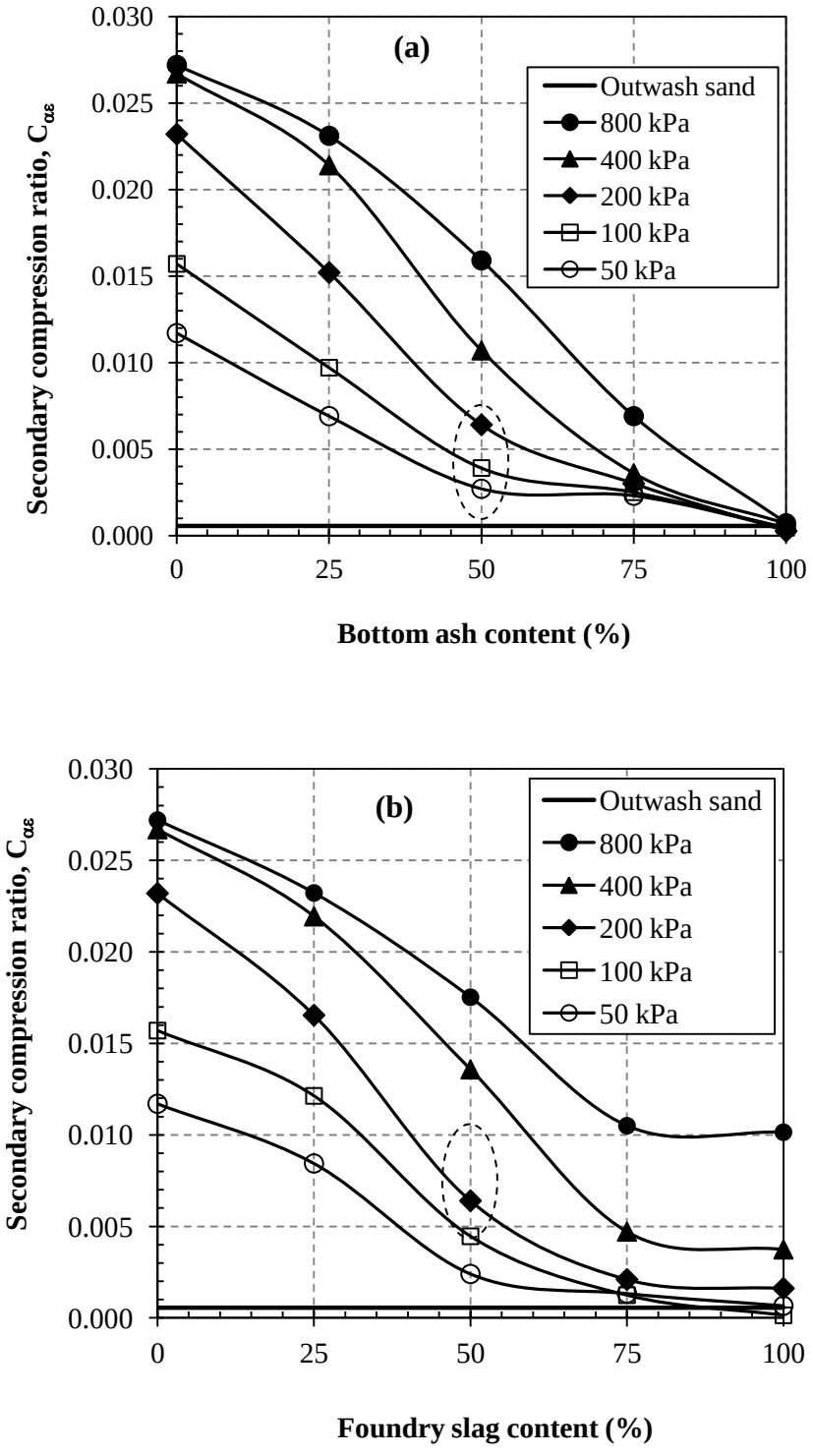

Fig. 2.11. Variation of secondary compression of (a) RAS:BA mixtures with BA content and (b) RAS:FS mixtures with FS content

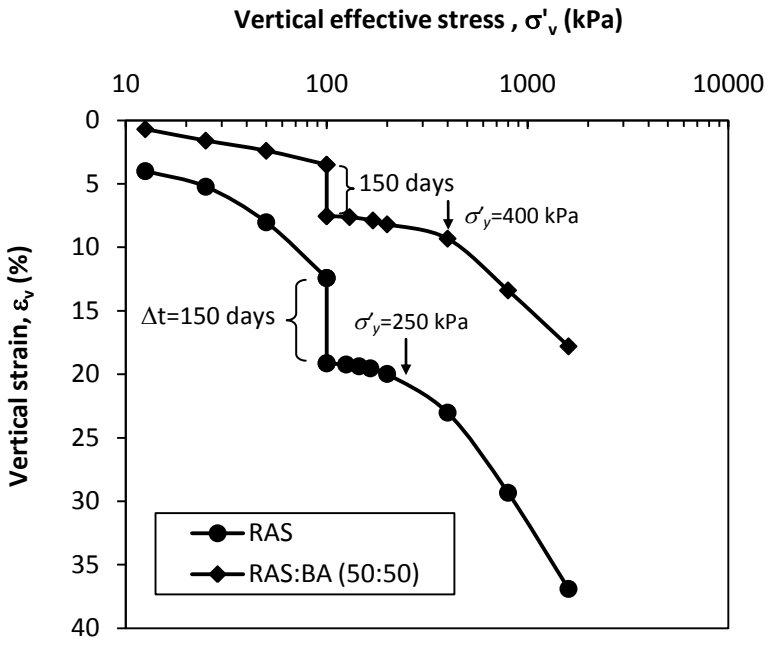

Fig. 2.12. Preconsolidation pressure of RAS:BA mixture resulting from secondary compression

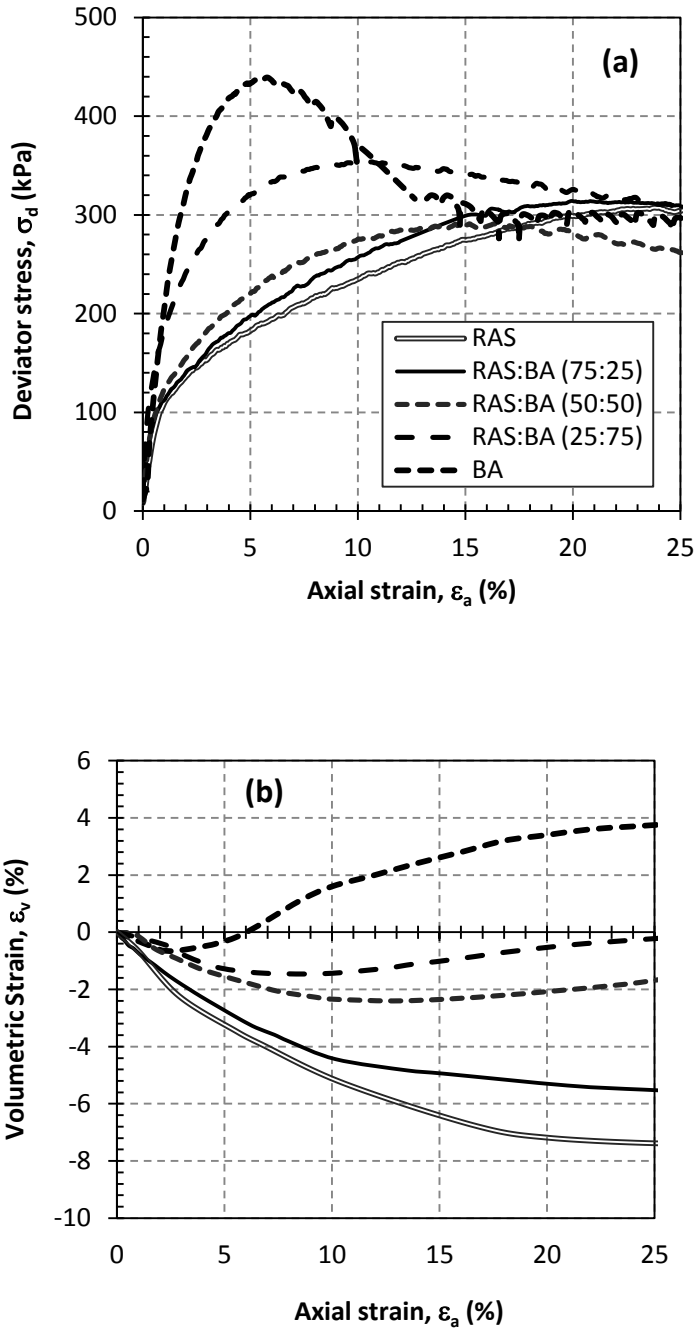

Fig. 2.13. Results of CD triaxial tests: (a) stress-strain behavior of RAS:BA mixtures; (b) volumetric change behavior of RAS:BA mixtures

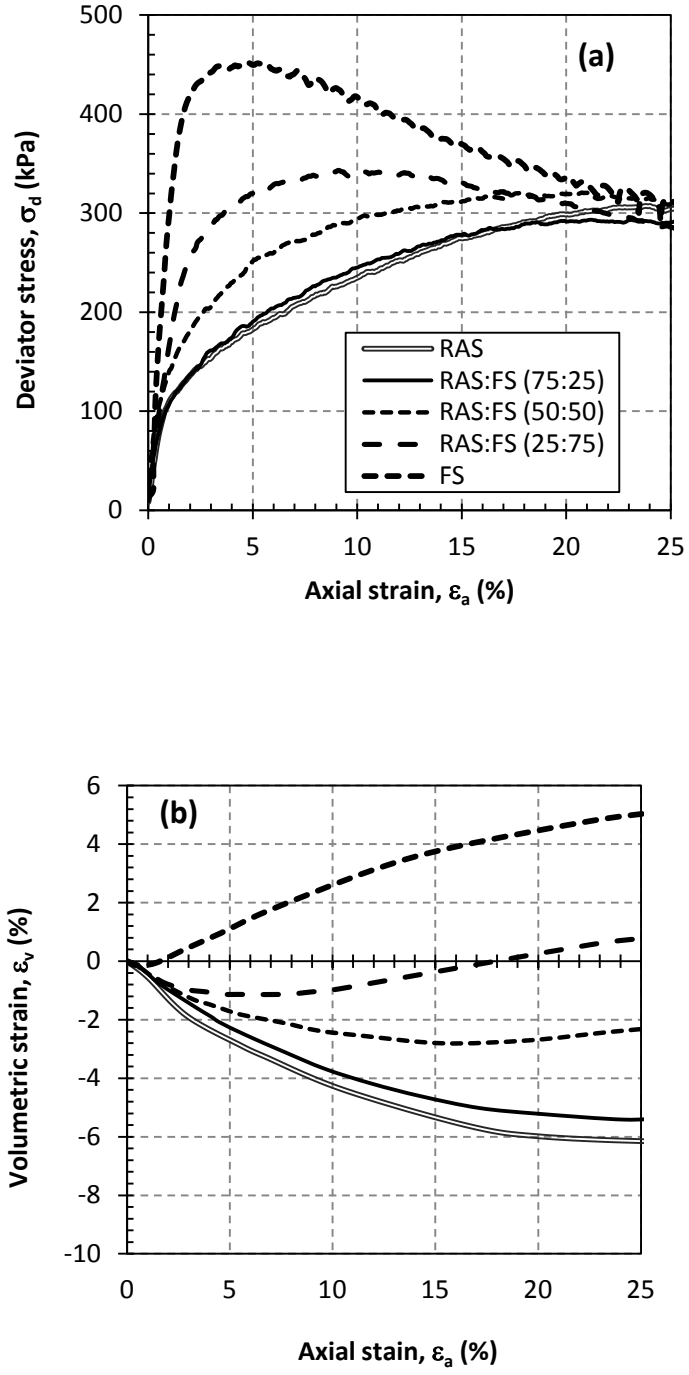

Fig. 2.14. Results of CD triaxial tests: (a) stress-strain behavior of RAS:FS mixtures; and (b) volumetric change behavior of RAS:FS mixtures

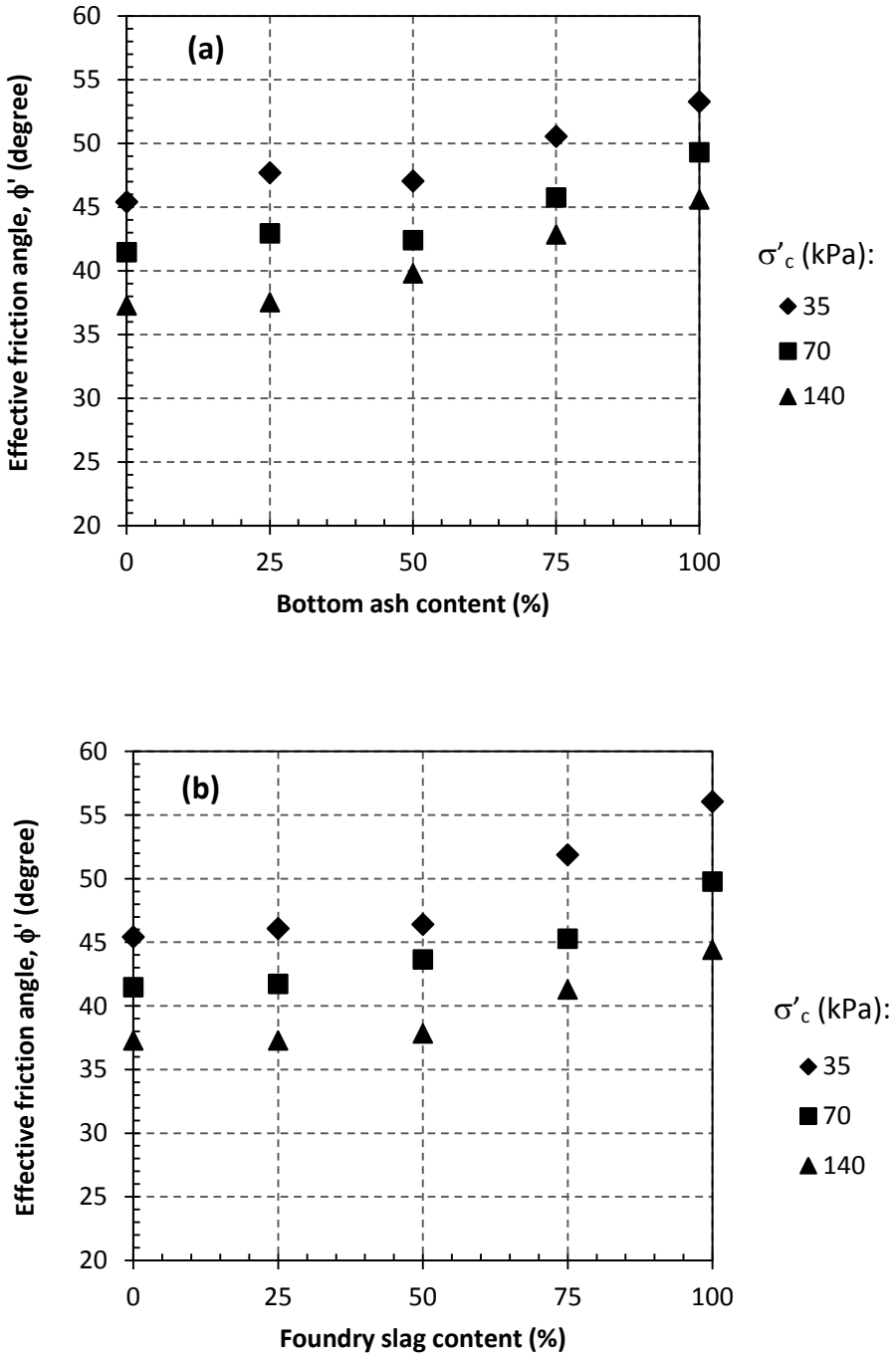

Fig. 2.15. Variation of friction angle of (a) RAS:BA mixtures with BA content and (b) RAS:FS mixtures with FS content at different confining stresses

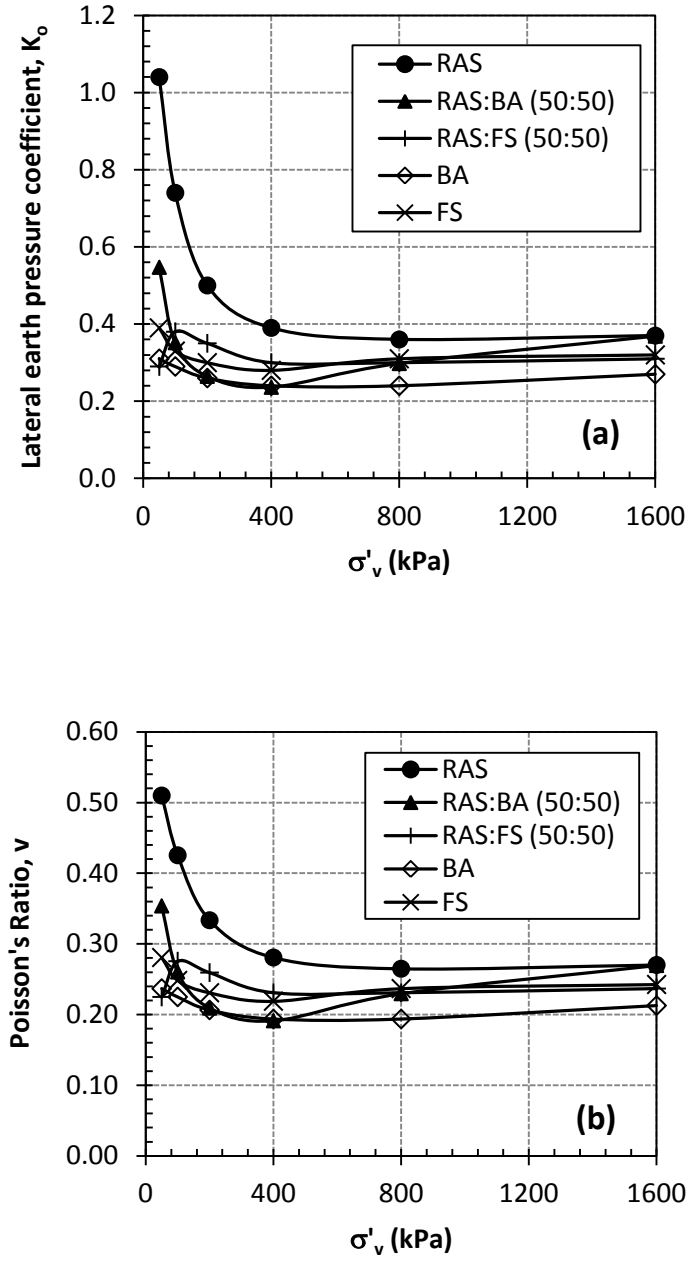

Fig. 2.16. Variation of K_o (a) and Poisson's ratio (b) of RAS:BA/FS mixtures with overburden pressure

Chapter 3 Evaluation of Fly Ash Stabilization of Recycled Asphalt Shingles for Use in Structural Fills

Abstract: The majority of tear-off roofing shingles and manufacturing shingle scraps are currently disposed of as solid waste in landfills. Landfills are also the end place for the majority of coal combustion byproducts like fly ash. In this study, geotechnical properties of recycled asphalt shingles (RAS) stabilized with a self-cementing fly ash (FA) for use as structural fill material were systematically evaluated. Compaction, hydraulic conductivity, compressibility, shear strength, and coefficient of lateral earth pressure at rest (K_o) of stabilized RAS were evaluated. The maximum dry unit weight (γ_{dmax}) of RAS:FA mixtures varies between 11.3 kN/m^3 and 13.8 kN/m^3 qualifying them as light-weight fill material and the compaction curves are not sensitive to water content. The hydraulic conductivity of RAS:FA varies between 2×10^{-4} cm/s and 3×10^{-5} cm/s for FA content varying between 0% and 20% resulting in a largely drainable material. RAS has a friction angle (ϕ') of 36^o and cohesion (c') of 24 kPa. Addition of 20% FA reduces the ϕ' to 33^o but increases the c' to 100 kPa making it sufficiently strong as a fill material. However, compared to compacted sand, RAS is highly compressible. Stabilizing RAS with more than 10% of FA, keeps the long-term settlement of a typical highway embankment below the typical settlement limit. Stabilized RAS has a K_o below 0.1 indicating lower lateral pressures behind retaining walls compared to typical soils. Overall results indicate that RAS stabilized with FA has potential as a lightweight material for use as highway embankment fill or retaining wall backfill.

Keywords: Recycled asphalt shingle, fly ash, structural fill, engineering properties.

Introduction

Using industrial solid waste in construction contributes to savings in energy consumed in production of virgin aggregates and reduction in greenhouse gas emissions, consequently resulting in more sustainable construction (Edil 2006, Lee et al. 2010). Nearly 80% of structures in the U.S. are covered by asphalt shingles (Krivit 2007). Asphalt shingle waste is produced by removing the asphalt shingles from the roofs of existing houses during renovation (called post-consumer asphalt shingle or tear-off shingle) or rejecting asphalt shingles/shingle tabs discarded in the manufacturing process of new asphalt shingles (called manufactured shingle scrap). Approximately 11 million Mg of asphalt roofing shingle waste are generated in the U.S. per year (Krivit 2007). Re-roofing jobs account for 10 million Mg, with another 1 million Mg manufacturing scrap. Currently the majority of produced asphalt shingle waste in the U.S. is disposed in landfills (Zickell 2003, Townsend 2007). The majority of current reuse application of recycled asphalt shingles (RAS) consists of incorporation in hot mix asphalt (HMA) to benefit from the asphalt cement and sand contents of RAS. However, many DOT specifications limit the incorporation of RAS in HMA to 5% due to adverse effect of higher percentages of RAS on mechanical properties of HMA (Button et al. 1995, Grodinsky 2002, Krivit 2007). Other applications of RAS include as fuel and mineral supplement in cement kilns, as dust control in gravel roads, as compacted road base and subbase, and as cold patch on paved roads. Reuse of RAS in these applications is also limited due to unavailability of basic knowledge of properties and standard specifications. Consequently, current applications of RAS reuse consists of only 10 to 20% of the total produced asphalt shingle waste in the U.S. (Turley, 2011).

Another possible application that will potentially generate large-volume use of the asphalt shingle waste is its use as structural fill material in highway embankments and backfill

behind retaining walls. For these applications, certain geotechnical properties are required and there is a dearth of such information. RAS is a highly compressible material (Soleimanbeigi et al. 2012), which limits its ability for use as a structural fill material. To control its excessive compressibility, stabilization of RAS with self-cementing fly ash, which is a widely available industrial byproduct, is considered. In this study, the geotechnical properties of RAS stabilized with self-cementing fly ash are evaluated for structural fill applications. The beneficial use of self-cementing fly ash has been investigated by several researchers and several demonstration projects have been successfully constructed using self-cementing fly ash in conjunction with a variety of materials from natural soils to recycled asphalt pavements (Patelunas 1986; DiGioia 1986; McLaren and DiGioia 1987; Misra 2000; Srivastava and Collins 1989; Ferguson, 1989; Ferguson and Levorson, 1999; Edil et al. 2002; Bin-Shafique et al. 2004; Lin et al. 2008; ACAA 2008; Lin et al. 2009; Wen and Edil 2009; Wen et al. 2011). According to the American Coal Ash Association (ACAA 2009) survey about 63 million Mg fly ash (FA) was produced in 2009 of which only about 39% was reused in different applications like concrete production, structural fills, waste stabilization, road base/subbase and soil modification. The remaining fly ash is typically disposed in utility disposal sites. Reuse of RAS stabilized with self-cementing fly ash will potentially have beneficial contribution in saving landfill space and reducing energy consumption and green house gas emissions due to production of natural aggregates through the beneficial use of two under recycled industrial byproducts.

The objective of this research is to evaluate mechanical properties of RAS stabilized with self-cementing fly ash for use as structural fill in highway embankment fill and retaining wall backfill thus opening up an application for both waste materials. The compaction, hydraulic conductivity, compressibility, shear strength, and coefficient of earth pressure at rest of stabilized

RAS have been evaluated in a systematic manner and improvements and suitability as a structural fill are assessed. The environmental implications are considered beyond the scope of this investigation; however, there are procedures available to implement such an assessment (Li et al. 2006; Kosson et al. 1996; Kosson et al. 2002; Komonweeraket et al. 2011).

Background

A typical asphalt shingle is produced by impregnating a layer of organic or fiberglass mat with air-blown liquid asphalt. Once coated with appropriate thickness of asphalt, one side of the shingle is covered by granules to protect the shingle against physical damage and damage from ultraviolet rays of sun, and the other side is coated by fine sand or fly ash to prevent adhering of individual shingles to each other during packing and transport. The compositions of a typical, new residential asphalt shingle produced today include 32 to 42% coating filler, 28 to 42% granules, 16 to 25% asphalt content, 2 to 15% mat, and 0.2 to 2% adhesive (Grodinsky et al. 2002; Krivit 2007).

Only a few scientific investigations have been conducted on engineering properties and field performance of RAS in geotechnical applications. A qualitative study conducted by Iowa Department of Transportation showed that ground shingles mixed with crushed limestone as a surface treatment were effective for dust control in unpaved rural roads, resulted in better lateral control of vehicles, reduced the loss of granular onto the ditches, and resulted in a quieter and smoother roadway (Marks 1997). Vermont Agency of Natural Resources (Vermont ANR) reported that a mixture of RAS:RAP:Gravel with 10:30:60 ratio placed and compacted on a series of municipal roadways, resists rutting and erosion, mitigates dust and in general requires less maintenance than the conventional gravel control section (Grodinsky et al. 2002).

Laboratory investigations on geotechnical properties of RAS were first conducted to evaluate performance of RAS as base-course (Hooper and Marr 2004; Warner 2007). The maximum dry unit weight (γ_{dmax}) of RAS from the standard Proctor compaction tests varied between 8.8 kN/m^3 and 12.3 kN/m^3. The California bearing ratio (CBR) of RAS was 6%, which categorized RAS as only a suitable material for subgrade (Hooper and Marr 2004). The resilient modulus of RAS was only appropriate for base/subbase layers when mixing 50% by weight of Grade 2 granular backfill (GP-GM) to RAS (Warner 2007). RAS mixed with granular material is however appropriate for use as structural fill in highway embankment or backfill behind retaining walls (Soleimanbeigi et al. 2012). The RAS content in the RAS:"Granular Material" mixture is selected based on the desired shear strength, compressibility and overburden pressure.

Materials

Samples of RAS were taken from Stratford Building Supply Co. in Stratford, Wisconsin. The non-friable RAS samples were processed from tear-off roofing shingle waste to remove common impurities including nails, paper, plastic and wood chips. The percent impurities measured from the RAS sample was less than 0.3% by weight. Fig. 3.1 (a) shows the typical shape of RAS particles as well as sand cover and mineral coating on RAS particle surfaces. The particles are plate-like, irregular in shape, highly angular, and rough in surface texture due to granular surface particles. The angularity of RAS particles reduces to semi-round to round as the particle size is reduced.

To stabilize RAS, a sample of self-cementing fly ash was obtained from Columbia Power Plant near Portage, Wisconsin. The compositional properties of the fly ash include 6.0% loss on ignition (LOI), minimum 50% of SiO_2, Al_2O_3, and Fe_2O_3, and minimum 75% of strength activity

at 7 days. The specific gravity of class C fly ash is 2.70 (Edil et al. 2006). This fly ash is classified as Class C fly ash in accordance to ASTM C618. Although a class C fly ash is investigated, other self-cementing fly ashes that do not meet class C specification, thus not suitable for concrete production and class F fly ashes activated with lime or cement may also provide the necessary stabilization to RAS.

An alternative to fly ash stabilization is to add granular materials to RAS to reduce its compressibility. Since the majority of RAS particles are plate-like in shape, addition of granular materials to RAS is expected to result in better packing of the particles, producing a mixture with lower compressibility and higher shear strength. This approach without stabilization is presented by Soleimanbeigi et al. (2012). Here a mixture of RAS and a granular additive stabilized with fly ash is also considered. Bottom ash (BA) was selected as the granular industrial byproduct additive to RAS. Fig. 3.1 (b) shows a light microphotograph of BA particles. The particles are internally porous, angular and rough in surface texture. Some pores of the particles are filled with dust. To compare engineering properties of stabilized RAS with those of a natural granular structural fill, mechanical tests were also conducted on a sample of Wisconsin glacial outwash sand (GOS) as a reference material. The light microphotograph of outwash sand particles is shown in Fig. 3.1 (c). The particles of GOS are smooth in surface, semi-round to round and free of dust.

Fig. 3.2 shows the particle size distribution curves of RAS, BA and GOS samples tested according to ASTM D 422. The majority of particles in each sample are sand size (between 0.075 mm and 4.75 mm) according to the Unified Soil Classification System (USCS). Table 3.1 summarizes the grain size indices and material classification according to the USCS.

The specific gravity (G_s) of RAS measured in accordance with ASTM D854 (method B) is 1.74, which is a positive attribute for use as a light-weight fill material. The low G_s of RAS is attributed to asphalt cement content and cellulose fiber content, which together comprise from 18 to 50% of RAS. The typical G_s of asphalt cement is between 1.02 and 1.05 (Roberts et al. 1996) and that of cellulose fiber is between 1.3 and 1.5 (Klyosov 2007). Bottom ash has a G_s of 2.67, which is comparable to G_s of GOS (2.71).

Methods

The engineering properties of RAS and stabilized RAS with 10%, 20% and 50% Class C fly ash content were obtained following the standard guide for use of coal combustion by-products in structural fills (ASTM E 1861-97). The compaction tests were performed to determine the dry unit weight of RAS and stabilized RAS. The hydraulic conductivity tests were conducted in a systematic manner to evaluate the drainage capacity of structural fill constructed with RAS or stabilized RAS. One-dimensional compression tests were conducted to investigate compressibility properties of RAS or stabilized RAS. Consolidated drained triaxial compression tests were conducted to evaluate shear strength and finally, K_o-consolidation tests were performed to estimate the coefficient of lateral earth pressure to estimate lateral earth pressure exerted behind retaining walls by RAS or stabilized RAS.

Compaction

Standard Proctor compaction tests following ASTM D 698 (method B) were conducted on different RAS:FA mixtures. Typically, a 1-h delay time between wetting/mixing and compaction was specified to simulate construction delays (ACAA 2003). Delay time causes density and

strength of the stabilized soil be reduced because a portion of the compactive energy must be used to overcome the bonding of the soil particles by cementation; therefore, a portion of the cementation potential is lost (ACAA 2003). RAS:FA mixtures with 10%, 20% and 50% self-cementing fly ash content were compacted 1 h after wetting. The compaction test was also conducted on a sample of RAS:BA:FA mixture with 40%:40%:20% ratio as a potential mixture.

Hydraulic Conductivity

Hydraulic conductivity tests with flexible-wall permeameters were conducted on compacted RAS and stabilized RAS specimens following ASTM D 5084-03 test procedure to evaluate the effect of confining stress (σ_c') on hydraulic conductivity. Each moistened RAS:FA mixture was compacted to 95% of standard γ_{dmax} at optimum water content (w_{opt}). The compacted mixture was cured at 25^{o}C and 100% relative humidity for 7 days. The hydraulic conductivity tests were conducted immediately after 7-day curing period. Each sample mixture was consolidated to the desired effective stress (σ_c'=35 kPa, 70 kPa and 140 kPa) for 24 h after the end of primary consolidation. The time for the end of consolidation is established when no further volume change is observed in the backpressure burette during consolidation. After consolidation phase, the hydraulic conductivity was measured according to the falling head rising tail method.

One-dimensional Compression

Settlement of an embankment with large lateral extension can be considered one-dimensional and estimated from the results of one-dimensional consolidation tests. To evaluate compressibility of RAS and stabilized RAS, one-dimensional compression tests were performed on compacted stabilized RAS with different Class C fly ash content, the stabilized RAS:BA

mixture with 20% Class C fly ash content, and GOS following ASTM D 2435-96. The standard consolidometer ring with 64 mm diameter and 25 mm height was used for the tests. Each specimen was compacted at the w_{opt} and relative compaction level of 95% inside the consolidometer ring in three lifts of equal thickness by a manual hammer. The specimens were then cured for 7 days in 100% humidity room. Pore pressure transducers were connected to the base of the specimens in the consolidometer cells to measure any generated excess pore water pressures (Δu) during consolidation test. Drainage was allowed from the top. The specimens were loaded incrementally from 12.5 kPa with load increment ratio (LIR) of 1.0 and load increment duration (LID) of 24 h until the maximum vertical stress (σ_v') level of 1600 kPa. The specimen deformations were measured by a LVDT placed on the loading plate. The LABVIEW software (National Instruments, Austin, TX) and a data acquisition card (UPC601-U) were used for automated incremental loading and recording of vertical deformation.

Triaxial Strength Tests

Consolidated drained (CD) triaxial compression tests were performed on RAS and stabilized RAS to evaluate shear strength and volumetric behavior. For each mixture three tests were performed under σ_c' of 35 kPa, 70 kPa and 140 kPa. The confining pressures were selected to represent typical effective stresses in highway embankments or retaining wall backfills. Each moistened RAS:FA mixture was compacted in a split mold using a standard Proctor compaction hammer. The split mold had a diameter of 73 mm and a height of 145 mm height. For each mixture the number of tamps per layer was determined by trials to obtain a density corresponding to the compaction level of 95%. After compaction the specimen was carefully removed from the split mold, wrapped using shrink wrap and cured for 7 days in a 100%

humidity room. After curing, each specimen was placed in the triaxial cell chamber and backpressure-saturated according to ASTM D4767 so that a B value greater than 95% was attained. The specimen was subsequently isotropically consolidated under a given σ_c'. The specimen volume change during consolidation phase was monitored in the backpressure burette until no significant change in volume was observed. The shearing of each specimen in CD condition was performed under constant strain rate. The shearing rate of 0.1 mm/min was selected based on the time for primary consolidation and the ultimate strain of the specimen at failure as suggested by Bishop and Henkel (1962). The pore water pressure was monitored during shearing to ensure no Δu is generated. The volume change of each specimen during shearing was recorded from the volume change of water in backpressure burette.

K_o-Consolidation Tests

To evaluate coefficient of lateral earth pressure at rest (K_o) of RAS and stabilized RAS, a specifically developed K_o-Consolidation cell by Edil and Wang (2000) was used. Fig. 3.3 shows the schematic of the apparatus. The cell has the diameter of a conventional consolidation ring (64 mm) and consists of a hollowed chamber with an inner ring thickness of 1 mm instrumented with strain gages. During application of σ_v' to the sample, the air pressure is applied into the lateral chamber around the inner ring to maintain the lateral displacement of the ring to a minimum. K_o is calculated by measuring the lateral air pressure, σ_h', upon application of σ_v' on the sample, $K_o = \sigma_h'/\sigma_v'$. The standard consolidation test procedure with LID of 24 h was followed for the K_o tests. A program was written in LABVIEW to automate the test and acquire the data.

Results and Discussions

Compaction behavior

Fig. 3.4 shows the variation of dry unit weight (γ_d) versus water content (w) for RAS, different RAS:FA mixtures and a mixture of RAS:BA:FA. RAS and RAS:FA mixtures have well-defined compaction curves with γ_{dmax} varying from 11.3 kN/m^3 for RAS to 15.9 kN/m3 for RAS:FA mixture with 50% Class C fly ash content. The γ_{dmax} of different RAS:FA mixtures are lower than γ_{dmax} of typical compacted sandy soils which typically ranges between 17 and 20 kN/m^3 (18.30 kN/m^3 for the Wisconsin GOS sample). The w_{opt} ranges from 8.6% for RAS to 13.2% for the RAS:BA:FA mixture indicating that the materials are not overly sensitive to compaction moisture content, which is an advantage in wet climates. The low γ_{dmax} of stabilized RAS makes it a favorable alternative to compacted sandy soils for construction of highway embankments over weak subgrade.

Hydraulic conductivity

The hydraulic conductivity of RAS and stabilized RAS at different σ_c' is shown in Fig. 3.5. Compared to GOS, RAS and stabilized RAS have lower the hydraulic conductivity. The hydraulic conductivity also reduces with increasing σ_c'. Possible reason is the compressibility of RAS particles which facilitates densification of the specimen at higher σ_c' which consequently results in lower hydraulic conductivity. The hydraulic conductivity of stabilized RAS also decreases with increasing fly ash content. Addition of silt-size fly ash increases the fines content of the sample and consequently reduces the hydraulic conductivity. The hydraulic conductivities of RAS and stabilized RAS generally vary, depending on confining pressure, between 2×10^{-4} cm/s and 9×10^{-6} cm/s which is equivalent to hydraulic conductivity of very fine sand, silty sand,

and silty clay soil (USBR 1987). The drainage capacity of different materials is also classified according to USBR (1987) and accordingly marked on Fig. 3.5. "Good Drainage" represents drainage capacity of clean gravel and sand while "Poor Drainage" represents drainage capacity of very fine sand, silty sand and silty clay soil. Drainage capacity of RAS and RAS:FA straddles good to poor depending on FA content and confining pressure.

Compressibility

Fig. 3.6 shows the compression curves of RAS and stabilized RAS in terms of vertical strain, ε_v, versus logarithm of vertical stress, σ_v'. Compared to outwash sand, pure RAS is highly compressible for structural fill applications. Under a σ_v' of 200 kPa, which is a typical overburden pressure in highway embankments, the ε_v of GOS is only 2.0% whereas RAS exhibits a ε_v of 17.5%. High compressibility of RAS is attributed to three mechanisms: (1) the cellulose felt within RAS particles creates voids in the particles. Under increasing σ'_v, the voids in cellulose felt tend to close rapidly. The voids between the plate-like RAS particles also tend to close due to the flexibility of RAS particles; (2) the sand particles either on RAS particle surface or separated from RAS particles, penetrate into asphalt coating of other RAS particles under increasing σ'_v; and (3) the smaller spherical RAS particles in the matrix [see Fig. 3.1(a)], tends to deform under σ'_v due to viscous asphalt cement. Asphalt cement and cellulose felt components together constitute between 35 to 50% by weight of RAS particles.

The compressibility of the stabilized RAS is systematically reduced with increasing self-cementing fly ash content. For σ'_v up to 200 kPa, compressibilities of GOS and stabilized RAS with 20% Class C fly ash are comparable. At higher σ'_v, the compressibility of the stabilized RAS increases possibly because of the breakage of bonding between RAS particles created by

fly ash cementation. Further increase of the fly ash content to 50%, although considered to be very high, reduces the compressibility of the stabilized RAS to levels comparable to those of the GOS specimen under σ_v' even greater than 200 kPa. The compressibility of stabilized RAS:BA mixture is also shown in Fig. 3.6. The ε_v of RAS:BA mixture stabilized with 20% Class C fly ash content is lower than ε_v of RAS stabilized with 20% fly ash for σ_v' larger than 200 kPa but comparable up to σ_v' = 200 kPa. This is attributed to more competent BA particles replacing some of the compressible RAS particles.

Settlement of a laterally wide earth structure is usually calculated using compressibility parameters obtained from the results of one-dimensional compression tests. The compressibility parameters for granular material obtained from the result of one-dimensional compression test include effective yield stress, σ_y', pre-yield modified compression index, $C_{pry} = \Delta\varepsilon/\Delta \log \sigma_v'$, post-yield modified compression index, $C_{psy} = \Delta\varepsilon/\Delta \log \sigma_v'$, and secondary compression ratio, $C_{\alpha\varepsilon} = \Delta\varepsilon/\Delta \log t$. The σ_y' corresponds to the stress that divides the soil compression curve into a region of small and elastic deformation called pre-yield curve and a region of plastic deformation called post-yield compression curve. The values of σ_y', C_{pry}, and C_{psy} were obtained from the ε_v versus $log\ \sigma_v'$ curves of RAS and stabilized RAS according to the graphical construction of Casagrande (Casagrande 1936b). Fig. 3.7 shows variation of compressibility parameters of stabilized RAS with fly ash content. The increase in fly ash content increases σ_y' while reducing C_{pry} and C_{psy}. The C_{pry} of stabilized RAS with fly ash content more than 20% is reduced to lower than C_{pry} of GOS. Coduto (1999) classified the compressibility of soils based on C_{pry} and C_{psy} as summarized in Table 3.2. Accordingly, the stabilized RAS is classified as *very slightly compressible* to *slightly compressible* when the σ_v' is in the pre-yield range ($\sigma_v' < \sigma_y'$). For σ_v' in

the post-yield range ($\sigma_v' > \sigma_y'$), the material is classified as *moderately compressible* to *highly compressible*.

Fig. 3.8 shows the variation of ε_v with logarithm of time for RAS and stabilized RAS under σ_v' = 100 kPa. The time for complete dissipation of Δu under the applied σ_v' is marked as the end of primary consolidation (t_p) on Fig. 3.8. As indicated, the primary consolidation accounts for a negligible compression of RAS and stabilized RAS; and the majority of settlement is due to secondary compression. The ε_v of RAS nonlinearly increases with logarithm of time after t_p and follows a constant rate after the standard LID of 24 h. Stabilization of RAS using Class C fly ash reduces the $C_{\alpha\varepsilon}$. Fig. 3.9 shows the variation of $C_{\alpha\varepsilon}$ with fly ash content calculated for one log cycle after the standard LID under different σ_v'. The increase in fly ash content to more than 10% reduces the $C_{\alpha\varepsilon}$ significantly. Under σ_v' of 200 kPa, which is a typical stress level for highway embankments, the $C_{\alpha\varepsilon}$ is reduced from 0.041 for unstabilized RAS to 0.005 for stabilized RAS with 20% fly ash content.

Fig. 3.10(a) shows the effect of secondary compression on σ_y' of unstabilized and stabilized RAS, i.e., the effect of aging. The LID under σ_v' of 100 kPa was extended from 24 h to 150 days during one-dimensional consolidation test. After the 150-day loading period, the test continued with standard LID of 24 h. The long-term compression increased the σ_y' of RAS from 65 kPa to 250 kPa and of stabilized RAS with 20% fly ash from 300 kPa to 420 kPa. The effect of secondary compression on σ_y' is more significant on RAS than on stabilized RAS possibly due to greater reduction in void ratio in RAS. The C_{pry} of RAS decreases from 0.07 to 0.03 as a result of this aging effect. The long-term compression under a constant σ_v' i.e., aging also affects the secondary compression rate at subsequent σ_v'. Fig. 3.10(b) shows the variation of ε_v with time under σ_v' of 200 kPa for unstabilized and stabilized RAS before and after aging for 150 days. The

$C_{\alpha\varepsilon}$ of RAS decreased from 0.0249 to 0.0020 and of RAS stabilized with 20% Class C fly ash decreased from 0.0066 to 0.0009 after a 150-day compression period under σ_v' of 100 kPa. The results indicate that, aging not only reduces the secondary compression of both unstabilized and stabilized RAS, also is an effective alternative to stabilization for reducing compressibility of RAS. In this respect, RAS behaves like some clay soils.

Shear strength

The stress-strain and volumetric behavior of unstabilized and stabilized RAS in consolidated drained triaxial compression tests are shown in Fig.11 along with that of GOS for comparison. Unstabilized RAS exhibits a stress-strain and volumetric behavior similar to that of loose sand. There is no peak on stress-strain curve and the volume change is contractive at different σ_c'. RAS has comparable peak shear strength to GOS but unlike GOS, the peak shear strength occurs at larger axial strain. Stabilization of RAS with self-cementing fly ash increases the shear strength and the peak point on the stress-strain curves develops at smaller axial strain resembling the stress-strain behavior of dense sand. The volume change of stabilized RAS tends to be more dilative. Stabilization has more prominent effect on stress-strain and volume change of RAS at smaller σ_c'. At σ_c'=35 kPa, stabilization of RAS with 20% fly ash increased the shear strength from 170 kPa to 420 kPa (reflecting a 150% increase) and changed the volumetric behavior from contractive to dilative whereas at σ_c'=140 kPa with the same fly ash content, the shear strength increased from 440 kPa to 630 kPa (reflecting a 43% increase) and the volume change remained contractive.

The deviator stress at failure was selected as either the peak deviator stress or the deviator stress corresponding to 15% axial strain whichever is reached earlier (ASTM D4767). Fig. 3.12

shows the effective friction angle and cohesion of unstabilized and stabilized RAS. The friction angle of unstabilized RAS is 36^o which is comparable to the friction angle of GOS. Pure RAS also exhibited an apparent cohesion (c') of 20 kPa possibly due to slight binding of RAS particles together during compaction. This apparent cohesion can be neglected for practical purposes. The friction angle decreases and cohesion increases with increasing fly ash content of stabilized RAS indicating diminishing contribution of confining stress to strength development and increasing contribution of cementation.

Coefficient of lateral earth pressure

Fig. 3.13 shows the variation of K_o with σ_v' of unstabilized and stabilized RAS along with GOS for comparison. The K_o of RAS nonlinearly decreases with increasing σ_v' from about 1.0 at σ_v' lower than 100 kPa to 0.36 at σ_v' higher than 500 kPa. On the other hand, stabilization of RAS with 20% Class C fly ash significantly reduces K_o to less than 0.1 under σ_v' smaller than 400 kPa. The stronger interlock and higher friction between particles generally tend to reduce K_o (Jáky 1944; Ladd et al. 1977; Mesri and Hayat, 1993). Under higher σ_v', K_o increases to 0.2 presumably due to breakage of cementation of the bonds between the RAS particles. The K_o of GOS sample nonlinearly decreases from 0.6 under σ_v' of 25 kPa and approaches to 0.4 under σ_v' higher than 400 kPa. The K_o of normally consolidated soils typically ranges from 0.35 to 0.7 (Coduto 1998; Holtz and Kovacs 2004). With γ_{dmax} of 13.8 kN/m^3 and K_o less than 0.1, stabilized RAS exhibits remarkably smaller lateral earth pressure than typical compacted soils, which is highly beneficial behind retaining structures and expected to result in significant reduction in the dimensions of retaining walls.

Practical Implication

The total or differential settlement that can be tolerated by a pavement is rarely specified except in the case of bridge approaches for which the tolerable settlement is commonly specified as 12 mm to 25 mm. For roadway embankments the allowable settlement after paving depends on the length of the fill and rate at which settlement develops. If the variations in settlement are uniformly distributed along the length of the embankment, settlement of 150 mm to 300 mm can be tolerated in long embankments (NCHRP Synthesis of Highway Practice 8). Although the maximum settlement of highway embankments are allowed between 300 mm and 600 mm (NCHRP Synthesis of Highway Practice 29 and Stark et al. (2004), 300 mm is a more widely accepted limit and is adopted here.

To illustrate the performance of embankment fill constructed with stabilized RAS and preloaded RAS, example calculations were made on embankments 12 m wide at the top and 2, 5, 10, and 15 m high constructed on a 10 m thick sand deposit. Since compacted RAS and stabilized RAS have comparable shear strength to typical compacted sand, emphasis was made on evaluation of embankment settlements during the life-time period rather than side slope stability. Settlements were evaluated using the following relationship:

$$s = \sum_{i=1}^{n} s_i = \sum_{i=1}^{n} h_i C_{\alpha\varepsilon,i} log\left(\frac{t}{t_o}\right) \quad (3.1)$$

where s is the embankment settlement, s_i is the settlement of a layer with thickness h_i (h_i was selected 0.5 m in the calculations), n is the number of layers to which the embankment height H was divided ($H=nh_i$), t is time, and t_o is an arbitrary reference time that for the calculations herein was taken 1 d after completion of construction. The material properties for the settlement calculations are summarized in Table 3.3.

Fig. 3.14 shows the variation of settlement of an embankment 10 m high, constructed with RAS, stabilized RAS, preloaded RAS and sand during 40 years after construction. The majority of settlements occur within 1 year after completion of the construction. The total settlement of the embankment constructed with RAS is about 1025 mm, which is far more than the allowable settlement. Aging by preloading of RAS reduces the total settlement to 83 mm which reflects 92% reduction in settlement. Stabilization of RAS with 10% fly ash reduces the total embankment settlement to 300 mm reflecting 70% reduction. Increase of fly ash content to 20% results in negligible total settlement during the 40-year lifetime. The average height of the embankments constructed in the U.S. is 4.5 m (Wright 1996). Having identical subgrade soil conditions, shorter embankments exhibit smaller settlement than those plotted in Fig. 3.14. Fig. 3.15(a) shows the variation of settlement with time and height of the embankments which preloading technique is used to reduce compressibility of RAS. The total settlement of the preloaded RAS fill with 5 m high in average is 30 mm. Fig. 3.15(b) plots the variation of settlement with time of RAS fill stabilized with 10% fly ash. The total settlement of an average fill constructed with the stabilized RAS is 70 mm. Fig. 3.15(c) indicates that total settlement of embankment fills with preloaded RAS or stabilized RAS up to 15 m high during the 40-year lifetime is within the allowable settlement limit. The variation of total settlement with percent fly ash is illustrated in Fig. 3.15(d). Stabilization of RAS with 10% fly ash significantly reduces the total settlement. The settlement reduction is more noticeable in embankments with lower height. Increase of fly ash content to 20% results in negligible total settlement for embankments with different height. The fly ash content between 10 to 15%, which is also the typically used fly ash content with soils and base course materials (ACAA 2003), is recommended to reduce

compressibility of RAS as structural fill to an acceptable limit while maintaining adequate drainage capacity (Fig. 3.5).

Conclusions

In this research the geotechnical properties of recycled asphalt shingles (RAS) stabilized with a self-cementing fly ash were evaluated for potential reuse as structural fill in highway embankments or backfill behind retaining structures. Compaction, hydraulic conductivity, compressibility, shear strength and coefficient of lateral earth pressure at rest characteristics of RAS stabilized with self-cementing fly ash were evaluated in a systematic manner. The following observations are made:

1. The maximum dry unit weight of RAS and stabilized RAS is lower than that of typical compacted soils. The maximum dry unit weight of the stabilized RAS increases with increase in fly ash content. The lower maximum dry unit weight of RAS and stabilized RAS makes them a favorable lightweight fill material over weak soils.
2. The hydraulic conductivity of unstabilized and stabilized RAS is comparable to that of silty sands. The hydraulic conductivity is reduced with increasing confining pressure due to compressibility of RAS particles. The hydraulic conductivity is also reduced with increase in fly ash content. Due to significant reduction in drainage capacity, maximum fly ash content in stabilized RAS is recommended to be limited to 20%.
3. RAS alone is too compressible as a structural fill material. Stabilization of RAS significantly reduces short-term and long-term compressibility of the material. RAS stabilized with 10 to 20% Class C fly ash under low to moderate σ_v' (i.e., 25 to 200 kPa) has the compressibility comparable to that of compacted sandy soil. Stabilization

of RAS mixed with a granular material like bottom ash results even lower compressibility compared to the stabilization of pure RAS. Aging by preloading for a specific time such as 150 days is an alternative method to reduce long-term compressibility of RAS. The effect of preloading on reducing the compressibility is more significant for unstabilized RAS than for stabilized RAS.

4. The stress-strain and volumetric behavior of RAS resemble those of loose sandy soils. RAS alone exhibits sufficient shear strength as a structural fill material. Stabilization of RAS further increases the shear strength and changes the volumetric behavior from compressive to dilative.
5. Stabilization of RAS significantly reduces the K_o of RAS. Lower maximum dry unit weight and K_o of stabilized RAS than those of typical compacted sandy soils make the stabilized RAS a favorable backfill material behind retaining walls with potential to greatly reduce the dimensions of the walls.

Based on the results of this research, stabilized RAS is considered to be a viable material for use as structural fill in highway embankments and backfill behind retaining walls. Structural fill is an alternative application to use in hot mix asphalt, which is likely to allow use of large volume of waste asphalt shingles and help to save landfill space, reduce disposal costs, energy consumption, and green house gas emissions due to mining and production of virgin aggregates. Additionally, stabilized RAS offer certain superior fill material characteristics compared to conventional materials such as light weight and reduced lateral pressures. However, RAS samples obtained from different sources and with different particle sizes may have different mechanical behavior and need to be tested for specific applications. Further studies need to be

made to generalize use of stabilized RAS in structural fills and to evaluate the potential effect of high ground temperatures in certain climatic regions.

Acknowledgement

Support for this study was provided by the Recycled Materials Resource Center, which is supported by the Federal Highway Administration. The opinions, findings, conclusions, or recommendations expressed herein are those of the author(s) and do not necessarily represent the views of the sponsors.

References

American Coal Ash Association (ACAA). (2009). Coal Combustion Product (CCP) Production & Use Survey Results. Aurora, CO. September 15, 2009 [online].

American Coal Ash Association (ACAA). (2003). *Fly Ash Facts for Highway Engineers*. Washington, DC.

American Society for Testing and Materials (ASTM). (1997). "Standard guide for use of coal combustion by-products in structural fills." *Designation E 1861-97*, PA.

American Society for Testing and Materials (ASTM). (1963). "Standard test method for particle-size analysis of soils." *Designation D 422-63*, PA.

American Society for Testing and Materials (ASTM). (2000). "Standard test methods for specific gravity of soil solids by water pycnometer." Designation *D 854-00*, PA.

American Society for Testing and Materials (ASTM). (2000). "Standard test methods for laboratory compaction characteristics of soil using standard effort [[f12,400 ft lbf/ ft^3 (600 kN m/m^3)]." *Designation D 698-00a*, PA.

American Society for Testing and Materials (ASTM). (1995). "Standard test methods for measurement of hydraulic conductivity of saturated porous materials using a flexible wall permeameter." *Designation D 5084-03*, PA.

American Society for Testing and Materials (ASTM). (1996). "Standard test method for one-dimensional consolidation properties of soils." *Designation D 2435-96*, PA.

Bin-Shafique, M. S., Senol, A., Edil, T. B., and Benson, C. H. (2004). "Incorporating Fly Ash Stabilized Subbase into Pavement Design-Case Study." *Geotechnical Engineering*, Institute of Civil Engineers, United Kingdom, 157(GE4), 239-249.

Bishop, A.W. and Henkel, D.J. (1962). *The Measurement of Soil Properties in the Triaxial Test*. 2nd ed., London, Edward Arnold.

Button, J. W., Williams D., and Scherocman, J.A. (1995). "Roofing Shingles and Toner in Asphalt Pavements." Research Report 1344-2F, Texas Transportation Institute, College Station, Texas.

Casagrande, A. (1936a). "The determination of the pre-consolidation load and its practical significance." Discussion D-34, *Proc. Fist Int. Conf. Soil Mech. Found. Engr.*, Cambridge, Vol. 3, 60-64.

Cetin, B., Aydilek, A. H. and Li, L. (2012). "Manganese and chromium leaching from high carbon fly ash stabilized highway base layers." *GeoCongress 2012, Geo Institute, American Society of Civil Engineers*, Oakland, Ca. CD-ROM.

Coduto, D. P. (1999). *Geotechnical Engineering Principles and Practices*. Prentice Hall.

DiGioia, A. M., McLaren, R. J., Burns, D. L., Miller, D. E., (1986). "Fly Ash Design Manual for Road and Site Application." Vol. 1: Dry or Conditioned Placement, Manual Prepared for EPRI, Interim Report, CS-4419, Electric Power Research Institute, Palo Alto, CA.

Edil, T. B. (2006). "Green Highways: Strategy for Recycling Materials for Sustainable Construction Practices." *Proceedings of the Seventh International Congress on Advances in Civil Engineering*, 2006, Yildiz Technical University, Istanbul, Turkey, 91-112**.**

Edil, T. B., and Wang, X. (2000). "Shear strength and K_o of peats and organic soils." *Geotechnics of High Water Content Materials, ASTM Special Technical Publication,* pp. 209-225.

Ferguson, G. (1989). "Use of Coal Ash in Highway Construction: Kansas Demonstration Project." *GS-6460, Research Project 2422-15, Electric Power Research Institute*, Palo Alto, CA.

Ferguson, G., Levorson, S. M. (1999). "Soil and Pavement Base Stabilization with Self-Cementing Coal Fly Ash." American Coal Ash Association, Alexandria, VA.

Grodinsky, C., Plunkett, N., and Surwilo, J. (2002). "Performance of Recycled Asphalt Shingles for Road Applications." *Final Report,* State of Vermont's Agency of Natural Resources.

Hooper, F., and Marr, W. (2004). “Effects of Reclaimed Asphalt Shingles on Engineering Properties of Soils.” *Recycled Materials in Geotechnics, Geotechnical Special Publication,* No. 127, ASCE, 137-149.

Jáky, J. (1948). “Earth pressure in soils.” *Proceedings of the Second International Conference on Soil Mechanics and Foundation Engineering*, Rotterdam, Vol. 1, 103-107.

Kim, B. and Prezzi, M. (2008). “Evaluation of the mechanical properties of class-F fly ash.” *Waste Management*, Vol. 28, 649-659.

Krivit, D. (2007). Recycling of Tear-Off Shingles: Best Practices Guide. Final report prepared for the Construction Materials Recycling Association (CMRA).Klyosov A.A. (2007). *Wood-plastic composites*. John Wiley & Sons, Inc. Hoboken, NJ.Kosson, D. S., van der Sloot, H. A., and Eighmy, T. T. (1996). "An approach for estimation of contaminant release during utilization and disposal of municipal waste combustion residues." *Journal of Hazardous Materials*, 47(1-3), 43-75.

Kosson, D. S., Van Der Sloot, H. A., Sanchez, F., and Garrabrants, A. C. (2002). “An integrated framework for evaluating leaching in waste management and utilization of secondary materials.” *Environmental Engineering Science*, 19(3), 159-204.

Holtz, D. R. and Kovacs, W. D. (2004). *An introduction to geotechnical engineering*. Pearson Education Taiwan Ltd.

Komonweeraket, K. Benson, C.H., Edil, T.B., and Bleam, W.F.(2010). “Leaching Behavior and Mechanisms Controlling the Release of Elements from Soil Stabilized with Fly Ash.” *Geo-Frontiers 20111,* Dallas, TX, CD-ROM.

Ladd, C.C., Foote, R., Ishihara, K., Schlosser, F., and Poulos, H.G. (1977). “Stress-Deformation and Strength Characteristics.” State-of-the-Art Report, *Proceedings of the Ninth International Conference on Soil Mechanics and Foundation Engineering*, Tokyo, Vol. 2, 421-494.

Lee, J. C., Edil, T. B., Tinjum, J. M. and Benson, C. H. (2010). “Quantitative Assessment of Environmental and Economic Benefits of Using Recycled Construction Materials in Highway Construction.” *Journal of the Transportation Research Board,* No. 2158 Paper 10-2505, National Research Council, Washington D. C., 2010, 138-142.

Li, L., Benson, C. H., Edil, T. B. and Hatipoglu, B. (2006). “WiscLEACH: A Model for Predicting Ground Water Impacts from Fly-Ash Stabilized Layers in Roadways.” *GeoCongress 2006,* Atlanta, GE, ASCE, CD-ROM.

Li, L., Benson, C. H., Edil, T. B. and Hatipoglu, B. (2008). "Sustainable Construction Case History: Fly Ash Stabilization of Recycled Asphalt Pavement Material." *Geotechnical and Geological Engineering,* 26(2), 177-188.

Li, L., Edil, T. B., and Benson, C. H. (2009). "Mechanical Performance of Pavement Geomaterials Stabilized with Fly Ash in Field Applications." *Coal Combustion and Gasification Products* 1, pp. 43-49, doi: 10.4177/CCGP-D-09-00018.1

Marks, V. J., and Petermeier, G. (1997). "Let Me Shingle Your Roadway." *Research Project HR-2079, Iowa Department of Transportation,* Ames, Iowa

Mesri, G., and Hayat, T. M. (1993). "The coefficient of earth pressure at rest." *Canadian Geotechnical Journal*, 30(4), 647–666.

McLaren, R.J., DiGioia, A.M. (1987). "The Typical Engineering Properties of Fly Ash." *Geotechnical Practice for Waste Disposal '87, Geotechnical Special Publication*, No. 13, 683–697.

Misra, A. (2000). "Utilization of western coal fly ash in construction of highways in the Midwest." Mid-America Transportation Center, MATC project No. MATC UMC 96-2, Lincoln, NE.

Patelunas, G. M. (1986). "High Volume Fly Ash Utilization Projects in the United States and Canada." *Electric Power Research Institute*, Report No. CS-4446, Palo Alto, CA.

Srivastava, L. and Collins, R. J. (1989). "Ash Utilization in Highways: Delaware Demonstration Project." Interim Report, GS-6481, Research Project 2422-3, Electric Power Research Institute, Palo Alto, CA.

Soleimanbeigi, A., Edil, T., and Benson, C. (2012). "Recycled asphalt shingles mixed with granular byproducts as structural fill." *Journal of ASTM International*, 9(1), 1-19.

Townsend, T., Powell, J., and Xu, C. (2007). "Environmental issues associated with asphalt shingle recycling." *Construction Materials Recycling Association, US EPA Innovations Workgroup*.

Turley, W. (2010). Personal Communication. *Construction Materials Recycling Association*, Eola, IL.

U.S. Bureau of Reclamation (USBR). (1987). *Design of small dams*. Denver, CO.

Warner, J. D. (2007). "The beneficial reuse of asphalt shingles in roadway construction." *MSc thesis, Department of Civil and Environmental Engineering, University of Wisconsin-Madison*.

Wen, H. and Edil, T. B. (2009). "Sustainable Reconstruction of Highways with In-Situ Reclamation of Materials Stabilized for Heavier Loads." *BCR2A Conference, Proc.* 2nd Int. Conf. on Bearing Capacity of Roads, Railways and Airfields 2009, Champaign, IL, CD-ROM, 1011-1017.

Wen, H., Warner, J. D., Edil, T. B. and Wang, G. (2010). "Laboratory Comparison of Crushed Aggregate and Recycled Pavement Material With and Without High Carbon Fly Ash" *Geotechnical and Geological Engineering*, 28(4), 405-411.

Wright, P. H. (1996). *Highway Engineering*. John Wiley & Sons, Inc.

Zickell, A. J. (2003). "Asbestos Analysis of Post Consumer Asphalt Shingles." *Technical Report #41. Chelsea Center for Recycling and Economic Development, Technical Research Program.*

Table 3.1. Grain size indices and USCS classifications RAS, bottom ash and outwash sand

Material	d_{10} (mm)	d_{50} (mm)	C_u	C_c	% fines	USCS symbol	USCS name
RAS	0.17	1.1	7.6	1.6	3.8	SW	Well graded sand
Bottom ash	0.19	0.9	6.3	0.8	1.9	SP	Poorly graded sand
Glacial outwash sand	0.21	0.5	3.1	0.8	0.0	SP	Poorly graded sand

d_{10}: effective particle size (particle size for which 10% of the sample is finer than d_{10}); d_{50}: average particle size (particle size for which 10% of the sample is finer than d_{50}); C_u: coefficient of uniformity (d_{60}/d_{10}); C_c: coefficient of curvature ($C_{30}^2/(C_{10} \times C_{60})$); G_s: specific gravity; USCS: Unified Soil Classification System

Table 3.2. Classification for material compressibility (after Coduto 1998)

Modified Compression Index	Compressibility Classification
0-0.05	Very Slightly compressible
0.05-0.10	Slightly compressible
0.10-0.20	Moderately compressible
0.20-0.35	Highly compressible
> 0.35	Very Highly compressible

Table 3.3. Material properties for settlement evaluation

Properties		Sand	RAS	Preloaded RAS*	RAS:FA (90:10)	RAS:FA (80:20)
γ_d (kN/m^3)		18.3	11.3	11.8	12.5	13.8
σ'_y (kPa)		340	65	250	190	310
$C_{\alpha\varepsilon}$	0-5 m	0.0002	0.0117	0.0020	0.0045	0.0012
	5-10 m	0.0005	0.0157	0.0020	0.0061	0.0022
	10-15 m	0.0007	0.0195	0.0020	0.0095	0.0044

* After aging with a preload surcharge

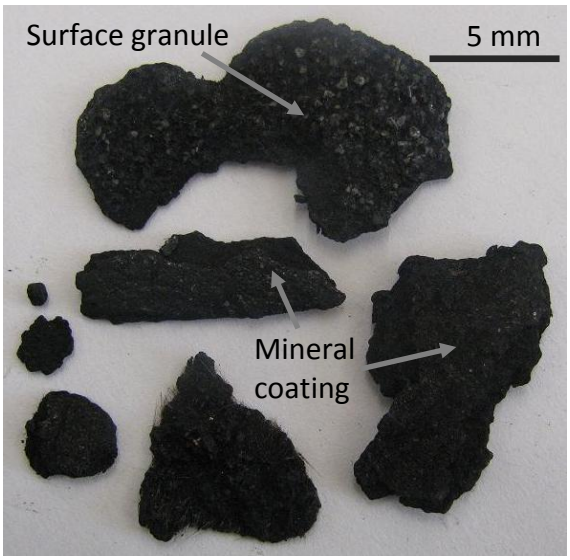

(a)

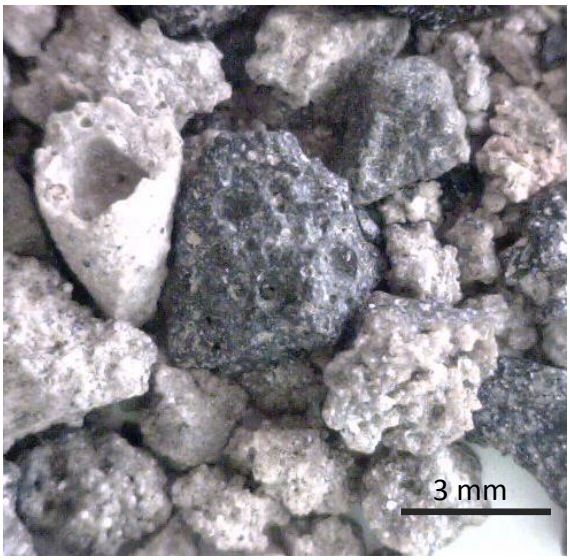

(b)

(c)

Fig. 3.1. Photograph of RAS (a), light microscope photomicrographs of bottom ash (b), and Wisconsin glacial outwash sand (c)

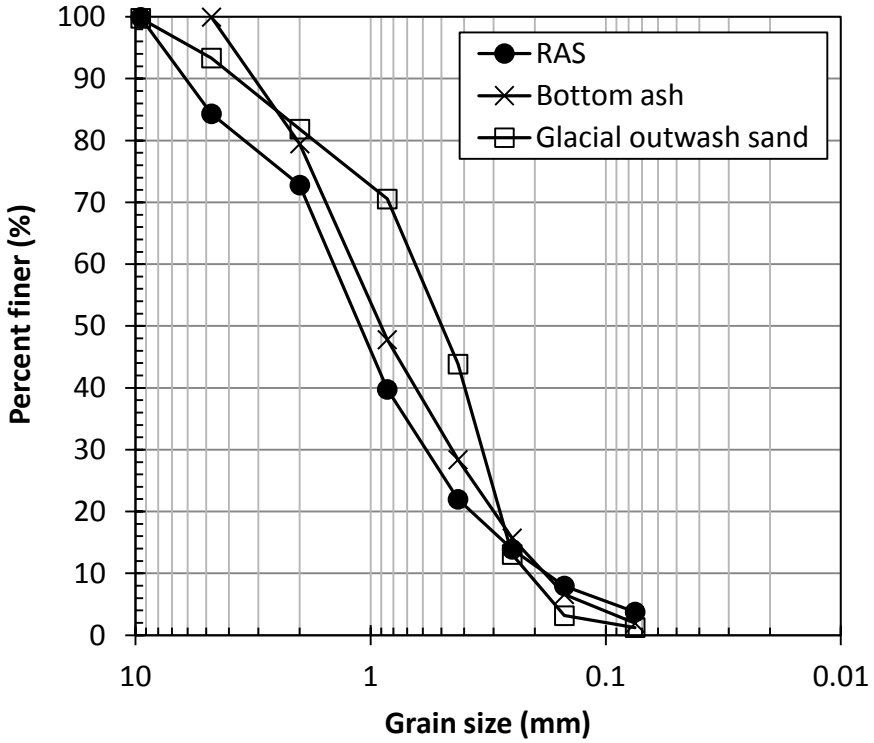

Fig. 3.2. Grain size distribution of RAS, bottom ash, and Wisconsin glacial outwash sand

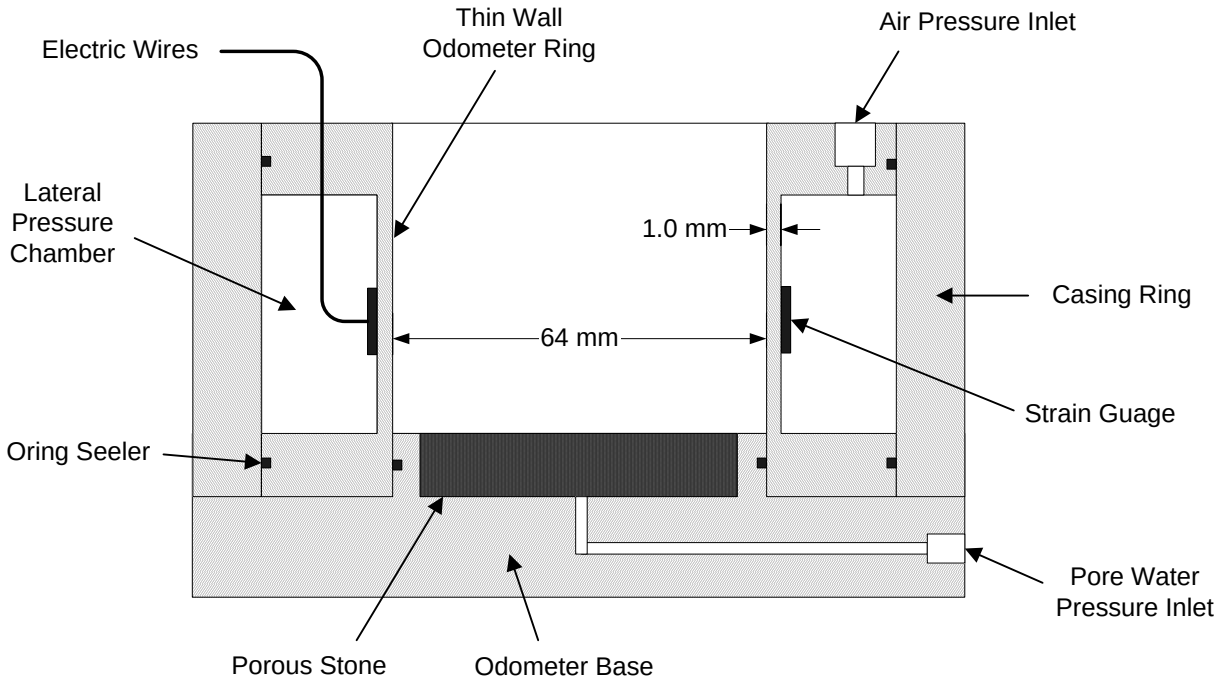

Fig. 3.3. K_o-Consolidation cell (after Edil and Wang 2000)

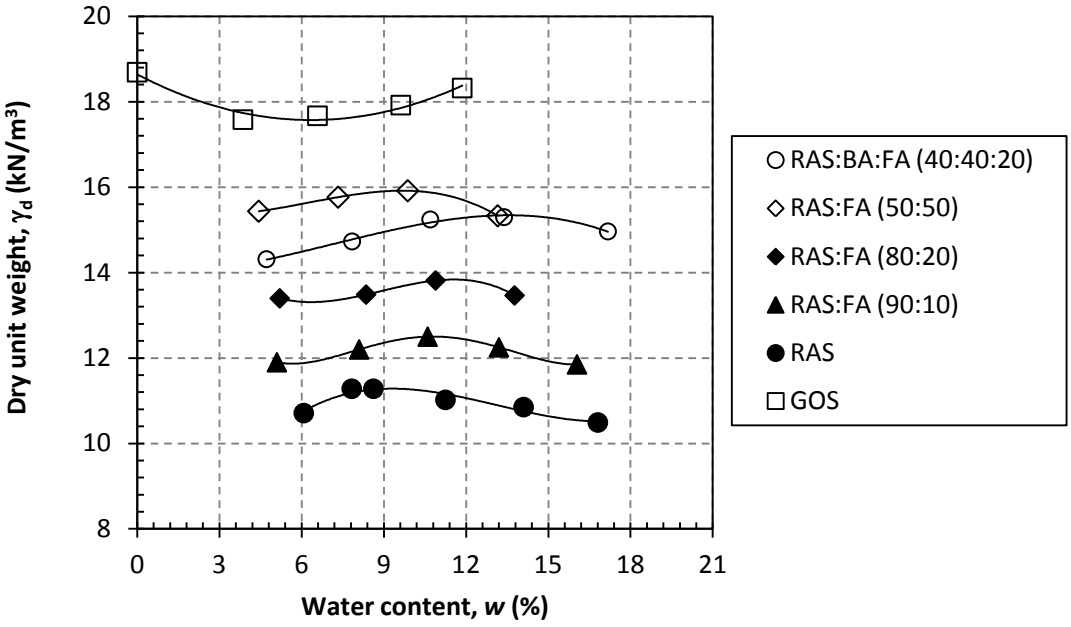

Fig. 3.4. Dry unit weight versus water content of RAS (:BA):FA mixtures

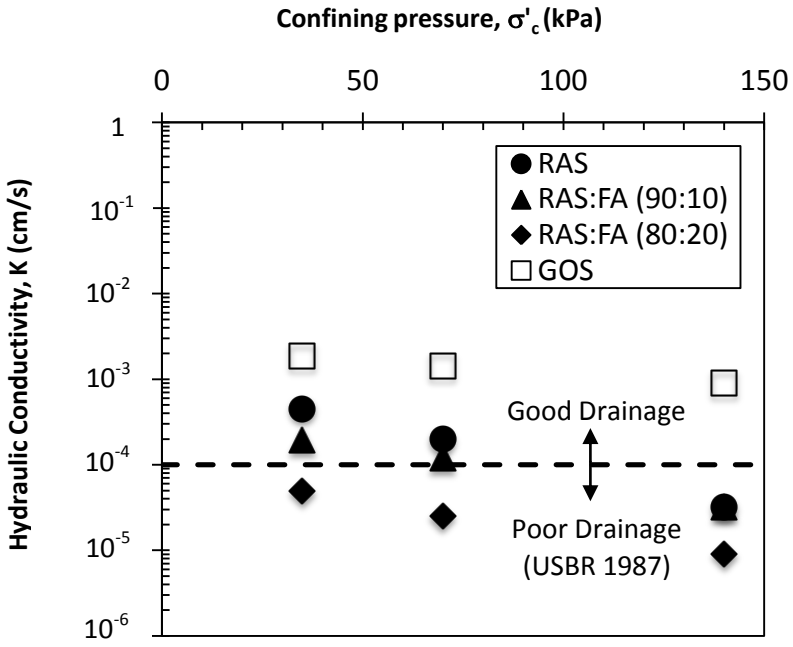

Fig. 3.5. Hydraulic conductivity of pure and stabilized RAS versus effective confining pressure

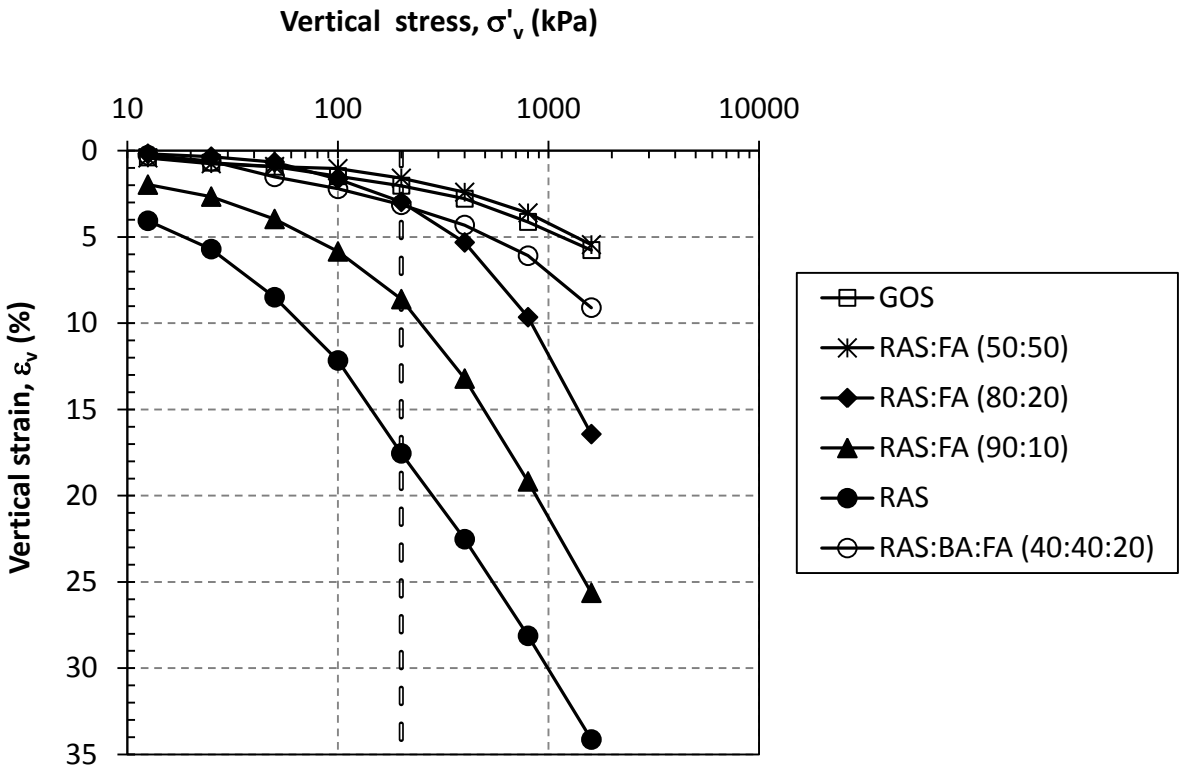

Fig. 3.6. One-dimensional compression curves

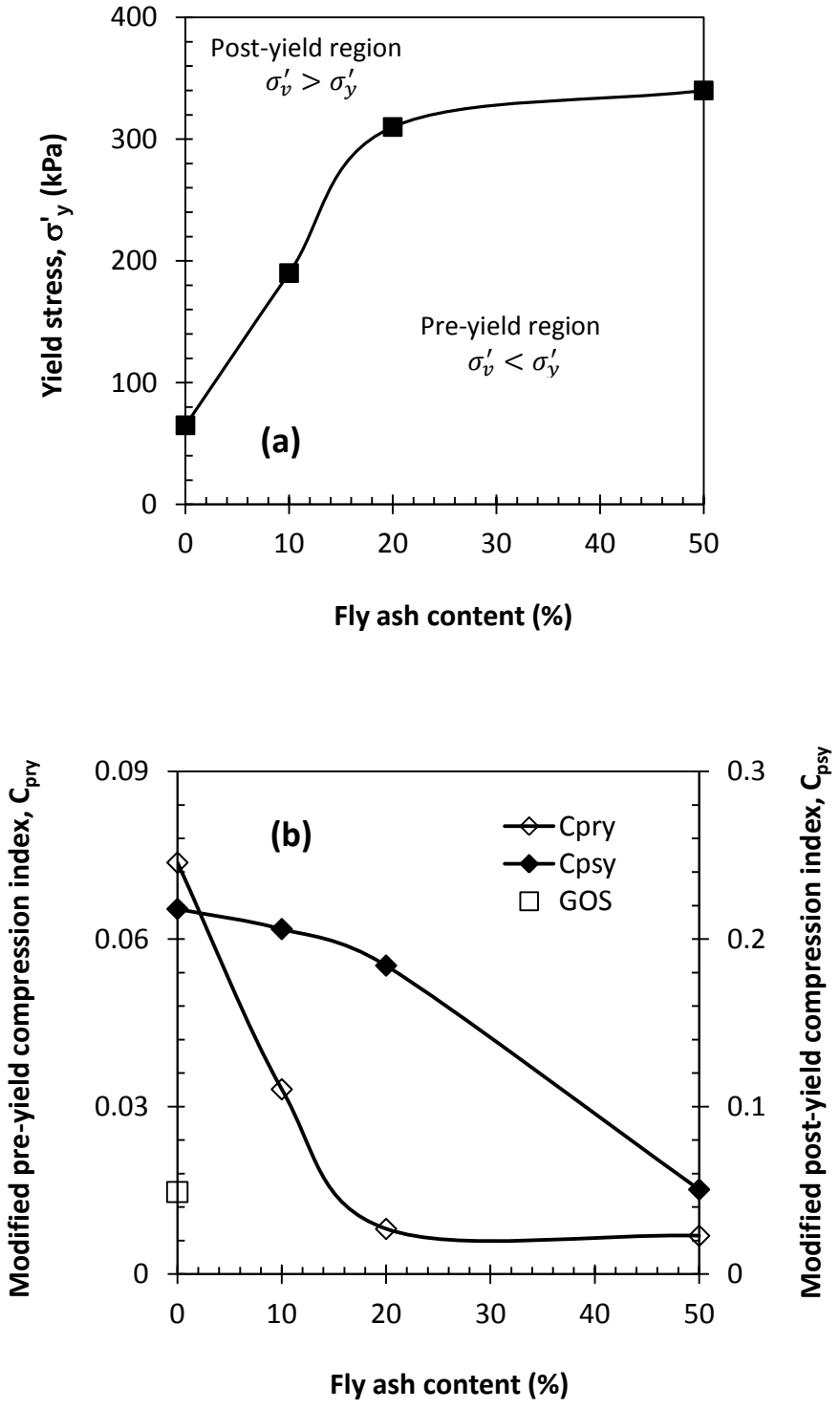

Fig. 3.7. Compressibility parameters: (a) variation of $\boldsymbol{\sigma_y'}$, and (b) $\boldsymbol{C_{pry}}$ and $\boldsymbol{C_{psy}}$ of stabilized RAS with Class C fly ash content

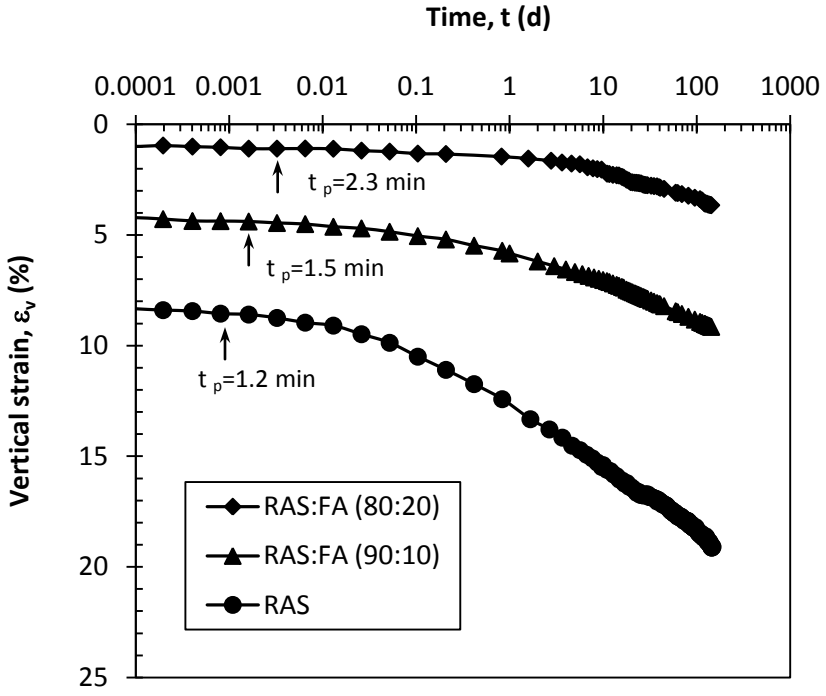

Fig. 3.8. Variation of ε_v with time for RAS and stabilized RAS for $\boldsymbol{\sigma'_v}$=100 kPa

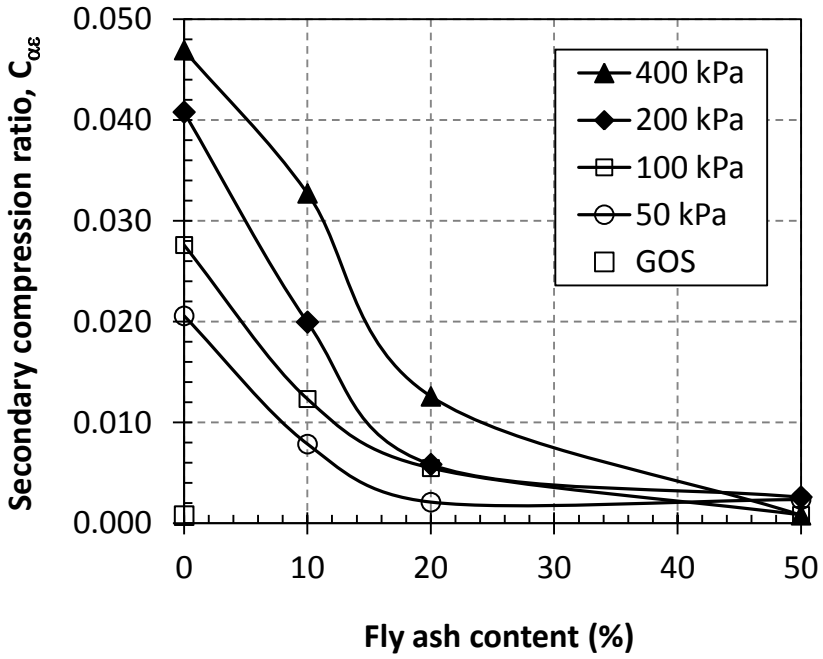

Fig. 3.9. Variation of long term compression of stabilized RAS with fly ash content

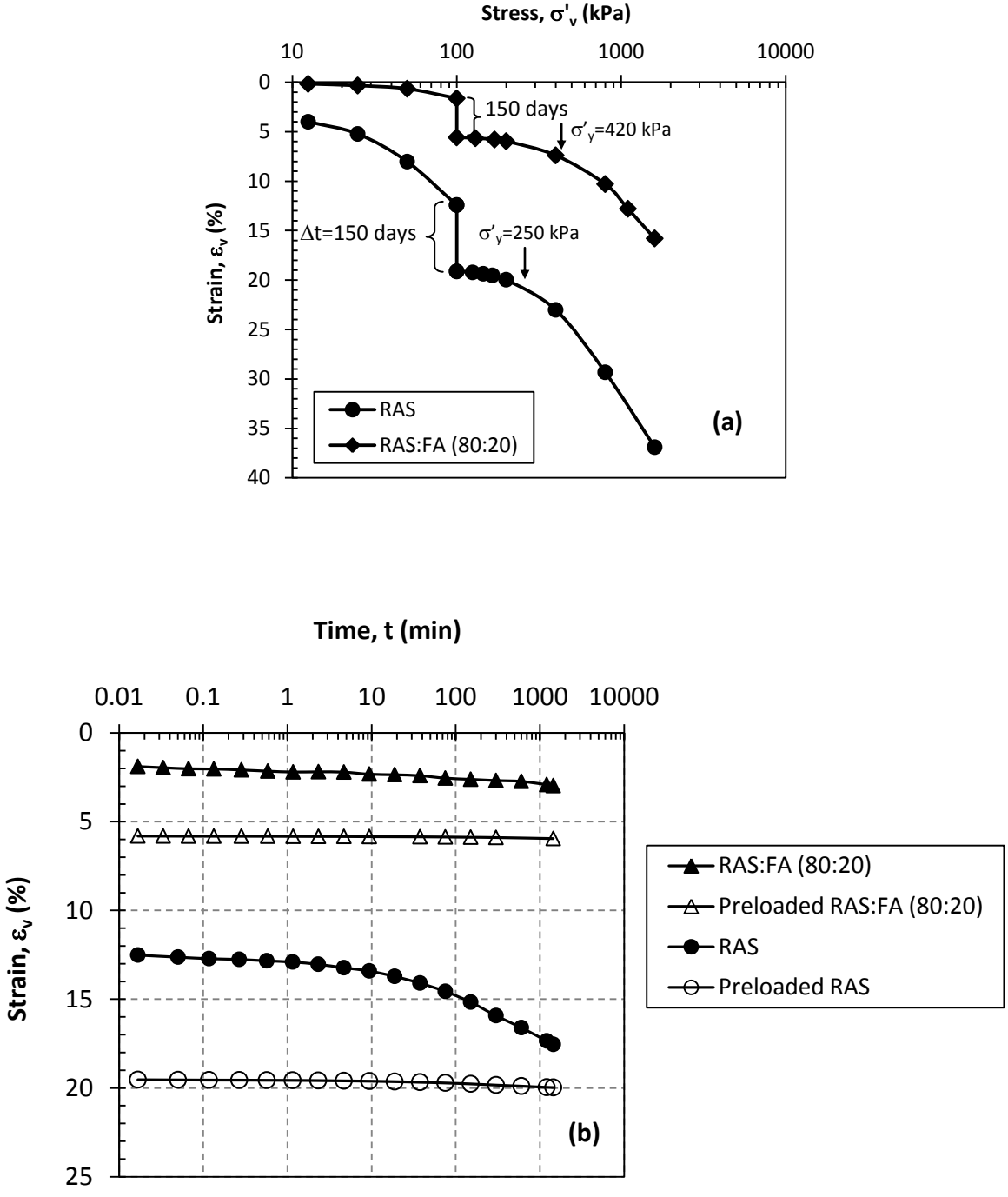

Fig. 3.10. Yield pressure of pure and stabilized RAS resulting from secondary compression (a), and effect of secondary compression on compression rate (b)

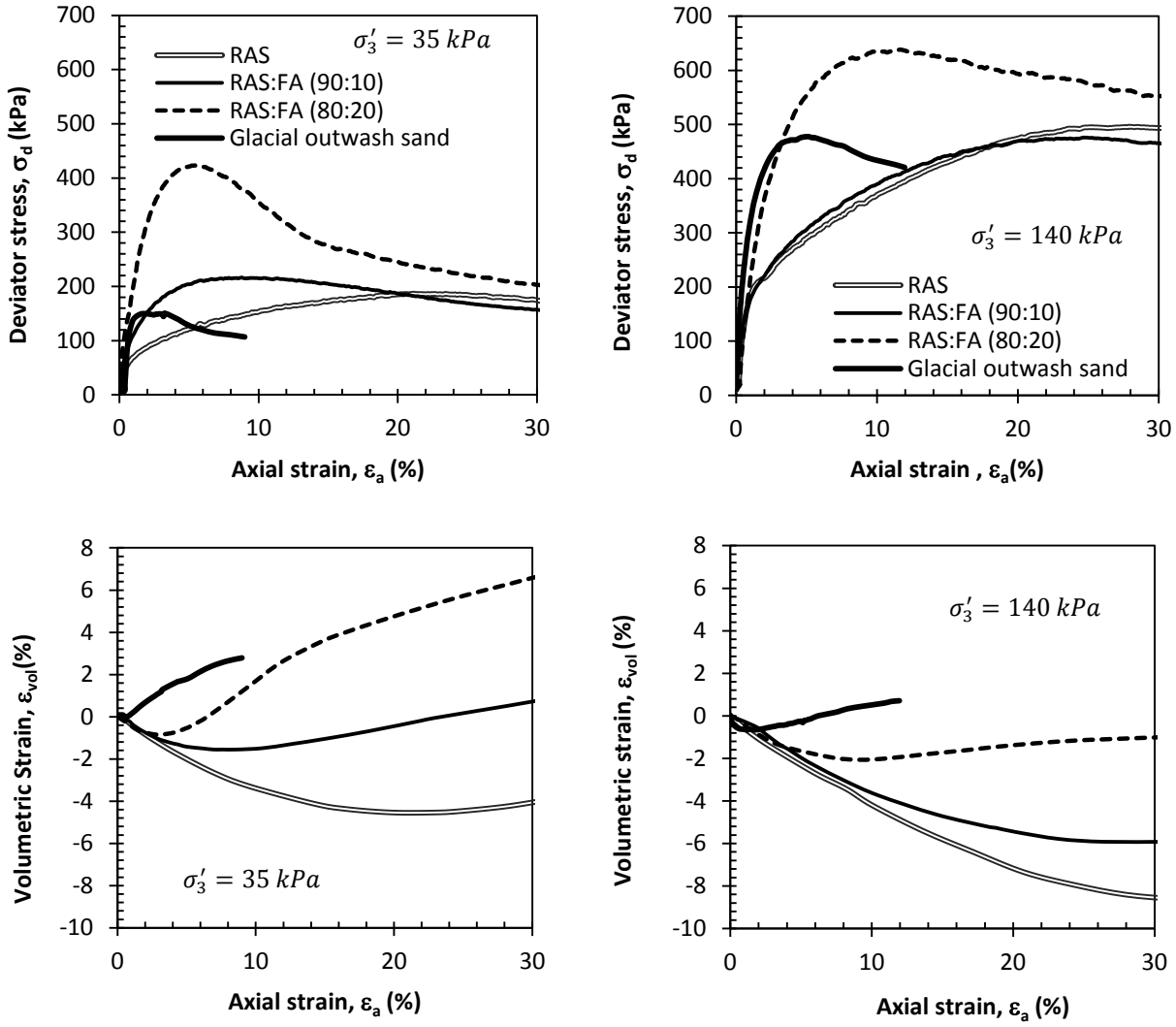

Fig. 3.11. Stress-strain and volumetric behavior of pure and stabilized RAS

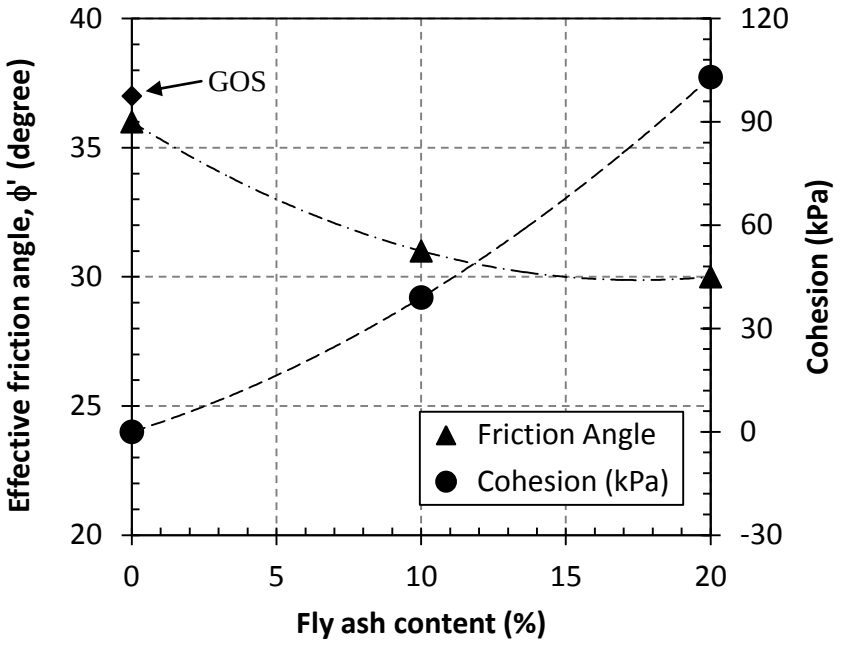

Fig. 3.12. Effective friction angle and cohesion of pure and stabilized RAS

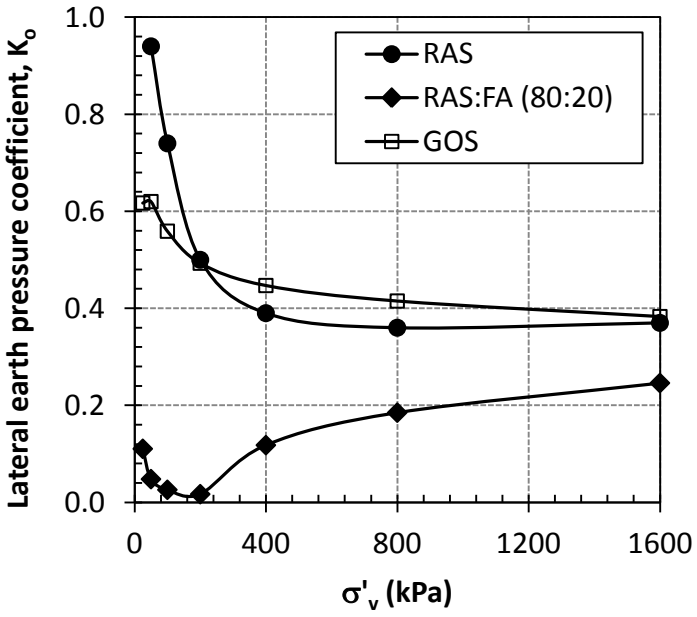

Fig. 3.13. Variation of K_o of pure and stabilized RAS with $\boldsymbol{\sigma'_v}$

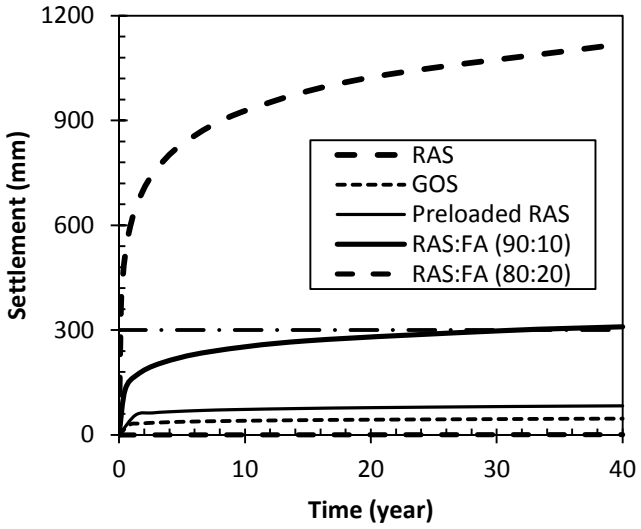

Fig. 3.14. Variation of embankment settlement with time

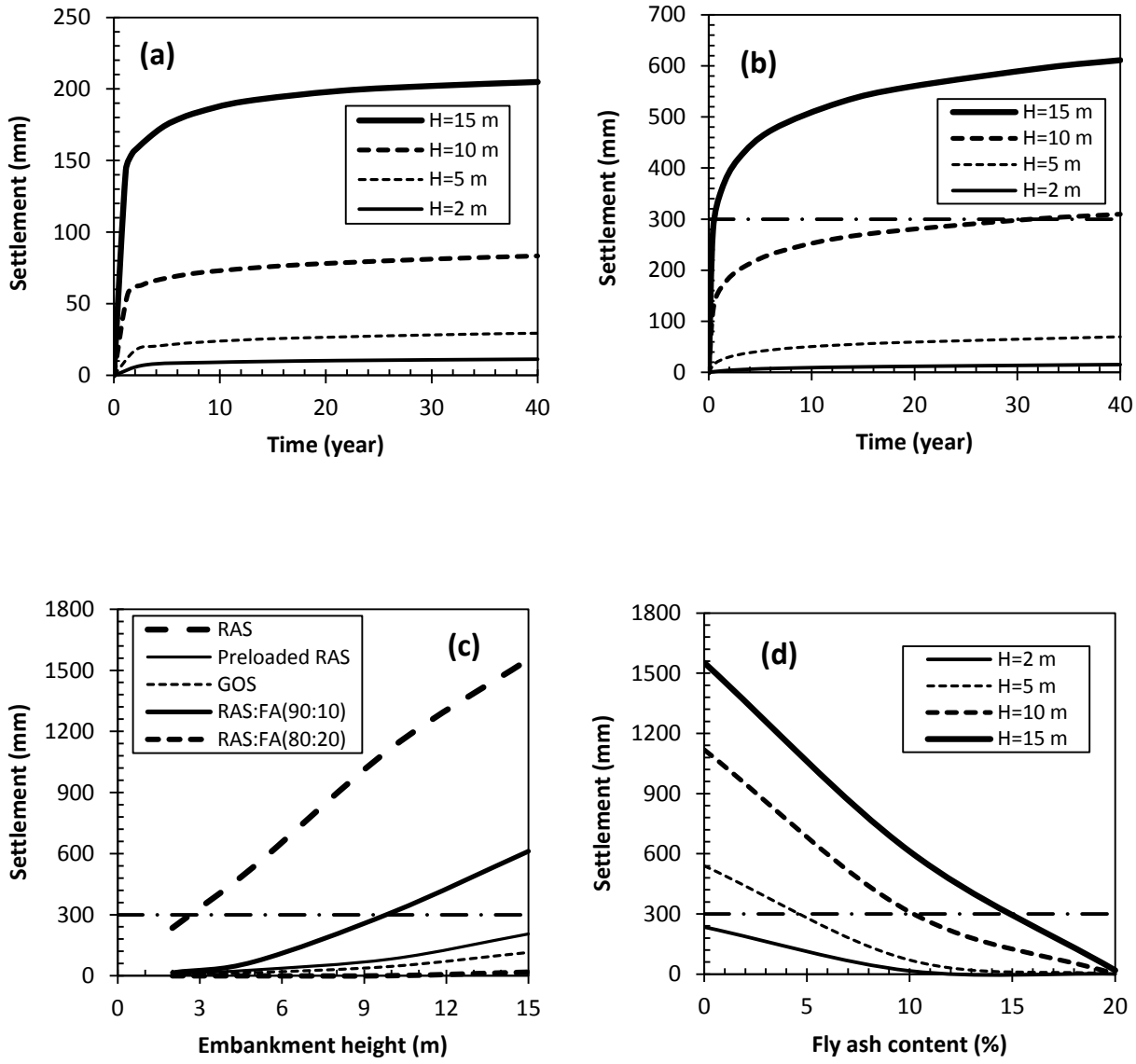

Fig. 3.15. Variation of settlement of preloaded RAS (a) and RAS stabilized with 10% fly ash (b) with time and embankment height; variation of settlement with embankment height (c) and fly ash content in RAS (d)

Chapter 4 Effect of Temperature on Geotechnical Properties of Recycled Asphalt Shingle Mixtures

Abstract: Shear strength, compressibility, and hydraulic conductivity of recycled asphalt shingles (RAS) mixed with bottom ash (BA) or with self-cementing fly ash (FA) were evaluated in a systematic manner at temperatures ranging from 5 ^{o}C to 35 ^{o}C, representing seasonal field temperature variation. Increasing temperature reduced the shear strength and increased the compressibility and hydraulic conductivity of compacted RAS-BA mixture and FA stabilized RAS. When the temperature increased from 5 ^{o}C to 35 ^{o}C, the effective friction angle (ϕ') of compacted RAS-BA mixture containing 25% RAS decreased from 41^{o} to 35^{o}, and of the mixture containing 50% RAS decreased from 41^{o} to 29^{o}. The ϕ' of RAS stabilized with 20% FA decreased from 46^{o} to 26^{o} however the effective cohesion (c´) increased from 45 kPa to 70 kPa and the compressive strength remained higher than that of compacted sand. In contrast, secondary compression ratio ($C_{\alpha\varepsilon}$) exponentially increased with temperature. Thermal cycling induced thermal preloading to RAS-BA and RAS-FA mixtures and significantly reduced the compressibility. Thermal preloading reduced $C_{\alpha\varepsilon}$ of RAS-BA mixture from 0.0078 to 0.0004 and that of RAS-FA mixture from 0.0016 to 0.0002 which is comparable to $C_{\alpha\varepsilon}$ for compacted sand (0.0003). To reduce long-term settlement of an embankment made with materials containing RAS, construction is recommended during warm seasons. In this way, the majority of settlement occurs during construction and settlement during service time of the embankment will be negligible. The hydraulic conductivity of both RAS-BA and RAS-FA mixtures increased with increasing temperature which is beneficial to drainage capacity of structural fill containing RAS.

Keywords: Recycled asphalt shingle, bottom ash, fly ash, temperature, structural fill, geotechnical properties.

Introduction

About 80% of homes in the U.S. are roofed by asphalt shingles. Asphalt shingle waste is produced from tear-off roofing shingles after demolition or renovation of houses or scraps from shingle manufacturers. Approximately 11 million Mg of waste asphalt roofing shingles are generated per year in the U.S. of which 10 million Mg are tear-off roofing shingles and 1 million Mg is factory scraps (Sengoz and Topal 2004; VANR 1999; Zickell 2003 and Townsend et al. 2007). Typical asphalt shingles are comprised of 16-35% asphalt binder, 2-15% cellulose felt, 20-38% mineral granule/aggregates, and 8-40% mineral filler/stabilizer (Krivit, 2007; Townsend et al. 2007). Asphalt shingle waste is recycled and ground to produce recycled asphalt shingles (RAS). Currently, RAS is used in hot mix asphalt (HMA) to benefit from oil and sand content in RAS, as cold patch to repair surface pavement, as supplemental fuel in cement kiln dust industry, and as temporary paving in rural roads and trails. However, all of these applications only reuse between 10 and 20% of asphalt shingle waste and the remaining is landfilled (Turley, 2011). Identifying other potential uses for RAS is one means to increase the fraction of reclaimed shingles that are reused.

Structural fill, including highway embankment fills or backfill behind retaining walls, is an application that could use large volumes of reclaimed asphalt shingles. Such use will contribute to a more sustainable roadway infrastructure by reducing energy and natural resources consumption as well as greenhouse gas (GHG) emissions associated with mining and production of conventional structural fill (Kilbert 2002; Gambatese and Rajendran 2005; Carpenter et al. 2007; US EPA 2009). Soleimanbeigi (2012) and Soleimanbeigi et al. (2012) evaluated engineering properties of RAS, RAS mixed with bottom ash (BA), and RAS stabilized with self-cementing fly ash (FA) at room temperature and found that the compacted RAS, although

possesses favorable shear strength for fill applications, exhibits excessive compressibility whereas RAS:BA mixtures and RAS stabilized with self-cementing fly ash are lightweight materials with compressibility that is acceptable for structural fill applications such as highway embankments and backfill behind retaining structures. The suitability of RAS for inclusion in structural fill was verified at room temperature. However, RAS particles contain viscous asphalt binder and viscosity of asphalt binder is sensitive to temperature (Roberts et al. 1996; West et al. 2010, Lee et al 2011; ASTM D 2493). Therefore, temperature change may affect engineering properties of the compacted RAS:BA mixtures or stabilized RAS.

Although RAS mixtures proved to provide suitable engineering properties as structural fill at constant laboratory temperature, understanding the effect of seasonal field temperature on engineering properties of the compacted RAS:BA mixtures or fly ash-stabilized RAS is imperative to ensure stability, acceptable settlement and drainage capacity of highway embankments at different seasons.

The effect of temperature on engineering properties of the compacted RAS:BA mixtures and RAS stabilized with self-cementing fly ash are presented along with design and construction guidelines for optimum performance of structural fills containing RAS. For this purpose, a thermo-mechanical system including temperature-controlled triaxial cell, consolidometer and permeameter was developed to investigate the effect of temperature change on shear strength, compressibility and hydraulic conductivity of the compacted RAS:BA mixtures and fly ash-stabilized RAS.

Temperature Variation in Structural Fills

The type of application determines the temperature range for which the mechanical properties of the geo-materials are investigated. For accurate characterization of mechanical properties of the

compacted RAS:BA mixtures or stabilized RAS, the laboratory mechanical property tests were conducted at temperatures close to those expected in the field. The temperature range for thermo-mechanical behavior of structural fills depends on the mean annual earth temperature and the seasonal ground temperature of the locality. The earth temperature is relatively constant at depths greater than 9 m below the ground surface, and corresponds roughly to the water temperature measured in groundwater wells 9 m to 15 m deep (Hillel 1982; Marshal and Holmes 1988; Geo4Va 2012). This temperature is referred to as mean earth temperature; T_m. Fig. 4.1 shows the T_m contours across the United States. The T_m varies between 3 ^oC in north of Minnesota to 25 ^oC in south of Florida. In Wisconsin where this study is conducted, the T_m varies from about 4.5 ^oC in Superior (north) to 10 ^oC in Beloit (south). The seasonal soil temperature change on either side of T_m depends on the type of soil and depth below the ground surface. Deeper soil experiences less seasonal variation in temperature than the soil in shallower depths and lags behind the seasonal changes in overlaying air temperature. At a particular location, the seasonal soil temperature change adds from -10 to +10 ^oC to the range of T_m as shown in Fig. 4.2 (Marshal and Holmes 1988; Hu and Feng 2003; ASHRAE 2007). The temperature to which the compacted RAS:BA mixtures and stabilized RAS in embankment fills in the U.S. could be subjected ranges from -5 ^oC to 35 ^oC. In this study, however, the practical lowest test temperature is set conservatively at 5 ^oC.

Materials

RAS samples were obtained from B.R. Amons & Sons Company in Elkhorn, Wisconsin. Visual inspection indicated that RAS samples were free of impurities such as wood chips, plastics, and nails. Warner (2007) concluded that RAS particles with maximum size (d_{max}) of 10 mm, result in higher dry unit weight and higher stiffness and strength. Therefore, in this study, the RAS supply

was screened to limit the d_{max} to 10 mm. Bottom ash and self-cementing (Class C) fly ash samples were obtained from Columbia Power Station in Wisconsin. Fig. 4.3 shows the particle size distribution curves of RAS, BA and GOS samples tested according to ASTM D 422. The majority of particles in each sample are sand size (between 0.075 mm and 4.75 mm) according to the Unified Soil Classification System (USCS). Table 4.1 summarizes the grain size indices and material classification according to the USCS. RAS and BA particles have almost similar grain size distributions; therefore, grain size distribution of different RAS:BA mixtures will fall within a narrow range. The specific gravity (G_s) of RAS measured in accordance with ASTM D854 (method B) is 1.74, which is a positive attribute as a light-weight fill material. The low G_s of RAS is attributed to asphalt cement content and cellulose fiber content, which together comprise from 18 to 50% of RAS. The typical G_s of asphalt cement is between 1.02 and 1.05 (Roberts et al. 1996) and that of cellulose fiber is between 1.3 and 1.5 (Klyosov 2007). Bottom ash has the G_s of 2.67, which is comparable to G_s of outwash sand sample (2.71).

RAS particles are plate-like, irregular in shape, highly angular and have rough surface texture. The angularity of RAS particles reduces to semi-round to round as the particle size decreases. BA particles are angular to highly angular, internally porous and have rough surface texture. Some pores of the particles are filled with dust. On the other hand, particles of outwash sand are solid, semi-round to round and have smooth surface texture. Particle surfaces are clean, shinny and free of dust (Soleimanbeigi et al. 2012). Pure RAS has a well-defined compaction curve with the maximum dry unit weight (γ_{dmax}) of 11.3 kN/m^3 and optimum water content (w_{opt}) of 8% (Fig. 4.4). The γ_d of the compacted RAS:BA mixture increases with increasing BA content. Although BA and outwash sand have comparable specific gravities, the high porosity of

BA particles reduces the γ_{dmax} to 15 kN/m^3 which is lower than γ_{dmax} of typical compacted sand. As the BA content increases the γ_d of the mixture becomes less susceptible to water content.

Methods

Thermo-Mechanical Testing System

Temperature-controlled triaxial compression, one-dimensional (1D) compression, and flexiable-wall hydraulic conductivity tests were conducted. The test cells consisted of conventional cells equipped with a heating and cooling system. To uniformly change the temperature of the specimen in the triaxial compression and the flexible-wall hydraulic conductivity tests, a copper coil tubing (with 6 mm outside diameter) was spiraled around the specimen to circulate heated or cooled water. There is a 3.0 cm distance between the copper coil and the specimen to avoid contact during shearing in the triaxial compression tests whereas the coil was spiraled with 1.0 cm distance outside the consolidometer ring in the 1D compression tests. The heating and cooling system was designed to induce the temperature range of 5 ^{o}C to 35 ^{o}C on the specimens. The 1D compression cell consists of a 8-mm thick stainless steel consolidometer ring placed inside a polyvinyl chloride (PVC) cylinder. The consolidometer ring is 102 mm in diameter and 47 mm in height. The PVC cylinder helps minimize heat transfer from or into the specimen.

Heating System

The water is heated inside a heating bath using a 250 W heater. A 12 V compact mini circulating pump, which is placed outside of the heating bath, circulates the warm water from the heating bath into the spiraled copper coil inside the test cells. Tygon plastic tubes were used to minimize temperature loss during water circulation. Temperatures in the heating bath (T_b), in the cell

chamber (T_c), and inside the specimen (T_s) were measured using three K-type thermocouples. To control and maintain the target temperature of the specimen, a LabView program was written to regulate the electrical power to the heater by means of a relay installed in the electrical circuit. A temperature tolerance of ±0.5 ^{o}C was allowed. Fig. 4.5 illustrates the schematic of the heating system. To avoid disturbance of the specimens due to insertion of thermocouples inside them, a correlation between the temperature inside the specimen and inside the cell chamber was obtained. The required time to bring the specimen temperarure, T_s, to the target temperature (i.e. 35 ^{o}C) is approximately 100 min in the triaxial and one-dimensional compression tests and 240-min in the hydraulic conductivity tests due to larger diameter specimens. The target temperature of the specimen for the subsequent tests is controlled by the temperature inside the cell (see Appendix A, Fig. 4.A.1 for the variation of T_b, T_c, and T_s).

Cooling System

The minimum temperature considered in this study is 5 ^{o}C. The cooling bath is a PVC box filled with ice in equilibrium with water shown in Fig. 4.5. The target temperature of the specimen for temperatures cooler than the room temperature (i.e., 4 to 20 ^{o}C) is controlled by regulating the power supply to the circulating pump using a program written in LabView. The circulating pump is switched off if T_c is below the target temperature. A tolerance of ±0.5 ^{o}C was allowed for T_c to reduce the number of turn-on/off of the pump. Fig. 4.A.1 in Appendix A illustrates that the approximate time required to bring the specimen temperature down to 5 ^{o}C is 100 min in the triaxial and one-dimensional compression cells and 300 min in the permeameter due to larger diameter specimens.

Specimen Preparation

The specimens prepared for thermo-mechanical tests include RAS:BA mixtures and stabilized RAS with self-cementing fly ash. Table 4.1 summarized the testing program for all of the tests. For triaxial compression tests, each specimen was compacted in five layers in a split mold with 74 mm diameter and 148 mm height at w_{opt} and 95% of standard Proctor maximum dry unit weight (γ_{dmax}). The number of tamps per layer using a standard Proctor hammer was determined such that the same compaction energy as in the standard compaction effort (592 kN.m/m^3) is applied to each specimen. Hydraulic conductivity specimens were compacted in a split mold with 150 mm diameter and 116 mm height following the ASTM D 5084. For consolidation tests, each specimen was compacted in three layers in the consolidometer ring at w_{opt} and 95% of γ_{dmax} obtained from standard Proctor compaction test. Similarly, the number of tamps per layer using a standard Proctor hammer was determined such that the same compaction energy as in the standard compaction effort is applied to each specimen.

The compacted RAS:FA mixture specimens were carefully removed from their molds, wrapped using shrink wrap to keep the water content constant according to ASTM C 593 and cured in a 100% humidity room. Since the hydration rate of fly ash is temperature dependent a 28-d curing period was considered to achieve the majority of hydration of the stabilized RAS specimen tests.

Test Procedure

Triaxial Compression

After assembling the temperature controlled triaxial system, each specimen was backpressure-saturated according to ASTM D4767 so that a B-value greater than 95% was attained. Following the saturation, each specimen was consolidated for 24 h under the chosen

effective confining pressure (i.e., σ'_3=35 kPa, 70 kPa and 140 kPa) at room temperature. Due to relatively high hydraulic conductivity of both RAS:BA and stabilized RAS specimens, pore water pressure quickly dissipated when σ'_3 was applied. The specimen volume change during consolidation phase was monitored in the backpressure burette until no significant volume change was observed. After 24-h consolidation period, the temperature of the specimen was brought to the target temperature (i.e., 5 ^{o}C or 35 ^{o}C) over 100 min. Axial loading was then carried out at an axial strain rate of 3.0%/h, which is considered to provide drained condition during loading based on comparison with similar soils as well as computations made using the pore water expulsion rate during the consolidation stage. The volume change of each specimen during shearing was recorded from the water elevation in the graduated backpressure burette.

To evaluate the effect of temperature change history on the stress-strain behavior, thermal cycle was also applied to each specimen. For thermal cycling tests, after consolidation for 24 h at room temperature, the temperature of each specimen was increased to 35 ^{o}C, kept constant for 48 h and then decreased to room temperature for another 24 h before shearing. The volume change of each specimen during consolidation, temperature change and shearing was also recorded.

One-Dimensional Compression

The compacted RAS:BA mixtures or stabilized RAS were tested under three σ'_v (50 kPa, 100 kPa and 200 kPa) which represent the typical road embankment overburden pressures. The compressibility of each specimen under a given σ'_v was evaluated at three different temperatures, i.e. 5 ^{o}C, 20 ^{o}C and 35 ^{o}C. The loading of each specimen started from 12.5 kPa and increased at room temperature with the load increment ratio (LIR) of 1 up to the target σ'_v after which the

temperature changed to target temperature and σ'_v was maintained constant for at least 10 d. The effect of thermal cycling on compressibility of the compacted RAS:BA mixtures or stabilized RAS was also evaluated. After compression at 35 ^oC for 10 d, the test continued for one month at room temperature and the compressibility was evaluated. To evaluate the effect of compaction and construction at warm seasons, a RAS:BA mixture was compacted at 35 ^oC inside the consolidometer ring and incrementally loaded (LID=1, LIR=1) from σ'_v =12.5 kPa to 200 kPa at 35 ^oC. The specimen temperature was then reduced to room temperature and the compression test was continued for six weeks.

Hydraulic Conductivity

The specimens for hydrauliuc conductivity tests were consolidated at three levels of confining pressure (i.e., σ'_3=35, 70, and 140 kPa). The specimens were backpressure-saturated using the B-test procedure according to ASTM 5084-03. To saturate the specimen, the cell pressure and backpressure were increased incrementally until the B-value over 95% was attained. Each specimen was consolidated for 24 h at room temperature after saturation. The excess pore water pressure in the compacted RAS:BA mixtures or stabilized RAS dissipates shortly after the confining pressure is applied. The volume change of each specimen was obtained by measurement of water elevation in the backpressure burette. The hydraulic gradients of 0.5 and 2.0 were respectively applied to the compacted RAS:BA mixture and stabilized RAS specimens following the recommendations per ASTM 5084-03.

Results and Discussion

Shear Strength

RAS Mixed with Bottom Ash

Temperature change has negligible effect on the stress-strain and volumetric change behavior of the compacted BA. However, when the RAS content increases to 25%, the stress-strain and volumetric change behavior of the compacted RAS:BA mixture becomes sensitive to temperature change. As the specimen temperature increases from room temperature to 35 ^{o}C, the peak deviator stress, σ'_{dmax}, reduces and the volumetric behavior becomes more compressive. The stress-strain and volumetric change behavior of the specimen sheared at 35 ^{o}C resemble those of sandy soil in loose state. The axial strain corresponding to σ'_{dmax} increases at increased temperature. There is no clear failure plane and the specimen bulges during shearing. On the other hand, the σ'_{dmax} increases and the volumetric behavior changes to dilative when the specimen temperature reduces to 5 ^{o}C. The stress-strain and volumetric change behavior resemble those of compacted sand in dense state. The shearing of the specimen occurs along a clear failure plane. The details can be viewed in Appendix A Fig. 4.A.2 to Fig. 4.A.4.

To evaluate sensitivity of compressive strength (σ'_{df}) of the compacted RAS:BA mixture with respect to temperature change, σ'_{df} measured at different temperatures was divided by σ'_{df} at room temperature to obtain normalized compressive strength denoted as S_n. Fig. 4.6 shows the variation of S_n with temperature. The sensitivity of S_n to temperature change increases with increasing RAS content in the mixture as expected. As the temperature increases, S_n becomes less susceptible to temperature change. As temperature rises from 20 ^{o}C to 35 ^{o}C, the S_n is reduced, on average, by 10% for the RAS:BA mixture containing 25% RAS, and by 20% for

RAS:BA mixture containing 50% RAS. The S_n–T curves do not appear to follow a clear trend with confining pressure.

The effective friction angle (ϕ') of the RAS:BA mixtures at different temperatures were obtained from the Mohr-Coulomb failure envelope and presented in Fig. 4.7(a) along with the friction angle of BA not mixed with RAS. These mixtures did not have a cohesion intercept. The ϕ' of the compacted RAS:BA mixtures decreases with increasing temperature. While the $\phi'$of bottom ash is nearly insensitive to temperature change, the ϕ' of the mixture containing 25% RAS is reduced from 41^o to 36^o and of the mixture containing 50% RAS is reduced from 41^o to 29^o when the temperature rises from 5 ^{o}C to 35 ^{o}C. To obtain a design graph for practical use, the ϕ' at different temperatures were interpolated from Fig. 4.7(a) and presented in Fig. 4.7(b). The increase of RAS content makes the ϕ' of the mixture more sensitive to temperature change. As the temperature increases, the variation of ϕ' with RAS content becomes more pronounced. At T=35 ^{o}C, when the RAS content increases from 0 to 50%, the ϕ' of the RAS:BA mixture reduces from 44^o to 29^o reflecting 27% reduction while at T=5 ^{o}C the ϕ' of the mixture reduces from 44^o to 41^o which reflects only 7% reduction. In general, reduction in ϕ' of compacted RAS:BA mixtures due to seasonal temperature change in the U.S. does not appear to endanger stability of typical highway embankments containing RAS.

Change in stress-strain, volumetric, and strength behavior of RAS:BA mixture at different temperatures is attributed to change of viscosity of asphalt binder in RAS particles. The viscosity of asphalt binder in RAS is reduced with increasing temperature (Frigio et al. 2011; ASTM D2493). Consequently, the deformability of the asphalt binder on the contact surfaces between individual RAS particles and also between RAS and BA particles increases resulting in higher shearing at the contact surface under a given deviatoric stress increment. Reduction of

viscosity of asphalt binder also increases compressibility of individual RAS particles. Increased deformability of the particles and larger shear strain at the contact surface between RAS and BA particles reduces tendency of the particles to roll over each other during shearing and therefore the volumetric change tends to exhibit contractive behavior. On the other hand, the viscosity of asphalt binder in RAS particles increases when the temperature is reduced. Consequently, the deformability of RAS particles as well as the shear strain along the contact surface between RAS and BA particles decreases when the specimen undergoes shear stress. With increased stiffness of the RAS particles at reduced temperature, the particles tend to roll over each other during shearing, exhibiting a dilative behavior.

RAS Stabilized with Fly Ash

The engineering properties of stabilized RAS at room temperature are appropriate for use as structural fill (Soleimanbeigi et al. 2012). The effect of temperature change on ϕ' and cohesion intercept (c') of stabilized RAS with 20% self-cementing fly ash is illustrated in Fig. 4.8(a). The ϕ' noticeably reduces from 46^{o} to 26^{o} (43%) when the temperature increases from 5 ^{o}C to 35 ^{o}C, however, the c' increases from 44 kPa to 71 kPa. The reduction in ϕ' is attributed to reduction in σ'_{df} due to increased deformability of RAS component in the stabilized RAS specimen at increased temperature as illustrated in Appendix A Fig. 4.A.5. The increase of c' is possibly due to accelerated hydration of self-cementing fly in the compacted RAS:FA mixture which creates stronger bond between the RAS particles at higher temperature. Effect of temperature on acceleration of hydration of fly ash has been investigated elsewhere (Rao and Shivananda 2005; Veisi et al. 2010).

During drained shear failure of each compacted RAS:BA or stabilized RAS specimen in triaxial cell, no pore water pressure was developed and the σ'_3 is constant . Therefore, the compressive strength of the compacted RAS:BA mixtures or stabilized RAS may be obtained from the Mohr-Coulomb failure criterion as:

$$\sigma'_{df} = \frac{2c' \cos\phi' + 2\sigma'_3 \sin\phi'}{1 - \sin\phi'} \quad (4.1)$$

In which ϕ' for the compacted RAS:BA mixtures is obtained from Fig. 4.7(b) and c' and ϕ' for the stabilized RAS is obtained from Fig. 4.8(a). Fig. 4.8(a) also compares the compressive strength (σ'_{df}) of stabilized RAS with that of a natural granular material (in this study glacial outwash sand) at different temperatures at σ'_3=70 kPa. Although the σ'_{df} of the stabilized RAS exhibits 40% reduction from 580 kPa to 340 kPa due to increasing temperature from 5 ^{o}C to 35 ^{o}C, the σ'_{df} remains consistently higher than that of the sand. The variation of σ'_{df} with temperature of glacial sand is almost negligible. The reduction in ϕ' due to temperature rise, reduces σ'_{df} more noticeably at higher stress level (σ'_3=140 kPa) than lower stress level (σ'_3=35 kPa) as shown on Fig. 4.8(b) as the variation of S_n (σ'_{df} of stabilized RAS normalized by σ'_{df} of outwash sand) with temperature. The S_n linearly decreases with increasing temperature at the same rate under different stress levels. The shear strength of stabilized RAS is therefore sufficient for application in typical structural fill at different climates in North America.

Effect of Thermal Cycle on the Stress-Strain Behavior

The reduction of viscosity of asphalt binder in RAS particles was considered the main contributing factor to increased deformation of compacted RAS:BA mixture when the temperature increased. As shown in Appendix A Fig. 4.A.2, the volumetric change behavior of compacted RAS:BA mixture at increased temperature is compressive. Therefore, the compacted RAS:BA material experiencing an increase in temperature should have lower void ratio under applied compressive stresses resulting in higher shear strength and stiffness when the temperature is reduced to room temperature compared to a specimen compressed in isothermal condition. Fig. 4.9(a) shows the permanent volume reduction of a specimen isotropically compressed at 35 ^{o}C for 48 hours. The reduction in void ratio resulted in an increased stiffness and strength (σ'_{df}) of the specimen compared to those of the specimen compressed at constant room temperature [Fig. 4.9(b)]. The practical implication of this behavior is that the RAS:BA embankment fill compacted and came to equilibrium with the operating stresses at warm temperatures will exhibit higher shear strength and stiffness later during mild and cold seasons. In this respect, construction of embankments containing RAS during cold seasons of the year is not recommended because it will lead to greater changes in stiffness and strength as the temperature rises.

Modeling of Stress-Strain Behavior

The nonlinear stress-strain curves of both clay and sand have been successfully approximated with a high degree of accuracy by a simplified and practical hyperbolic model (Kondner and Zelasko 1963; Duncan and Chang 1970). The hyperbolic relationship between the deviatoric stress and axial strain is represented by:

$$\frac{\varepsilon_a}{\sigma_d^{'}} = \frac{1}{E_i} + \frac{\varepsilon_a}{\sigma_{d,ult}^{'}} \tag{4.2}$$

where $\sigma_{d,ult}^{'}$ is the asymptotic value of $\sigma_d^{'}$ which is related to $\sigma_{df}^{'}$ by means of a factor defined R_f as:

$$R_f = \sigma_{df}^{'} / \sigma_{d,ult}^{'} \tag{4.3}$$

and E_i is the initial stress dependent tangent modulus of soil expressed as:

$$E_i = \kappa p_a \left(\frac{\sigma_3}{p_a}\right)^{\eta} \tag{4.4}$$

where κ is the modulus number, η is the modulus exponent and p_a is the atmospheric pressure. To characterize Eq. 4.4, $\varepsilon_a / \sigma_d^{'}$ is plotted versus ε_a. The E_i and $\sigma'_{d,ult}$ are obtained from the intercept and slope of the best fitted line to the data points. Parameters κ and η are readily obtained by plotting the values of E_i against σ'_c on log-log scale and fitting a straight line to the data. The hyperbolic model parameters of the compacted RAS:BA mixtures are given in Appendix A Table 4.A.1. The hyperbolic model allows the prediction of expected systematic change in E_i and σ'_{df} with temperature change and can be used in numerical analyses of embankments constructed of RAS containing materials. Fig. 4.10(a) shows the linear variation of E_i obtained from hyperbolic model with σ'_3 in a log-log scale. The slope of the line (η) increases and the intercept of the line with σ'_3 of unity (κ) decreases with increasing RAS content indicating that E_i decreases and becomes more sensitive to σ'_3 when RAS content increases. Fig. 4.10(b) shows the variation of κ and η with temperature. Similarly, η increases and κ decreases with increasing temperature indicating that E_i of the mixture reduces and becomes more sensitive to σ'_3 with increasing temperature. The hyperbolic model parameters were used to predict the experimental stress-strain data [Fig. 4.10(c) and Fig. 4.A.5]. The hyperbolic model represents

the stress-strain data of the compacted RAS:BA mixtures and stabilized RAS reasonably well up to the σ'_{df}. To predict the compressive strength using the hyperbolic model, the axial strain at failure, ε_f, for each specimen compressed at a given σ'_3 and sheared at different temperatures were measured and presented in Fig. 4.A.6. As illustrated, the ε_f increases with increasing RAS content, σ'_3 and temperature. Having ε_f, the compressive strength (i.e. σ'_{df}) of compacted RAS:BA mixture is obtained from Eq. 4.2 and the effective friction angle is obtained from Eq. 4.1. This approach allows prediction of friction angle for a RAS:BA mixture of a given RAS content at a given confining pressure and temperature.

One-Dimensional Compression

RAS Mixed with Bottom Ash

Fig. 4.11 presents the variation of vertical strain (ε_v) with time of the compacted RAS:BA mixtures compressed under σ'_v =200 kPa at different temperatures. After 24 h compression at room temperature, the specimen heated to 35 ^oC, exhibits higher vertical strain and strain rate than the replicate specimen compressed at room temperature (22 ^oC). The increase of ε_v with time significantly slows down when the temperature of the specimen is reduced 5 ^oC. As mentioned in the triaxial compression test section, change of viscosity of asphalt binder in RAS particles with temperature is considered to be the major controlling factor in deformational behavior of RAS:BA mixtures at elevated temperatures.

Fig. 4.12 shows that logarithm of vertical strain rate ($\dot{\varepsilon_v}$) linearly varies with temperature for the compacted RAS:BA specimens. The slope of the lines is independent of stress level and elapsed time after temperature change as illustrated in Figs. 4.12(a) and (b). This slope is defined as thermal coefficient of compression and denoted as $C_{T\varepsilon}$. The unit of $C_{T\varepsilon}$ is per min-degree

Celsius [1/ ^{o}C]. Since $C_{T\varepsilon}$ is independent of time and stress level, it may be regarded as an inherent property of the material. Fig. 4.12(c) shows that $C_{T\varepsilon}$ increases with increasing RAS content in the mixture. The equation of the fitting line is therefore given by:

$$\frac{d\varepsilon}{dt} = \dot{\varepsilon} = Ae^{C_{T\varepsilon}T} \tag{4.5}$$

$$\text{or} \qquad \frac{dln\dot{\varepsilon}}{dT} = C_{T\varepsilon} \tag{4.6}$$

The secondary compression ratio is most commonly defined as (Ladd et al. 1977):

$$C_{\alpha\varepsilon} = \frac{d\varepsilon}{dlogt} \tag{4.7}$$

where *t* is the elapsed time. From Eq. 4.7, the strain rate is obtained as:

$$\dot{\varepsilon} = \frac{C_{\alpha\varepsilon}ln10}{t} \tag{4.8}$$

By substitution of Eq. (4.8) into Eq. (4.6):

$$\frac{\Delta ln\frac{C_{\alpha\varepsilon}ln10}{t}}{\Delta T} = C_{T\varepsilon} \quad \rightarrow \; ln\frac{C_{\alpha\varepsilon}ln10}{t}\Big|_{\mathrm{T}} - ln\frac{C_{\alpha\varepsilon}ln10}{t}\Big|_{\mathrm{T_o}} = C_{T\varepsilon}\,\Delta\mathrm{T} \rightarrow \; ln\left(\frac{C_{\alpha\varepsilon,T}}{C_{\alpha\varepsilon,T_o}}\right) = C_{T\varepsilon}\,\Delta\mathrm{T}$$

Therefore:

$$C_{\alpha\varepsilon,T} = C_{\alpha\varepsilon,T_o}e^{C_{T\varepsilon}\,\Delta T} \tag{4.9}$$

Eq. 4.9 indicates that secondary compression ratio ($C_{\alpha\varepsilon}$) of the compacted RAS:BA mixture is an exponential function of temperature change. Fig. 4.13 shows the variation of $C_{T\varepsilon}$ with RAS content.

The $C_{\alpha\varepsilon}$ for the compacted RAS:BA mixtures compressed at elevated temperatures were determined for over 1000 min after the temperature change following the initial 24 h compression period under a given σ'_v. The data points in Figs. 4.14(a) and (b) illustrate the variation of $C_{\alpha\varepsilon}$ with temperature at different σ'_v. The response is consistent with the exponential function of temperature given in Eq. 4.9. At a given temperature, the $C_{\alpha\varepsilon}$ also

increases with increasing σ'_v. It appears that increasing σ'_v increases the micro shear stresses along the contact surface between RAS and BA particles, which in turn accelerates the shear strain along the surface, resulting in increasing $C_{\alpha\varepsilon}$. Soleimanbeigi et al. (2012) showed that secondary compression ratio of RAS mixed with foundry slag or stabilized RAS is a power function of the applied stress level. It is expected that the compacted RAS:BA mixtures follow the same behavior.

From the ε_v-log t curves at a given σ'_v, the strain rates ($\dot{\varepsilon}$) at different times were determined. The variations of $\dot{\varepsilon}$ with σ'_v for a mixture containing 75% of BA at T=22 ^oC and T=35 ^oC are plotted in Fig. 4.15. In a log-log plot, strain rate linearly increases with stress level and the slopes of the lines are almost the same at different elapsed times after loading. At a given temperature and time, the equation of the best fitting line over the data points is therefore given by:

$$\frac{d\varepsilon}{dt} = \dot{\varepsilon} = A{\sigma'_v}^m \tag{4.10}$$

$$\text{or} \quad \frac{dln\dot{\varepsilon}}{dln\sigma'_v} = m \tag{4.11}$$

where m is the slope of the $\dot{\varepsilon} - log\sigma'_v$ curves in log scale and A is the strain rate corresponding to the unit of σ'_v. By substitution of Eq. 4.8 into Eq. 4.11 we obtain:

$$\frac{\Delta ln\frac{C_{\alpha\varepsilon}ln10}{t}}{\Delta ln\sigma'_v} = m \rightarrow \frac{ln\frac{C_{\alpha\varepsilon}ln10}{t}\Big|_{\sigma'_v} - ln\frac{C_{\alpha\varepsilon}ln10}{t}\Big|_{\sigma'_{vo}}}{ln\sigma'_v - ln\sigma'_{vo}} = m \rightarrow \frac{C_{\alpha\varepsilon}}{C_{\alpha\varepsilon o}} = \left(\frac{\sigma'_v}{\sigma'_{vo}}\right)^m$$

or:

$$C_{\alpha\varepsilon} = C_{\alpha\varepsilon o}\left(\frac{\sigma'_v}{\sigma'_{vo}}\right)^m \tag{4.12}$$

Eq. 4.12 indicates that secondary compression ratio of the compacted RAS:BA mixture is a power function of the stress level. The value of the exponent *m* varies from about 1.0 to 0.75 with increasing RAS content as shown in Fig. 4.13. Similar results were obtained by Soleimanbeigi et al. (2012) for the compacted RAS:FS mixtures or stabilized RAS. Fig. 4.16(a) shows a comparison between the measured and predicted $C_{\alpha\varepsilon}$ using Eq. 4.12 for different RAS containing mixtures compressed at various stress levels. The coefficient of correlation, r, is 0.98 which validates Eq. 4.12 as significant representation of the experimental data.

Combining Eq. 4.9 and Eq. 4.12, the following relationship is obtained:

$$C_{\alpha\varepsilon} = C_{\alpha\varepsilon o} e^{C_{T\varepsilon}(T-T_0)} \left(\frac{\sigma'_v}{\sigma'_{vo}}\right)^m \tag{4.13}$$

Eq. 4.13 provides an estimate of $C_{\alpha\varepsilon}$ of the compacted RAS:BA mixture at temperature T and stress level σ'_v from the measured $C_{\alpha\varepsilon o}$ at temperature T_o and stress level σ'_{vo}. To assess how well Eq. 4.13 captures the experimental data, the predicted $C_{\alpha\varepsilon}$ from Eq. 4.13 are plotted in Fig. 4.14 and compared with the measured $C_{\alpha\varepsilon}$ for the compacted RAS:BA mixtures compressed at elevated stress levels and temperatures. Using Eq. 4.13, the three curves in Fig. 4.14(a) were generated from a single point of $C_{\alpha\varepsilon}$=0.00286 at T=22 ^oC and σ'_v=100 kPa for the mixture containing 25% RAS and the three curves in Fig. 4.14(b) were generated from a single point of $C_{\alpha\varepsilon}$=0.00728 at T=22 ^oC and σ'_v=100 kPa for the mixture containing 50% RAS. The calculated values of $C_{\alpha\varepsilon}$ in Figs. 4.14(a) and (b) show that Eq. 4.13 captures experimental $C_{\alpha\varepsilon}$ measured at different temperatures and stress levels. Fig. 4.16(b) compares the predicted and measured $C_{\alpha\varepsilon}$. Since the $C_{\alpha\varepsilon}$ exponentially varies with temperature, the scale of the plot was changed to logarithmic to properly show different values of $C_{\alpha\varepsilon}$. The coefficient of correlation, r, is 0.99

which indicates good agreement between the measured and calculated $C_{\alpha\varepsilon}$ and validates Eq. 4.13 as a significant representation of the experimental data.

Eq. 4.13 can be used to predict the $C_{\alpha\varepsilon}$ of the stabilized RAS or granular materials containing RAS at different stress levels and temperatures from a measured $C_{\alpha\varepsilon}$ at a particular stress level and temperature. This is especially important when performing numerical analysis of embankments containing RAS for settlement calculations. The vertical stress changes at different elevations in an embankment fill and also temperature changes with different seasons. Since $C_{\alpha\varepsilon}$ varies with stress level and temperature, the embankment fill settles at different rates at different points in the embankment.

To obtain a practical graph for design purpose, $C_{\alpha\varepsilon}$ at intermediate temperatures were interpolated from the measured $C_{\alpha\varepsilon}$-T data points in Fig. 4.14 and plotted in Fig. 4.17. The graphs in Fig. 4.17 may be used in design practice to determine the required RAS content in the RAS:BA mixture corresponding to a desired $C_{\alpha\varepsilon}$ at a given temperature and stress.

Fig. 4.18 shows the compression curve of a RAS:BA specimen with 25% RAS, compacted at 35 ^{o}C in the consolidometer ring and incrementally loaded to σ'_v=200 kPa at 35 ^{o}C. After compression for 24 h under σ'_v=200 kPa, the temperature was reduced to room temperature and compression continued. The measured $C_{\alpha\varepsilon}$ is 0.0004 which is significantly lower than the corresponding $C_{\alpha\varepsilon}$ of an identical specimen compressed at room temperature throughout the test. As shown in Fig. 4.18, under each incremental σ'_v, the specimen compressed at higher temperature exhibits higher vertical strain than the specimen compressed at room temperature. Therefore, the specimen compressed at higher temperature has lower void ratio compared to the specimen compressed at room temperature. The temperature rise induces thermal preloading in the compacted RAS:BA mixture and reduces the $C_{\alpha\varepsilon}$ to as low as that for Wisconsin outwash

sand (Table 4.2). The practical implication of this behavior is that compaction and construction of embankments containing RAS should be undertaken in the warm season of the year. During construction at higher temperature, the void ratio of the fill containing RAS reduces at a higher rate reducing the potential for settlement during the following seasons.

RAS Stabilized with Fly Ash

Three stabilized RAS specimens were first compressed at room temperature for 24 h under σ'_v=200 kPa. The compression of the specimens then continued at three different temperatures, i.e. 5, 22, and 35 ^{o}C for 10 days. Fig. 4.19(a) shows the compression curves. The vertical strain at 5 ^{o}C and 22 ^{o}C is fairly constant with logarithm of time after 24 h. However, at 35 ^{o}C the vertical strain rapidly increases when the temperature increases and eventually becomes constant. Unlike the compacted RAS:BA mixture for which the log ($\dot{\varepsilon}$)-T relationship was linear at different time, the variation of log ($\dot{\varepsilon}$)-T for fly ash stabilized RAS is only linear for the $\dot{\varepsilon}$ immediately after the temperature change as indicated in Fig. 4.19(b). The coefficient of thermal creep, $C_{T\varepsilon}$, is 0.168. The $C_{\alpha\varepsilon}$ calculated using Eq. 4.9 with $C_{T\varepsilon}$ =0.168 agrees well with the experimental data at times immediately after temperature change as illustrated in Fig. 19(c).

To evaluate possible thermal preconsolidation on stabilized RAS, the compression of the specimens after 10 days at 35 ^{o}C was continued at 22 ^{o}C for another 5 weeks. The $C_{\alpha\varepsilon}$ of the specimen which experienced temperature rise, was reduced to 0.0002 which reflects 8 times reduction compared to $C_{\alpha\varepsilon}$ of the specimen compressed at constant room temperature during the test [see Fig. 4.19(a)]. The temperature rise induced thermal preloading to the compacted stabilized RAS and reduced $C_{\alpha\varepsilon}$ to as low as that for Wisconsin outwash sand (Table 4.2). The practical implication of this behavior is the appropriateness of compaction and construction with

RAS:FA mixtures in the warm season of the year. During construction at higher temperature, the void ratio of the RAS containing fill reduces at a higher rate and therefore negligible settlement is expected during the following seasons.

Hydraulic Conductivity

Fig. 4.20 shows that the hydraulic conductivity of the compacted RAS:BA mixture and stabilized RAS generally increases with temperature. The hydraulic conductivity of the compacted RAS:BA mixture compressed at σ'_3=70 kPa increases from 9×10^{-4} cm/s to 1.3×10^{-3} cm/s which reflects 40% increase while the hydraulic conductivity of stabilized RAS increases from 2.6×10^{-4} cm/s to 4.8×10^{-4} cm/s reflecting 85% increase. Two mechanisms are assumed to be involved. First, the change in viscosity of circulating water with temperature and second, the change in void ratio of the specimen due to deformability of RAS particles containing viscous asphalt binder.

The hydraulic conductivity of a porous medium is separated into the product of two multiples, one reflecting property of the porous medium and one reflecting fluid properties:

$$K = k\frac{\rho g}{\mu} \tag{4.14}$$

where K is the hydraulic conductivity of the porous medium, k is the intrinsic permeability of the porous medium, ρ is density of water, μ is the viscosity of water and g is the gravitational acceleration. To verify the first assumption, variation of water density and viscosity with temperature is considered in the range of 5 ^{o}C to 35 ^{o}C. Water density is reduced slightly (0.8%) while water viscosity is reduced by 50% (see Appendix A Fig. 4.A.9). Assuming there is no

change in intrinsic permeability with temperature, the ratio of hydraulic conductivity at elevated temperature to the hydraulic conductivity at room temperature (K_o) is obtained from:

$$\frac{K}{K_o} = \frac{\rho}{\rho_o} \cdot \frac{\mu_o}{\mu} \tag{4.15}$$

where $\rho_o$is the water density and μ_o is the water viscosity at room temperature. The normalized measured hydraulic conductivity of RAS:BA specimens along with Eq. 4.15 is plotted in Fig. 4.21. The deviation of data points from the curve reflects the effect of differences in void ratio on the hydraulic conductivity due to temperature change. Fig. 4.21 shows that at temperatures higher than the room temperature the reduction in void ratio has a decreasing effect on the hydraulic conductivity while at temperatures lower than the room temperature the increase in void ratio has increasing effect. The intrinsic permeability is generally related to porosity and average pore or particle diameter. Fig. 4.22 shows that the volumetric strain (or void ratio) of each specimen decreases with increasing temperature. However, since the hydraulic conductivity generally increases with temperature, the reduction in void ratio, shown in Fig. 4.22, is not a dominant factor for hydraulic conductivity of RAS:BA or stabilized RAS with temperature. Therefore, the reduction of viscosity of permeating water is the major contributing factor to increased hydraulic conductivity of the compacted RAS:BA mixture or stabilized RAS.

Summary and Implications

The effect of seasonal temperature change typically observed in the field on geotechnical properties of compacted RAS:BA mixture and stabilized RAS with Class C fly ash was

evaluated. The range of temperature considered herein encompasses the extreme seasonal temperature change observable in the US.

Shear strength of both compacted RAS:BA mixtures and stabilized RAS consistently decreases with increasing temperature. As the RAS content in the RAS:BA mixtures increases the temperature change has a more pronounced effect on the shear strength of the mixture. However, shear strength of embankments constructed with the compacted RAS:BA mixtures (with RAS content no more than 50%) or stabilized RAS with at least 20% self-cementing fly ash remains within a range sufficient to provide stability of the typical road embankment fills in the climatic ranges of North America (i.e., up to 35 ^{o}C fill temperatures).

Temperature change, on the other hand, has significant and limiting impact on compressibility of the compacted RAS:BA mixture and stabilized RAS with self-cementing fly ash. The secondary compression index increases exponentially with temperature. During the cold seasons (temperatures lower than 10 ^{o}C), the compression of the RAS:BA mixture or stabilized RAS is comparable to that of natural granular material and is practically negligible. However, the compressibility exponentially increases during warm seasons (when the temperature rises to 20 to 35 ^{o}C). This indicates that an embankment fill containing RAS constructed during the cold to mild seasons of the year may exhibit significant settlement during the warm season. In any region in North America, if the embankment is constructed during the warm season, the majority of the compression will occur during construction and negligible settlement can be expected in the seasons following the warm season. The design graphs were developed to predict subsequent settlement of an embankment constructed at a temperature around 20 ^{o}C as a function of RAS content, temperature, and stress levels for RAS:BA mixtures. In using the design graph, one may

meet the design specifications for the maximum allowable settlement of a road embankment (such as required by a state transportation agency).

The hydraulic conductivity of the RAS:BA mixture or stabilized RAS provides adequate drainage capacity for the embankment fill. The drainage capacity of the material increases with temperature due to reduction in water viscosity.

Previous research results showed that compressibility of the BA is greater than natural sand. The acceptable BA content of the compacted RAS:BA mixture can be safely replaced by natural granular material content and the results and design graphs obtained herein can be used conservatively for the compacted RAS mixtures with sands and gravels. The results obtained in this research is also specific to the type and maximum particle size of the recycled asphalt shingles used. The materials used are processed industrial materials or byproducts. Therefore, it is expected that their behavior will vary in a narrow range and thus only one source is used for the test materials. While the overall behavior is not likely to vary significantly, the quantitative values of the various parameters may be different if materials from other sources are used and therefore should be evaluated for design.

Conclusions

On the premise that recycled asphalt shingles (RAS) are too compressible for use as structural fill material led to an investigation of mixing RAS with a less compressible granular industrial byproducts such as bottom ash (BA) or stabilize with a self-cementing fly ash. Such improvement resulted in acceptable structural fill behavior at moderate temperatures. The effect of temperature change on mechanical properties of these improved mixtures is evaluated herein. Thermo-mechanical systems including temperature-controlled triaxial compression, one-dimensional compression, and permeameter cells were developed and the test procedures were

devised to closely simulate the field conditions in the laboratory. Based on the test results the following conclusions are made:

1- Shear strength of RAS:BA mixtures and stabilized RAS decreases with temperature. However, the reduction of shear strength due to seasonal temperature changes expected in the U.S. does not endanger stability of typical highway embankments. The hyperbolic model represents the stress-strain data of RAS:BA mixtures and stabilized RAS well up to the maximum deviator stress.

2- The vertical strain and strain rate in one-dimensional compression increases with temperature. The coefficient of thermal compression, defined as the slope of the log of strain rate versus temperature, is an inherent property of the material and is independent of time and stress level. Secondary compression index of compacted RAS:BA mixtures and fly ash-stabilized RAS is an exponential function of temperature change and power function of stress level. The developed relationship is useful when performing numerical analysis to account for the effect of temperature and stress level to properly evaluate long-term settlements. The design graphs indicating variation of secondary compression rate with RAS content, temperature and stress level were developed to select suitable RAS content in a mixture with a granular material like bottom ash under a given stress level and temperature.

3- Thermal cycling induces thermal preloading to the mixtures containing RAS, which, in turn, reduces compressibility and increases shear strength. Based on these results, to achieve the optimum behavior, construction of embankments made with materials containing RAS is recommended during warm seasons.

4- Hydraulic conductivity of RAS:BA mixture and stabilized RAS increases with temperature. The increase of hydraulic conductivity is mostly due to reduction of water viscosity with temperature. However, there is no concern regarding drainage capacity of RAS:BA or FA stabilized RAS at elevated temperatures.

Acknowledgment

Funding for this research was provided by the recycled material resource center (RMRC) and Solid Waste Research Program (SWRP) at the University of Wisconsin-Madison. Authors also greatly appreciate B.R. Amon & Sons, Inc. to provide samples of recycled asphalt shingles for this research.

References

Carpenter, A. C., Gardner, K. H., Fopiano, J., Benson, C. H., and Edil, T. B. (2007). "Life Cycle Based Risk Assessment of Recycled Materials in Roadway Construction." *Waste Management*, 27(10), 1458-1464.

Duncan J. M. and Chang, C. Y. (1970). "Nonlinear analysis of stress and strain in soils" *Journal of Soil Mechanics and Foundation Engineering Division*, 96(SM5): 1629-1651.

Edil, T., Benson, C., Bin-Shafique, M., Tanyu, B., Kim, W., and Senol, A. (2002). "Field evaluation of construction alternatives for roadway over soft subgrade," *Transportation Research Record*, 1786, Transportation Research Board, National Research Council, Washington, DC, 36-48.

Frigio, F., Tabatabaee, N., and Bahia, H. (2011). "Estimating the effect of RAP, RAS, and warm mix additives on high temperature viscosity of blended binders." *Transportation Research Board* (Submitted).

Fox, P. J. and Edil, T. B. (1996). "Effects of stress and temperature on secondary compression of peat." *Canadian Geotechnical Journal*, 33, 405-415.

Gambatese, J. A. and Rajendran, S. (2005). "Sustainable Roadway Construction: Energy Consumption and Material Waste Generation of Roadways." *Proceeding of Construction Research Congress*, San Diego, CA.

Geo4VA (2011). Earth Temperature and Site Geology. Virginia Tech, http://www.geo4va.vt.edu/A1/A1.htm, Accessed February 2011.

Hanson, J. L. (1996). *Thermal precompression of peat.* PhD Dissertation, Univ. of Wisconsin-Madison, Madison, WI.

Hillel, D. (1982). *Introduction to soil physics*. Academic Press, San Diego, CA.

Houston, S. L., Houston, W. N., and Williams, N. D. (1985). "Thermo-mechanical behaviour of seafloor sediments." *Journal of Geotechnical Engineering.,* 111, 1249-1263.

Hu, Q., and Feng, S. (2003). "A daily soil temperature dataset and soil temperature climatology of the contiguous United States." *Journal of Applied Meteorology*. 42, 1139-1156.

Klyosov A. A. (2007). *Wood-plastic composites*. John Wiley & Sons, Inc. Hoboken, NJ.

Kilbert, C. J. (2002). "Policy instruments for a sustainable built environment." *Journal of Land Use and Environmental Law*, 17 (2), 379-394.

Kondner R. L., Zelasko J. S. (1963). "A hyperbolic stress-strain formulation for sand." *2nd Pan-American Conference on Soil Mechanics and Foundation Engineering Division*, Brazil, pp. 289-324.

Krivit, D. (2007). *Recycling of Tear-Off Shingles: Best Practices Guide*. Final report prepared for the Construction Materials Recycling Association (CMRA).

Ladd, C. C., Foote, R. Ishihara, K., Schlosser, F. and Poulos, H. G. (1977). "Stress-deformation and strength characteristics." State-of-the-Art Report, Proceedings of the Ninth International Conference on Soil Mechanics and Foundation Engineering, Tokyo, 2, 421-494.

Lade, P. V., and Liu, C. T. (1998). "Experimental study of drained creep behavior of sand." *Journal of Engineering Mechanics, ASCE,* 124, 912-920.

Lee, S. J., Amirkhanian, S. N., Shatanawi. S., and Thodesen, C. (2008). "Influence of compaction temperature on rubberized asphalt mixes and binders." *Canadian Journal of Civil Engineering*, 35, 908-917.

Marshall, T. J. and Holmes, J. W. (1988). *Soil Physics*. *2nd ed*. Cambridge Univ. Press, New York.

Mesri, G., and Castro, A. (1987). "The C_α/C_c concept and K_o during secondary compression." *Journal of Geotechnical and Geoenvironmental Engineering, ASCE,* 113, 230-247.

Mesri, G., Feng, T. W., and Benak, J. M. (1990). "Postdensification penetration resistance of clean sands." *Journal of Geotechnical and Geoenvironmental Engineering, ASCE,* 116, 1095-1115.

Rao, S. M, and Shivananda, P. (2005). "Role of curing temperature in progress of lime-soil reactions." *Geotechnical and Geological Engineering,* 23 (1), 79-85.

Roberts, F. L., Kandhal, P. S., Brown, E. R., Lee, D. Y. and Kennedy, T. W. (1996). *Hot Mix Asphalt Materials, Mixture Design, and Construction*. National Asphalt Paving Association Education Foundation. Lanham, MD.

Sengoz, B., and Topal, A. (2004). "Use of asphalt roofing shingle waste in HMA." *Construction and Building Materials*, 19, 338-346.

Soleimanbeigi, A., Edil, T. B., and Benson, C. H. (2012). "Recycled asphalt shingles mixed with granular byproducts as structural fill", *Journal of ASTM International,* Vol. 9, No. 1.

Soleimanbeigi, A**.,** Edil, T. B., and Benson, C. H. (2012). "Evaluation of fly ash stabilization of recycled asphalt shingles for use in structural fills", *Journal of Materials in Civil Engineering, ASCE, in press*.

Soleimanbeigi, A., Edil, T. B., and Benson, C. H. (2012). "Compressibility of reclaimed asphalt shingles mixtures: mechanism and practical implication", *Canadian Geotechnical Journal, prepared.*

Swiertz, D., Mahmoud, E., Bahia, H. (2011). "Estimating the Effect of RAP and RAS on Fresh Binder Low Temperature Properties without Extraction and Recovery." *In Transp. Res. Rec.: J. of the Transp. Res. Board*, Washington, DC, 2208, 48-55.

VANR (1999). "Recycled Asphalt Shingles in Road Application: An Overview of the State of Practice." <http://www.anr.state.vt.us/dec/wastediv/recycling/shingles.pdf> (Accessed June 9th 2012).

Veisi, M., Chittoori, B., Celaya, M., Nazarian, S., Puppala, A. J. and Solis, C. (2010). "Accelerated Stabilization Design of Subgrade Soils", Research Report FHWA/TX 06/0-5569-1, Center for Transportation Infrastructure Systems, The University of Texas at El Paso, El Paso, Texas,, 229 p.

West, R. C., Watson, D.E., Turner, P.A., and Casola, J. R. (2010). *Mixing and compaction temperatures of asphalt binders in hot-mix asphalt*. National Cooperative Highway Research Program, Report No. 648, Trans. Res. Board, Washington, DC.

Yoon, S., Balunaini, U., Yildirim, I. Z., Prezzi, M. and Siddiki, N. Z. (2009). "Construction of an embankment with a fly and bottom ash mixture: Field performance study." *Journal of Materials in Civil Engineering, ASCE*, Vol. 21, No. 6, pp. 271-278.

Table 4.1. Thermal test program for mechanical properties of RAS:BA mixture and stabilized RAS

Type of test	Material	σ'_3 or σ'_v (kPa)	T (^oC)	# of tests
Triaxial Compression	RAS:BA (50:50)	35, 70, 140	5, 20, 35	9
	RAS:BA (25:75)	35, 70, 140	5, 20, 35	9
	RAS:BA (0:100)	35, 70, 140	5, 35	6
	RAS:FA (80:20)	35, 70, 140	5, 20, 36	9
	RAS:BA (25:75)	70	20-35-20	1
1D Compression	RAS:BA (50:50)	50, 100, 200	5, 20, 35	9
	RAS:BA (25:75)	50, 100, 200	5, 20, 35	9
	RAS:BA (0:100)	50, 200	5, 35	4
	RAS:FA (80:20)	50, 200	5, 20, 35	6
	RAS:BA (25:75)	200	35-20	1
Hydraulic Conductivity	RAS:BA (50:50)	35, 70, 140	5, 20, 35	9
	RAS:FA (80:20)	35, 70, 140	5, 20, 35	9

Table 4.2. Secondary compression ratio of different materials

Material	$C_{\alpha\varepsilon}$
Berthierville Clay (Mesri and Castro 1987)	0.0185
California Tar Sand (Mesri and Castro 1987)	0.0014
Micaceous Antelope Valley Sand (Lade and Liu 1998)	0.0011
Lake Michigan Beach Sand (Mesri et al. 1990)	0.0004
Wisconsin outwash sand	0.0003
RAS-BA (25-75)	0.0078
RAS-BA (25-75): Thermally Precompressed	0.0004
FA Stabilized RAS	0.0030
FA Stabilized RAS :Thermally Precompressed	0.0002

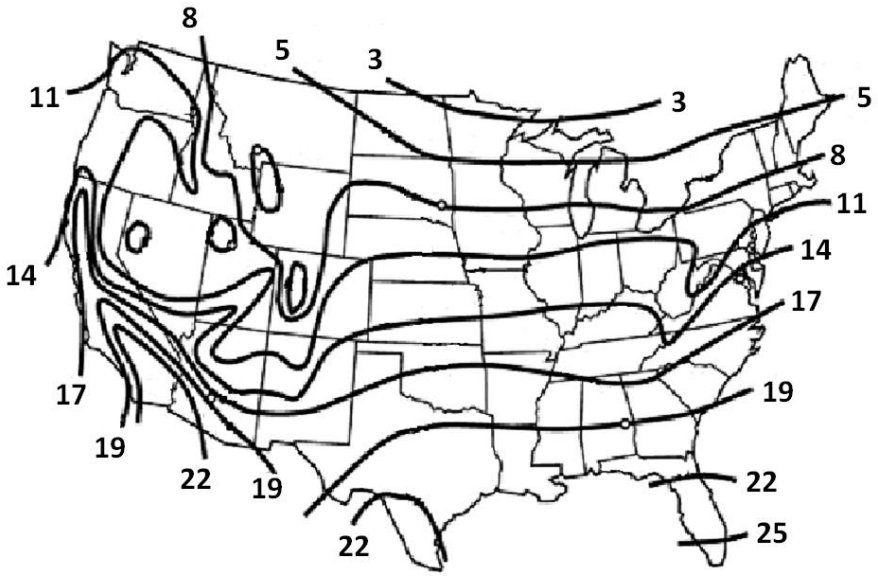

Fig. 4.1. Mean annual earth temperature observations (^{o}C) in U.S. (Geo4VA, 2011)

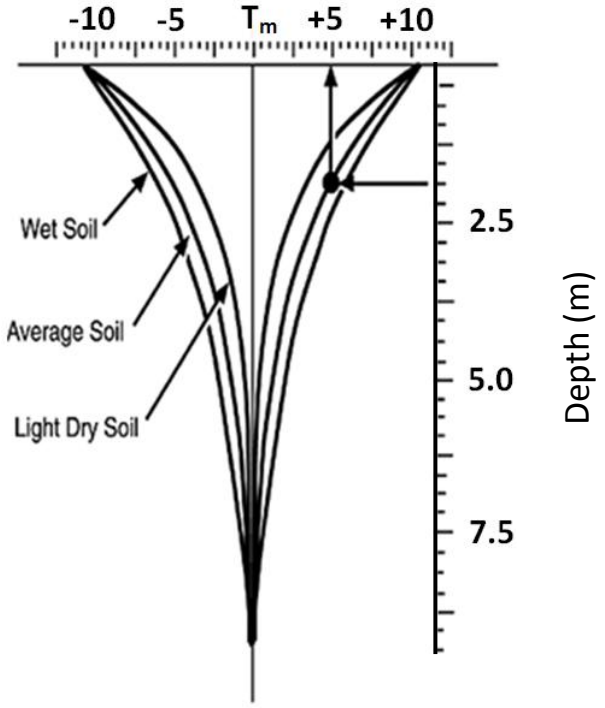

Fig. 4.2. Seasonal soil temperature change as a function of depth below ground surface (Geo4VA, 2011)

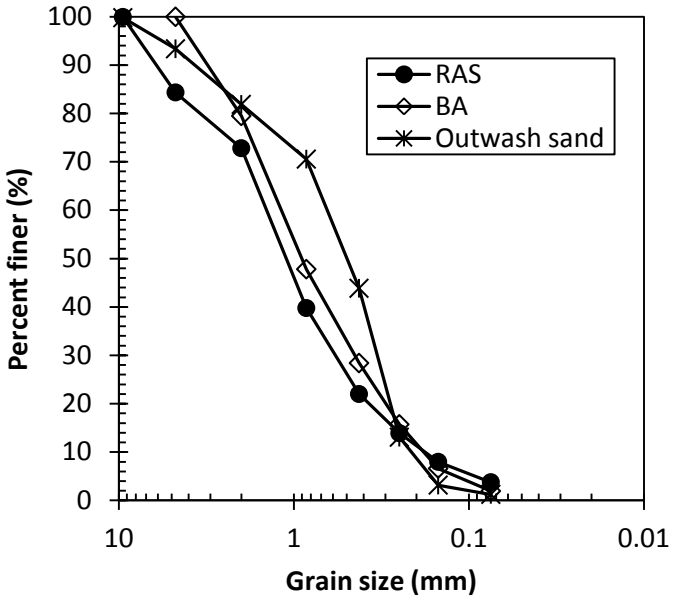

Fig. 4.3. Grain size distribution of RAS, BA and outwash sand

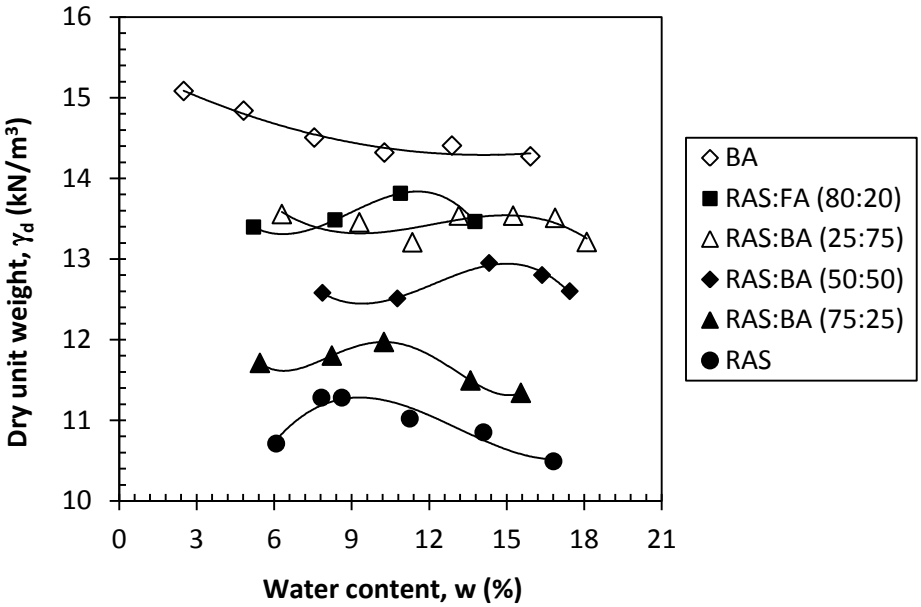

Fig. 4.4. Compaction curves of RAS:BA and stabilized RAS

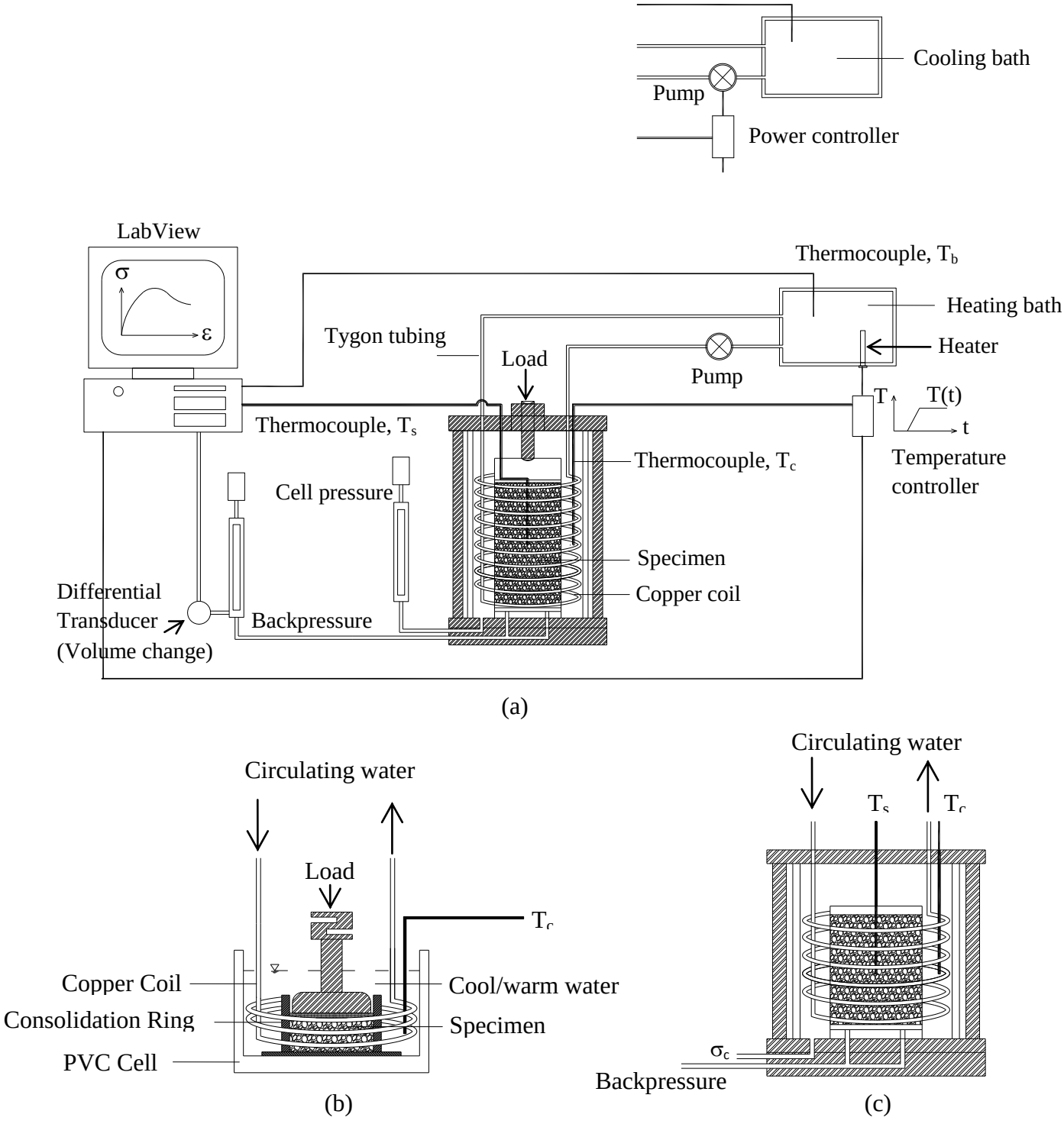

Fig. 4.5. Thermo-mechanical system: (a) temperature controlled triaxial cell (b) temperature controlled 1D compression cell and (c) temperature controlled permeameter

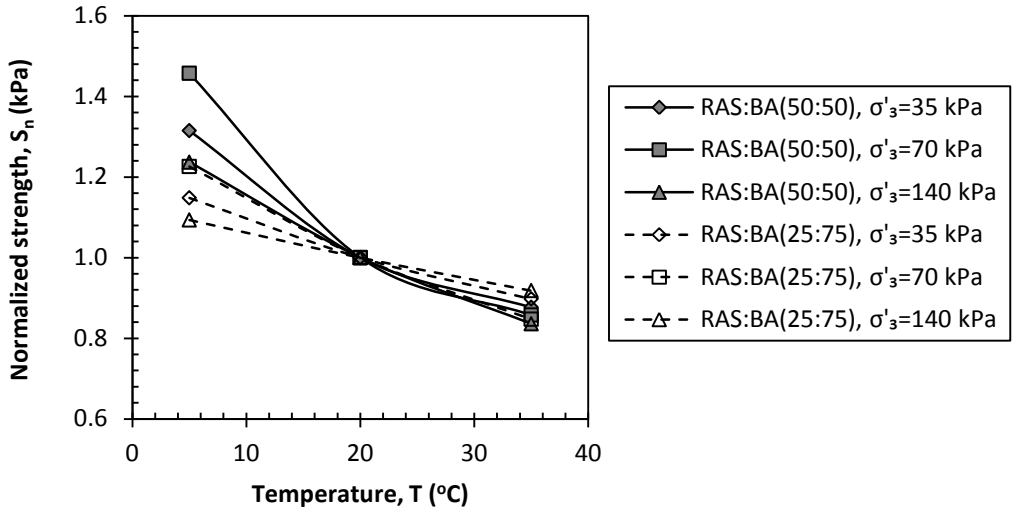

Fig. 4.6. Variation of normalized strength of RAS:BA mixtures at different temperatures

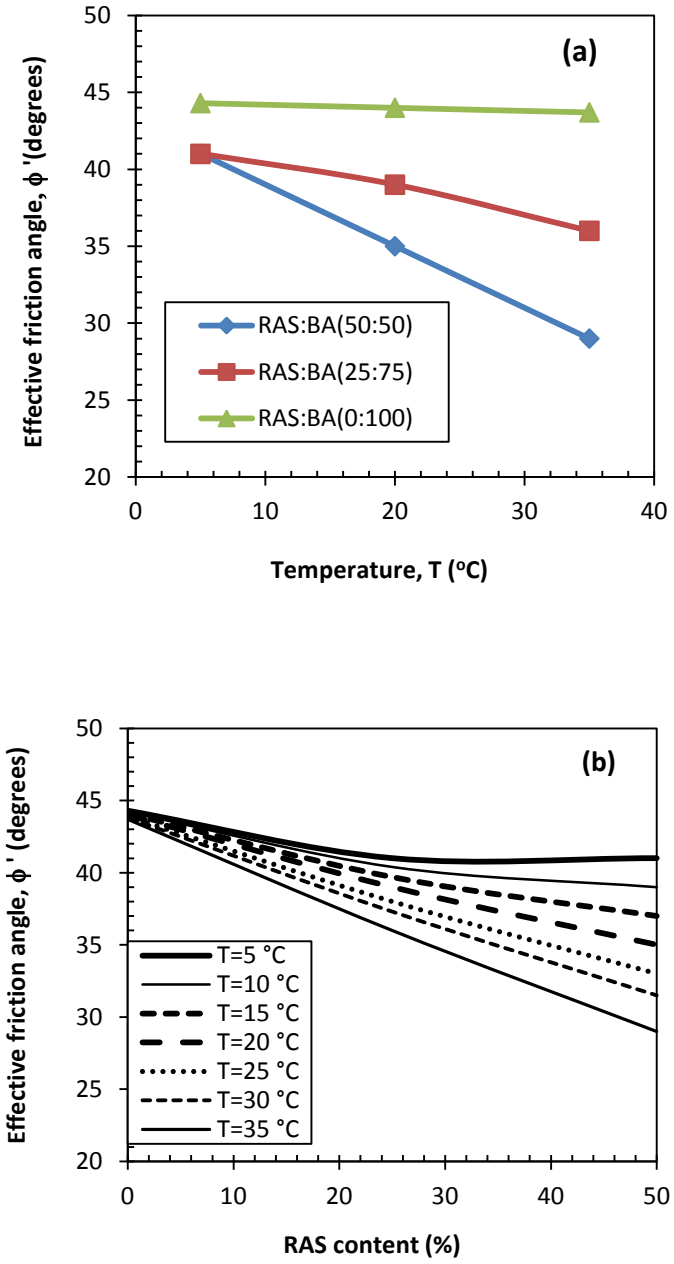

Fig. 4.7. Variation of effective friction angle with temperature (a) and with RAS content (b) of RAS:BA mixtures

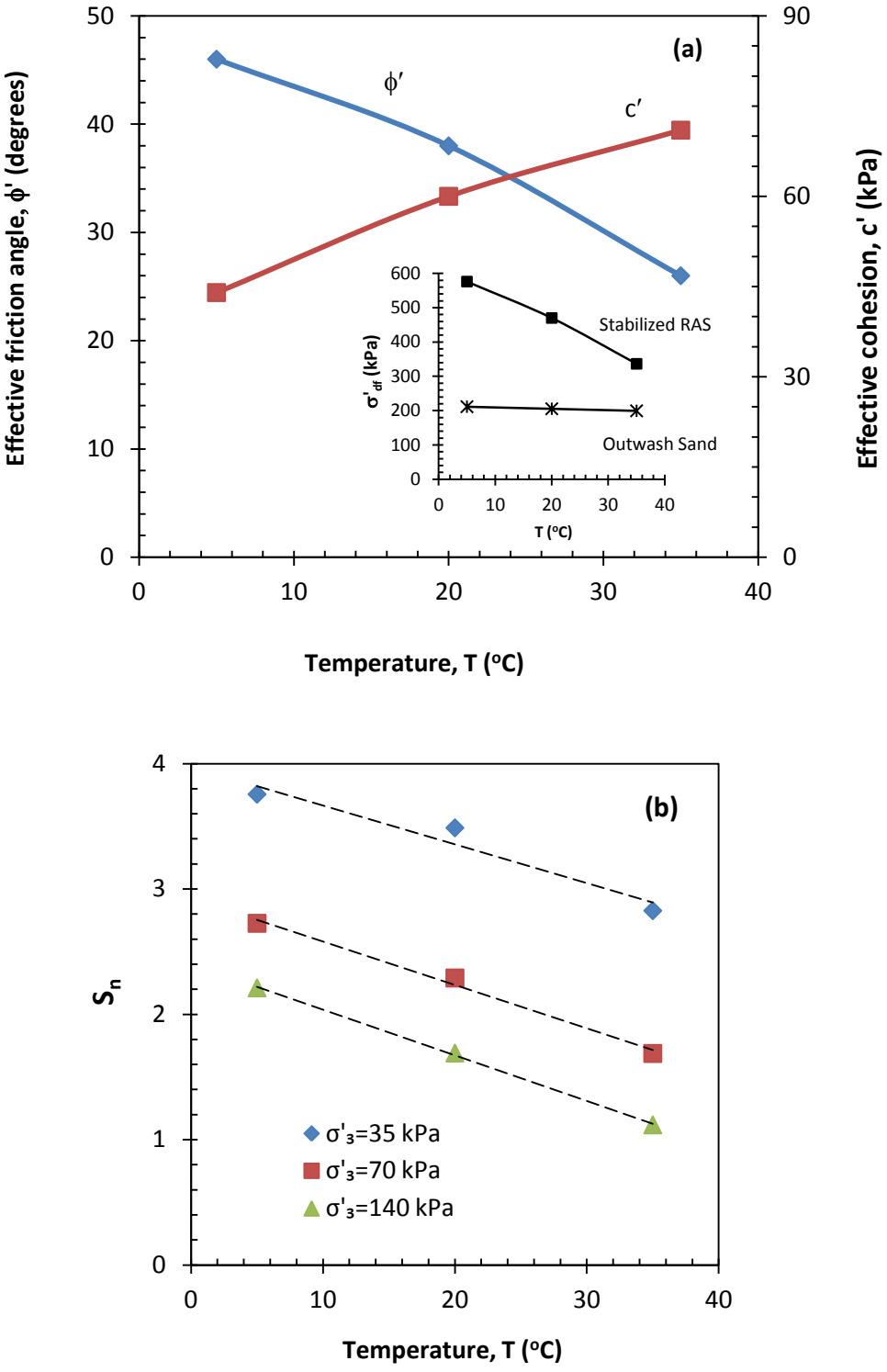

Fig. 4.8. Variation of (a) friction angle and cohesion of stabilized RAS and (b) normalized σ'_{df} with temperature

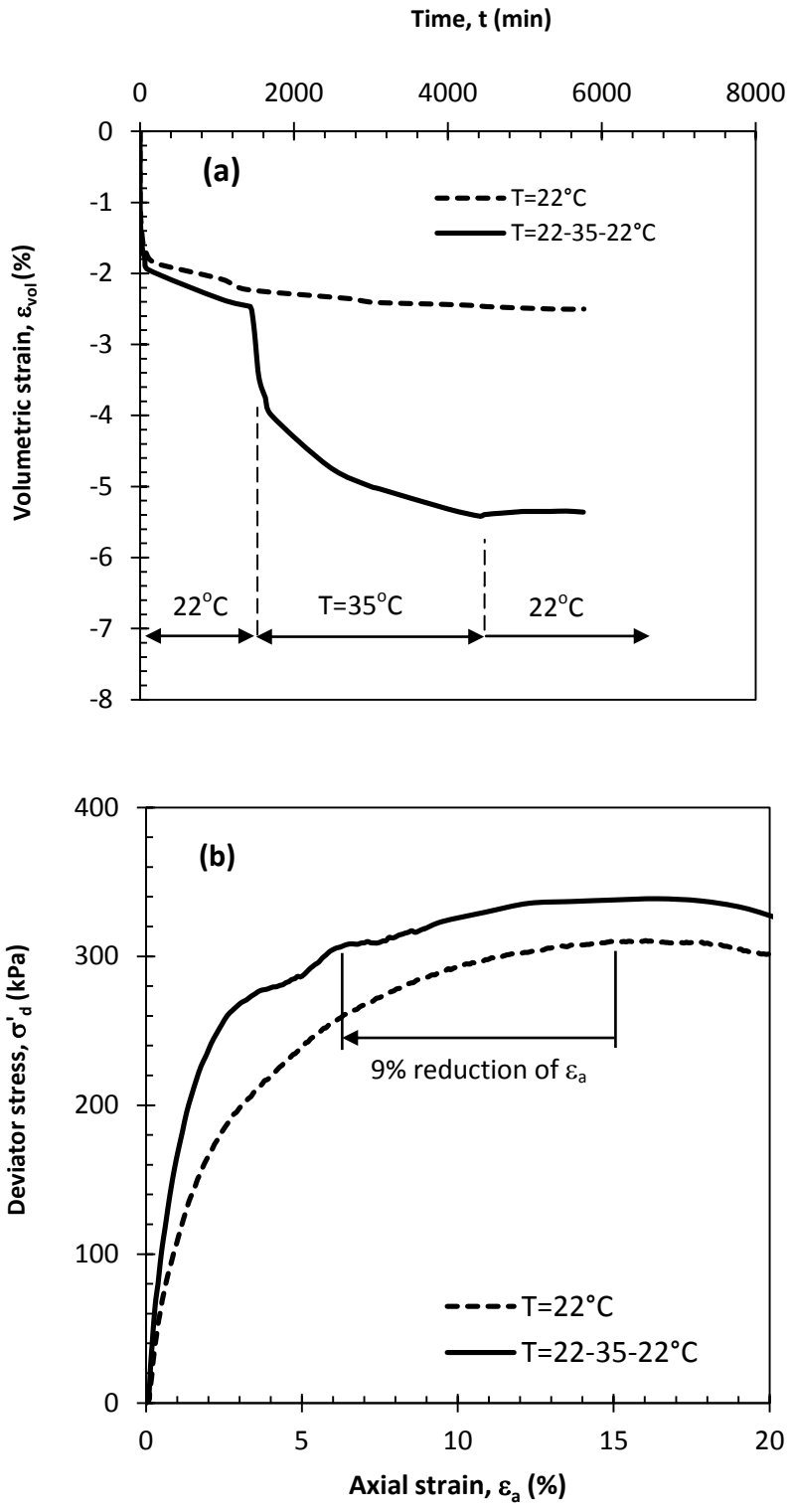

Fig. 4.9. Effect of thermal cycle on stress-strain behavior of RAS:BA mix

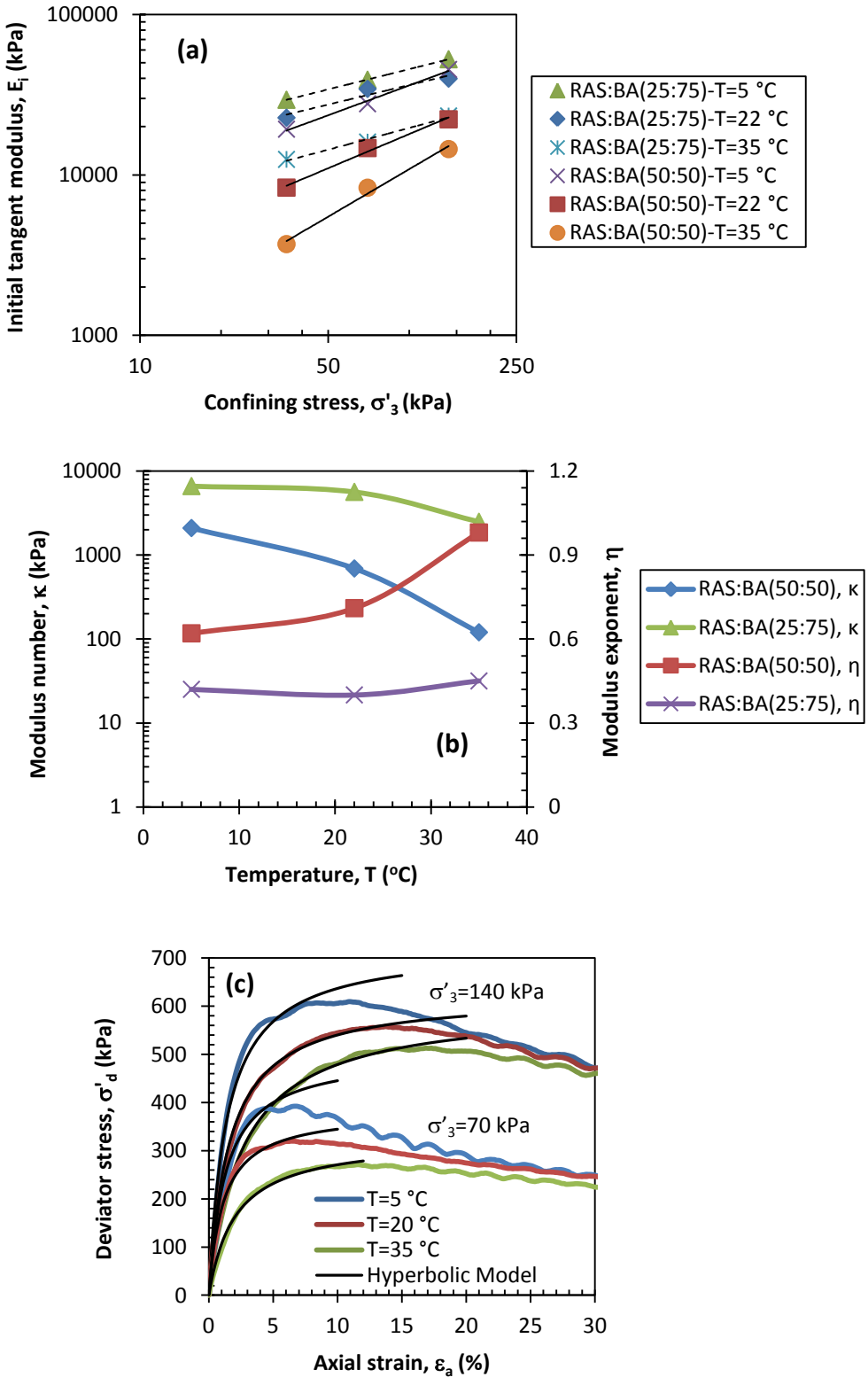

Fig. 4.10. Variation of (a) E_i with σ'_3 (b) κ and η of RAS:BA mixtures with temperature and (c) measured and predicted stress-strain curves at different temperatures

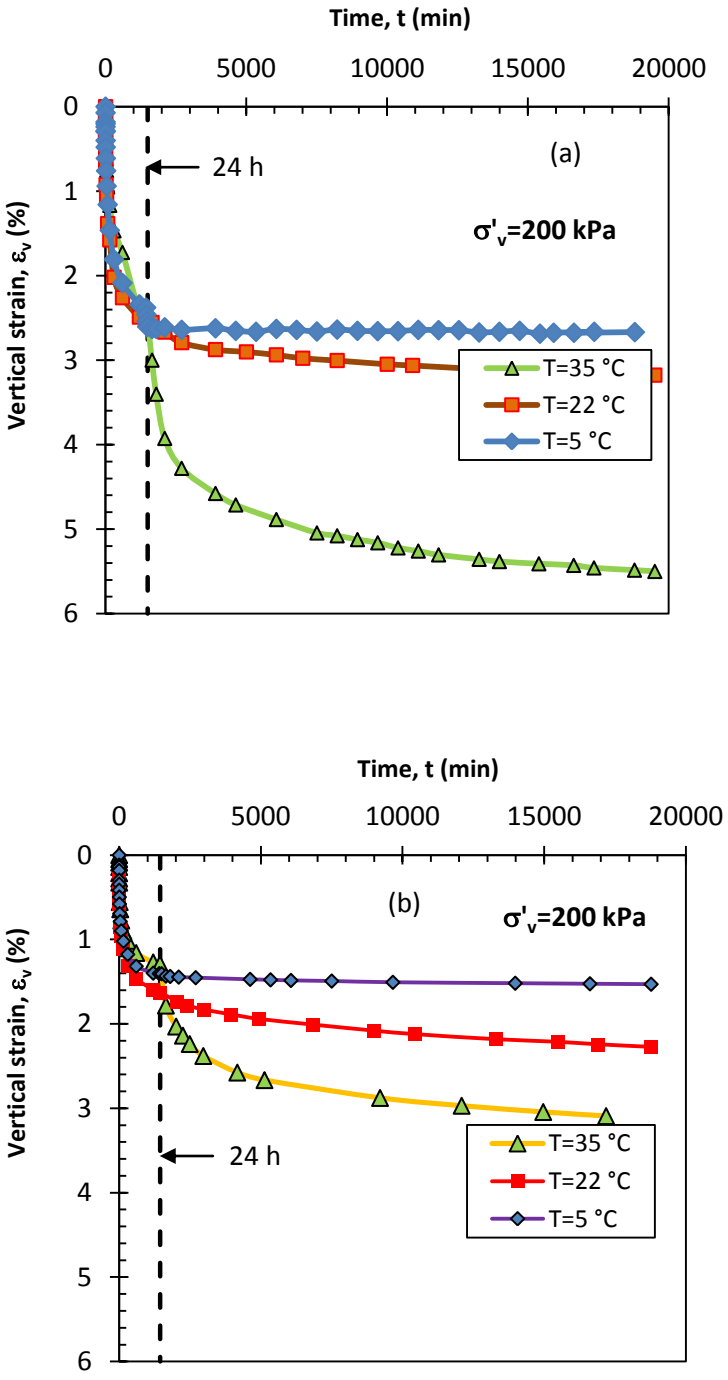

Fig. 4.11. Variation of ε_v with time at different temperatures for (a) RAS:BA (50:50) and (b) RAS:BA (25:75)

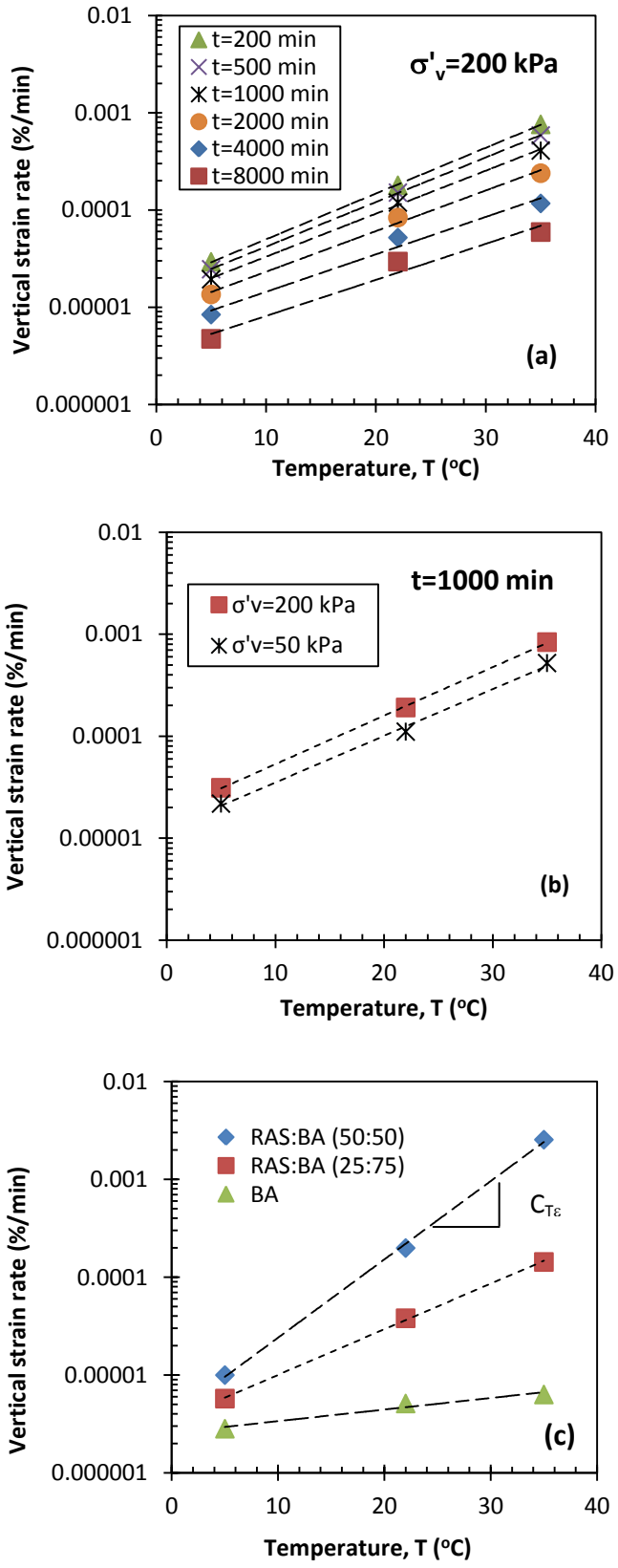

Fig. 4.12. Variation of strain rate of RAS:BA mixtures with temperature

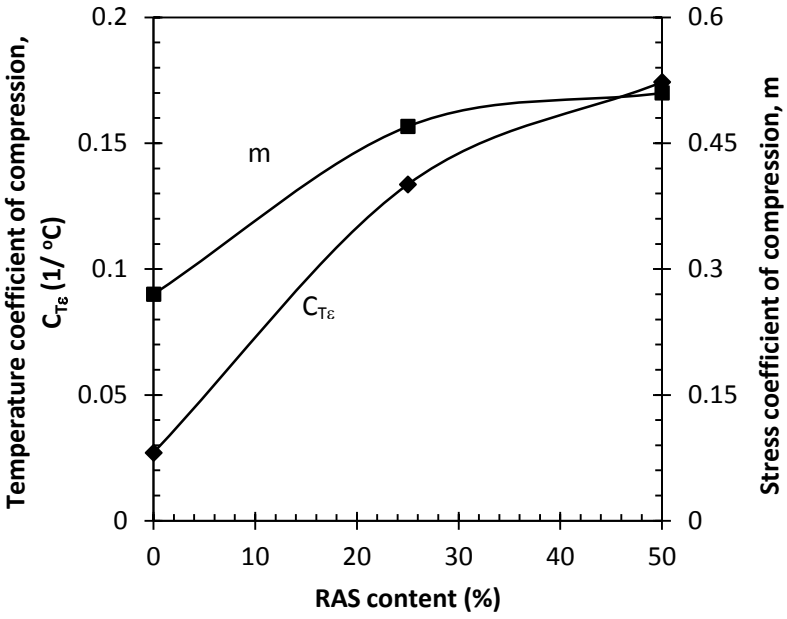

Fig. 4.13. Variation of $C_{T\varepsilon}$ and m with RAS content in the compacted RAS:BA mixture

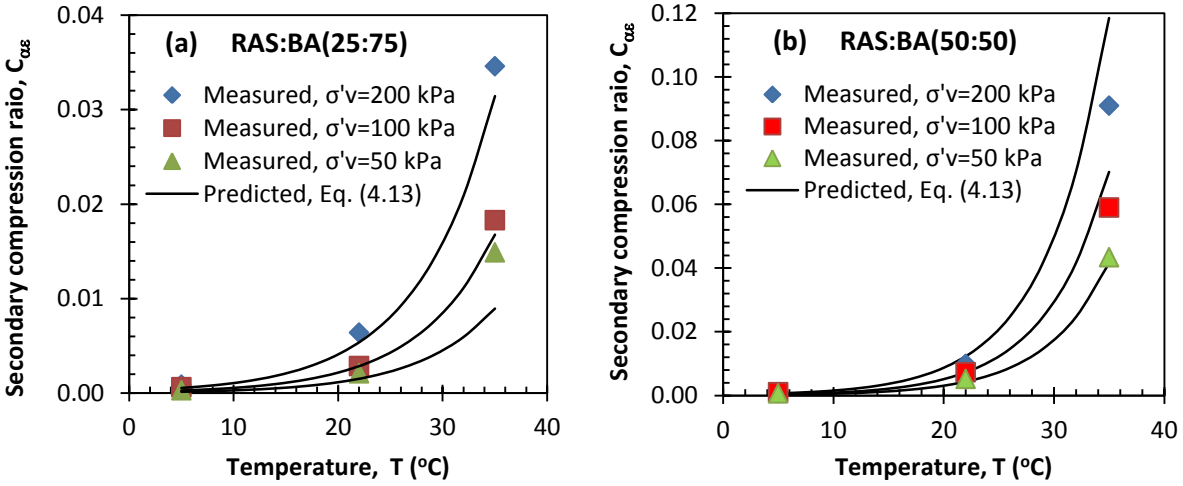

Fig. 4.14. Variation of $C_{\alpha\varepsilon}$ with temperature and stress level of compacted RAS:BA mixtures with (a) 25% RAS (b) 50% RAS

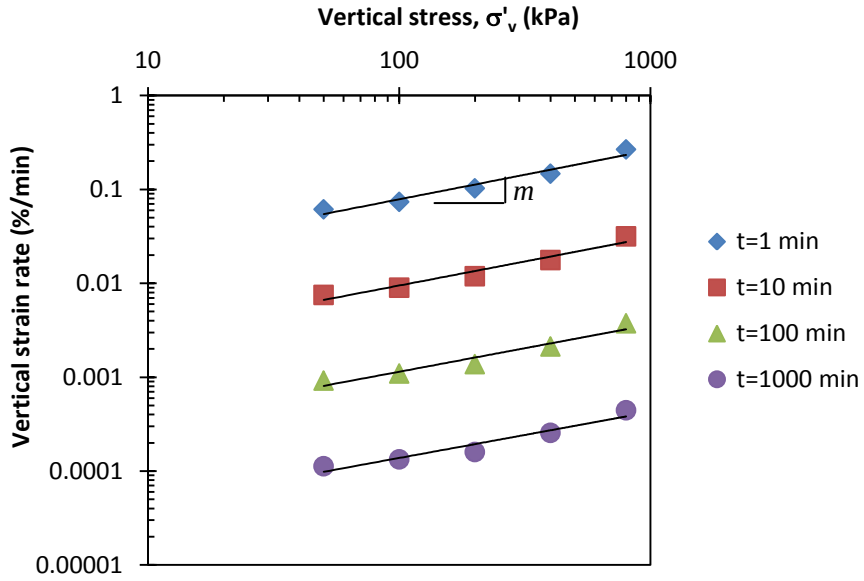

Fig. 4.15. Variation of vertical strain rate with vertical stress for compacted RAS:BA (25:75)

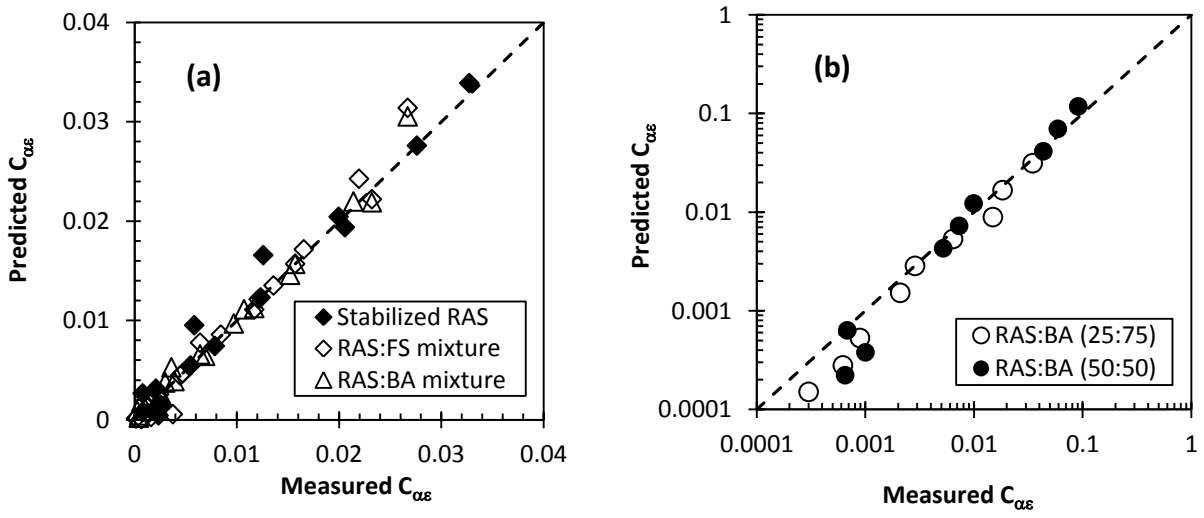

Fig. 4.16. Predicted versus measured $C_{\alpha\varepsilon}$ (a) for different RAS mixtures at room temperature (Soleimanbeigi et al. 2012) and (b) for RAS:BA mixtures at elevated temperatures

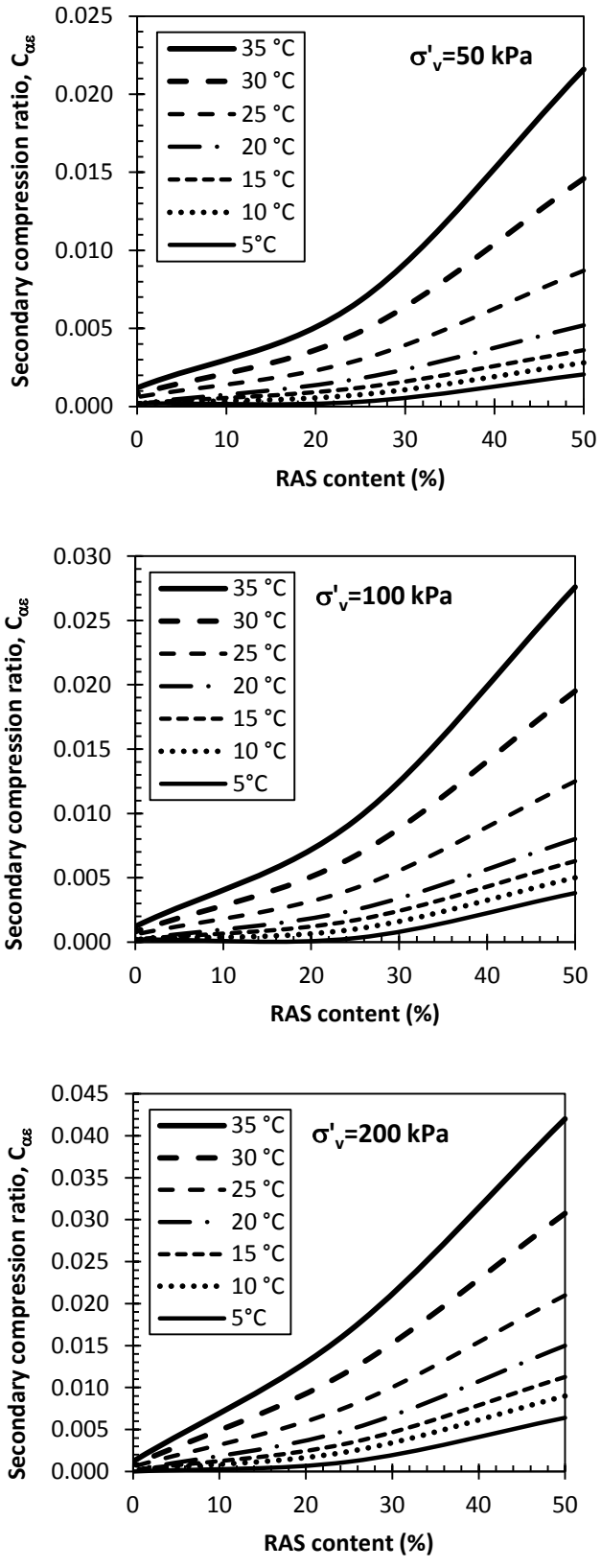

Fig. 4.17. Variation of $C_{\alpha\varepsilon}$ with RAS content at different temperatures and σ'_v

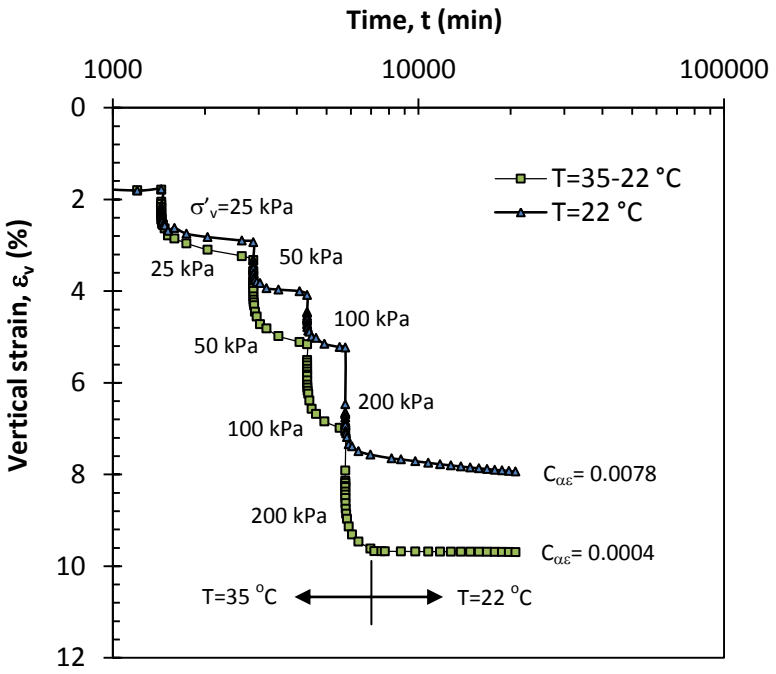

Fig. 4.18. Effect of construction at elevated temperature on compressibility of compacted RAS:BA mixture

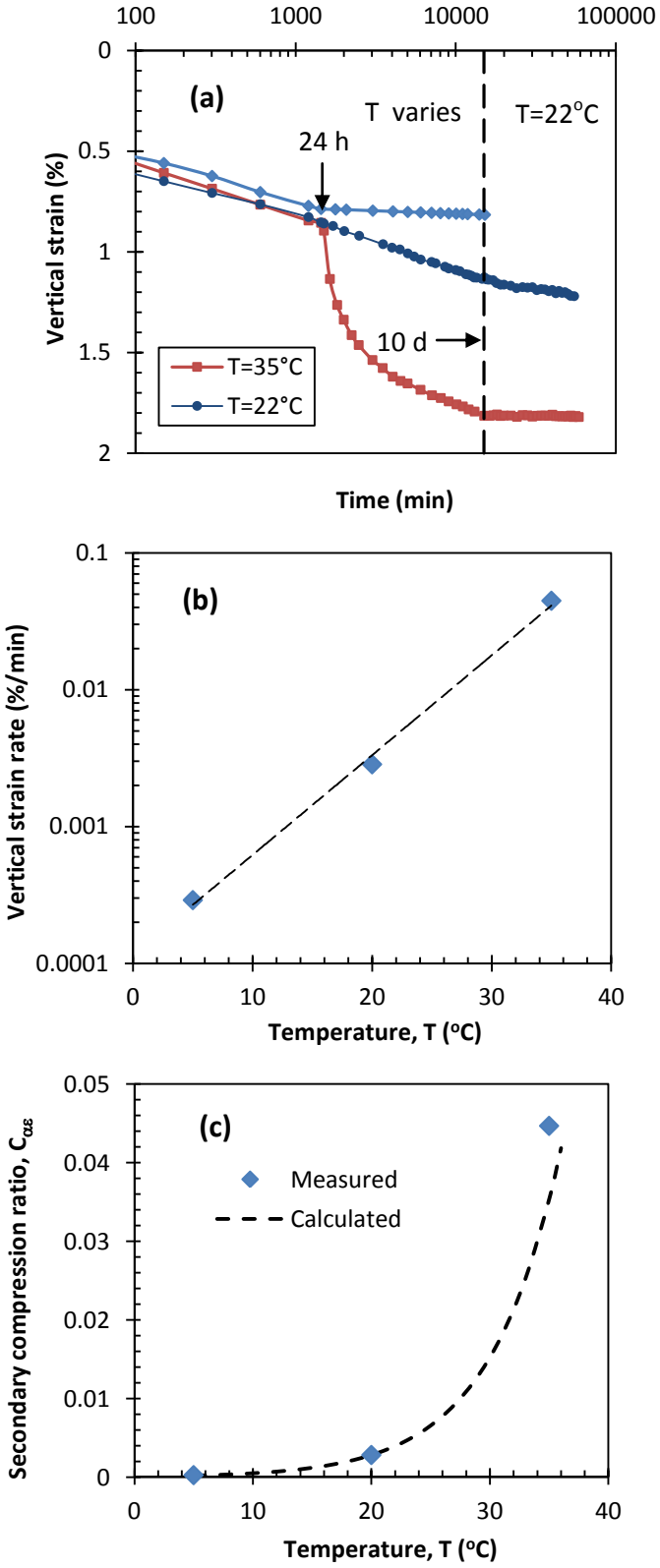

Fig. 4.19. Variation of vertical strain with time of stabilized RAS at different temperatures (a); train rate with temperature (b); and $C_{\alpha\varepsilon}$ with temperature (c)

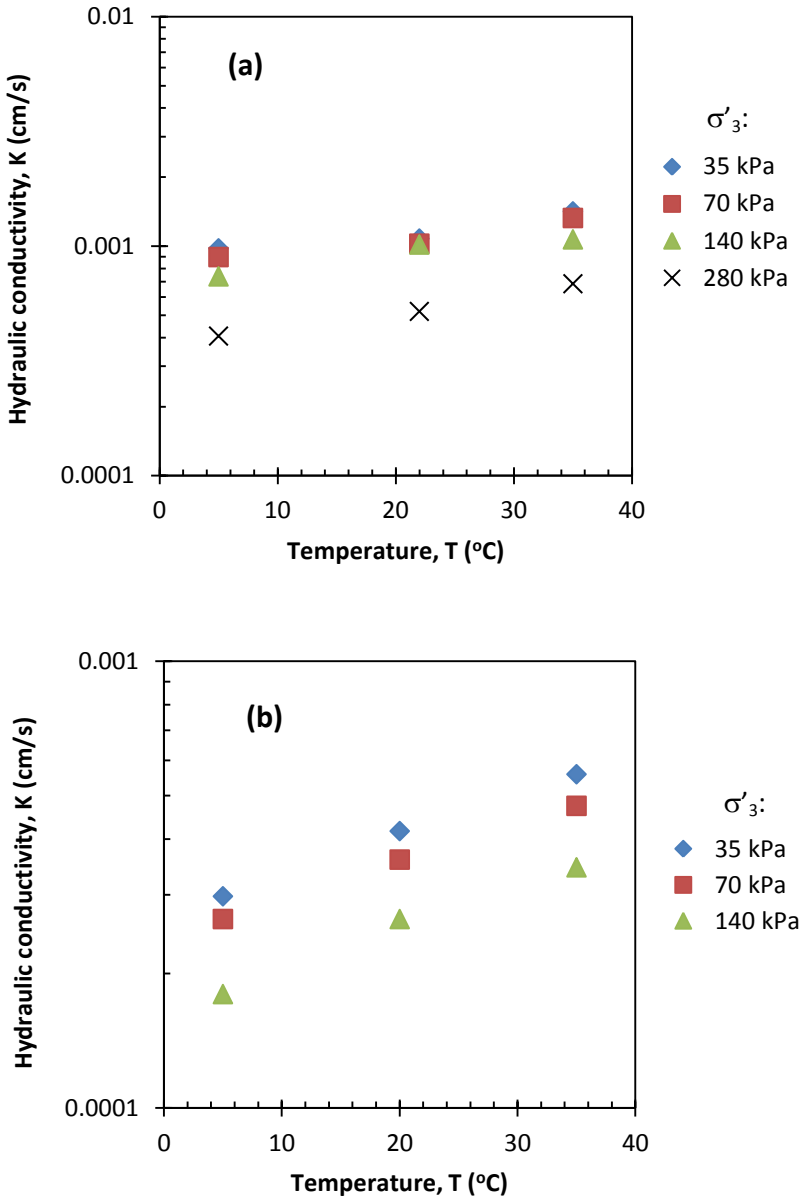

Fig. 4.20. Variation of hydraulic conductivity of (a) RAS:BA mixture; and (b) stabilized RAS with temperature

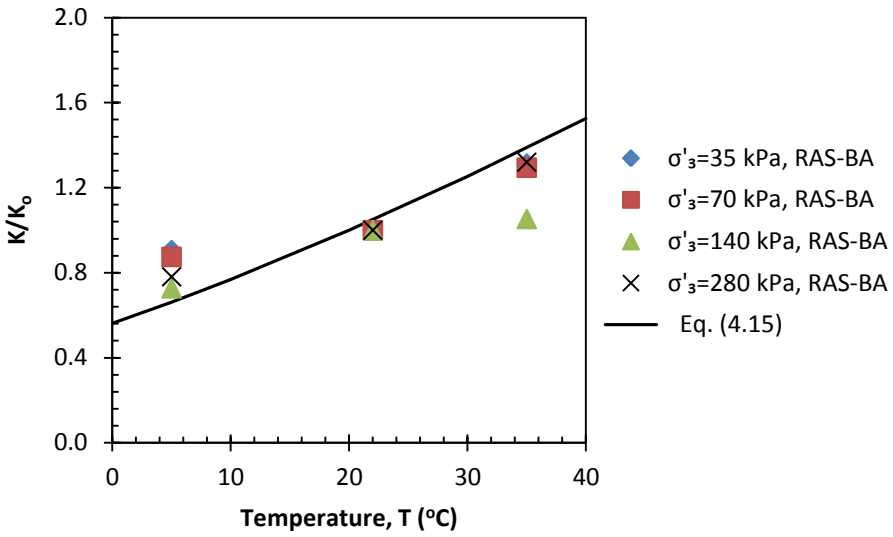

Fig. 4.21. Variation of normalized hydraulic conductivity of RAS:BA with temperature

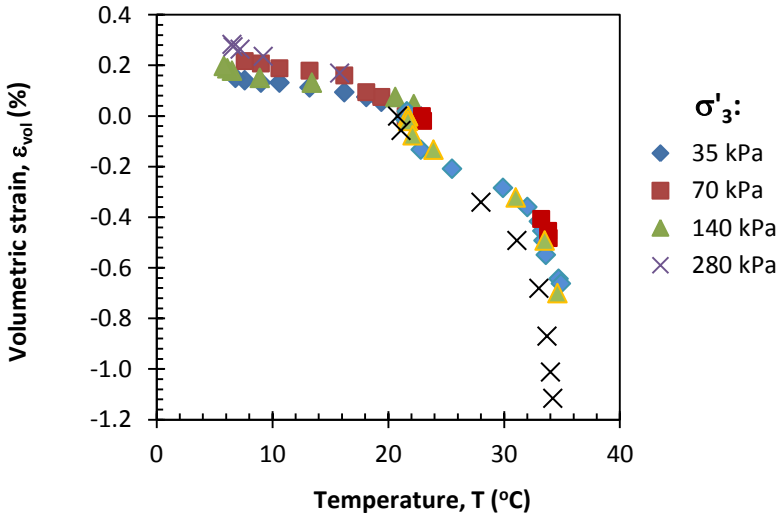

Fig. 4.22. Variation of volumetric strain of the specimen with temperature

APPENDIX

Table 4.A.1. Hyperbolic model parameters for stress-strain behavior of compacted RAS:BA mixtures

RAS (%)	σ'_3 (kPa)	35			70			140		
	T(^{o}C)	5	20	35	5	20	35	5	20	35
25	E_i (kPa)	29400	22700	12500	39200	34400	16000	52600	39800	23300
	$\sigma'_{d,ult}$	294	278	256	503	383	326	725	625	602
	σ'_{df}	239	208	187	392	320	271	610	558	512
	R_f	0.81	0.75	0.73	0.78	0.84	0.83	0.84	0.89	0.85
50	E_i (kPa)	19300	8300	3700	27800	14700	8300	45500	22200	14500
	$\sigma'_{d,ult}$	263	227	233	556	362	360	714	526	323
	σ'_{df}	237	180	158	452	310	266	629	509	425
	R_f	0.90	0.79	0.68	0.81	0.86	0.74	0.88	0.97	1.32

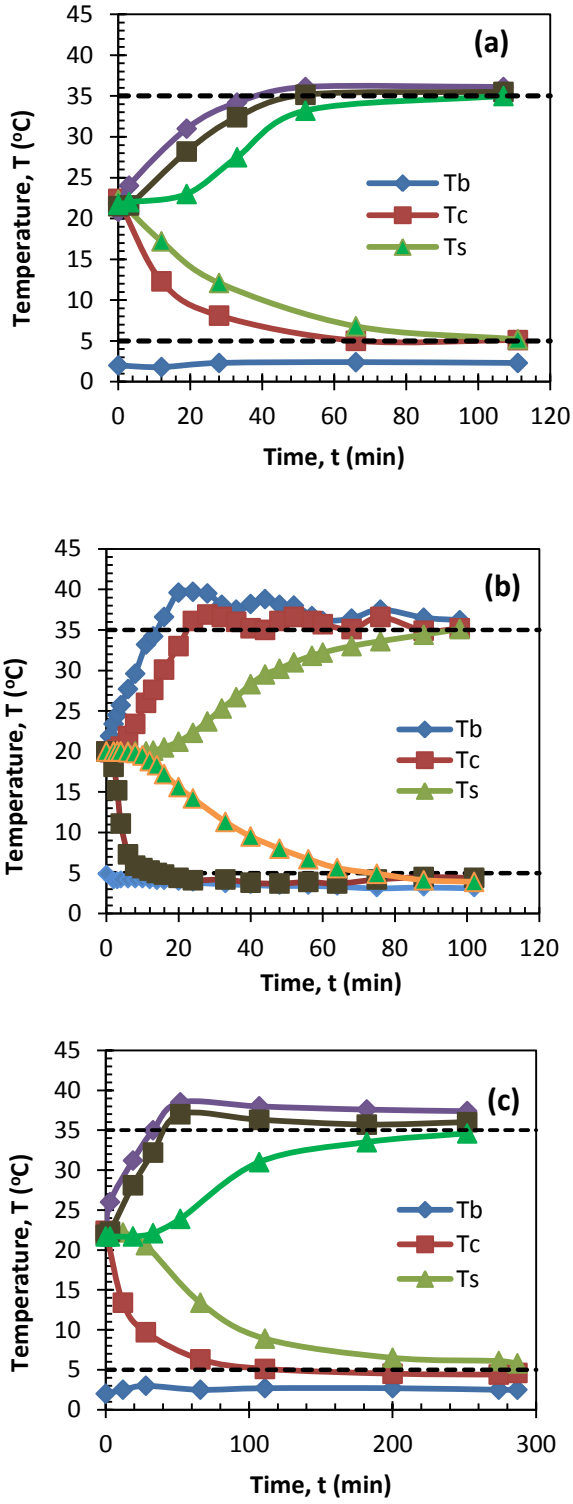

Fig. 4.A.1. Calibration curves for temperature variation in heating/cooling bath, cell and specimen for (a) temperature controlled triaxial cell; (b) temperature controlled consolidometer; and (c) temperature controlled permeameter (T_b=bath temperature, T_c=cell temperature, T_s=specimen temperature)

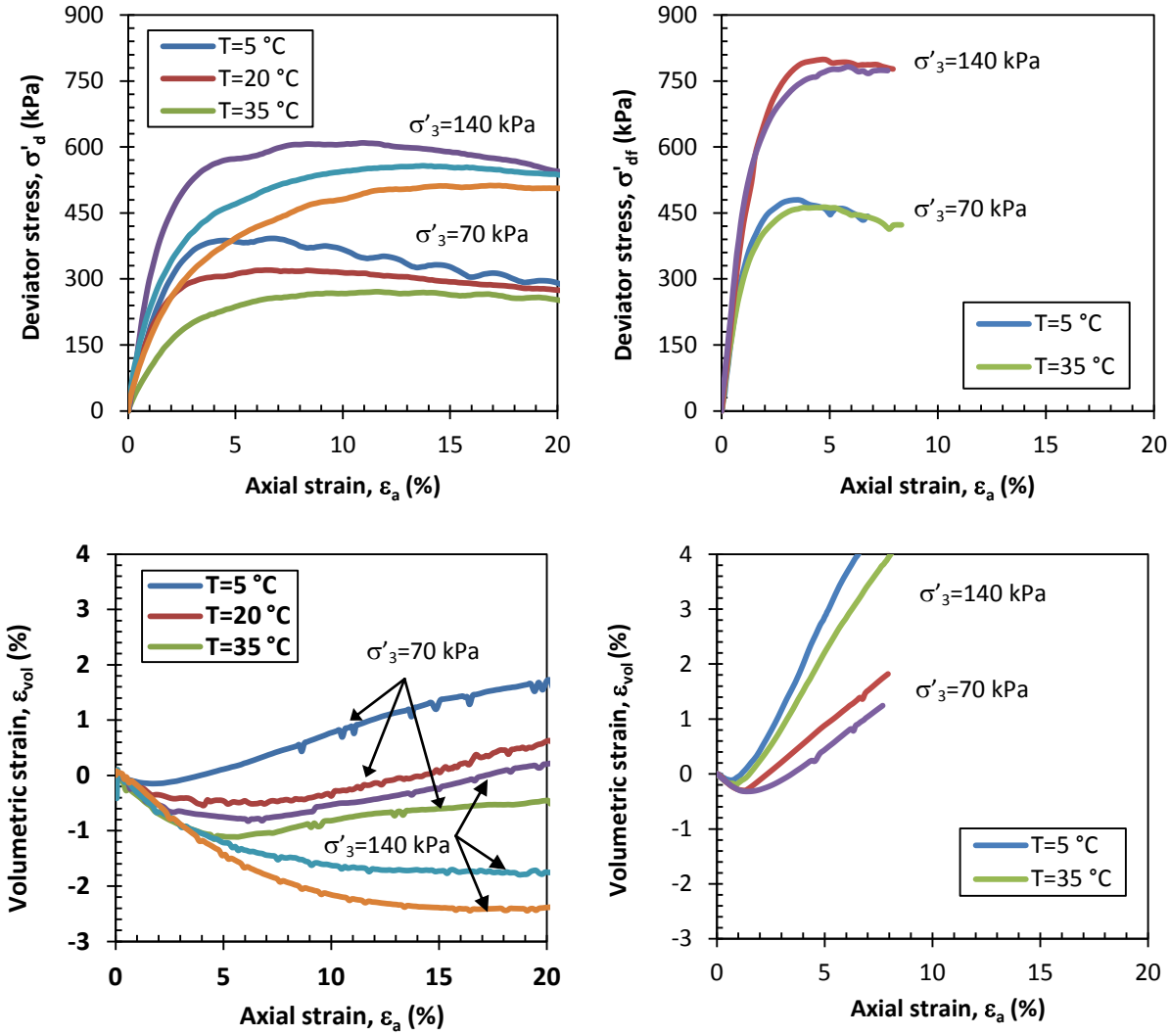

Fig. 4.A.2. Effect of temperature on stress-strain and volumetric change behavior of RAS:BA mixture with 25% RAS

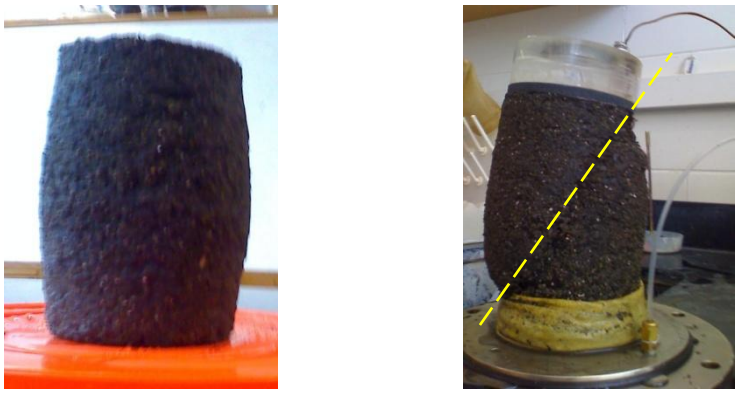

(a) T=22°C, 35°C (b) T=5°C

Fig. 4.A.3. Modes of failure of RAS:BA mixture specimen at different temperatures

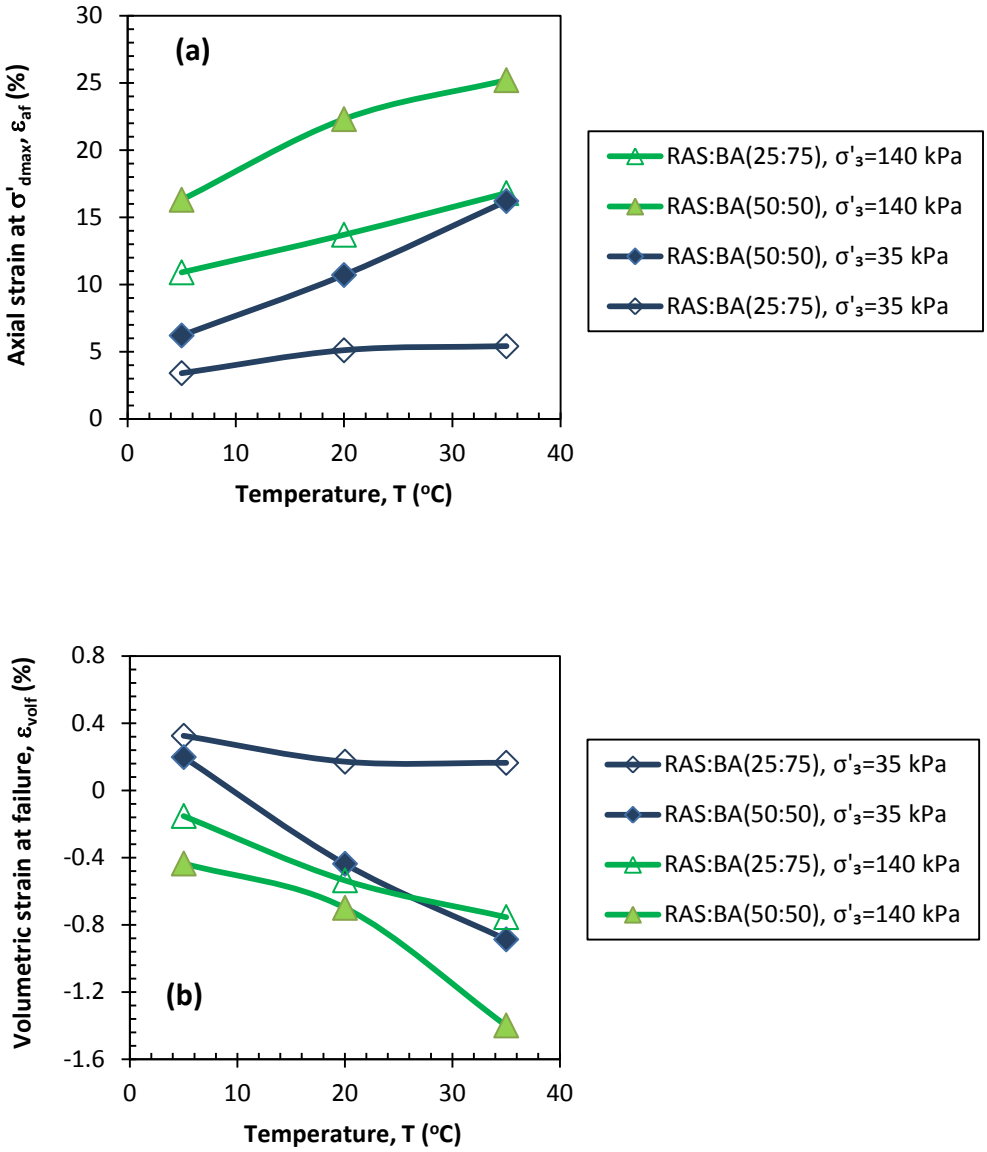

Fig. 4.A.4. Variation of axial strain at σ'_{max} (a) and volumetric strain (b) of RAS:BA mixtures with temperature

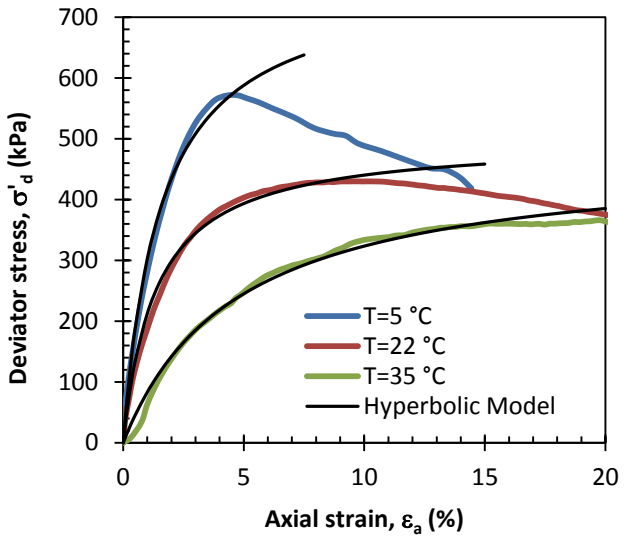

Fig. 4.A.5. Stress-strain behavior and hyperbolic curve fit of stabilized RAS at different temperatures

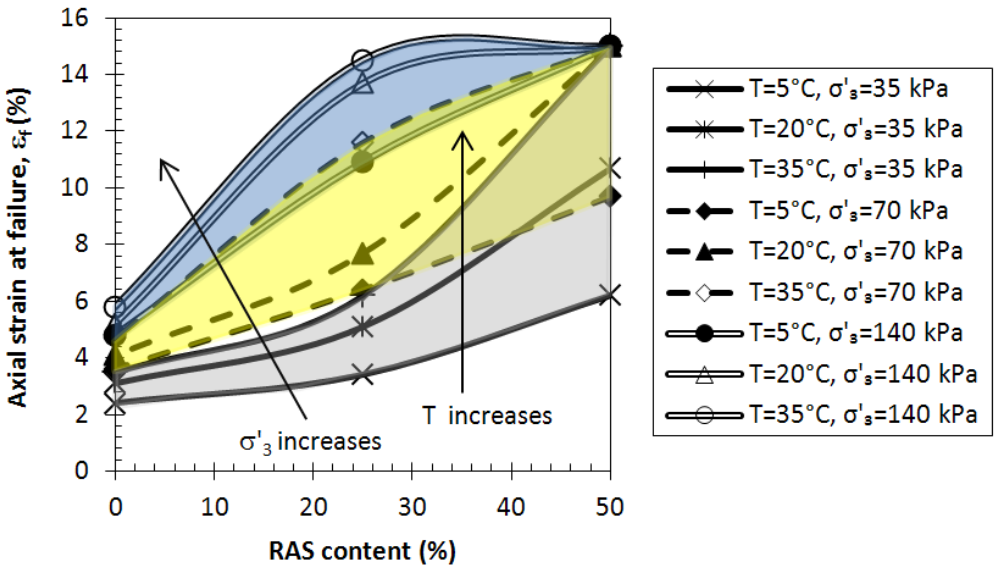

Fig. 4.A.6. Variation of axial strain at failure with temperature and confining pressure

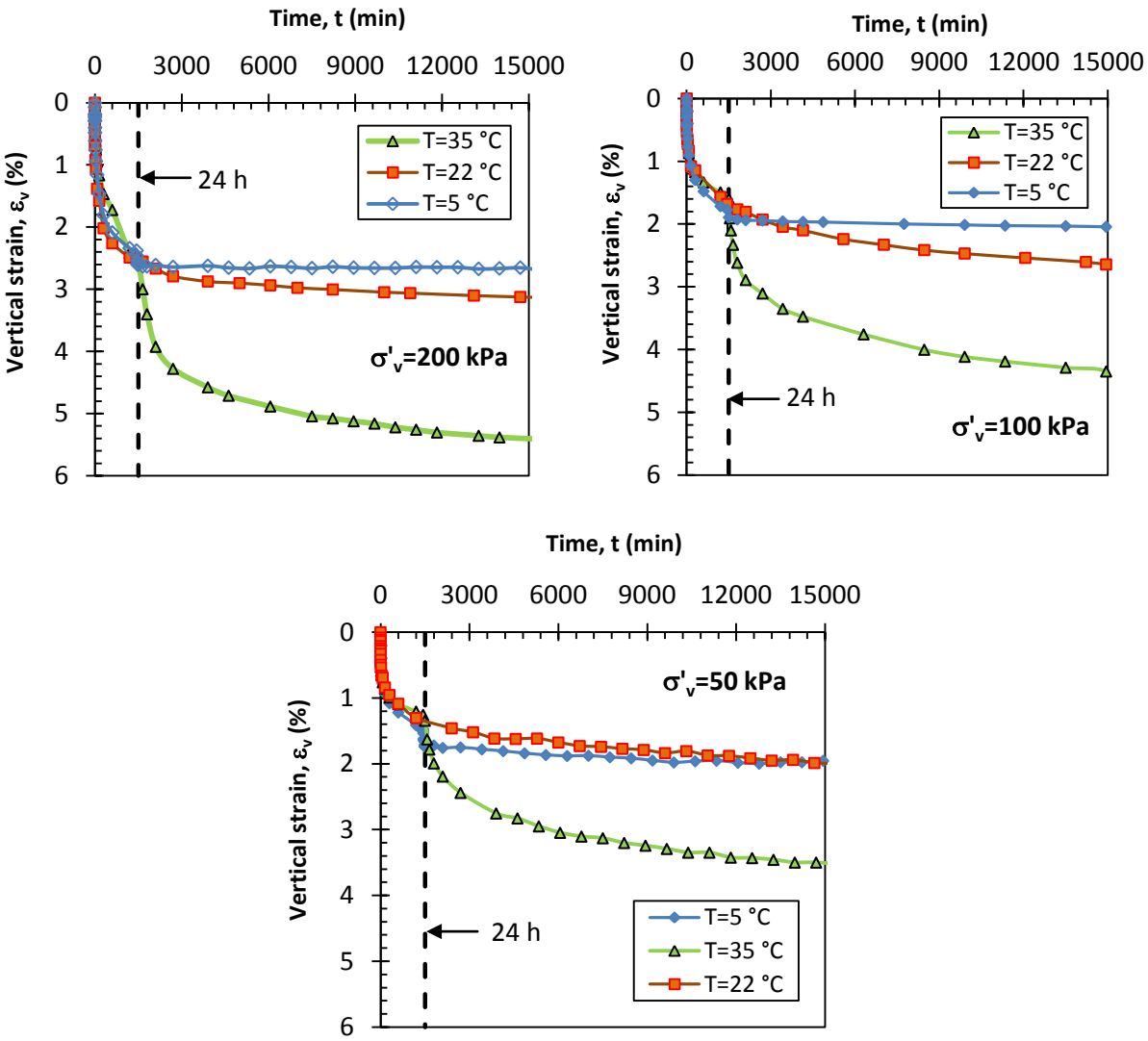

Fig. 4.A.7. Variation of vertical strain with time at different temperatures for RAS:BA (50:50)

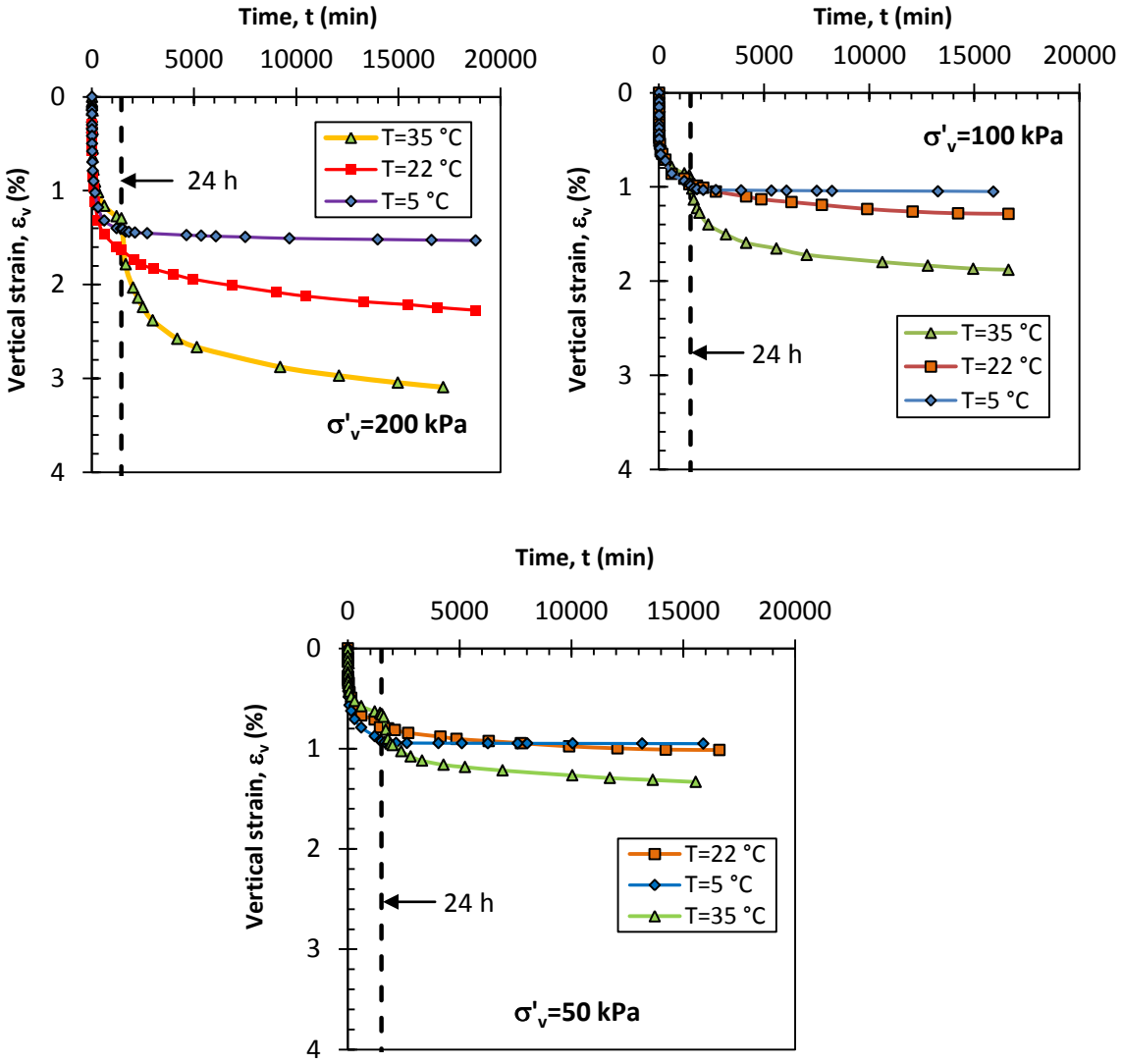

Fig. 4.A.8. Variation of vertical strain with time at different temperatures for RAS:BA (25:75)

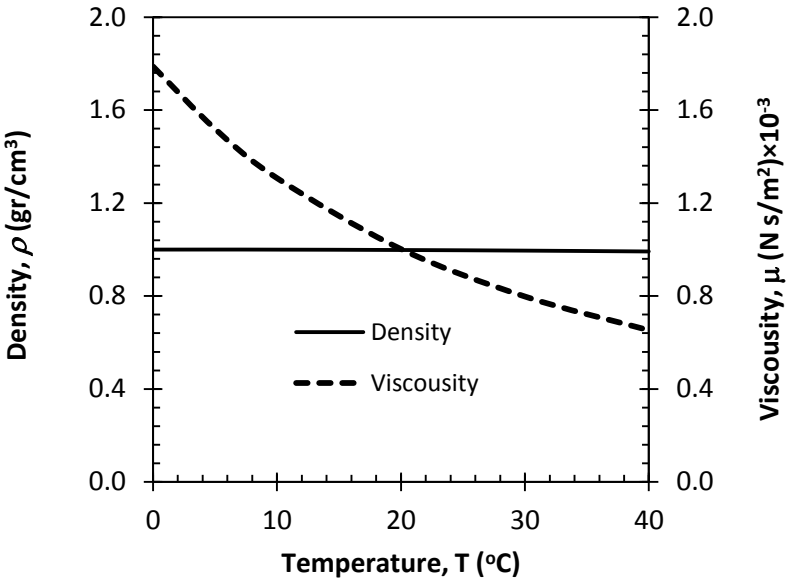

Fig. 4.A.9. Variation of density and viscosity of pore water with temperature

Chapter 5 Shear Creep Response of Recycled Asphalt Shingles

Abstract: Recycled asphalt shingles (RAS) mixed with granular materials or cementitiously stabilized to control their otherwise high compressibility become viable lightweight structural fill material in highway embankments or backfill behind retaining structures. In this research, deviatoric creep response of fly ash-stabilized RAS and RAS mixed with bottom ash (BA) were investigated. Systematic constant stress consolidated-drained triaxial tests were conducted on the stabilized RAS and compacted RAS:BA mixtures at different confining pressures, deviatoric stress levels and temperatures covering a typical range that can be expected in field applications. The results showed a classic creep response for both stabilized RAS and the compacted RAS:BA mixtures. The creep rupture was observed at deviatoric stress levels higher than 80% of the deviatoric stress at failure. The confining pressure also affected the shear creep rate. At higher confining pressure the shear creep rate decreased and the time to creep rupture increased. The temperature change also affected the axial strain and strain rate. The axial strain rate exponentially increases with increasing temperature. To minimize deviatoric strain and strain rate of fill materials containing RAS, construction is recommended during the warm season of the year. Based on the test results, the creep models were developed to evaluate the time-dependent deformation of embankments constructed with fly ash-stabilized RAS or RAS mixed with granular materials. To design the side slopes of the highway embankments containing RAS, the maximum deviatoric stress obtained from the triaxial shear test should be reduced by at least 20% to prevent the creep rupture.

Introduction

Recycled asphalt shingles (RAS) are produced by grinding tear-off roof shingles or manufacturer shingle scraps. Approximately 12 million Mg of asphalt shingle waste is produced per year in the United States, of which only 10 to 20% is reused (Turley 2011). To evaluate possible reuse of asphalt shingle waste in large volume applications, Warner and Edil (2012) investigated potential use of RAS in a pavement structure such as a subbase and Soleimanbeigi et al. (2012) investigated geotechnical properties of RAS, fly ash-stabilized RAS, and the compacted RAS mixed with granular material such as bottom ash (BA). RAS alone has favorable shear strength and drainage characteristics but is compressible. Both stabilized RAS and the compacted RAS:BA mixtures, however, are viable lightweight materials for use in highway embankments or retained backfill (Soleimanbeigi et al. 2012). Use of RAS helps provide a more sustainable geotechnical construction by reducing aggregate production and mining and reducing waste disposal.

Soil creep is the accumulation of time-dependent shear strain under a sustained shear stress that proceeds at a rate controlled by viscous resistance of soil structure (Mitchell and Soga, 2005). Recycled asphalt pavements (RAP) that contain asphalt binder is shown to be subject to creep rupture (Viyanant et al. 2007). RAS also contains asphalt binder and is expected to be subject to excessive creep strain under sustained deviatoric stress in roadway embankments or retained fills. Indeed, Soleimanbeigi et al. (2012) reported that temperature change affects engineering properties of the compacted RAS:BA mixtures and stabilized RAS due to change of viscosity of asphalt binder in RAS. In this study, consolidated drained triaxial tests under constant axial stress were conducted on the compacted RAS:BA mixtures and stabilized RAS to evaluate creep deformation and creep rupture. The tests were performed under different

deviatoric stress levels, confining pressures, and temperatures to more precisely simulate field conditions on creep behavior.

Creep Behavior

The creep response is represented by a relationship between creep strain and the logarithm of time, which may be linear, concave upward or downward as shown in Fig. 5.1. The creep response is often divided into three stages: primary, secondary and tertiary. Following the application of a deviatoric stress in primary stage, the creep rate decreases with time. During secondary stage, the strain rate reaches a constant value for an extended period of time, and under relatively high deviatoric stress levels, the creep rate may start increasing during tertiary stage until a possible creep rupture.

The effect of shear creep is most significant in clayey soil due to higher plasticity, activity and water content of clays (Mitchell and Soga, 2005). Shear creep phenomena have also been observed in sand (Murayama et al. 1984; and Augustesen et al. 2004) albeit sands exhibit smaller creep deformations than clays. The creep mechanism in RAS is attributed to the presence of viscous asphalt binder in the particles. Shear stresses in particulate materials are resisted by the friction at the particle contacts. The asphalt binder at RAS particle contacts affects the deformation response of the compacted RAS and makes the process sensitive to temperature. Singh and Mitchell (1968) developed an empirical model to predict the time-dependent strain rate under a given deviatoric stress during the primary and secondary stages of creep. This creep model, which has been found suitable for description of creep response of a wide variety of soils, is represented by:

$$\dot{\varepsilon}(t) = Ae^{\bar{\alpha}\bar{D}}\left(\frac{t_1}{t}\right)^m \tag{5.1}$$

where $\dot{\varepsilon}(t)$ is the strain rate, A, $\bar{\alpha}$ and m are the model parameters, $\overline{D}$ is the stress level ($\overline{D} = \sigma_d/\sigma_{df}$, where σ_d is the applied deviatoric stress and σ_{df} is the deviatoric stress at failure), t_1 is an arbitrary reference time and t is the elapsed time after application of the stress level. The simplified empirical model of Singh and Mitchell (1968) will be used in this study to evaluate creep response of fly ash-stabilized RAS or compacted RAS:BA mixtures. Due to presence of viscous asphalt binder in RAS particles, temperature change is expected to affect creep response of RAS:BA mixtures or stabilized RAS. The objective is to investigate the creep response at different temperatures.

Creep rupture is defined as the failure of the material at the end of the tertiary creep and the time to rupture, t_r, is the total elapsed time from loading to the final rupture. Singh and Mitchell (1968) clay model does not predict the tertiary creep deformation; however, the prediction of the time to creep rupture was considered by other investigators (Saito and Uezawa 1961; Campanella and Vaid 1974).

Materials

RAS samples were obtained from B.R. Amons & Sons Company in Elkhorn, Wisconsin. Visual inspection indicated that RAS samples were free of impurities such as wood chips, plastics, and nails. Warner (2007) concluded that RAS particles with maximum size (d_{max}) of 10 mm, when compacted, result in higher dry unit weight (γ_d), stiffness and strength. Therefore, in this study, the RAS supply was screened to limit the d_{max} to 10 mm. Bottom ash and self-cementing fly ash samples were obtained from Columbia Power Station in Wisconsin. Fig. 5.2 shows the particle size distribution curves of RAS and BA samples tested according to ASTM D 422. The majority of particles in each sample are sand size (between 0.075 mm and 4.75 mm) according to the

Unified Soil Classification System (USCS). Table 5.1 summarizes the grain size indices and material classification according to the USCS. The RAS and BA particles have almost similar grain size distributions; therefore, grain size distribution of different RAS:BA mixtures falls within a narrow range. The specific gravity (G_s) of RAS measured in accordance with ASTM D854 (method B) is 1.74, which is a positive attribute as a light-weight fill material. The low G_s of RAS is attributed to asphalt cement content and cellulose fiber content, which together comprise from 18 to 40% by weight of RAS. The typical G_s for asphalt binder is between 1.02 and 1.05 (Roberts et al. 1996) and for cellulose fiber is between 1.3 and 1.5 (Klyosov 2007). Bottom ash has the G_s of 2.67, which is comparable to that of sand.

RAS particles are plate-like, irregular in shape, highly angular and have rough surface texture. The angularity of RAS particles reduces to semi-round to round as the particle size decreases. BA particles are angular to highly angular, internally porous and have rough surface texture. Some pores of the particles are filled with dust (Soleimanbeigi et al. 2012). Pure RAS has a well-defined compaction curve with the maximum dry unit weight (γ_{dmax}) of 11.3 kN/m^3 and optimum water content (w_{opt}) of 8% (Fig. 5.3). The γ_d of the compacted RAS:BA mixture increases with increasing BA content. Although BA has comparable specific gravity to sand, the high porosity of BA particles reduces the γ_{dmax} to 15 kN/m^3, which is lower than γ_{dmax} of typical compacted sand. As the BA content increases the γ_d of the mixture becomes less susceptible to water content. Depending on the BA content in the compacted RAS:BA mixture, the γ_{dmax} varies between 11.3 kN/m^3 and 15.0 kN/m^3. Stabilized RAS with 25% self-cementing fly ash has also a well-defined compaction curve with the γ_{dmax} of 13.7 kN/m^3.

The materials used are processed industrial materials or byproducts. Therefore, it is expected that their behavior will vary in a narrow range and thus only one source is used for the

test materials. While the overall behavior is not likely to vary significantly, the quantitative values of the various parameters may be different if materials from other sources are used and therefore should be evaluated for design.

Experimental Program

The specimens prepared for the consolidated drained (CD) triaxial creep tests included the compacted RAS:BA mixtures with BA content of 50% and 75% and stabilized RAS with 20% self cementing fly ash. These mixtures are determined in previous research to be viable for use in structural fill applications (Soleimanbeigi et al. 2012). Table 5.2 summarizes the testing program for CD triaxial creep tests. Each sample was compacted at w_{opt} and 95% of standard Proctor γ_{dmax} in five layers in a split mold with 74 mm diameter and 148 mm height. The number of tamps per layer using a standard Proctor hammer was determined such that the same compaction energy as in the standard compaction effort (592 kN.m/m^3) was applied to each sample mixture. Each compacted RAS:FA specimen was carefully removed from the split mold and cured in a 100% humidity room in a sealed condition. Since the hydration rate of fly ash is time dependent, the 28-d curing period was considered to achieve the majority of hydration of stabilized RAS specimen and minimize the effects of subsequent temperature change on curing.

After assembling the triaxial creep cell, to monitor the volume change of the specimens during creep test, each specimen was backpressure-saturated according to ASTM D 4767 so that a B-value greater than 95% was attained. Following the saturation, each specimen was consolidated for 24 h under σ'_3=70 kPa. Due to high hydraulic conductivity of the compacted RAS:BA mixtures or stabilized RAS, pore water pressure dissipated shortly after the confining pressure was applied. The specimen volume change during consolidation phase was monitored

in the backpressure burette based on outflow of pore water until no significant volume change was observed. After 24-h consolidation period, creep tests at room temperature (i.e. 22^{o}C) were conducted by applying different stress levels, $\overline{D}$ (as a fraction of strength), ranging from 0.2 to 0.95 as summarized in Table 5.2 on the specimens. To evaluate the effect of confining pressure on creep response of the compacted RAS:BA mixture, each specimen was consolidated at four different confining stresses (i.e., 35 kPa, 70 kPa, 140 kPa, and 280 kPa) prior to loading at $\overline{D}$=0.9. The selected confining pressures were calculated based on a consideration of typical heights of highway embankments and the unit weight of the compacted RAS:BA mixtures or stabilized RAS. The stress ratio of 0.9 was selected to make sure that creep rupture occurs and investigate the effect of confining pressure on creep rupture. To determine the deviator stress at failure (σ_{df}), first consolidated drained tests were performed on compacted RAS:BA mixtures and stabilized RAS. Axial loading was applied at an axial strain rate of 3.0%/h, which is considered to provide drained condition during loading based on comparison with similar soils as well as computations made using the pore water expulsion rate during the consolidation stage. The volume change of each specimen during shearing was recorded from the volume change of water in backpressure tubing.

Creep tests at elevated temperatures were conducted in a temperature controlled triaxial cell. The cell consists of a conventional triaxial cell equipped with a heating and cooling system. The heating and cooling system was designed to induce a temperature range of 5 ^{o}C to 35 ^{o}C on the specimens. The selected temperature range represents the typical field temperature range in the US (Soleimanbeigi et al. 2012). Heating of each RAS:BA or stabilized RAS specimen was implemented by circulating heated water through a copper coil (6 mm outside diameter) placed inside the triaxial cell and spiraled around the specimen. There is a 3.0 cm distance between the

copper coil and the specimen to avoid contact during shearing. The water is heated inside a heating bath using a 250 W heater. A 12 V compact mini circulating pump, which is placed outside of the heating bath, circulates the heated water from the heating bath into the copper coil inside the triaxial cell. Tygon plastic tubes were used outside the triaxial cell to minimize temperature loss during water circulation. Temperatures in the heating bath, in the cell chamber, and inside the specimen were measured using three K-type thermocouples. To control and maintain the target temperature of the specimen, a LabView program was written to regulate the electrical power to the heater by means of a relay installed in the electrical circuit. A temperature tolerance of ±0.5 ^{o}C was allowed. Fig. 5.4 illustrates the schematic of the heating system. To avoid disturbance of the specimens due to insertion of thermocouples inside them, a correlation between the temperature inside the specimen and inside the cell chamber was obtained on a dummy specimen. Fig. 5.5 shows the variation of temperatures inside the heating bath (T_h), inside the cell (T_c), and inside the specimen (T_s). The required time to bring the T_s to the target temperature is less than 100 min. The target temperature of the specimen for the actual tests was then controlled by the temperature inside the cell considering the 100-min time lag. The cooling bath is a calibrated refrigerator that maintains the temperature of the water down to 5 ^{o}C. The circulating pump is placed inside a PVC box which is filled with water and placed inside the refrigerator. The target temperature of the specimen is controlled by regulating the power supply to the circulating pump using a program written in LabView. The circulating pump is switched off if T_c is below 5 ^{o}C. A tolerance of ±0.5 ^{o}C was allowed for T_c to reduce the number of turn-on/off of the pump. Similar to the heating system, the required time to bring the T_s to the target temperature is less than 100 min as illustrated in Fig. 5.5(a). The volume change of the specimen during heating and cooling of the cell was also recorded and shown in Fig. 5.5(b). The

volumetric expansion or compression during cooling or heating of the cell is less than 0.5% and occurs in less than 100-min. Since compression and loading of the specimens are conducted 24 h after temperature change, the volumetric change measurement during creep tests at elevated temperatures will not be affected by the volumetric change of the cell water during heating or cooling.

After consolidation at σ'_3=70 kPa, axial loading corresponding to a given $\overline{D}$ was applied to the specimen at room temperature for 24 h. The temperature of the specimen was then brought to the target temperature (i.e., 5 ^{o}C or 35 ^{o}C) over 100 min. The volume change of each specimen during creep deformation was recorded from the volume change of water in the backpressure burette. In addition to constant temperature creep tests, the effect of temperature cycle history on the creep behavior of compacted RAS:BA mixtures and fly ash-stabilized RAS specimens was also evaluated. For thermal cycling tests, after loading at a given $\overline{D}$, the temperature of each specimen increased to 35 ^{o}C for an extended period of time and then reduced to room temperature while recording the creep deformation.

Creep Response of RAS:BA Mixture

The results of CD triaxial compression tests on the compacted RA:BA mixtures are shown in Fig. 5.6. The increase of BA content in the mixture, increases the maximum deviator stress (σ_{df}) and transforms the volume change from compressive to dilative. Increase of confining pressure increases the σ_{df} and the corresponding axial strain and transforms the volumetric change behavior from dilative to compressive. Fig. 5.7 shows the results of creep test at room temperature on the compacted RAS:BA mixture which contains 50% RAS. The axial strain versus log time curves corresponding to different stress levels show that the compacted RAS:BA

mixture exhibits the first and second stages of classical creep behavior and creep rupture does not occur. The continued creep test at $\overline{D}$=0.8 for 6 weeks shows that axial strain linearly increases with log *t* in the second stage of creep. The axial strain rate linearly decreases with time in a logarithmic scale indicating that the compacted RAS:BA mixtures follow the classical creep behavior observed in clay. The slope of the line is the creep rate parameter denoted as *m* in Eq. (5.1). Table 5.3 includes *m* values for clay, sand, frozen sand and RAP. The materials with high creep potential like clay have *m* between 0.4 and 0.7 whereas materials with low creep potential like sand exhibits *m* between 0.9 and 1.0. The average best-fit *m* for the stress levels of $\overline{D}$=0.8 and 0.6 over the entire data points is 1.03 indicating that creep rupture should not be a concern when using compacted RAS:BA mixture with 50% BA as the structural fill. At $\overline{D}$=0.2, 0.4 and 0.6, the average best-fit *m* increases from 0.83 during t < 5700 min to 1.2 corresponding to t > 5700 min as indicated in Fig. 5.7(c). The increase in *m* (i.e. reduction in strain rate over time) might be due to reduction of void ratio of the RAS:BA specimen over time. The Poisson's ratio of the asphalt binder is approximately 0.5 indicating that the asphalt binder is an incompressible material. Reduction in void ratio over time might therefore have an impact on reducing the compressibility of the compacted RAS:BA specimens. The reduction in *m* over time was also observed in RAP (Viyanant et al. 2007). Fig. 5.8(a) shows the variation of log $\dot{\varepsilon}$ with $\overline{D}$ at different *t* after loading. The variation of log $\dot{\varepsilon}$ with $\overline{D}$ indicates a series of lines with identical slopes and different intercepts. The slope of the lines, which represents the parameter $\bar{\alpha}$ in Eq. 5.1 are averaged to 4.8. The y intercept of each line at $\overline{D}$=0 and corresponding to an arbitrary t_1 indicates parameter A in Eq. 5.1. The y intercept of the line corresponding to t_1=1 min at $\overline{D}$=0 is 0.061. The characterized creep model for the compacted RAS:BA mixture containing 50% BA is therefore represented by:

$$\dot{\varepsilon} = 0.061e^{3.83\bar{D}}\left(\frac{1}{t}\right)^{m}\ ,\ \begin{cases}\text{m} = 0.83 \text{ for t} < 5700 \text{ min}\\ \text{m} = 1.20 \text{ for t} > 5700 \text{ min}\end{cases} \quad (5.2)$$

Fig. 5.9 shows the results of creep tests on the compacted RAS:BA mixtures containing 75% BA. At a given stress level, the axial strains of the specimen are significantly reduced with increased amount of less compressible BA particles. The $\varepsilon - \log t$ curves show that the compacted RAS:BA mixture exhibits the first and second stages of classical creep behavior and creep rupture occurs at $\bar{D} > 0.8$. The axial strain rate linearly decreases with time in a logarithmic scale indicating that the compacted RAS:BA mixture containing 25% BA also follows the classical creep behavior. Additional creep tests at $\bar{D}$ < 0.80 showed that axial strain rate log-linearly decreases with time and the average best-fit *m* is 0.91 indicating less creep susceptibility with increasing BA content. Fig. 5.10 shows the linear variation of log strain rate with $\bar{D}$ at different times. The curves have similar slopes with the average of $\bar{\alpha}$=4.58. The intercept *A* at t_1=1 min is 0.022. The characterized creep model for RAS:BA mixture containing 75% BA is therefore represented by:

$$\dot{\varepsilon} = 0.022e^{4.58\bar{D}}\left(\frac{1}{t}\right)^{0.91} \quad (5.3)$$

Creep Rupture

The creep rupture is identified by increasing axial strain rate with time in the log $\dot{\varepsilon}$-log *t* curve.. Unlike the mixture with 50% BA, creep rupture for the mixture containing 75% BA occurred at $\bar{D}$ > 0.8 as illustrated in Fig. 5.9(b). The continued creep test at $\bar{D}$=0.8 for 6 weeks shows that axial strain linearly increases with log *t* in the second stage of creep without any sign of rupture. The time to rupture increased as $\bar{D}$ decreased from 0.95 to 0.83. Campanella and Vaid (1974) reported that time to creep rupture is controlled by the time it takes the cumulative axial strain to reach a critical strain value which for Haney Clay was approximately the strain corresponding to the maximum deviatoric stress. Similar observations were made by Ting (1983) for frozen sand

and Viyanant et al. (2007) for RAP. The increase of axial strain rate or creep rupture at $\overline{D}$ > 0.8 for the RAS mixture with 75% BA content can also be explained from the shape of the stress-strain curve at σ_3'=70 kPa shown in Fig. 5.6(a). The deviatoric stress reaches to the peak at axial strain of 5.8% followed by strain softening due to dilative response illustrated in Fig. 5.6(b). During the creep test, as the cumulative axial strain [see Fig. 5.9(a)] reaches to the value corresponding to the post-peak strength, the tertiary creep was initiated. The cumulative axial strain at the initiation of tertiary creep under $\overline{D}$=0.95 is 6.7% which is higher than 5.8%, the axial strain corresponding to peak deviatoric stress. However, as the BA content in the RAS mixture is reduced to 50%, the ductility of the mixture and the axial strain corresponding to peak deviatoric stress are increased as shown in Fig. 5.6. Therefore, the cumulative axial strain did not reach to the critical axial strain during the testing time and the creep rupture was observed.

The time corresponding to $\dot{\varepsilon}_{min}$ is the time to rupture, t_r. The t_r and $\overline{D}$ were plotted in semi log scale and shown in Fig. 5.11(a). The time to rupture increases with decreasing stress level. The relationship between t_r and $\overline{D}$ shows a nonlinear trend for both compacted RAS:BA mixture and stabilized RAS. The time to rupture nonlinearly increases with reducing $\overline{D}$. The nonlinear relationship between t_r and $\overline{D}$ were also observed for RAP (Viyanant et al. 2007) and Haney Clay (Campanella and Vaid 1974). As identified from Figures 9(b), the compacted RAS:BA mixture at $\overline{D}$=0.8 did not rupture after five weeks. Fig. 5.11(a) estimates that nonlinear relationships between time to rupture and stress level represents an asymptote to an upper yield stress of approximately 0.8 for the compacted RAS:BA mixture. Below the upper yield strength, the material is not expected to experience creep rupture under the applied deviatoric stress. The estimated upper yield strength for RAP was 0.60 which shows that RAP is more susceptible to rupture than RAS mixtures. The majority of RAP particles are covered by asphalt coating which

increases the shear strain in the particle contacts under an applied shear stress. However, in the RAS:BA mixture only 25% of the mass contains RAS particles with asphalt binder at the contact surfaces. In addition, the asphalt binder used in manufacturing the asphalt shingles is air-blown which is harder and has higher viscosity than the binder used in the hot mixed asphalt (Krivit 2007). Finn and Snead (1973) suggested that upper yield strength of a material is estimated from the intercept of a linear relationship between stress level and cube root of minimum strain rate. Fig. 5.11(b) shows the relationship between $\overline{D}$ and $(\dot{\varepsilon}_{min})^{\frac{1}{3}}$ for the compacted RAS:BA mixture and other materials. The intercept of the $\overline{D}$ axis determines the upper yield strength of 0.81 for the compacted RAS:BA mixtures indicating that if the materials are subjected to the deviatoric stress level lower than 0.81, the creep rupture is unlikely to occur. The estimated upper yield strength of Haney Clay is 0.74 and of RAP is 0.60. The results are similar to the upper yield strengths estimated from Fig. 5.11(a).

Effect of Temperature

The effect of temperature change on the log $\dot{\varepsilon}$- log *t* curves of the compacted RAS:BA mixture with 75% BA content is demonstrated in Figures 12(a) to (c). At a given *t* and $\overline{D}$, the strain rate increases with increasing temperature from 5 ^{o}C to 35 ^{o}C. At $\overline{D} = 0.4$, the initial strain rate increases from 0.088 %/min to 0.263 %/min when the temperature increase from 22 ^{o}C to 35 ^{o}C and reduces to 0.037 %/min when the temperature is lowered to 5 ^{o}C. However, the best-fit *m* is identical at different temperatures and is averaged to 0.86 at $\overline{D}$=0.4, 0.95 at $\overline{D}$=0.6 and to 1.01 at $\overline{D}$=0.8. Figures 13(a) to (c) represent the variation of $\dot{\varepsilon}$ with temperature at different $\overline{D}$ and *t*. At each $\overline{D}$, the log $\dot{\varepsilon}$ linearly varies with temperature and the best-fit curves over the data points have almost identical slopes at different *t* with a coefficient of variance varying between 10 and

15%. Similar behavior was observed for the compacted RAS:BA mixture with 25% RAS content. The slope of these curves is defined as the coefficient of thermal creep with unit of 1/ ^{o}C and is denoted by $C_{\varepsilon T}$. The $C_{\varepsilon T}$ decreases with increasing the stress ratio as shown in Fig. 5.13(d). The creep of the compacted RAS:BA mixture is more significant at larger stress levels. Design factor of safety for the slopes is generally low (i.e., slightly above 1) as opposed to design factor of safety for foundations (i.e., ~ 3.0), thus the mobilized stress levels in the slopes are large, which makes the compacted RAS:BA mixture more susceptible to potential creep problems. Therefore the $C_{\varepsilon T}$ corresponding to stress ratio of 0.8 is recommended for design consideration, which is 0.033 1/ ^{o}C for the mixture containing 50% RAS and 0.012 1/ ^{o}C for the mixture containing 25% RAS. From Fig. 5.13(a), the equation of the best fitting line is represented by:

$$\frac{dln\dot{\varepsilon}(t)}{dT} = C_{\varepsilon T} \tag{5.4}$$

By integration of Eq. 5.4 over the temperature change, the following relation is obtained:

$$\dot{\varepsilon}(T,t) = \dot{\varepsilon}(T_o,t)e^{C_{\varepsilon T}(T-T_o)} \tag{5.5}$$

where T_o is the room temperature. Eq. 5.5 indicates that the strain rate exponentially changes with temperature. By substitution of Eq. 5.1 to Eq. 5.5 we obtain:

$$\dot{\varepsilon}(T,t) = Ae^{\overline{\alpha}\overline{D}}\left(\frac{t_1}{t}\right)^m e^{C_{\varepsilon T}(T-T_o)} \tag{5.6}$$

or $$\dot{\varepsilon}(T,t) = Ae^{\overline{\alpha}\overline{D}+C_{\varepsilon T}\Delta T}\left(\frac{t_1}{t}\right)^m \tag{5.7}$$

Eq. 5.6 indicates that strain rate is an exponential function of temperature. The exponential effect of temperature on strain rate obtained in Eq. 5.7 is in close agreement with the well-known rate processes theory, which was developed in part from triaxial compression tests on clay specimens at elevated temperatures (Mitchell et al. 1968). The basis of the theory is that the atoms and molecules participating in a deformation process (termed flow units) are constrained from movement relative to each other by virtue of energy barriers separating adjacent equilibrium positions. The displacement of flow units to new positions requires that they become activated through acquisition of sufficient energy to overcome the energy barrier. From the consideration of statistical mechanics it is known that the flow units are in fact not at rest but vibrate with a frequency of $\frac{kT_a}{h}$ as a consequence of their thermal energy, where *k* is Boltzmann's constant (1.38×10^{-16} erg $^{o}K^{-1}$) and h is Planck's constant (6.624×10^{-27} erg sec^{-1}) and T_a is the absolute temperature in ^{o}K. In the absence of applied potentials to the material no consequences of the activation are observed since barriers will be crossed with equal frequency in all directions. However, if a directed potential such as a temperature change is applied to the material, the energy barriers are reduced and the flow units are displaced from their original equilibrium positions. The strain rate in response to variations in temperature are given by (Mitchell et al. 1968):

$$\dot{\varepsilon} = \mathrm{X}\frac{kT_a}{h} exp\left(-\frac{E}{RT_a}\right) \tag{5.8}$$

where X is the function of the flow units in the direction of deformation and the average component of displacement in the same direction; *R* is the universal gas constant ($8.314\ \frac{J}{mol.K}$) and *E* is the experimental activation energy (constant). If X and *E* are independent of temperature, then from Eq. 5.8:

$$\frac{\partial ln\left(\frac{\dot{\varepsilon}}{T}\right)}{\partial \frac{1}{T}} = -\frac{E}{R} \tag{5.9}$$

Therefore if identical specimens are subjected to creep tests under the same stress intensity but at different temperatures, there should be a linear variation between $\frac{\dot{\varepsilon}}{T}$ and $\frac{1}{T}$. The behavior was verified for clay (Mitchell et al. 1968; Mitchell and Soga 2005) and a similar behavior is observed for RAS mixtures.

Effect of Thermal Cycle

Fig. 5.14 shows the effect of thermal cycle on the strain rate of the compacted RAS:BA mixture. Creep tests at $\overline{D}$=0.8 were conducted on two identical specimens. Specimen 1 sustained the applied deviatoric stress at constant room temperature throughout the test. However, after 24 h compression, the temperature of specimen 2 increased to 35 ^{o}C during stage 1 as shown on Fig. 5.14. The axial strain rate of specimen 1 in this stage is 450×10^{-6} %/min whereas for specimen 2 increased to 2200×10^{-6} %/min. During stage 2 of the creep test, the temperature of specimen 2 reduced to room temperature. The average strain rate at this stage is reduced to 25×10^{-6} %/min reflecting 6 times reduction compared to strain rate of specimen 1 which is 150×10^{-6} %/min. At stage 3, the temperature of specimen 2 increased to 35 ^{o}C for 72 hr. The strain rate of specimen 2 increased to 110×10^{-6} %/min which is close to the 98×10^{-6} %/min for specimen 1. At stage 4, temperature of specimen 2 was reduced to room temperature. The corresponding strain rate reduced to 3.6×10^{-6} %/min which is 18 times lower than the strain rate of specimen 1 (64×10^{-6} %/min) at the same stage and is close to strain rate of bottom ash (1.7×10^{-6} %/min) at t > 13000 min. This observation indicates that thermal cycle induces preconsolidation on the compacted RAS:BA mixture and therefore the axial strain and strain rate is greatly reduced. The reduced strain rate might result from the increased rate of reduction in void space in the specimen due to

increased viscosity of asphalt binder in RAS which tends to deform and rearrange in denser configuration. The rapid reduction in void ratio occurred at higher temperature, reduces the compressibility at the subsequent room temperature. The results suggest that the construction of embankments incorporating RAS be made during warm seasons of the year to minimize the creep deformation during the rest of the year.

Effect of Confining Pressure

The effect of confining stress (σ'_3) on creep response of the compacted RAS:BA (25:75) mixture at $\bar{D}$=0.9 is illustrated in Fig. 5.15(a). Although Eq. 5.1 does not include the effect of σ'_3 on strain rate, however σ'_3 appears to affect the axial strain and strain rate of the compacted RAS:BA mixture. At σ'_3 =35 kPa, the axial strain rapidly increases and the specimen start to rupture after 2 min. As the σ'_3 increases to 70 kPa, the axial strain and strain rate decreases and the time to rupture increases to 12 min. However the trend is not consistent. The tests at 35 and 70 kPa initially experience lower strain but quickly accelerate to creep rupture while the tests at 140 kPa or higher, initially experience larger strain but take more time to rupture. The initial strain rates of the specimens at 35 and 70 kPa are significantly higher than those observed at 140 and 280 kPa. The smaller initial strain rate at low confining pressure may be due to possible induced overconsolidation due to compaction energy applied when preparing the specimen. On the other hand, the time to creep rupture and the creep rate parameter *m* consistently increases with increasing confining pressure as illustrated in Fig. 5.15(b). At shown in Fig. 5.6, the stress-strain behavior of the compacted RAS:BA specimen changes from strain softening to strain hardening with increasing confining pressure. The volumetric behavior also changes from dilative to compressive. compressive It appears that at higher σ'_3, the asphalt binder in RAS

particles deforms to reduce void spaces in the RAS:BA specimen. Since asphalt binder is incompressible, at reduced void space, the specimen exhibits lower axial strain under a given *t* and $\overline{D}$.

Creep Response of Fly Ash-Stabilized RAS

Fig. 5.16 shows the axial strain and strain rate of stabilized RAS at different stress levels. The material exhibits a log-linear relationship between axial strain rate and time before initiation of creep rupture. The tertiary creep and creep rupture occurs at $\overline{D} \geq 0.85$ whereas at $\overline{D} \leq 0.8$ the material exhibits secondary creep response where the strain rate log-linearly reduces with time with no indication of creep rupture after five weeks. The average best-fit *m* over $\overline{D}$=0.8, 0.7 and 0.6 is 0.78 for t < 10000 min which indicates the creep susceptibility and possible rupture of the stabilized RAS. However, similar to the compacted RAS:BA mixture with 50% RAS, the continued creep test on the stabilized RAS showed that *m* increases to 1.25 over t > 10000 min. Similar behavior was observed during creep response of RAP (Viyanant et al. 2007). The *m* value for RAP at t < 1000 min was about 0.8 and increased to 1.4 between t=1000 min and t=15000 min and increased dramatically to 2.6 at t > 15000 min. Viyanant et al. (2007) hypothesized that the asphalt coating on the grain size becomes compressed so that there is little bitumen at the grain contacts of the aggregate particles and since the direct particle contacts are less susceptible to creep, less creep would be observed. However there were no direct observations to confirm their hypothesis. During creep of stabilized RAS, the volumetric change of the specimen was measured in the backpressure burette. Fig. 5.16(c) shows the volumetric change of stabilized RAS under different stress levels. At $\overline{D} \geq 0.8$, despite initial compression of the specimen, volumetric strain increased and material exhibits dilative behavior at the initiation

of creep rupture. However at $\overline{D} \leq 0.8$, the material exhibits compression and the void ratio is reduced. At $\overline{D}$=0.6, the void ratio gradually reduces from 0.4 to 0.34 during the creep test. Since asphalt binder and sand particles in the mixture are incompressible, reduction in void ratio will reduce deformability of the specimen which subsequently reduces the axial strain and strain rate. Parameters A and $\bar{\alpha}$ obtained from y intercept and slope of the log axial strain rate with stress level are 0.032 %/min and 4.60 %/min respectively.

Creep Rupture

As shown in Fig. 5.16(b), the stabilized RAS experienced creep rupture at $\overline{D} > 0.8$. The time to rupture, t_r and $\overline{D}$ were plotted in semi log scale and shown in Fig. 5.11(a). The time to rupture is increased with decreasing the stress level. The time to rupture nonlinearly increases with reducing $\overline{D}$. As identified from Fig. 5.16(b), the stabilized RAS did not rupture after five weeks under $\overline{D}$=0.80. Fig. 5.11(a) estimates that nonlinear relationships between time to rupture and stress level represents an asymptote to an upper yield stress of approximately 0.8 for the stabilized RAS. Below the upper yield strength, the material is not expected to experience creep rupture under the applied deviatoric stress. The estimated upper yield strength for RAP was 0.60 which shows that RAP is more susceptible to rupture than RAS mixtures. The upper yield strength of stabilized RAS from the Finn and Snead (1973) method is estimated as $\overline{D}$=0.82 which is intercept of $\overline{D}$ axis as shown in Fig. 5.11(b). If the stabilized RAS is subjected to the deviatoric stress level lower than 0.82, the creep rupture is unlikely to occur. The result is similar to the upper yield strengths estimated from Fig. 5.11(a).

Effect of Temperature

Fig. 5.17 shows the effect of temperature rise and thermal cycle on creep response of stabilized RAS. Increasing temperature increases the axial strain under sustained load and the volumetric change behavior becomes more compressive. Temperature rise accelerates the axial strain and volume reduction which therefore reduces the strain when the temperature drops back to room temperature. Axial strain rate of the specimen that experienced a temperature rise showed a 10-fold reduction compared to the specimen that deformed at a constant room temperature during the test. Similar to the compacted RAS:BA mixture, if the structural fill containing stabilized RAS material is constructed during warm seasons, the majority of deviator strain on the side slopes occurs during the construction and the strain rate during the subsequent seasons decreases. Unlike the compacted RAS:BA specimens, systematic creep tests on stabilized RAS at different temperatures did not result in consistent variations between axial strain rate and temperature. The coefficient of thermal creep decreased with time. The reason may be attributed to temperature dependency of hydration process of fly ash. Although the asphalt binder viscosity reduces with temperature, the increase in bonding strength between the particles (Soleimanbeigi et al. 2012) will reduce susceptibility of the stabilized RAS with temperature.

Summary and Implication

Compacted RAS:BA mixtures and stabilized RAS are favorable lightweight material for possible use as structural fill. In this research, creep response of the compacted RAS:BA mixtures and stabilized RAS was investigated for use in highway embankment fills. The results show that the materials have similar classical creep behavior to soils with the log axial strain rate linearly decreasing with log time. The creep rate parameters are 0.8 and 0.9 respectively for the RAS:BA

mixtures containing 50% and 25% RAS and 0.78 for the stabilized RAS indicating that these materials are susceptible to creep rupture especially at high stress levels. The upper yield strength below which the creep rupture does not occur was estimated to about 0.80 for both RAS:BA mixture and stabilized RAS. The design engineer should keep the maximum shear stress to at least 20% below the shear strength when designing slopes of the highway embankment or retaining structures to make sure no creep rupture will occur during lifetime of the earth structures. The reduction in shear stress results in flatter slopes for the embankments indicating that larger amount of RAS will be used, which is beneficial to the purpose of reusing asphalt shingle waste. Results of deviatoric creep tests at elevated temperatures showed that temperature change affects creep response of RAS containing fills. The axial strain rate is an exponential function of temperature. The slope of the log axial strain rate with time defined as coefficient of thermal creep is constant at different times and stress levels but varies with RAS content in the mixture and is 0.033 1/ ^{o}C for 50% RAS content and 0.012 1/ ^{o}C for 25% RAS content. The creep model parameters developed in this study can be used in numerical analysis to evaluate creep deformations of earth structures constructed with RAS.

To reduce axial strain rate and possibility of creep rupture, construction of embankments containing RAS are recommended in warm seasons. At higher temperature, the axial strain occurs at higher rate during construction due to reduced viscosity of asphalt binder. Therefore, during the rest of the year when the temperature drops, the increased viscosity of the asphalt binder in RAS and reduced void spaces in the structural fills reduce the strain rate and creep of the RAS contained embankment fill. Although the laboratory test results indicate that the strain rate during the next heating cycle of 35 ^{o}C, i.e., representing the summer heating in the season following construction, is still higher than the strain rate of natural soils, it is significantly lower

(20 times) than the strain rate during the first heating cycle of 35 ^{o}C, i.e., representing construction in the first summer. It is noted that the laboratory temperature simulating the first and second summers was considered the same (i.e. 35 ^{o}C). However, when the embankment is constructed and the road is paved, surface pavement will almost act as a thermal insulator and the temperature in the RAS containing embankment in the second summer is expected to be lower than whatever the temperature is during the first summer when the RAS mixture is directly exposed to warm weather during construction, which indicates lower anticipated creep rate.

Conclusions

In this paper deviatoric creep behavior of compacted RAS:BA mixture and fly ash-stabilized RAS was evaluated at varying temperatures and stresses. At large deviatoric stress levels, creep rupture should be a concern when using the compacted RAS:BA mixture or stabilized RAS as structural fill. To minimize potential of creep rupture in a structural fill, the design engineer should keep the maximum shear stress to at least 20% below the shear strength when designing slopes of the highway embankment or retaining structures to make sure no significant creep rupture is likely to occur during lifetime of the earth structures. The strain rate exponentially increases with temperature which can be beneficial to minimize the creep deformation and possible creep rupture if the construction of the structural fill is conducted during a warm season. Construction of the RAS containing structural fill during mild or cold seasons of the year is not recommended, as there will be greater potential for creep in subsequent warm season. Reclaimed asphalt shingles can be used in construction of highway embankment fills taking into account their intrinsic characteristics such as compressibility and temperature sensitivity during design

and construction. Such high-volume use not only resolves the disposal problem of the material but also helps provide a more sustainable roadway construction using recycled materials.

References

Augustesen, A., Liingaard, M., and Lade, P.V. (2004). "Evaluation of time-dependent behavior of soils." *International Journal of Geomechanics, ASCE,* 4(3): 137-156.

Campanella, R.G., and Vaid, Y.P. (1974). "Triaxiual and plain strain creep rupture of an undisturbed clay." *Canadian Geotechnical Journal*, 11(1): 1-10.

Finn, W. D. L., and Snead, D. (1973). "Creep and creep rupture of an undisturbed sensitive clay." *In Proceedings of the 8th International Conference on Soil Mechanics and Foundation Engineering.* USSR National Society for Soil Mechanics and Foundation Engineering, Moscow, 1.1, 135-142.

Klyosov A.A. (2007). *Wood-plastic composites*. John Wiley & Sons, Inc. Hoboken, NJ.

Krivit, D. (2007). *Recycling of Tear-Off Shingles: Best Practices Guide*. Final report prepared for the Construction Materials Recycling Association (CMRA).

Mitchell, J. K. (1969). "Temperature effects on engineering properties and behavior of soils." *Highway Research Board*, Special Report No. 103, Washington, DC, 9-28.

Mitchell, J. K., Campanella, R. G. and Singh, A. (1968). "Soil creep as a rate process." *Journal of Soil Mechanics and Foundation Division, ASCE,* 94, 231-253.

Mitchell, J. K., Singh, A. and Campanella, R. G. and (1969). "Bonding, effective stresses and strength of soils." *Journal of Soil Mechanics and Foundation Division, ASCE,* 95, 1219-1246.

Mitchell, J. K. and Soga, K. (2005). *Fundamentals of soil behavior*. John Wiley & Sons, Inc., New York.

Monkman, F. C., and Grant, N. J. (1956). "An empirical relationship between rupture life and minimum creep rate in creep-rupture tests." *Proceedings of the American Society of Testing and Materials*, 56, 593-620.

Murayama, S., Michihiro, K., and Sakagami, T. (1984). "Creep characteristics of sand", *Soils and Foundations,* 24(2): 1-15.

Viyanant, C., Rathje, E. M., and Rauch, F. A. (2007). "Creep of compacted recycled asphalt pavement", *Canadian Geotechnical Journal*, 44, 687-697.

Rao, S. M. and Shivananda, P. (2005). "Role of curing temperature in progress of soil-limereactions." *Technical Note, Geotechnical and Geological Engineering*, 23, 79-85.

Roberts, F. L., Kandhal, P. S., Brown, E. R., Lee, D. Y. and Kennedy, T. W. (1996). *Hot Mix Asphalt Materials, Mixture Design, and Construction*. National Asphalt Paving Association Education Foundation. Lanham, MD.

Singh, A., and Mitchell, J. K. (1968). "General stress-strain-time function for soils." *Journal of the Soil Mechanics and Foundations Division, ASCE,* 94(SM1): 693-709.

Soleimanbeigi, A., Edil, T. B., and Benson, C. H. (2012). "Recycled asphalt shingles mixed with granular byproducts as structural fill", *Journal of ASTM International*, 9(1): 1-19.

Soleimanbeigi, A**.**, Edil, T. B., and Benson, C. H. (2012). "Evaluation of fly ash stabilization of recycled asphalt shingles for use in structural fills", *ASCE Journal of Materials in Civil Engineering,* 25(1):1-12.

Soleimanbeigi, A., Edil, T. B., and Benson, C. H. (2012). "Effect of temperature on geotechnical engineering properties of recycled asphalt shingles mixtures", *Journal of Geotechnical and Geoenvironmental Engineering, ASCE (prepared for submission).*

Saito, M., and Uezawa, H. (1961). "Failure of soil due to creep." In Proceedings of the fifth International Conference on Soil Mechanics and Foundation Engineering, Paris, July 17-22, Dunod, Paris, pp. 315-318.

Ting, J.M. (1983). "On the nature of the minimum creep rate-time correlation for soil, ice and frozen soil." *Canadian Geotechnical Journal*, 20, 176-182.

Turley, W. (2011). Personal Communication. *Construction Materials Recycling Association*, Eola, IL.

Veisi, M., Chittoori, B., Celaya, M., Nazarian, S., Puppala A. J. and C. Solis (2010). *Accelerated stabilization design of subgrade soils*. Center for Transportation Infrastructure Systems, University of Texas at El Paso, Conducted for Department of Transportation in cooperation with Federal Highway Administration, Research Report No. 055691.

Warner, J., and Edil, T. (2012). "An Evaluation of Reclaimed Asphalt Shingles for Beneficial Reuse in Roadway Construction." *Journal of ASTM International*, 9(1), DOI: 10.1520/JAI103665

Table 5.1. Grain size indices and USCS classifications RAS, bottom ash and outwash sand

Material	d_{10} (mm)	d_{50} (mm)	C_u	C_c	Fines (%)	Gs	USCS symbol	USCS name
RAS	0.17	1.1	7.6	1.6	3.8	1.74	SW	Well graded sand
Bottom ash	0.19	0.9	6.3	0.8	1.9	2.67	SP	Poorly graded sand

d_{10}: effective particle size (particle size for which 10% of the sample is finer than d_{10}); d_{50}: median particle size (particle size for which 10% of the sample is finer than d_{50}); C_u: coefficient of uniformity (d_{60}/d_{10}); C_c: coefficient of curvature ($C_{30}^2/(C_{10} \times C_{60})$); G_s: specific gravity; USCS: Unified Soil Classification System

Table 5.2. Creep test program on RAS:BA mixtures or stabilized RAS

Materials	T (^{o}C)	σ'_3 (kPa)	$\overline{D}$	# of Tests
RAS:BA (50:50)	20	70	0.2, 0.4, 0.6, 0.8, 0.9	5
RAS:BA (50:50)	5, 35	70	0.4, 0.6, 0.8	6
RAS:BA (25:75)	20	70	0.2, 0.4, 0.6, 0.8, 0.83, 0.86, 0.9, 0.95	8
RAS:BA (25:75)	20	35, 70, 140, 280	0.8	3
RAS:BA (25:75)	5, 35	70	0.4, 0.6, 0.8	6
RAS:BA (25:75)	20-35-20	70	0.8	1
Stabilized RAS	20	70	0.6, 0.7, 0.8, 0.9, 0.95	5
Stabilized RAS	20-35-20	70	0.8	1

Table 5.3. Creep rate parameter m for different soils

Material	m	Reference
Osaka clay	1.0	Singh and Mitchell (1969)
San Fransisco Bay mud	0.75	Singh and Mitchell (1969)
Seattle clay	0.5	Singh and Mitchell (1969)
Haney clay	0.4-0.7	Campanella and Vaid (1974)
Sand	0.9-1.0	Augustesen et al. (2004)
RAP	0.7-0.9	Viyanant et al. (2007)
Frozen sand	0.75-0.85	Ting (1983)

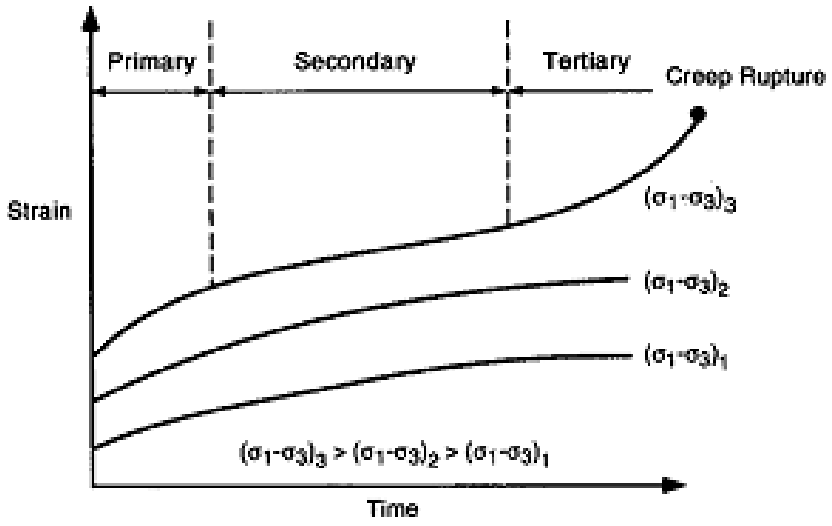

Fig. 5.1. Creep under constant deviator stress (after Mitchell and Soga 2005)

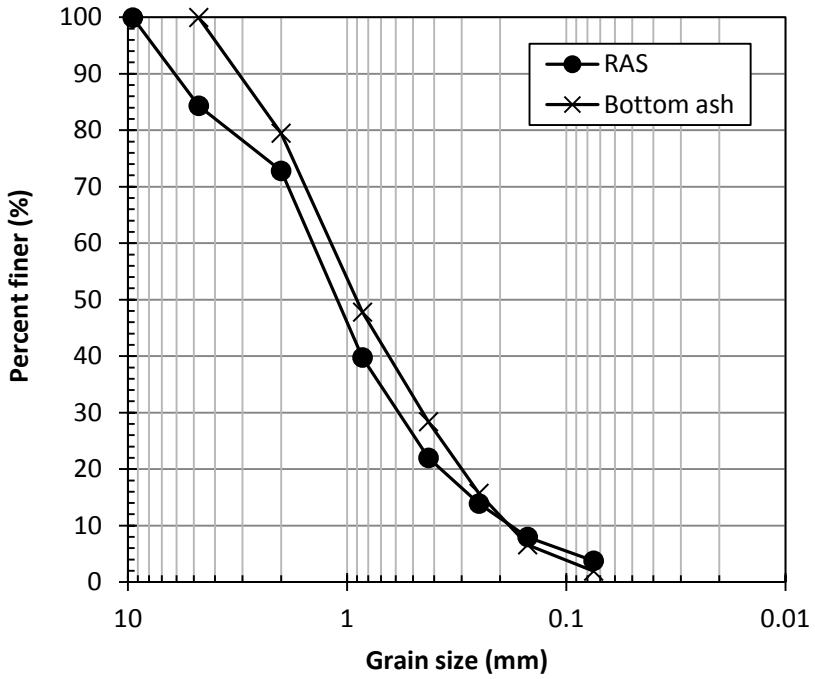

Fig. 5.2. Grain size distribution of RAS and bottom ash

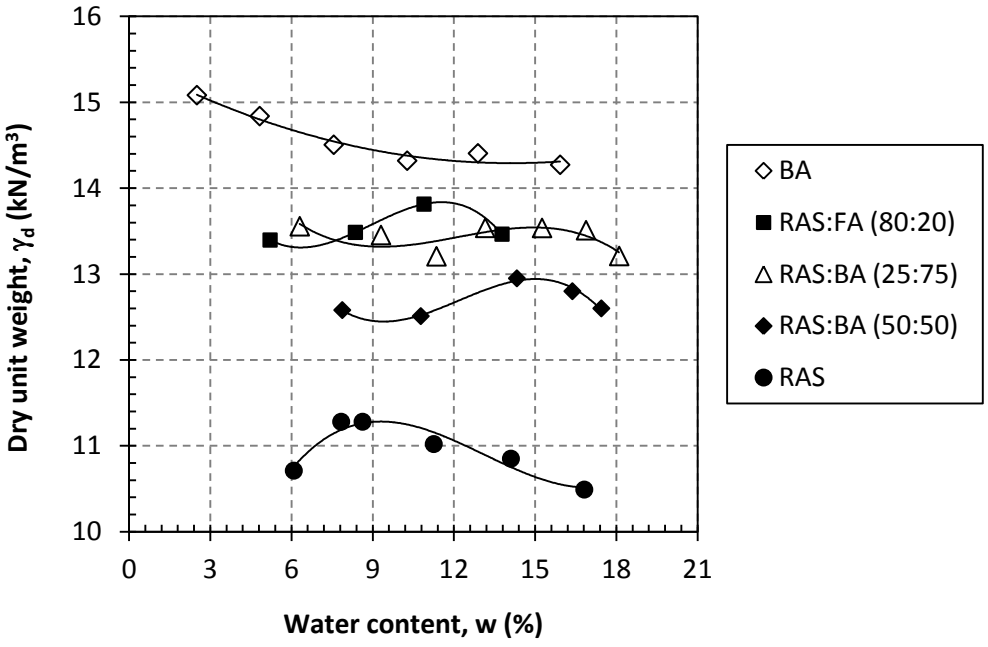

Fig. 5.3. Compaction curves of RAS:BA mixture and stabilized RAS

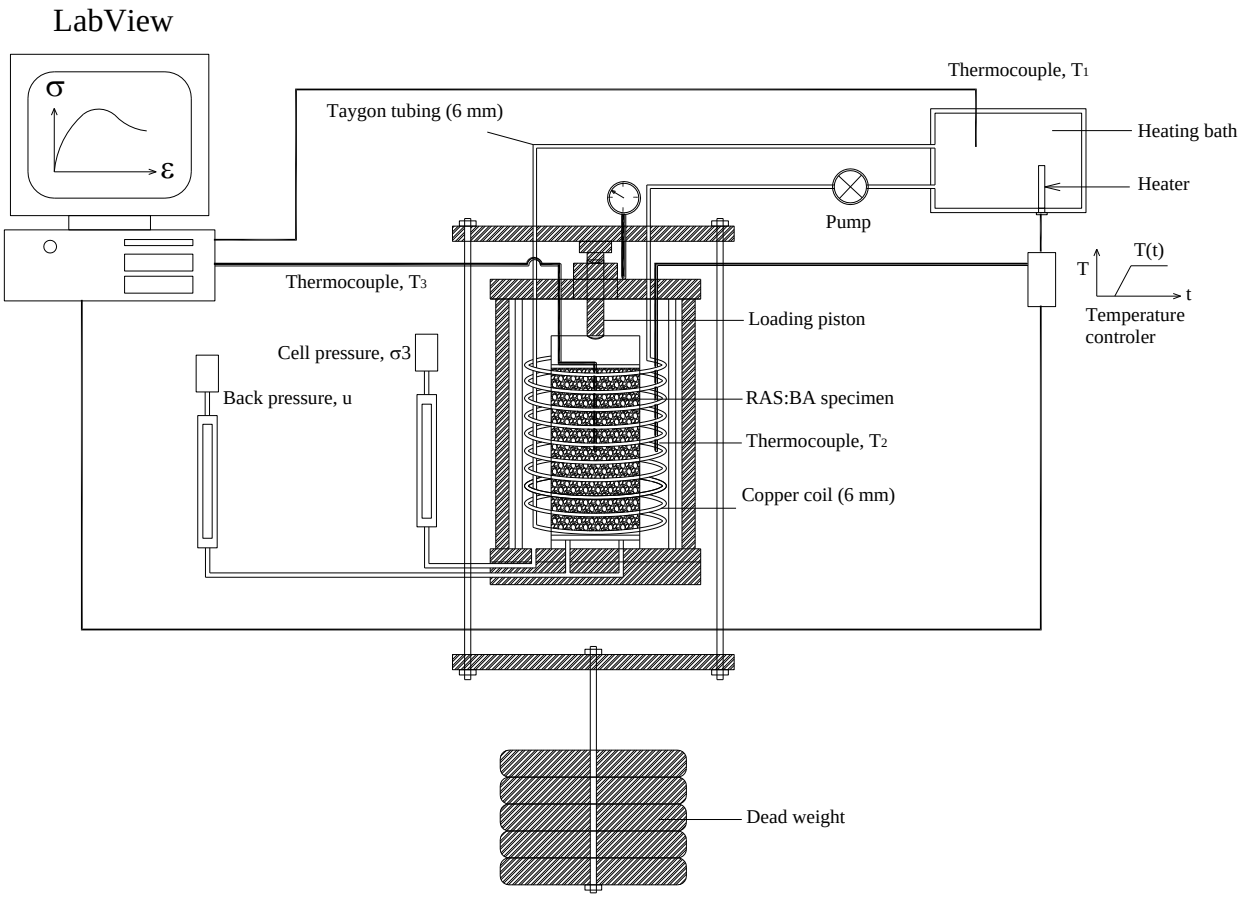

Fig. 5.4. Schematic of temperature controlled triaxial creep system

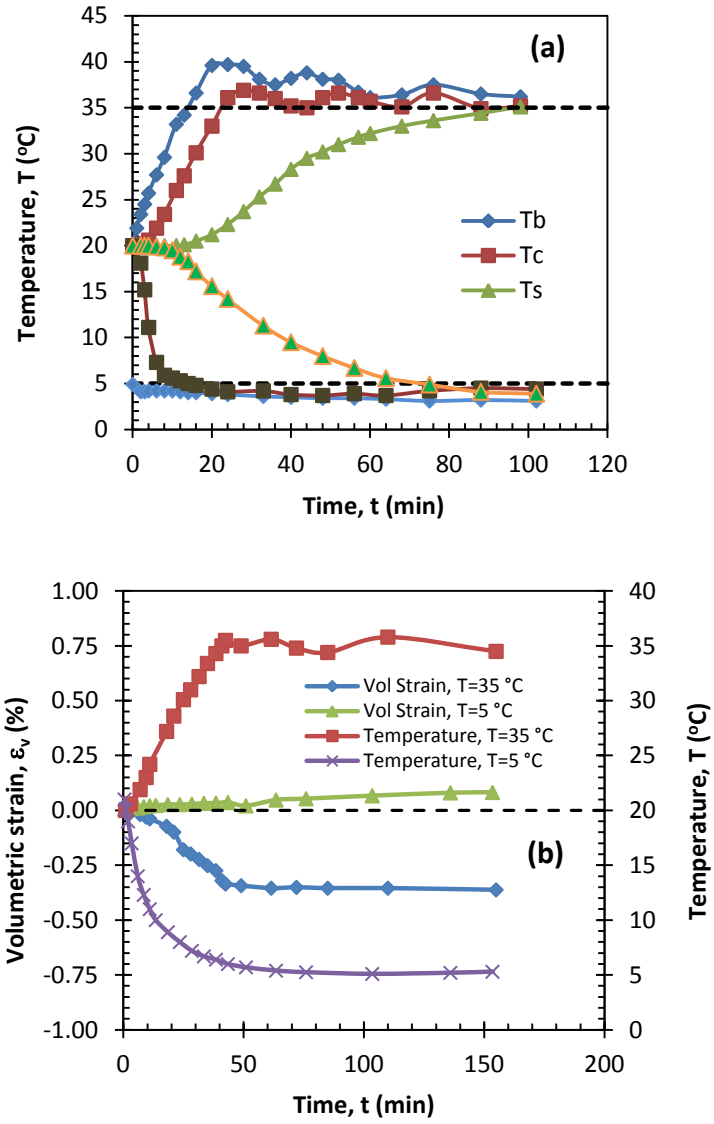

Fig. 5.5. Calibration curves for temperature variation in heating/cooling bath, cell and specimen for the temperature controlled triaxial cell (T_b=bath temperature, T_c=cell temperature, T_s=specimen temperature) (a), volumetric strain of in triaxial cell (b)

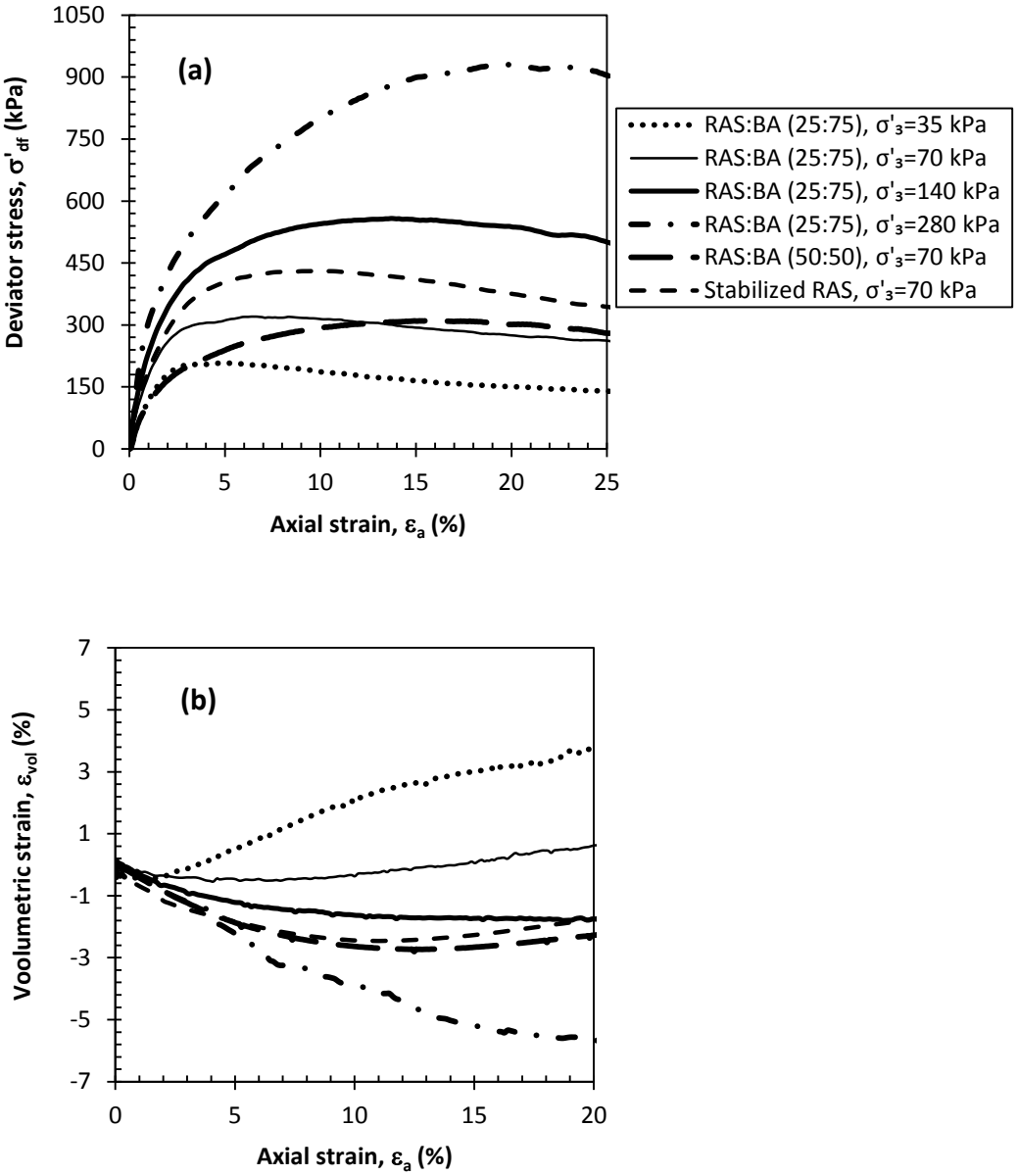

Fig. 5.6. Results of CD triaxial compression tests: (a) stress-strain behavior and (b) volumetric change behavior of compacted RAS:BA mixture and stabilized RAS

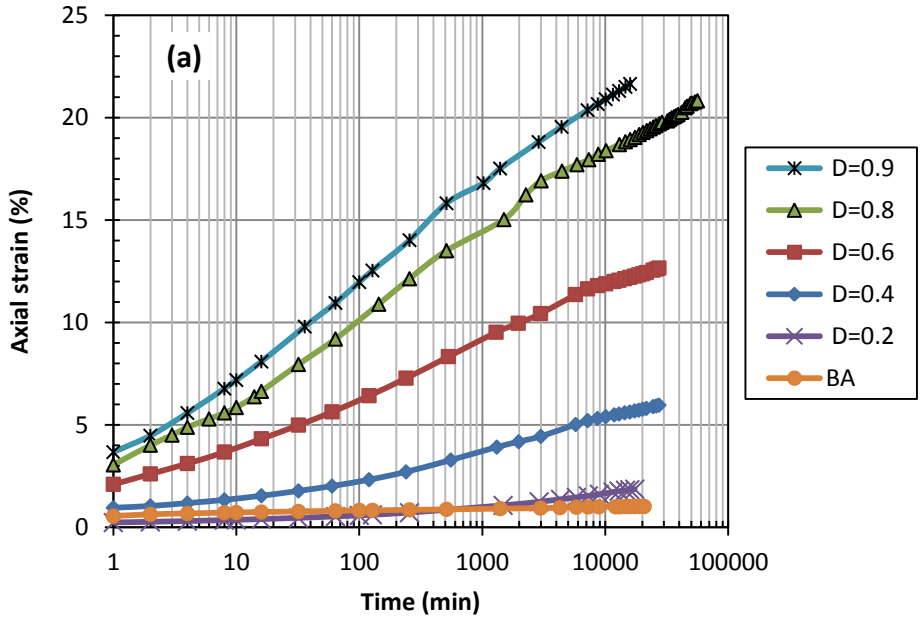
(a)
Axial strain (%)
Time (min)
25
20
15
10
5
0
1
10
100
1000
10000
100000
D=0.9
D=0.8
D=0.6
D=0.4
D=0.2
BA

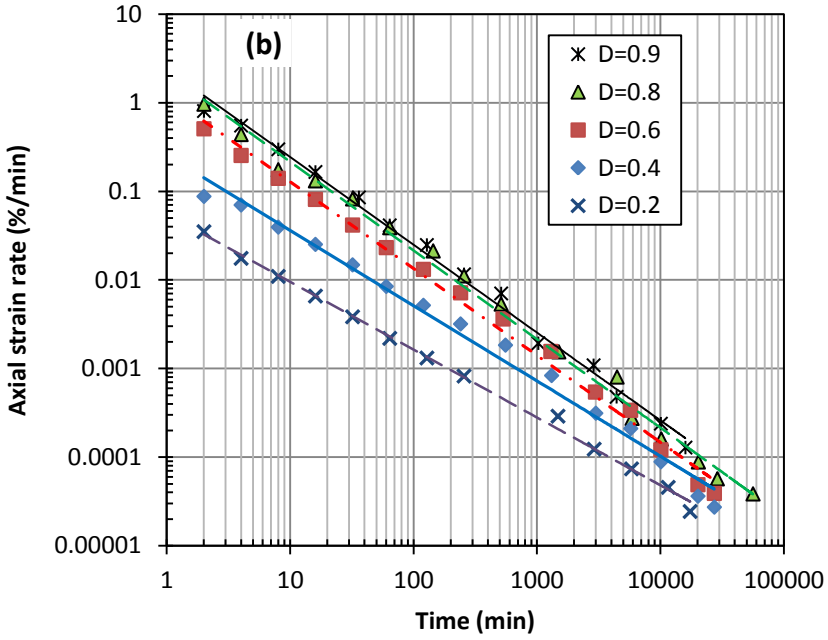
(b)
Axial strain rate (%/min)
Time (min)
10
1
0.1
0.01
0.001
0.0001
0.00001
1
10
100
1000
10000
100000
D=0.9
D=0.8
D=0.6
D=0.4
D=0.2

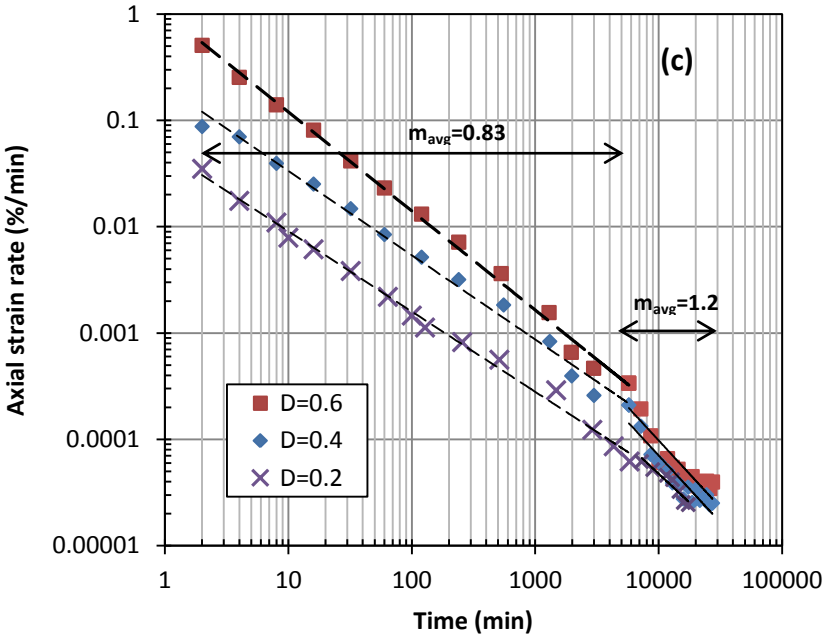

Fig. 5.7. Axial strain (a) and axial strain rate (b) (all specimens) and (c) (specimens with D=0.2 to 0.6) versus time for RAS:BA (50:50) at σ'_3=70 kPa

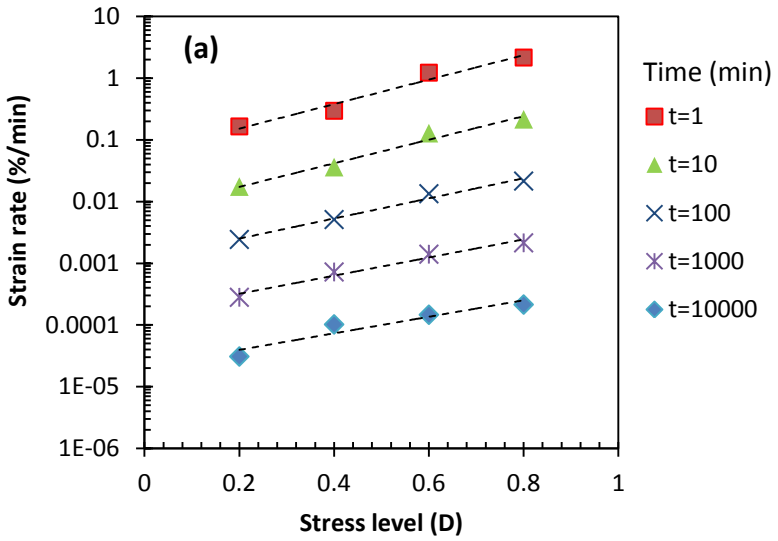

Fig. 5.8. Axial strain rate versus stress level

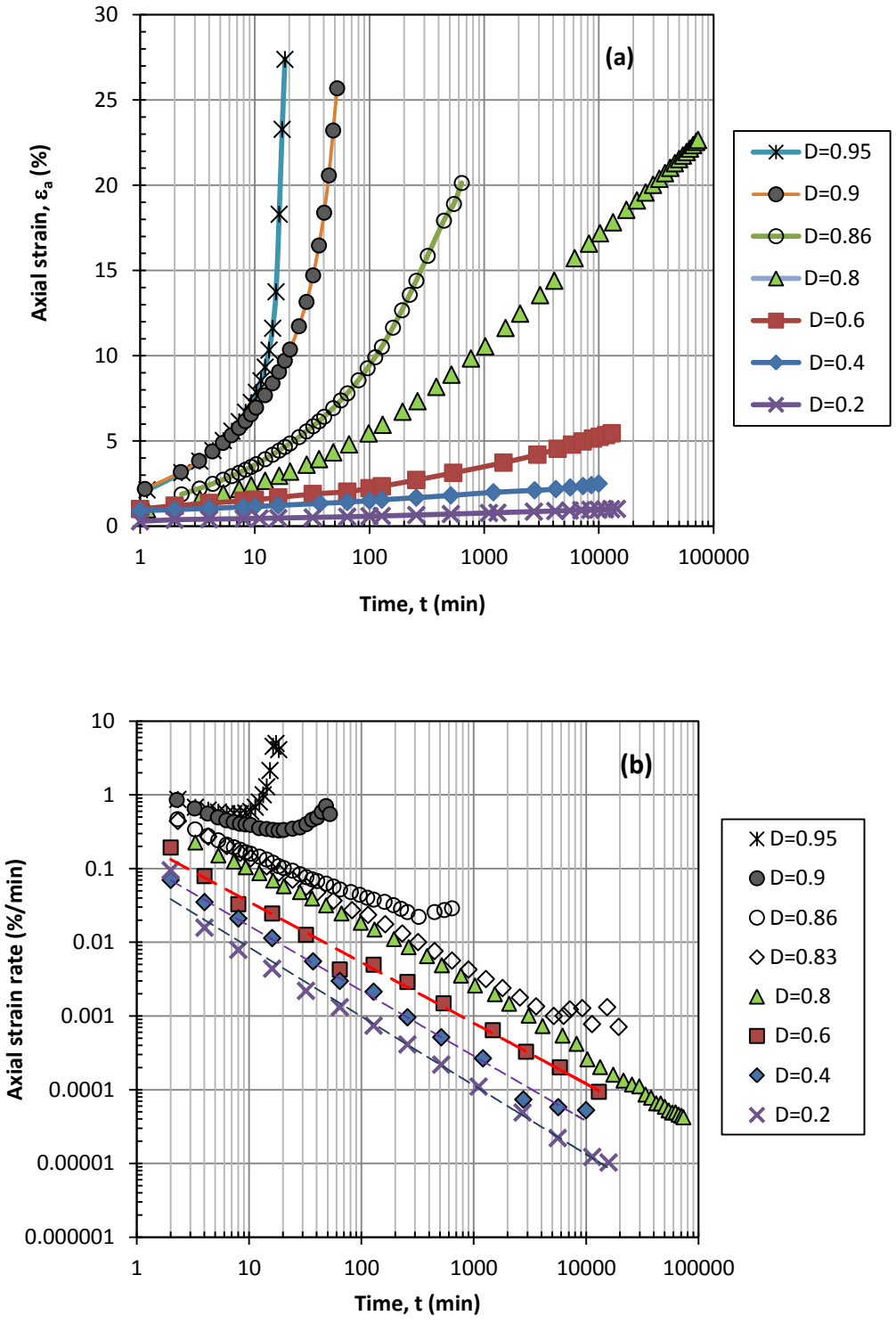

Fig. 5.9. Axial strain (a) and axial strain rate (b) versus time for RAS:BA (25:75) at σ'_3=70 kPa

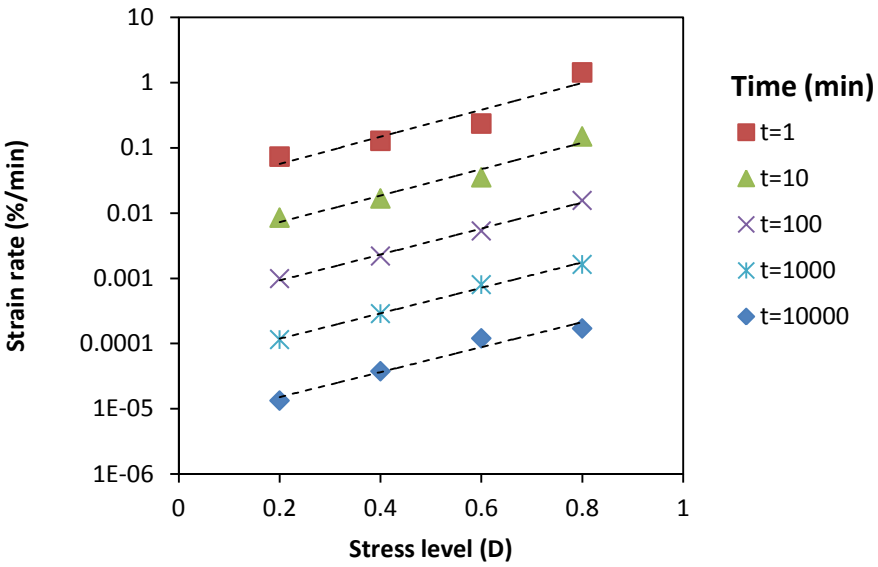

Fig. 5.10. Axial strain rate (a) versus stress level for RAS:BA (25:75) at σ'_3=70 kPa

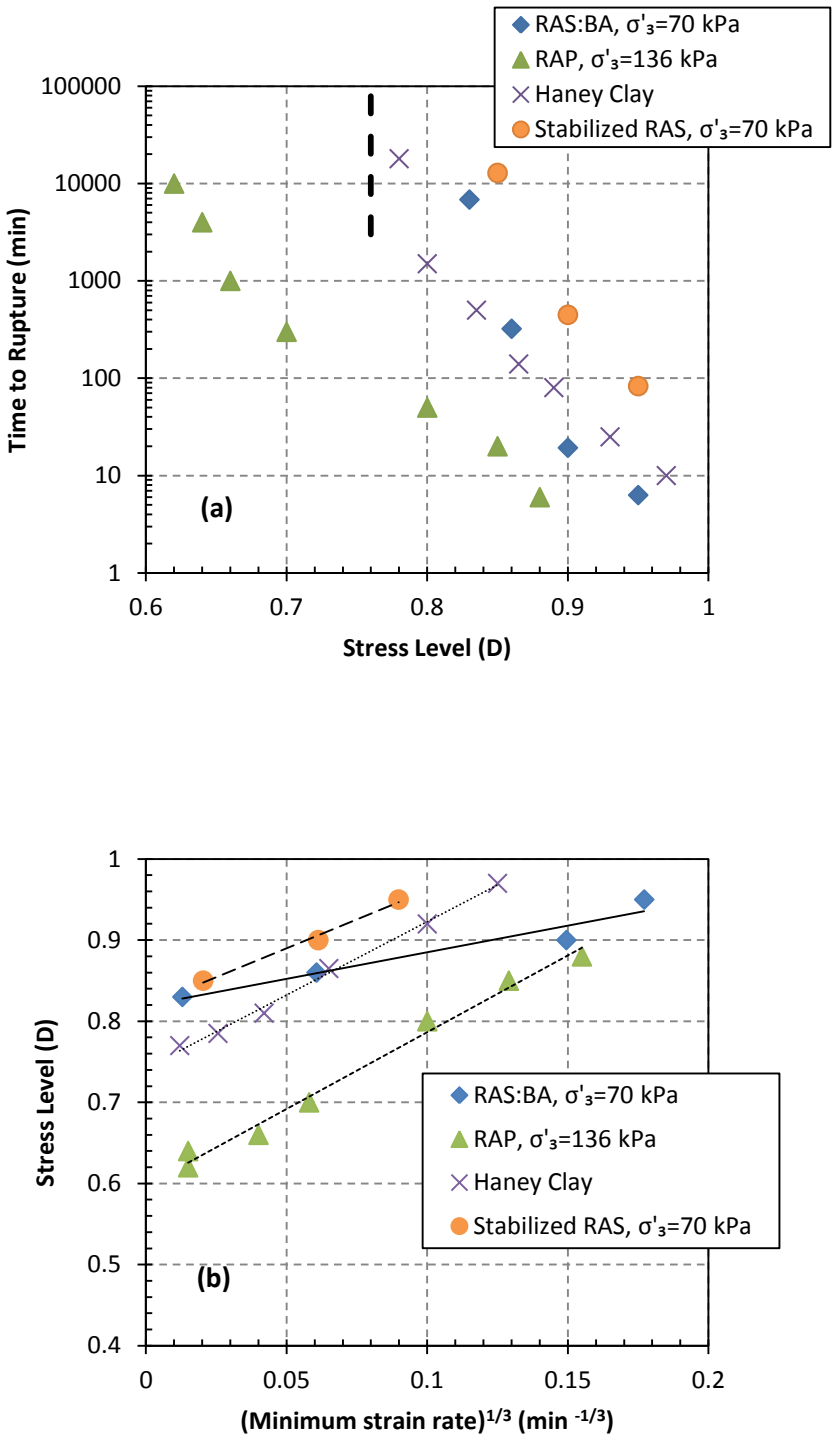

Fig. 5.11. Time to rupture (a) and upper yield stress (b)

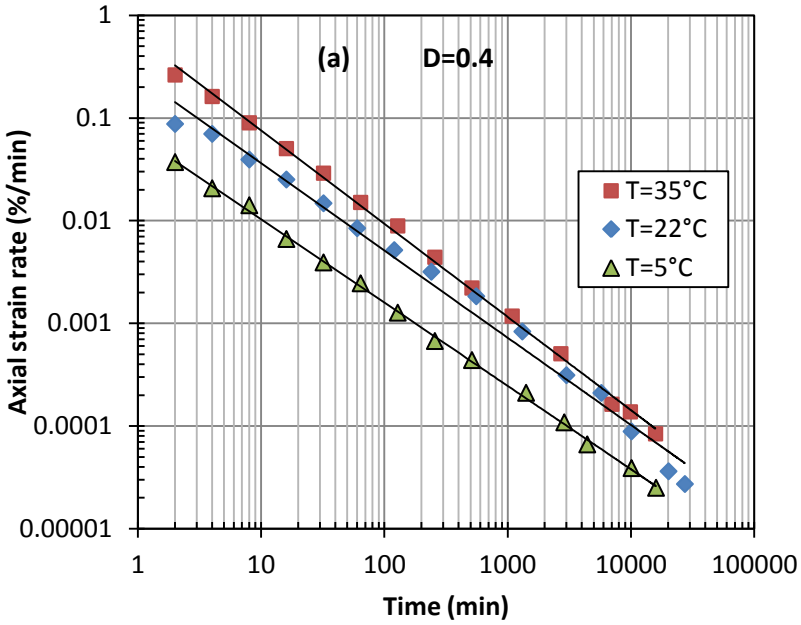
(a)
D=0.4
T=35°C
T=22°C
T=5°C
Axial strain rate (%/min)
Time (min)
1
0.1
0.01
0.001
0.0001
0.00001
1
10
100
1000
10000
100000

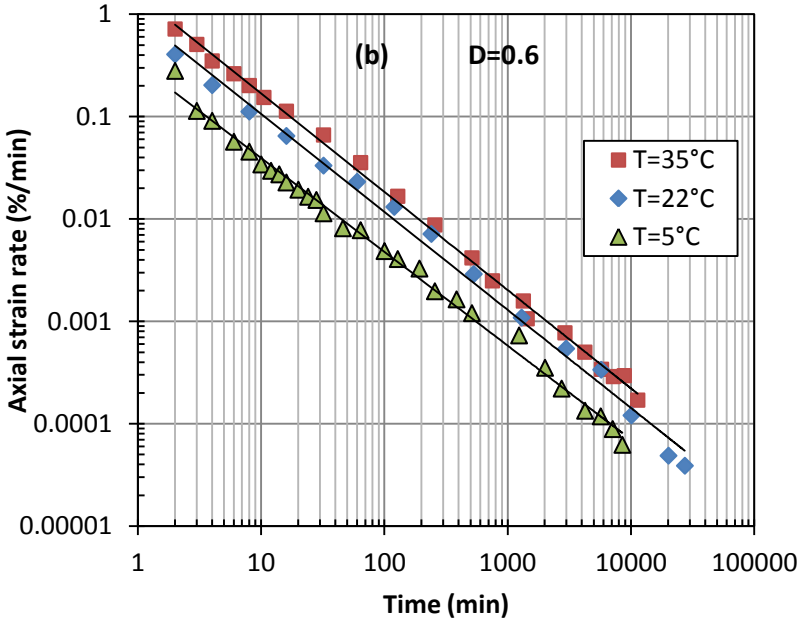
(b)
D=0.6
T=35°C
T=22°C
T=5°C
Axial strain rate (%/min)
Time (min)
1
0.1
0.01
0.001
0.0001
0.00001
1
10
100
1000
10000
100000

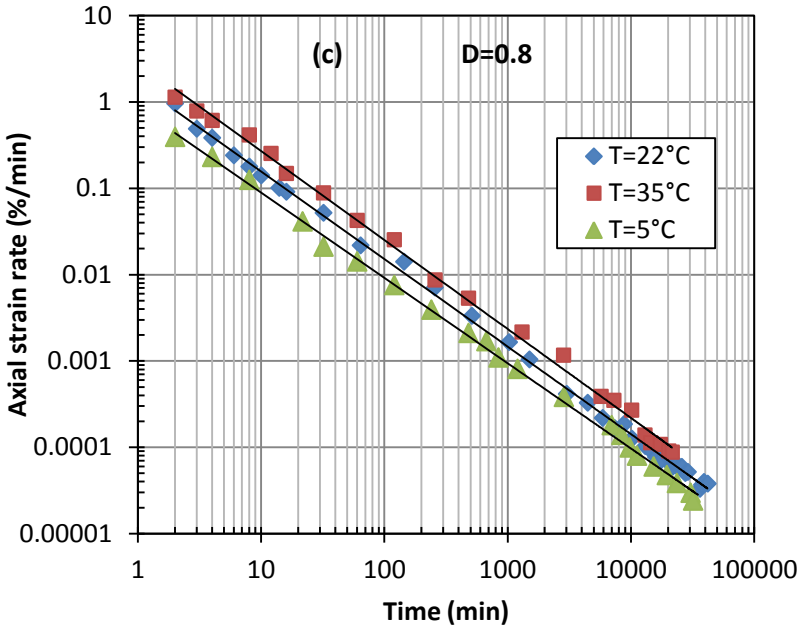

Fig. 5.12. Axial strain rate with log of time at different temperatures under (a) D=0.4; (b) D=0.6; and (c) D=0.8

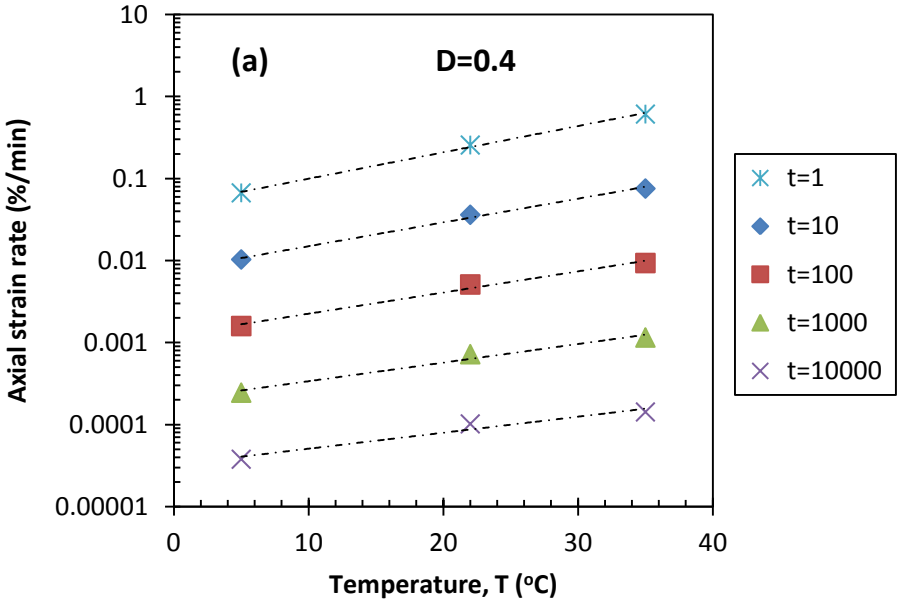

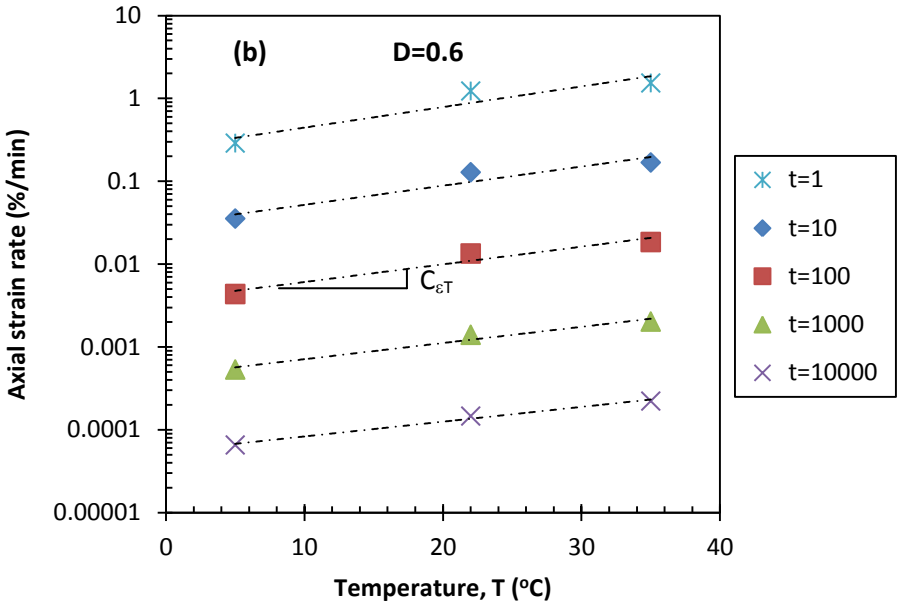
(b)
D=0.6
Axial strain rate (%/min)
Temperature, T (°C)
$C_{\varepsilon T}$
t=1
t=10
t=100
t=1000
t=10000
10
1
0.1
0.01
0.001
0.0001
0.00001
0
10
20
30
40

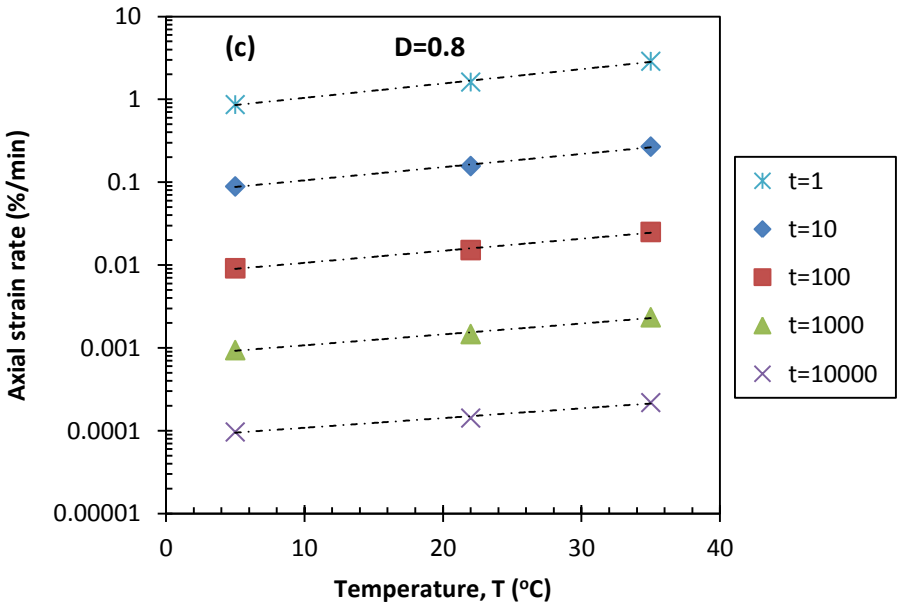
(c)
D=0.8
Axial strain rate (%/min)
Temperature, T (°C)
t=1
t=10
t=100
t=1000
t=10000
10
1
0.1
0.01
0.001
0.0001
0.00001
0
10
20
30
40

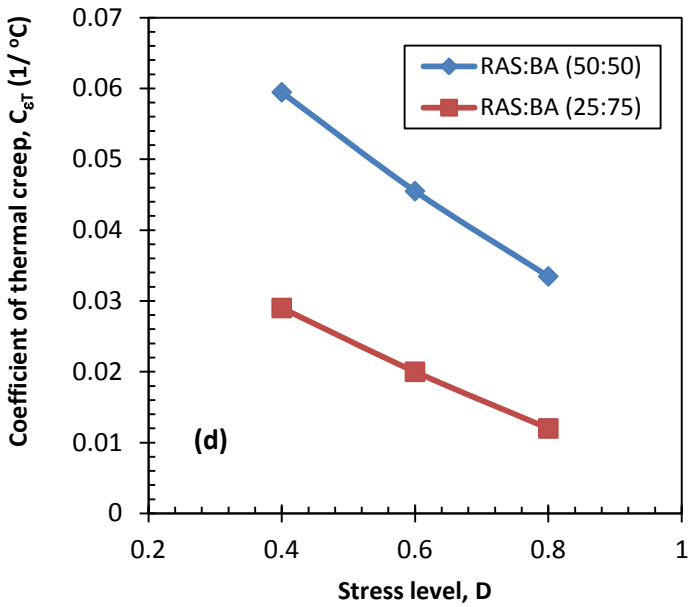

Fig. 5.13. Axial strain rate with temperature at different times under (a) D=0.4; (b) D=0.6; and (c) D=0.8 and (d) variation of $\boldsymbol{C_{\varepsilon T}}$ with stress level

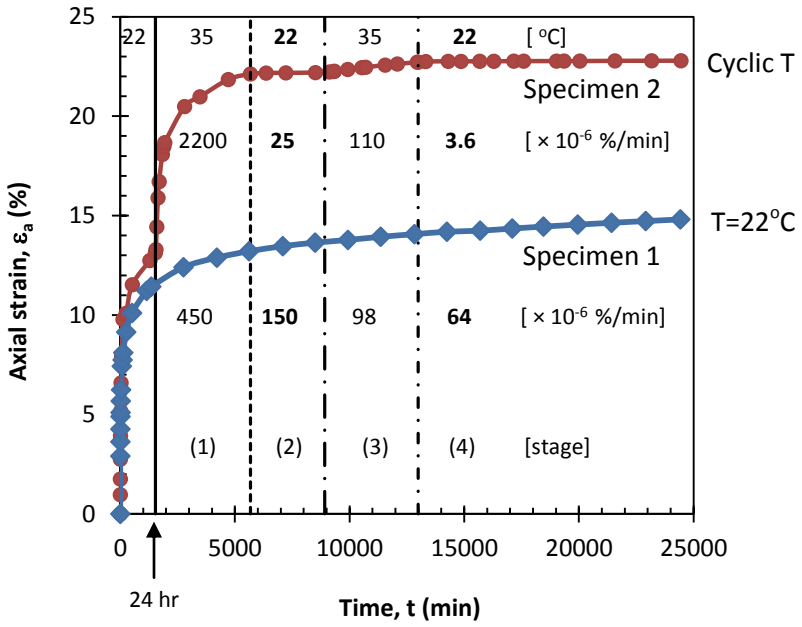

Fig. 5.14. Axial strain with time at constant and varying temperatures for RAS:BA (25:75)

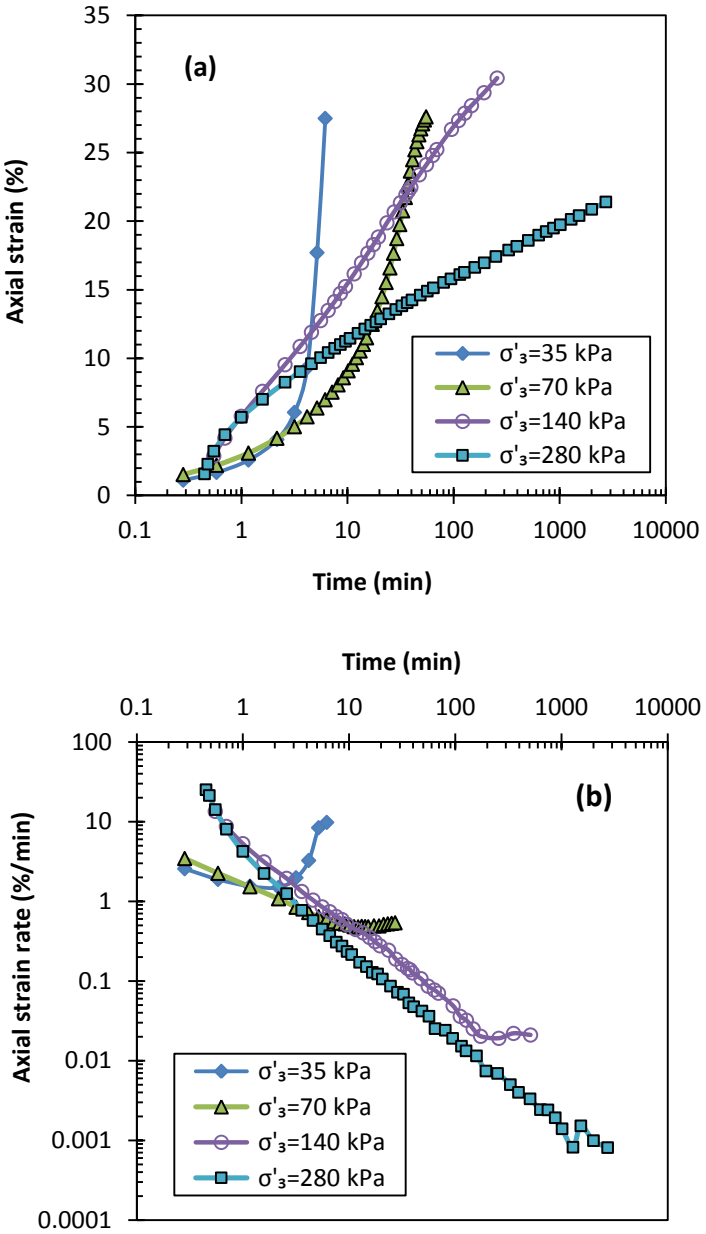

Fig. 5.15. Effect of confining stress on (a) axial strain and (b) strain rate

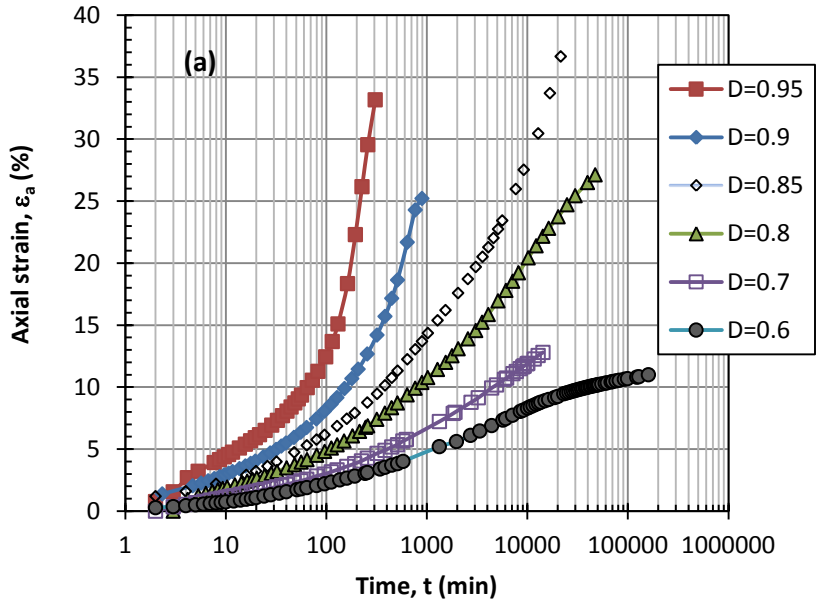
(a)
Axial strain, ε_a (%)
Time, t (min)
D=0.95
D=0.9
D=0.85
D=0.8
D=0.7
D=0.6

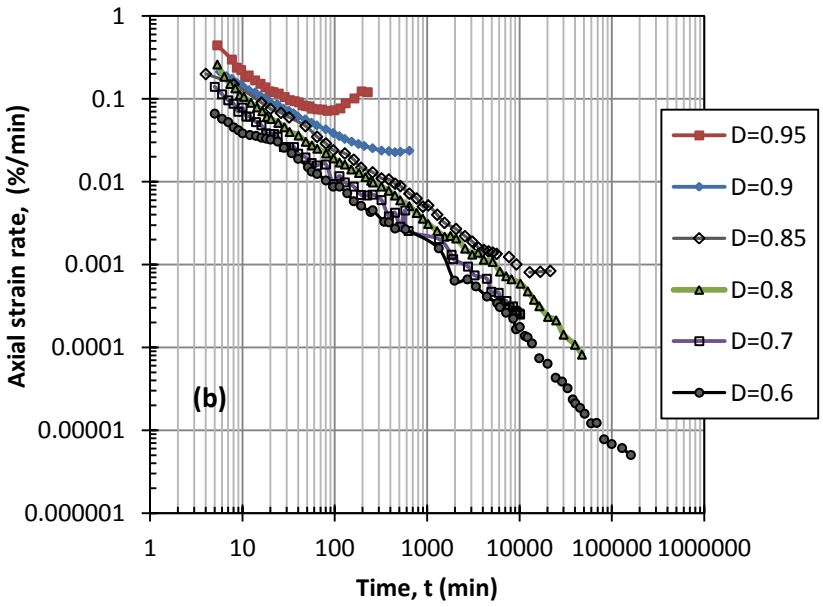
(b)
Axial strain rate, (%/min)
Time, t (min)
D=0.95
D=0.9
D=0.85
D=0.8
D=0.7
D=0.6

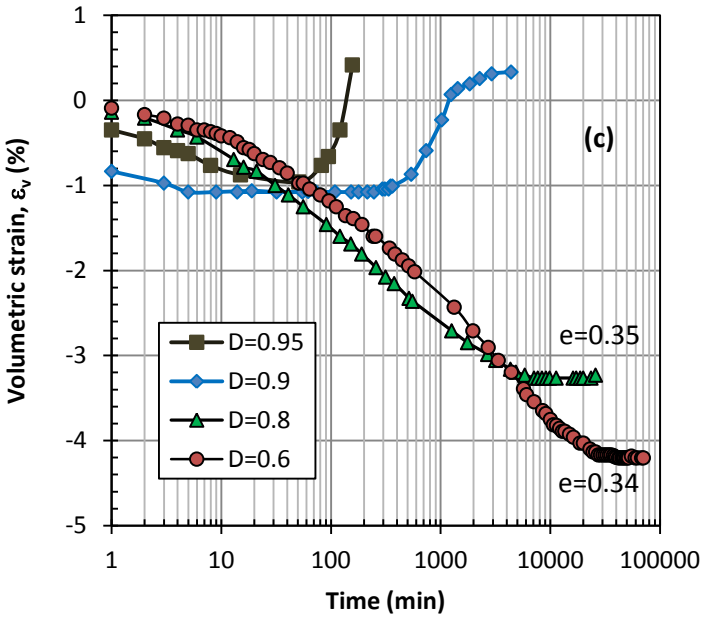

Fig. 5.16. Axial strain (a) axial strain rate (b) and volumetric strain (c) with time at different stress levels for stabilized RAS

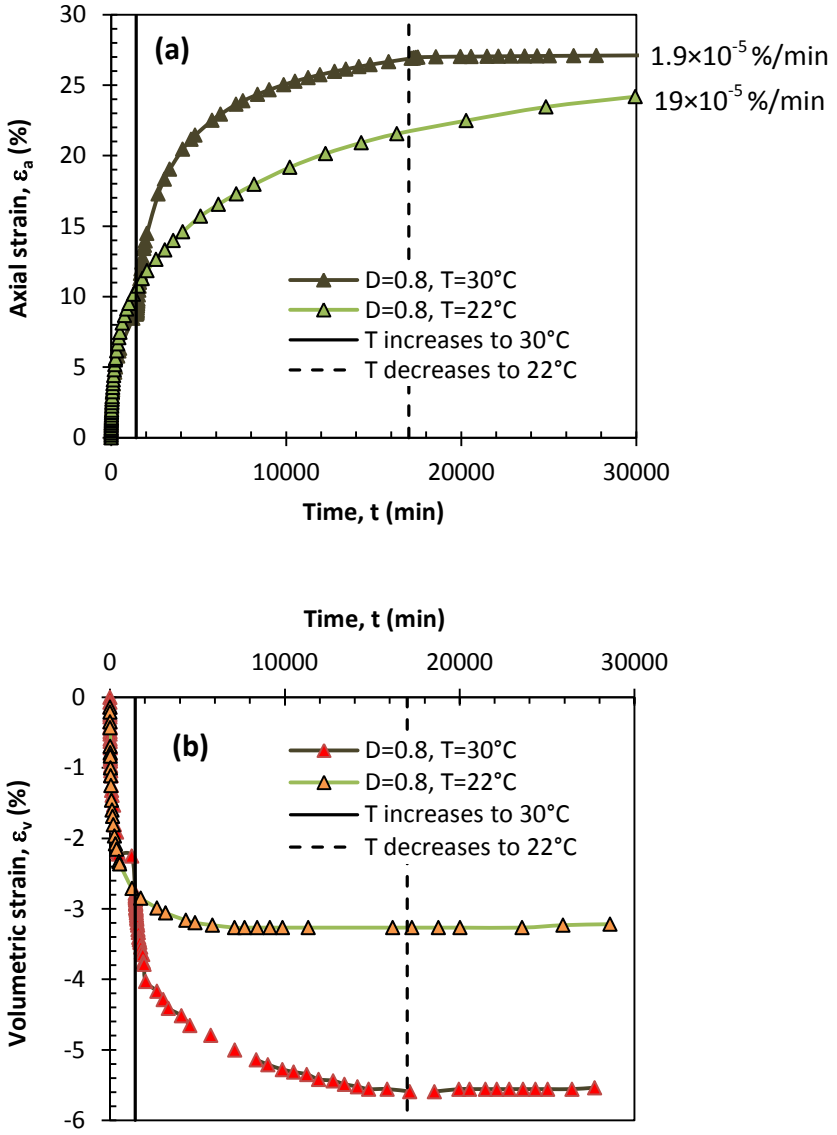

Fig. 5.17. Axial strain and volumetric change with time at different temperatures

Chapter 6 Summary and Conclusion

In this study, recycled asphalt shingles (RAS) were evaluated for potential use as structural fill in highway embankments or backfills behind retaining walls. To reduce compressibility of RAS, addition of granular materials as additives to RAS and stabilization using self cementing fly ash were considered. Geotechnical properties of compacted RAS:BA/FS mixtures and stabilized RAS including compaction behavior, hydraulic conductivity, shear strength, compressibility and coefficient of earth pressure at rest were evaluated in a systematic manner. Since RAS particles contains viscous asphalt binder, to evaluate possible seasonal temperature change on mechanical properties of RAS containing fills, a thermo-mechanical system was developed to investigate the effect of temperature change on geotechnical properties. The range of temperature considered herein encompasses the extreme seasonal temperature change observed in North America.

The following specific observations are made based on the test results:

Compaction Behavior

RAS:BA/FS mixture and stabilized RAS have lower γ_{dmax} than typical compacted soils and varies between 11.3 kN/m^3 and 15.2 kN/m^3. The maximum dry unit weight of the RAS:BA/FS mixture or stabilized RAS increases with increasing BA/FS or fly ash content. Low dry unit weight makes them favorable alternatives to natural compacted soils for construction of structural fill over weak soils.

Drainage Capacity

The hydraulic conductivity of the RAS:BA/FS mixture or stabilized RAS provides adequate drainage capacity as structural fills. The hydraulic conductivity slightly decreases with increasing confining pressure due to high compressibility of RAS particles. The hydraulic conductivity of the mixture increases with increase in bottom ash/foundry slag content and becomes almost insensitive to confining pressure when the bottom ash/foundry slag content of the mixture increases to more than 50%. The hydraulic conductivity of stabilized RAS is comparable to that of silty sands. The hydraulic conductivity is also reduced with increasing fly ash content. Due to reduction in drainage capacity, maximum fly ash content in stabilized RAS is recommended to be limited to 20%. The drainage capacity of the material increases with temperature due to reduction in water viscosity. There is no concern regarding drainage capacity of RAS:BA or fly ash stabilized RAS at elevated temperatures.

Shear Strength

RAS alone exhibits sufficient shear strength as a structural fill material. Shear strength of compacted RAS:BA/FS mixtures or stabilized RAS are similar to those of compacted sandy soils and is sufficient for construction of structural fills. The shear strength of both compacted RAS:BA mixture and stabilized RAS consistently decreases with increasing temperature. As the RAS content in the RAS:BA mixture increases the temperature change has more pronounced effect on the shear strength of the mixture. However, shear strength of the embankment fills constructed with the compacted RAS:BA mixtures (with RAS content no more than 50%) or stabilized RAS with 20% self-cementing fly ash remains within the range sufficient to provide

stability of the typical road embankment fill in the climate ranges of North America (i.e., up to 35 ^{o}C fill temperatures).

Compressibility

The short-term and long-term compressibility of pure RAS are significantly higher than those of compacted sandy soils. The high compressibility is due to asphalt cement and cellulose felt contents in RAS. Systematic addition of bottom ash or foundry slag to RAS or stabilization of RAS reduces compressibility of the mixture. At small to moderate stress levels typical in highway embankments, addition of more than 50% by weight bottom ash/foundry slag to RAS or stabilization with more than 10% self cementing fly ash, greatly reduces the short-term and the long-term compression and categorizes the RAS:BA/FS mixtures or stabilized RAS as slightly to very slightly compressible material. Aging by preloading for a specific time such as 150 days is an alternative method to reduce long-term compressibility of RAS. Previous research results showed that compressibility of the BA or FS is greater than natural sand. The acceptable BA or FS content of the compacted RAS:BA/FS mixture can be safely replaced by natural granular material content and the results and design graphs obtained herein can be used conservatively for the compacted RAS mixtures with sands or gravels. The results obtain in this research is also specific to the type and maximum particle size of the recycled asphalt shingles used. The developed design graphs help determine RAS content in the mixture based on overburden pressure and allowable long term settlement.

Temperature change, on the other hand, affects compressibility of the compacted RAS:BA mixture and stabilized RAS with self-cementing fly ash. The secondary compression index increases exponentially with temperature. During the cold seasons (temperatures lower

than 10 ^{o}C), the compression of the RAS:BA mixture or stabilized RAS is comparable to that of natural granular material and is practically negligible. However, the compressibility exponentially increases during warm seasons (when the temperature rises to 20 to 35 ^{o}C). This indicates that an embankment fill containing RAS or stabilized RAS constructed during the cold to mild seasons of the year may exhibit significant settlement during the warm season. In any region in North America, if the embankment is constructed during the warm season, the majority of the compression will occur during construction and negligible settlement can be expected in the seasons following the warm season. The design graphs were developed to predict subsequent settlement of an embankment constructed at a temperature around 20 ^{o}C as a function of RAS content, temperature and stress levels for RAS:BA mixtures. In using the design graph, one may meet the design specifications for the maximum allowable settlement of a road embankment.

Coefficient of Lateral Earth Pressure

Coefficient of lateral earth pressure of RAS:BA/FS mixtures or stabilized RAS are comparable to those of compacted sand. Adequate drainage capacity and lower dry unit weight of RAS:BA/FS mixtures or stabilized RAS make them favorable alternatives to sand and gravel in terms of lower lateral earth pressures behind retaining structures with potential to greatly reduce the dimensions of the walls. Stabilization of RAS significantly reduces the K_o of RAS.

Deviatoric Creep Response

Deviatoric creep behavior of compacted RAS:BA mixture and fly ash-stabilized RAS was evaluated at varying temperatures and stresses. At large deviatoric stress levels, creep rupture

should be a concern when using the compacted RAS:BA mixture or stabilized RAS as structural fill. To minimize potential of creep rupture in a structural fill, the design engineer should keep the maximum shear stress to at least 20% below the shear strength when designing slopes of the highway embankment or retaining structures to make sure no significant creep rupture is likely to occur during lifetime of the earth structures. The strain rate exponentially increases with temperature which can be beneficial to minimize the creep deformation and possible creep rupture if the construction of the structural fill is conducted during a warm season. Construction of the RAS containing structural fill during mild or cold seasons of the year is not recommended, as there will be greater potential for creep in subsequent warm season. Reclaimed asphalt shingles can be used in construction of highway embankment fills taking into account their intrinsic characteristics such as compressibility and temperature sensitivity during design and construction. Such high-volume use not only resolves the disposal problem of the material but also helps provide a more sustainable roadway construction using recycled materials.

Based on the results of this research, RAS mixed with granular materials or stabilized with self cementing fly ash is considered to be a viable material for use as structural fill in highway embankments and backfill behind retaining walls. Structural fill is an alternative application to use in hot mix asphalt, which is likely to allow use of large volume of waste asphalt shingles and help to save landfill space, reduce disposal costs, energy consumption, and green house gas emissions due to mining and production of virgin aggregates. Additionally, RAS in mixture or stabilized offers certain superior fill material characteristics compared to conventional materials such as light weight and reduced lateral pressures. The materials used are processed industrial materials or byproducts. Therefore, it is expected that their behavior will vary in a narrow range and thus only one source is used for the test materials. While the overall

behavior is not likely to vary significantly, the quantitative values of the various parameters may be different if materials from other sources are used and therefore should be evaluated for design.

Appendix Compressibility of Reclaimed Asphalt Shingles Mixtures: Mechanism and Practical Implication

Abstract: Asphalt shingle waste has been identified by Environmental Protection Agency (EPA) as top five priority material for reuse application. Over 11 million Mg asphalt shingle waste is produced in the U.S. each year for which land-filling is the main end place. While shear strength and hydraulic conductivity of reclaimed asphalt shingles (RAS) are comparable to granular soils, significant compressibility is the main issue for use of RAS in structural fill applications. In this study, to limit the compressibility of RAS, stabilization with self-cementing fly ash and mixtures of RAS with another granular by-product, namely foundry slag (FS) were considered with an emphasis on mechanisms, analytical relationships, and practical implications for use of RAS as highway structural fill. Results showed that compressibility is reduced to below allowable limits by increasing granular additive content (e.g. FS) to more than 50% by weight or by stabilizing RAS with more than 10% fly ash. The secondary compression ratio is a power function of stress level indicating that the RAS containing embankment settles at different rates along the height of the embankment. The use of reclaimed asphalt shingles in the construction of highway embankments and backfills consume large quantities of materials and contributes to a more sustainable roadway construction.

Keywords: reclaimed asphalt shingle, RAS, compressibility, foundry slag, fly ash, embankment, backfill.

Introduction

Sustainable construction saves resources and contributes to the reduction of global warming by reducing greenhouse gas emissions. An important source of greenhouse gases in highway construction is related to mining and the production of high volume construction materials (Wen and Edil, 2009; Lee et al. 2010). As the world population grows the amount and type of generated solid waste increases. The use of solid waste materials in high-volume applications in construction is not only a promising solution to the waste disposal problems, but it also contributes to reducing greenhouse gas emissions and energy consumption by avoiding mining and aggregate production.

Approximately 11 million Mg of waste asphalt roofing shingles are generated per year in the U.S. of which 10 million Mg are tear-off roofing shingles and 1 million Mg is factory scraps (Townsend et al. 2007; NERC, 2011). The most common disposal method of the asphalt shingle waste is landfilling. Reuse of asphalt shingle waste has been identified by the U.S. Environmental Protection Agency (EPA) and Federal Highway Administration (FHWA) as a top priority.

The current applications of RAS include use in hot mix asphalt (HMA), as cold patches in surface pavement or as supplementary fuel in cement kiln dust industry. However, these applications only use from 10% to 20% of the total produced asphalt shingle waste (Turley, 2011). Another possible application which involves large quantities of material is in structural fills which include highway embankment fills or backfill behind retaining walls. In particular, in areas where the underlying soils are compressible or weak, use of a light-weight material such as RAS will potentially reduce the settlement and increase the global stability of the earth structure. Preliminary compression test results indicated that pure RAS is too compressible for use as

structural fill (Benson et al. 2010). To reduce compressibility of RAS, addition of granular materials with verified suitability as structural fill was considered. Foundry slag (FS) is a combination of limestone and metal impurities in metal casting industry, which is collected from top of the molten metal in the furnace. The molten slag is cooled, crushed and screened to create granular slag. According to the U.S. Geological Survey, about 17 to 24 million Mg foundry slag was produced in 2008 of which about 90% were used in a variety of engineering applications such as aggregate in Portland cement concrete, asphalt concrete, aggregate base, fill material and railroad ballast. Of the total used FS, 40% was used as road base-course and 10% was used as fill material. The engineering properties of foundry slag are suitable for use as structural fill and working platforms over soft subgrades (Emery, 1982; Ahmed, 1993; Edil et al. 2002; Tanyu et al. 2005).

To control its excessive compressibility, stabilization of RAS with self-cementing fly ash, which is a widely available industrial byproduct, is also considered. In this study, the compressibility of RAS stabilized with self-cementing fly ash is evaluated for structural fill applications. The beneficial use of self-cementing fly ash has been investigated by several researchers and several demonstration projects have been successfully constructed using self-cementing fly ash in conjunction with a variety of materials from natural soils to recycled asphalt pavements (Patelunas 1986; DiGioia et al. 1986; McLaren and DiGioia 1987; Ferguson, 1989; Misra 2000; Bin-Shafique et al. 2004; Li et al. 2008; ACAA 2009; Li et al. 2009; Wen and Edil 2009; Wen et al. 2011). According to the American Coal Ash Association (ACAA 2009) survey about 68 million Mg fly ash (FA) was produced in 2010 of which only about 38% was reused in different applications like concrete production, structural fills, waste stabilization, road base/subbase and soil modification. The remaining fly ash is typically disposed in utility disposal

sites. Reuse of RAS stabilized with self-cementing fly ash will potentially have beneficial contribution in saving landfill space and reducing energy consumption and green house gas emissions due to production of natural aggregates through the beneficial use of two under recycled industrial byproducts. The environmental implications of self cementing fly ash are considered beyond the scope of this investigation; however, there are procedures available to implement such an assessment (Li et al. 2006; Kosson et al. 2002; Komonweeraket et al. 2011).

Mixing foundry slag with RAS or stabilizing RAS with self-cementing fly ash are expected to reduce the compressibility problem associated with RAS on one hand while allowing beneficial reuse application for two additional solid wastes on the other hand. Previous research results showed that the compacted RAS:FS mixtures or stabilized RAS have sufficient shear strength to provide stability for structural fills (Benson et al. 2010, Soleimanbeigi et al. 2012). Therefore, the objective of this research is to investigate compressibility of the compacted RAS:FS mixtures or stabilized RAS as a construction material in highway embankments and backfills.

Materials and Methods

Materials

RAS samples used in this study were obtained from Stratford Building Supply Company in Stratford, Wisconsin. Visual inspection indicated that RAS samples were free of impurities such as wood chips, plastics, and nails. Warner (2007) concluded that RAS particles with maximum size (d_{max}) of 10 mm, result in higher dry unit weight (γ_d) and higher strength. Therefore, in this study, the RAS supply was screened to limit the d_{max} to 10 mm. FS samples were obtained from the Grede Foundries in Wisconsin. To compare the engineering properties of RAS:FS mixtures

to those of natural soils, a sample of glacial outwash sand (GOS) in Wisconsin was also used in this study.

Constituents of a typical asphalt shingle include 20-35% asphalt cement, 2-15% cellulose felt, 20-38% mineral granules/aggregates, and 8-40% mineral filler/stabilizer (Townsend et al. 2007). Fig. A.1 shows typical shape of RAS particles, light microscope (LM) photomicrographs of FS and outwash sand particles and scanning electron microscope (SEM) photomicrographs of FS fines particles. RAS particles are plate-like, irregular in shape, highly angular and have rough surface texture. The angularity of RAS particles reduces to semi-round to round as the particle size decreases. During manufacturing, one side of the asphalt shingles is covered by sand to protect them against physical damage. The other side is covered by mineral filler to protect the shingles against adhesion during packing and shipment [Fig. A.1(a)]. Particles of outwash sand are solid, semi-round to round and have smooth surface texture as displayed in Fig. A.1(b). The FS particles are angular to highly angular, internally porous and have rough surface texture as shown in Fig. A.1(c). Fines particles of FS are highly angular, irregular in shape with sharp edges as illustrated in the SEM micrograph in Fig. A.1(d). Fig. A.2 shows the grain size distribution for RAS, FS, and GOS determined according to ASTM D 422. More than 80% of particles of each material are sand size with fines contents less than 5%. According to the Unified Soil Classification System (USCS) RAS and FS, although they are not soil, are classified as well graded sand, whereas GOS is classified as poorly graded sand. The grain size indices and the classification are summarized in Table A.1. The specific gravity of RAS evaluated according to ASTM D 854 (Method B) is 1.74, which is lower than the specific gravity of GOS, i.e. 2.71 (see Table A.1). The low specific gravity of RAS is attributed to organic cellulose felt and asphalt cement contents, which together constitute between 20 to 40% by mass of RAS. The

specific gravity of asphalt binder is generally between 1.0 and 1.04 (Roberts et al. 1996). FS has a specific gravity of 2.36, which is also lower than the specific gravity of the GOS and falls within the range reported in the literature (RMRC, 2010). To stabilize RAS, a sample of self-cementing fly ash was obtained from Columbia Power Plant near Portage, Wisconsin. The compositional properties of the fly ash include 6.0% loss on ignition (LOI), minimum 50% of SiO_2, Al_2O_3, and Fe_2O_3, and minimum 75% of strength activity at 7 days. The specific gravity of class C fly ash is 2.70 (Edil et al. 2006). This fly ash is classified as Class C fly ash in accordance to ASTM C618. Although a class C fly ash is investigated, other self-cementing fly ashes that do not meet class C specification, thus not suitable for concrete production and class F fly ashes activated with lime or cement may also provide the necessary stabilization to RAS.

The results of the rigid wall hydraulic conductivity tests following ASTM D 5856 showed that the compacted RAS:FS mixture or stabilized RAS will provide sufficient drainage capacity for structural fills. The hydraulic conductivity of the compacted RAS:FS mixture varies between 2×10^{-3} cm/s and 1×10^{-4} cm/s depending on the RAS content in the mixture and decreases as the RAS content increases. The hydraulic conductivity of RAS stabilized with 10% fly ash is 1.2×10^{-4} cm/s and with 20% fly ash is 2.5×10^{-5} cm/s. Consolidated drained triaxial compression test results also showed that the compacted RAS:FS mixtures or fly ash stabilized RAS have sufficient shear strength to provide stability for typical highway embankment fills. Fig. A.3(a) shows the variation of friction angle (ϕ') and cohesion (c') of the compacted RAS:FS mixtures with FS content. The ϕ' and c' remain almost unchanged with FS content up to 50% after which both ϕ' and c' increase. The increase of ϕ' is attributed to the increased number of the angular FS particles with rough surfaces in the matrix of the RAS:FS mixture [see Figs. A.1(c), (d)]. The sharp edge of the FS particles may create bonds to the asphalt binder of the RAS particles and

increase the c′ of the mixture. Fig. A.3(b) shows the variation of ϕ′ and c′ of stabilized RAS with fly ash content. The friction angle decreases but cohesion increases with increasing fly ash content. The ϕ′ for the compacted RAS:FS mixtures or stabilized RAS are within the ϕ′ range (31^o to 45^o) for typical compacted sandy soils (Holtz and Kovacs, 2011) and are hence considered sufficient to provide stability for typical highway embankments.

Methods

Compaction and one-dimensional compression tests were conducted on RAS:FS mixtures with FS contents of 0, 25, 50, 75, and 100% and on stabilized RAS with fly ash contents of 10, 20 and 50%.

Compaction

Systematic standard Proctor compaction tests following ASTM D 698 (method B) were performed to obtain relationship between dry unit weight and water content of the RAS:FS mixtures and stabilized RAS. Minimum five compaction tests were conducted to obtain the variation of γ_d with water content (w) of each RAS:FS or RAS:FA mixture.

One-dimensional Compression

Settlement of an embankment with large lateral extension can be considered one-dimensional and estimated from the results of one-dimensional consolidation tests. To evaluate compressibility of the compacted RAS:FS mixtures or stabilized RAS, one-dimensional compression tests were conducted following ASTM D 2435-96 using a standard consolidometer

ring with 64-mm diameter and 25-mm height. Each specimen was compacted at the w_{opt} and relative compaction level of 95%. The compaction in the consolidometer ring was conducted in three lifts of equal thickness by a manual hammer. The compacted RAS:FA mixtures were cured for 7 days in 100% humidity room. The RAS:FS specimens were soaked in the consolidometers for 24 hours before applying vertical loads. Pore pressure piezometers were connected to consolidometer cells to measure any generated excess pore water pressures under each stress level. The specimens were loaded incrementally from 12.5 kPa with load increment ratio (LIR) of 1.0 and load increment duration (LID) of 24 hours until the maximum vertical stress level (σ'_{vmax}) of 1600 kPa. The range of the stress level was selected to clearly obtain compression curves and define compressibility parameters for RAS:FS mixtures. The one-dimensional consolidation test was also performed on the glacial outwash sand sample for comparison. The LABVIEW software (National Instruments, Austin, TX) and a data acquisition card (UPC601-U) were used for automated incremental loadings and recording of vertical deformations.

Results and Discussion

Compaction Characteristics

Fig. A.4(a) shows that pure RAS has a well-defined compaction curve with a γ_{dmax} of 11.3 kN/m^3 and w_{opt} of 9%. Systematic addition of FS to RAS only slightly reduces γ_{dmax} of the compacted RAS:FS mixture. The γ_{dmax} of RAS:FS mixture varies between 11.3 kN/m^3 for RAS to 10.9 kN/m^3 for a mixture containing 50% RAS. As the FS content in the RAS:FS mixture increases, the curvature of the parabolic shape of the compaction curve decreases. This is attributed to increase in granular FS particles. The γ_{dmax} of granular soils generally occurs at dry conditions and decreases with increasing water content until saturation where the dry unit weight increases

(Hilf, 1991; Drnevich et al. 2007). Low specific gravity and high porosity of FS particles result in low γ_{dmax} of FS with respect to typical compacted sand. The γ_{dmax} of the RAS:FS mixtures remains almost unchanged with different FS contents, making the compacted RAS:FS mixture a favourable lightweight material for embankment fill application. The RAS:FA mixtures also have bell-shaped compaction curves with γ_{dmax} varying from 11.3 kN/m^3 for RAS to 15.9 kN/m^3 for RAS:FA mixtures with 50% fly ash. The γ_{dmax} of different RAS:FA mixtures are lower than γ_{dmax} of typical compacted sandy soils which typically ranges between 17 and 20 kN/m^3 (18.30 kN/m^3 for the Wisconsin GOS sample). The w_{opt} ranges from 8.6% for RAS to 13.2% for the RAS:BA:FA mixture indicating that the materials are not overly sensitive to compaction moisture content, which is an advantage in wet climates.

Compressibility

Fig. A.5(a) shows the compression curves of the compacted RAS:FS mixtures as vertical strain, ε_v, versus logarithm of vertical effective stress, σ'_v. The compression curve of outwash sand specimen is also included for comparison. Compared to outwash sand, pure RAS is highly compressible for structural fill applications. High compressibility of RAS is attributed to three mechanisms: (1) the cellulose felt within RAS particles creates voids in the particles. For increasing σ'_v, the voids in cellulose felt tend to close rapidly. The voids between the plate-like RAS particles are also closed due to flexibility of the RAS particles; (2) the sand particles either on the RAS particle surface or separated, penetrate into asphalt coating of other RAS particles at increasing σ'_v; and (3) the smaller spherical RAS particles in the matrix [see Fig. A.1(a)], tend to deform under σ'_v.

On the other hand, under stress levels less than 200 kPa, which represent typical overburden pressure in highway embankments, the compressibility of the compacted FS is only slightly higher than the compressibility of outwash sand, which makes the foundry slag an appropriate additive to reduce compressibility of RAS. Fig. A.5(a) illustrates that systematic addition of FS to RAS, reduces compressibility of the compacted RAS:FS mixtures. Under σ'_v up to 200 kPa, addition of 50% foundry slag to RAS significantly reduces ε_v of the compacted RAS:FS mixtures form 17% to 7%.

Compared to the compacted outwash sand, the compressibility of the compacted FS rapidly increases when σ'_v increases to higher than 200 kPa. This is attributed to crushability, high angularity and rough surface texture of the FS particles. Some popcorn-like FS particles were observed to break under finger pressure. High angularity and rough surface texture of granular particles in general, increase the surface abrasion and possibility of particle breakage (Robert and de Souza, 1958; Marshal, 1967; Pestana and Whittle, 1995; Chuhan et al. 2003), which, in turn, increase the compressibility. To verify this, particle size distribution of FS samples were obtained after compaction and after 1D compression test. Fig. A.2 shows degradation of FS particles after compaction and compression (under σ'_v of 1600 kPa) tests in terms of changing grain size. The fines content increased from 3% to 6% after compaction and to 11% after 1D compression test. The median grain size, d_{50}, reduced from 1.8 mm to 1.1 mm after compaction and to 0.5 mm after 1D compression test.

Fig. A.5(b) shows that the compressibility of the stabilized RAS is systematically reduced with increasing self-cementing fly ash content. For σ'_v up to 200 kPa, compressibilities of GOS and stabilized RAS with 20% Class C fly ash are comparable. At higher σ'_v, the compressibility of the stabilized RAS increases possibly because of the breakage of bonding between RAS

particles created by fly ash cementation. Further increase of the fly ash content to 50%, although considered to be very high, reduces the compressibility of the stabilized RAS to levels comparable to those of the GOS specimen under σ_v' even greater than 200 kPa.

Fig. A.6 shows the variation of ε_v with time for different compacted RAS:FS mixtures or stabilized RAS under σ'_v of 100 kPa. The time at which excess pore water pressure, Δu as measured, is dissipated marks the end of primary consolidation, t_p. The generated Δu in the compacted RAS:FS mixtures or stabilized RAS dissipates in less than 2 min due to high hydraulic conductivity of the mixtures thus the primary consolidation accounts for negligible compression of the material and the majority of the compression is due to the secondary compression. The ε_v of RAS nonlinearly increases with logarithm of time after t_p and follows a constant rate after the standard LID of 24 h. The secondary compression is characterized by the secondary compression ratio, which is defined as the slope of ε_v versus log t curve (Ladd et al. 1977):

$$C_{\alpha\varepsilon} = \frac{d\varepsilon}{dlogt} \tag{A.1}$$

The values of $C_{\alpha\varepsilon}$ were determined from the ε_v - log t curves after t_p and corresponding to different compacted RAS:FS mixtures or stabilized RAS. Fig. A.7(a) shows the variation of $C_{\alpha\varepsilon}$ with RAS content at different σ'_v. The value of $C_{\alpha\varepsilon}$ increases with RAS content and stress level. At a given σ'_v, the increase of FS to more than 50% in the RAS:FS mixture, reduces the $C_{\alpha\varepsilon}$ by 80%. For example, for σ'_v = 200 kPa, the addition of 50% foundry slag to RAS reduces the $C_{\alpha\varepsilon}$ from 0.023 to 0.006. Stabilization of RAS using self cementing fly ash reduces the $C_{\alpha\varepsilon}$. Fig. A.7(b) shows the variation of $C_{\alpha\varepsilon}$ with fly ash content calculated for one log cycle before the standard LID under different σ_v'. The increase in fly ash content to more than 10% reduces the $C_{\alpha\varepsilon}$ significantly.

Under σ_v' of 200 kPa, which is a typical stress level for highway embankments, the $C_{\alpha\varepsilon}$ is reduced from 0.041 for unstabilized RAS to 0.005 for stabilized RAS with 20% fly ash content.

The long-term settlement of typical highway embankments were calculated based on $C_{\alpha\varepsilon}$ for different FS or FA contents in the mixture and will be discussed in the following section in this paper. The increase of $C_{\alpha\varepsilon}$ with stress level as illustrated in Fig. A.7 implies increasing settlement rate with overburden pressure within an embankment. Therefore, to evaluate the settlement of an embankment containing RAS, different $C_{\alpha\varepsilon}$ needs to be assigned at different elevation of the embankment. From the ε_v-log t curves at a given σ'_v, the strain rates ($\dot{\varepsilon}$) at different times were determined. The variation of $\dot{\varepsilon}$ with σ'_v for a mixture containing 75% of FS is plotted in Fig. A.8(a) and for stabilized RAS with 20% of FA is plotted in Fig. A.8(b). The strain rate log-linearly increases with stress levels and the slopes of the lines are almost the same at different elapsed times after loading. Similar behaviour was observed for the mixtures with different FS or FA contents. The equation of the best fitting line is therefore given by:

$$\frac{d\varepsilon}{dt} = \dot{\varepsilon} = A{\sigma_v'}^m \tag{A.2}$$

$$\text{or} \qquad \frac{dln\dot{\varepsilon}}{dln\sigma_v'} = m \tag{A.3}$$

where m is the slope of the $\dot{\varepsilon} - log\sigma_v'$ curves in log scale and A is the strain rate corresponding to the unit of σ'_v. From Eq. A.1, the strain rate is obtained as:

$$\dot{\varepsilon} = \frac{C_{\alpha\varepsilon} ln10}{t} \tag{A.4}$$

By substitution of Eq. A.4 into Eq. A.3 we obtain:

$$\frac{\Delta ln\frac{C_{\alpha\varepsilon} ln10}{t}}{\Delta ln\sigma_v'} = m \quad \rightarrow \frac{ln\frac{C_{\alpha\varepsilon} ln10}{t}\Big|_{\sigma_v'} - ln\frac{C_{\alpha\varepsilon} ln10}{t}\Big|_{\sigma_{vo}'}}{ln\sigma_v' - ln\sigma_{vo}'} = m \rightarrow \frac{C_{\alpha\varepsilon}}{C_{\alpha\varepsilon o}} = \left(\frac{\sigma_v'}{\sigma_{vo}'}\right)^m$$

or:

$$C_{\alpha\varepsilon} = C_{\alpha\varepsilon o}\left(\frac{\sigma_v^{'}}{\sigma_{vo}^{'}}\right)^m \quad \text{(A.5)}$$

Eq. A.5 indicates that secondary compression ratio of the compacted RAS:FS mixture or stabilized RAS is a power function of the stress level. The value of the exponent m varies from about 1.0 to 0.5 with increasing RAS content for the compacted RAS:FS mixtures and from 0.5 to 0.85 for the stabilized RAS with increasing fly ash content as illustrated in Fig. A.9. The values of $C_{\alpha\varepsilon}$ were calculated from Eq. A.5 for different mixtures and plotted in Fig. A.7. There is a good agreement between the measured and predicted $C_{\alpha\varepsilon}$. Fig. A.10 shows a comparison between the measured $C_{\alpha\varepsilon}$ and predicted $C_{\alpha\varepsilon}$ using Eq. A.5 for different compacted RAS:FS and stabilized RAS mixtures at various stress levels. The coefficient of correlation, r, is 0.98 indicating validity of the power function of $C_{\alpha\varepsilon}$ with respect to stress level. Eq. A.5 can be used to predict the $C_{\alpha\varepsilon}$ of the stabilized RAS or granular materials containing RAS at different stress levels from the measured $C_{\alpha\varepsilon}$ at a single stress level. This is especially important when performing numerical analysis of embankments for settlement calculations. The vertical stress differs at different elevations in an embankment fill. Since the $C_{\alpha\varepsilon}$ varies with stress levels, the embankment fill settles at different rates along the height.

In the preceding discussions so far, the effect of addition of less compressible granular material, e.g. foundry slag, was investigated for reducing secondary compression of RAS. Preloading is an alternative approach to reduce the long term compression of compressible geo-materials like peat and soft clay (Brawner, 1959a, b; Samson and La Rochelle, 1972; Mesri et al. 1997). In this study, the LID under σ'_v =100 kPa was maintained for 150 d during 1D consolidation test on RAS and RAS:FS mixture with 50% FS content. After the 150-day

duration, the consolidation test with standard LID=24 h continued until σ'_v =1600 kPa. Fig. A.11(a) shows the effect of preloading on compression curves. During the LID=150 d, the vertical strain increased from 12.4% to 19.1%. This results in the reduction in void ratio thus small compression at the following load increments up to the yield stress. The yield stress (σ'_y), which is the stress level that develops plastic strain in the material, increased from 65 kPa before preloading to 250 kPa after preloading. The $C_{\alpha\varepsilon}$ of RAS was also reduced significantly from 0.023 to 0.002, reflecting a 10-fold decrease, as obtained from the slope of the curves in Fig. A.11(b). The reason is attributed to decrease in void ratio of the compacted RAS specimen over time. The results indicate that preloading is an effective alternative way to reduce the compressibility of RAS.

Practical Implication

The total or differential settlement that can be tolerated by a pavement is rarely specified except in the case of bridge approaches for which the tolerable settlement is commonly specified as 12 mm to 25 mm. For roadway embankments the allowable settlement after paving depends on the length of the fill and rate at which settlement develops. If the variations in settlement are uniformly distributed along the length of the embankment, settlement of 150 mm to 300 mm can be tolerated in long embankments (NCHRP Synthesis of Highway Practice 8, 1971). Although the maximum settlement of highway embankments are allowed between 300 mm and 600 mm (NCHRP Synthesis of Highway Practice 29, 1975; and Stark et al. 2004), 300 mm is a more widely accepted limit and is adopted here.

To illustrate the settlement of embankment fills constructed with RAS:FS mixtures, stabilized RAS or preloaded RAS, example calculations were made on embankments 2, 5, 10,

and 15-m high constructed on a 15-m thick sand deposit. As illustrated in previous sections, due to the high hydraulic conductivity, primary consolidation accounts for negligible settlement of the RAS:FS or stabilized RAS fill and short term settlements of the fill occur during construction of the embankment. The long-term settlements due to secondary compression were evaluated using the following relationship:

$$s = \sum_{i=1}^{n} s_i = \sum_{i=1}^{n} h_i C_{\alpha\varepsilon,i} \log\left(\frac{t}{t_o}\right) \tag{A.6}$$

where s is the embankment settlement, s_i is the settlement of a layer with thickness h_i (h_i was selected 0.5 m in the calculations), n is the number of sublayers, i.e., the embankment height H divided by the sublayer thickness ($H=nh_i$), t is time, and t_o is an arbitrary reference time that for the calculations herein was taken 1 d after the completion of construction. The values of $C_{\alpha\varepsilon}$ used for settlement calculations were calculated from Eq. A.5. Depending on elevation of each sublayer in the embankment, the corresponding $C_{\alpha\varepsilon}$ to the vertical stress was used for settlement calculation.

Fig. A.12(a) shows the variation of settlement of an embankment 10-m high, constructed with either compacted RAS:FS mixtures, stabilized RAS, preloaded RAS or compacted sand, during 40-year lifetime after construction. The majority of the settlements occur within 1 year after completion of embankment construction. The long-term settlement of the embankment constructed with RAS is about 1050 mm which is far above the allowable limit. Preloading of RAS for five months reduces the long-term settlement to 108 mm, which reflects 90% reduction. Addition of 50% FS to RAS also reduces the long-term embankment settlement to 294 mm reflecting a 72% reduction. Increase of FS content to 75% results in only 90 mm settlement during the 40-year lifetime. Stabilization of RAS with 10% fly ash reduces the total embankment settlement to 300 mm reflecting 70% reduction. Increase of fly ash content to 20% results in

negligible total settlement during the 40-year lifetime. The average height of the embankments constructed in the U.S. is 4.5 m (Wright, 1996). Having identical subgrade soil conditions, shallow embankments exhibit smaller settlement than those plotted in Fig. A.12(a) for a 10-m high embankment. Fig. A.12(b) presents the variation of settlement with height of the embankments constructed with preloaded RAS, compacted RAS:FS mixtures, stabilized RAS and glacial outwash sand. The long-term settlement of embankments with average height, i.e. 4.5 m, constructed with these materials is smaller than the 300-mm allowable settlement. In general, for embankment height up to 15 m, preloaded RAS fills, RAS:FS fills with 50% and 75% FS content, and RAS stabilized with higher than 10% self cementing fly ash, result in long-term settlements below the allowable limit of 300 mm. Fig. A.12(c) shows the variation of long-term settlements of embankments of different heights with FS content in RAS:FS mixtures. RAS fills less than 5-m high exhibit long-term settlement within the allowable limit. For higher embankments, addition of more than 50% FS to RAS significantly reduces the long-term settlement. The variation of total settlement with percent fly ash is illustrated in Fig. A.12(d). Stabilization of RAS with 10% fly ash significantly reduces the total settlement. The settlement reduction is more noticeable in embankments with lower height. Increase of fly ash content to 20% results in negligible total settlement for embankments with different height. The fly ash content between 10 to 15%, which is also the typically used fly ash content with soils and base course materials (ACAA 2003), is recommended to reduce compressibility of RAS as structural fill to an acceptable limit while maintaining adequate drainage capacity.

The results of this study are easily generalized to develop guideline criteria for incorporation of RAS in natural granular materials. As illustrated in Fig. A.5, compacted FS is more compressible than the compacted glacial outwash sand. Therefore, the maximum

recommended RAS for incorporation in RAS:FS mixture is also recommended for incorporation in RAS:granular material mixtures where the "granular material" (e.g., sand, other slags) is similar to or less compressible than FS. To maintain adequate drainage capacity and keep the long-term settlement of the average embankment fill below the maximum allowable limit, the maximum recommended RAS content for incorporation into granular materials should be less than 50%. The maximum self cementing fly ash content in stabilized RAS is limited to 20% to reduce settlement while maintaining adequate drainage capacity.

Conclusions

In this study, compressibility of reclaimed asphalt shingles (RAS) mixed with foundry slag (FS) and also RAS stabilized with self-cementing fly ash (FA) were evaluated for potential use as structural fill in highway embankments. The following specific observations are made based on the test results:

1. The compacted RAS:FS mixtures have maximum dry unit weight of 11 kN/m^3 which is about 50% of maximum dry unit weight of typical compacted soils. The maximum dry unit weight of stabilized RAS with fly ash content up to 20% varied from 11 kN/m^3 to 13.8 kN/m^3. Low dry unit weight of the compacted RAS:FS mixtures or stabilized RAS makes them favorable alternatives to natural compacted soils for construction of lighter structural fills.
2. Compressibility of pure RAS is significantly higher than that of compacted sandy soils. Mixing RAS with granular foundry slag, stabilizing RAS with self cementing fly ash or preloading of RAS significantly reduces the compressibility. The excess pore water pressure dissipates during construction of the RAS containing fill and the majority of the

fill settlement is due to secondary compression which starts shortly after construction. For a typical stress level in highway embankments, addition of 50% by weight of foundry slag to RAS reduced the secondary compression ratio by 80% from 0.023 to 0.006. Stabilization of RAS with 20% fly ash reduced the secondary compression ratio to 0.003 and preloading reduced the ratio to 0.002.

3. The secondary compression ratio is a power function of vertical stress. The embankment fill containing RAS will settle at different rates along the elevation of the embankment. The exponent of the power function systematically reduces with increasing foundry slag or fly ash content. The developed relationship is useful to incorporate in numerical methods for precise long term settlement calculation of embankments containing RAS.
4. Long-term settlement of an embankment constructed with less than 50% RAS or with stabilized RAS containing more than 10% self cementing fly ash is lower than the allowable settlement limit. Typical highway embankments with height shorter than 5 m will exhibit long-term settlement lower than 100 mm, which is below the allowable limit.

Based on the results of this research, RAS:FS mixture or stabilized RAS is considered a viable material for use as fill in highway embankments. Such an application will use the majority of reclaimed asphalt shingles and contribute to reduction of greenhouse gas emissions by avoiding production of natural aggregates. The results obtained in this study are for the specific RAS, FS, and FA samples tested, which are typical of such material. However, RAS samples obtained from different sources and with different particle sizes may have different mechanical behavior and need to be tested for specific applications. Further studies are needed to generalize the use of RAS:FS mixture or stabilized RAS in structural fills and to evaluate the potential effect of high ground temperatures in certain climatic regions.

Acknowledgment

Support for this study was provided by the Recycled Materials Resource Center, which is supported by the Federal Highway Administration. The opinions, findings, conclusions, or recommendations expressed herein are those of the author(s) and do not necessarily represent the views of the sponsors.

References

Ahmed, I. (1993). *Use of Waste Material in Highway Construction*. Noyes Data Corporation, Park Ridge, New Jersey.

American Coal Ash Association. (2009). *Coal Combustion Product (CCP) Production & Use Survey Results*, ACAA, Aurora, Colorado, September 15, 2009 [online].

Benson, C., Edil, T., and Soleimanbeigi, A. (2010). "Use of recycled asphalt shingles in highway embankments." *Proceeding of 2010 Mid-Continent Transportation Research Forum*, August 19-21, Madison, WI.

Bin-Shafique, M. S., Senol, A., Edil, T. B., and Benson, C. H. (2004). "Incorporating Fly Ash Stabilized Sub-base into Pavement Design-Case Study." *Geotechnical Engineering*, Institute of Civil Engineers, United Kingdom, 157(GE4), 239-249.

Brawner, C. O. (1959a). "Preconsolidation in highway construction over muskeg." *Roads and engineering construction*, Monetary Times Production, Toronto, 97(9), 99-104.

Brawner, C. O. (1959b). The principles of preconsolidation in highway construction over muskeg. *Proceeding of the 5th Muskeg Research Conference*, NRC, Ottawa, ACSSM Technical Memorandum.

Chuhan, F. A., Kjeldstad, A., Bjorlykke, K., and Hoeg, K. (2003). Experimental compression of loose sands: relevance to porosity reduction during burial in sedimentary basins. *Canadian Geotechnical Journal*, 40(5): 995-1011.

DiGioia, A. M., McLaren, R. J., Burns, D. L., Miller, D. E. (1986). "Fly Ash Design Manual for Road and Site Application." Vol. 1: Dry or Conditioned Placement, Manual Prepared for EPRI, Interim Report, CS-4419, Electric Power Research Institute, Palo Alto, CA.

Drenvich, V. P., Evans, A. C., and Prochaska, A. B. (2007). "A study of effective soil compaction control of granular soils." *Joint Transportation Research Program*. Paper 234.

Edil, T., Benson, C., Bin-Shafique, M., Tanyu, B., Kim, W., and Senol, A. (2002). "Field evaluation of construction alternatives for roadway over soft subgrade." *Transportation Research Record*, 1786, Transportation Research Board, National Research Council, Washington, DC: 36-48.

Emery, J. J. (1982). "Slag utilization in pavement construction." *Extending Aggregate Resources*, ASTM STP No. 774, ASTM: 95-118.

Ferguson, G. (1989). "Use of Coal Ash in Highway Construction: Kansas Demonstration Project." *GS-6460, Research Project 2422-15, Electric Power Research Institute*, Palo Alto, CA.

Hilf, J. W. *Compacted Fill*. (1991). In Foundation Engineering Handbook, 2nd Edition (H.-Y. Fang (Ed.)). New York, Van Nostrand Reinhold, 249-316.

Krivit D. *Recycling of Tear-Off Shingles: Best Practices Guide*. 2007, Final report prepared for the Construction Materials Recycling Association (CMRA).

Kosson, D. S., Van Der Sloot, H. A., Sanchez, F., and Garrabrants, A. C. 2002. An integrated framework for evaluating leaching in waste management and utilization of secondary materials. *Environmental Engineering Science*, 19(3), 159-204.

Komonweeraket, K. Benson, C. H., Edil, T. B., and Bleam, W. F. (2010). "Leaching Behavior and Mechanisms Controlling the Release of Elements from Soil Stabilized with Fly Ash." *Geo-Frontiers 2011*, Dallas, TX, CD-ROM.

Ladd, C. C., Foote, R. Ishihara, K., Schlosser, F. and Poulos, H. G. (1977). "Stress-deformation and strength characteristics." State-of-the-Art Report, Proceedings of the Ninth International Conference on Soil Mechanics and Foundation Engineering, Tokyo, Vol 2, pp. 421-494.

Lee, J., Edil, T., Tinjum, J., and Benson, C. (2010). "Quantitative Assessment of Environmental and Economic Benefits of Using Recycled Construction Materials in Highway Construction." *Journal of Transportation Research Board*, 2158, 138-142.

Li, L., Benson, C. H., Edil, T. B. and Hatipoglu, B. (2006). "WiscLEACH: A Model for Predicting Ground Water Impacts from Fly-Ash Stabilized Layers in Roadways." *GeoCongress 2006*, Atlanta, GE, ASCE, CD-ROM.

Li, L., Benson, C. H., Edil, T. B. and Hatipoglu, B. (2008). "Sustainable Construction Case History: Fly Ash Stabilization of Recycled Asphalt Pavement Material." *Geotechnical and Geological Engineering*, 26(2), 177-188.

Li, L., Edil, T. B., and Benson, C. H. (2009). "Mechanical Performance of Pavement Geomaterials Stabilized with Fly Ash in Field Applications." *Coal Combustion and Gasification Products* 1, pp. 43-49, doi: 10.4177/CCGP-D-09-00018.1

Marshal, R. J. (1967). "Large scale testing of rockfill materials." *Journal of the Soil Mechanics and Foundations Division, ASCE,* 93: 27–43.

McLaren, R.J., DiGioia, A.M. (1987). "The Typical Engineering Properties of Fly Ash." *Geotechnical Practice for Waste Disposal '87, Geotechnical Special Publication*, 13, 683-697.

Mesri, G., Stark, T.D., Ajlouni, M.A., and Chen, C.S. (1997). "Secondary compression of peat with or without surcharging." *Journal of Geotechnical and Geoenvironmental Engineering, ASCE,* 123(5): 411-421.

Northeast Recycling Council. *Asphalt Shingles Manufacturing & Waste Management in the Northeast Fact Sheet*. NERC, November 2011.

NCHRP Synthesis of Highway Practice 8. (1971). *Construction of Embankments.* Transportation Research Board, National Research Council, Washington, D.C., 38 p.

NCHRP Synthesis of Highway Practice 29. (1975). *Treatment of Soft Foundations for Highway Embankments.* Transportation Research Board, National Research Council, Washington, D.C. 25 p.

Patelunas, G. M. (1986). *High Volume Fly Ash Utilization Projects in the United States and Canada.* Electric Power Research Institute, Report No. CS-4446, Palo Alto, CA.

Pestana, J. M., and Whittle, A. J. (1995). "Compression model for cohesionless soils." *Géotechnique*, 45: 611-631.

Recycled Materials Resource Center. 2010. *User Guidelines for By-products and Secondary Use Materials in Pavement Construction,* http://www.rmrc.unh.edu/tools/uguidelines/ index.asp, Accessed December 2010.

Roberts, J. E., and de Souza, J. M. 1958. The compressibility of sands, *Proc., American Society for Testing and Materials*, 58, 1269-1277.

Roberts, F.L., Kandhal, P.S., Brown, E.R., Lee, D.Y. and Kennedy, T.W. 1996. *Hot Mix Asphalt Materials, Mixture Design, and Construction.* National Asphalt Paving Association Education Foundation. Lanham, MD.

Samson, L., and La Rochelle, P. (1972). "Design and performance of an expressway constructed over peat by preloading." *Canadian Geotechnical Journal*, 9, 447–466.

Soleimanbeigi, A., Edil, T., and Benson, C. (2012). "Recycled asphalt shingles mixed with granular byproducts as structural fill", *Journal of ASTM International*, 9(1):1-19.

Stark, T. D., Arellano, D., Horvath, J. S., and Leshchinsky, D. 2004. NCHRP Report No. 529: Guidelines and recommended standards for geofoam applications in highway embankments. Transportaion Research Board, National Research Council, Washington, DC.

Tanyu, B.F., Benson, C.H., Edil, T.B., and Kim, W.H. (2005). "Equivalency of crushed rock and three industrial by-products used as a working platform during pavement construction." *Transportation Research Record*, 1874, Trans. Res. Board, National Research Council, Washington, DC, 59-69.

Townsend, T., Powell, J., and Xu, C. (2007). "Environmental issues associated with asphalt shingle recycling." *Constr. Mater. Recycling Association, US EPA Innovations Workgroup*.

Turley, W. (2011). Personal Communication. *Construction Materials Recycling Association*, Eola, IL.

U.S. Geological Survey. (2010). *Minerals Yearbook*. USGS, see http://minerals.usgs.gov/minerals/ pubs/commodity/iron_&_steel_slag/myb1-2008-fesla.pdf, Accessed December 2010.

Warner, J. D. (2007). *The beneficial reuse of asphalt shingles in roadway construction*. MSc Thesis, Department of Civil and Environmental Engineering, University of Wisconsin-Madison.

Wen, H. and Edil T. B. (2009). "Sustainable Reconstruction of Highways with In-Situ Reclamation of Materials Stabilized for Heavier Loads." *8th International Conference on Bearing Capacity of Roads, Railways, and Airfields*, Champaign, IL, June 19.

Wen, H., Warner, J. D., Edil, T. B. and Wang, G. (2010). "Laboratory Comparison of Crushed Aggregate and Recycled Pavement Material With and Without High Carbon Fly Ash." *Geotechnical and Geological Engineering*, 28(4), 405-411.

Wright, P. H. (1996). *Highway Engineering*. John Wiley & Sons.

Table A.1. Grain size indices and USCS classifications of RAS, foundry slag and outwash sand

Material	d_{10} (mm)	d_{50} (mm)	C_u	C_c	fines (%)	G_s	USCS symbol	USCS name
RAS	0.17	1.1	7.6	1.6	3.8	1.74	SW	Well graded sand
Foundry slag	0.18	1.6	11.4	2.7	4.8	2.36	SW	Well graded sand
Glacial outwash sand[a]	0.21	0.5	3.1	0.8	0.0	2.71	SP	Poorly graded sand

d_{10}: effective particle size (particle size for which 10% of the sample is finer than d_{10}); d_{50}: median particle size (particle size for which 10% of the sample is finer than d_{50}); C_u: coefficient of uniformity, d_{60}/d_{10}; C_c: coefficient of curvature, $C_{30}^2/(C_{10} \times C_{60})$; G_s: specific gravity; USCS: Unified Soil Classification System

[a] Data were taken from Bareither et al. (2008)

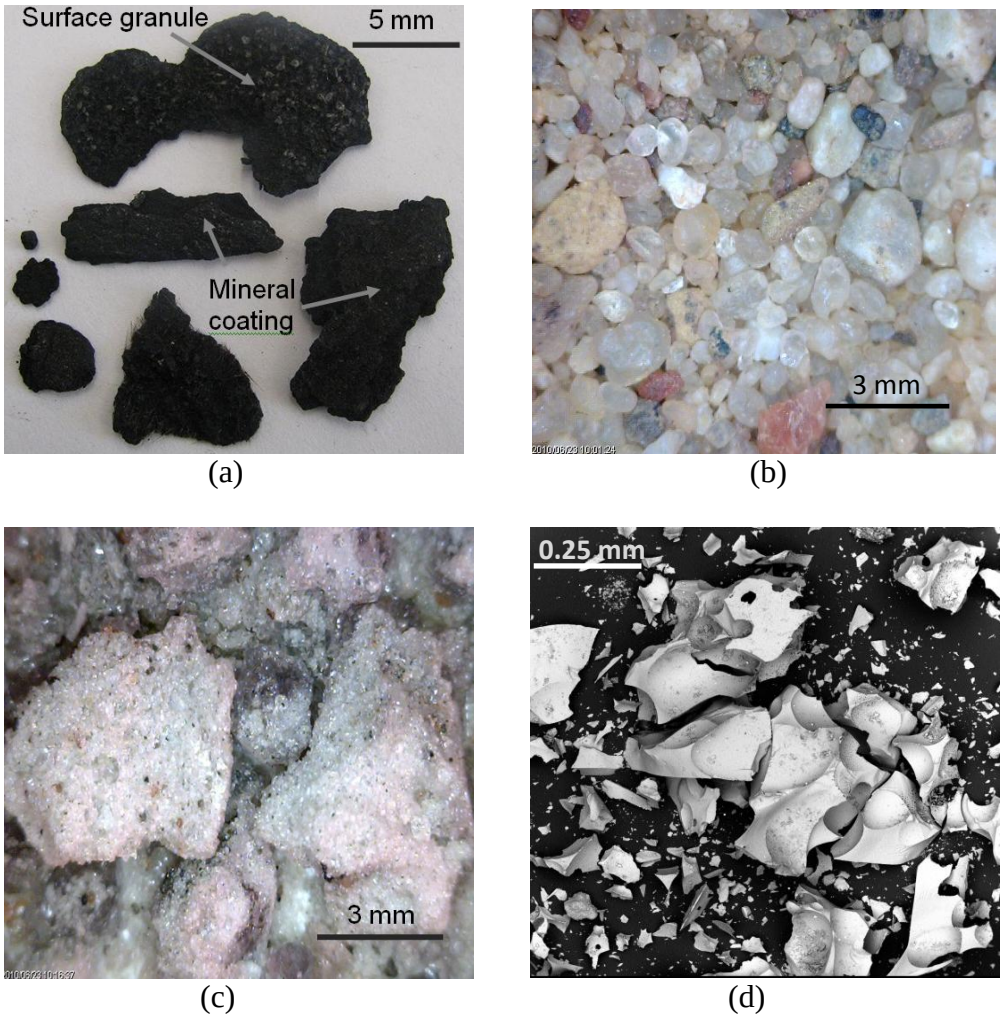

(a) (b)

(c) (d)

Fig. A.1. Photographs of (a) RAS, (b) glacial outwash sand, (c) foundry slag and (d) SEM micrographs of foundry slag particles

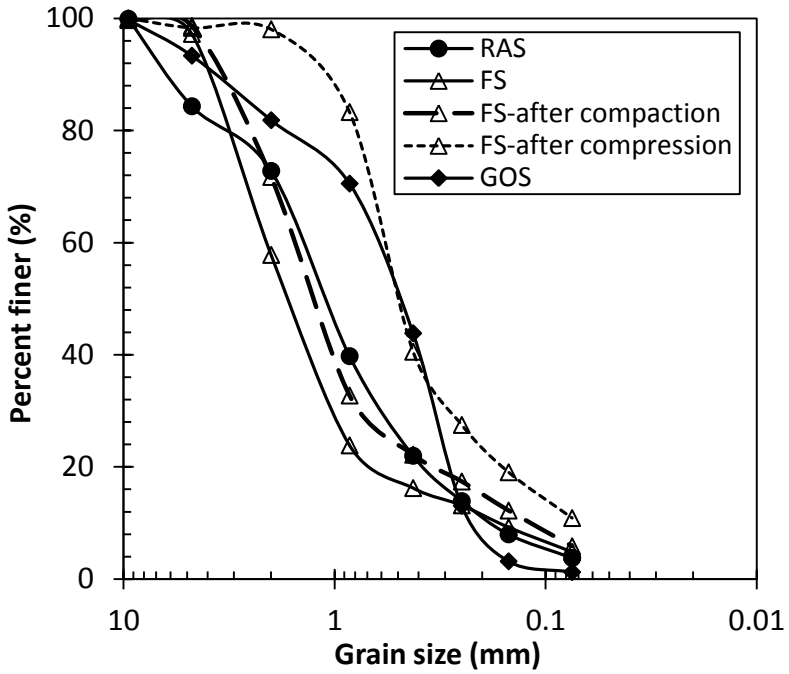

Fig. A.2. Grain size distribution of RAS, foundry slag, and glacial outwash sand

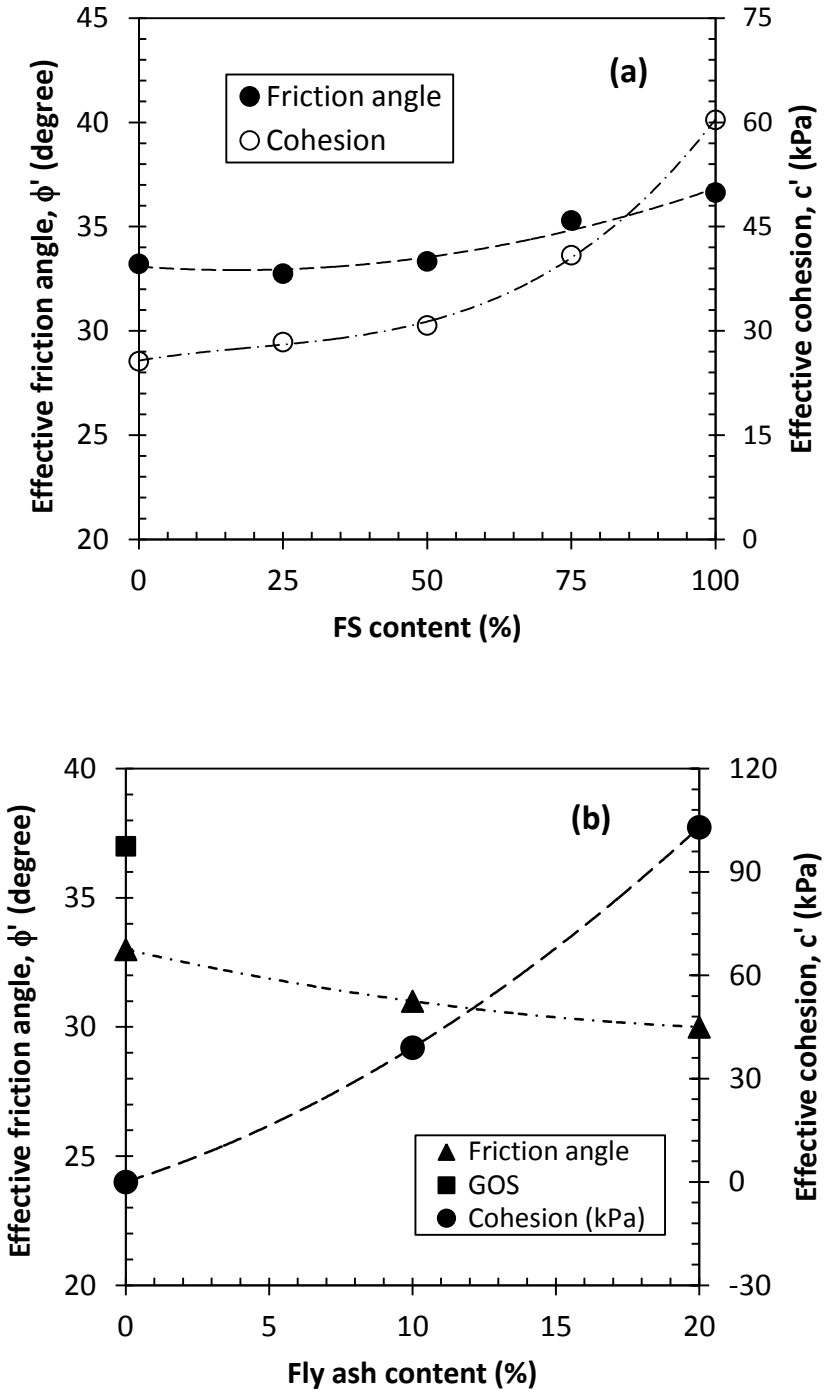

Fig. A.3. Variation of friction angle and cohesion of (a) compacted RAS:FS mixtures with FS content and (b) stabilized RAS with fly ash content

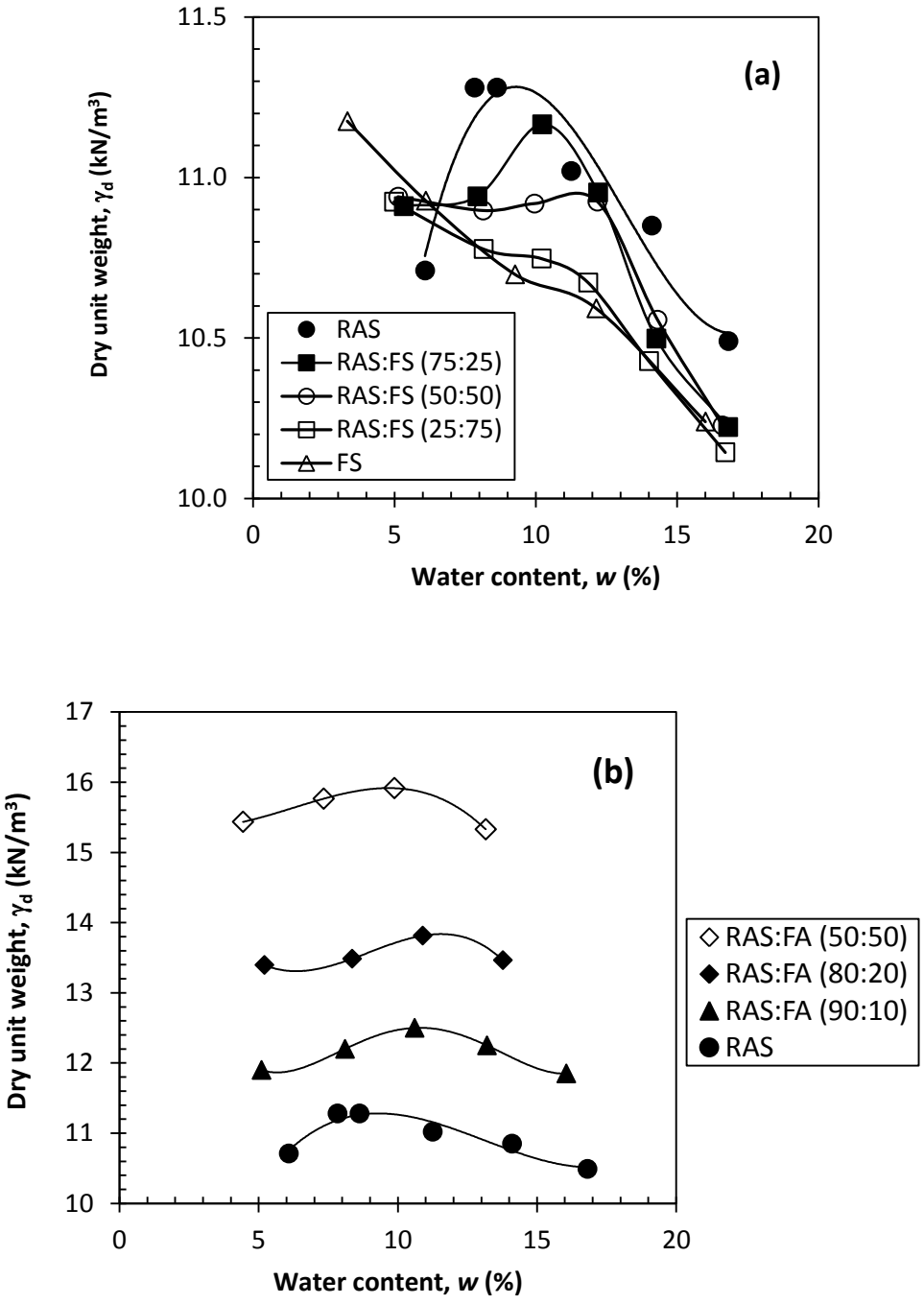

Fig. A.4. Dry unit weight versus water content of (a) compacted RAS:FS mixtures and (b) stabilized RAS

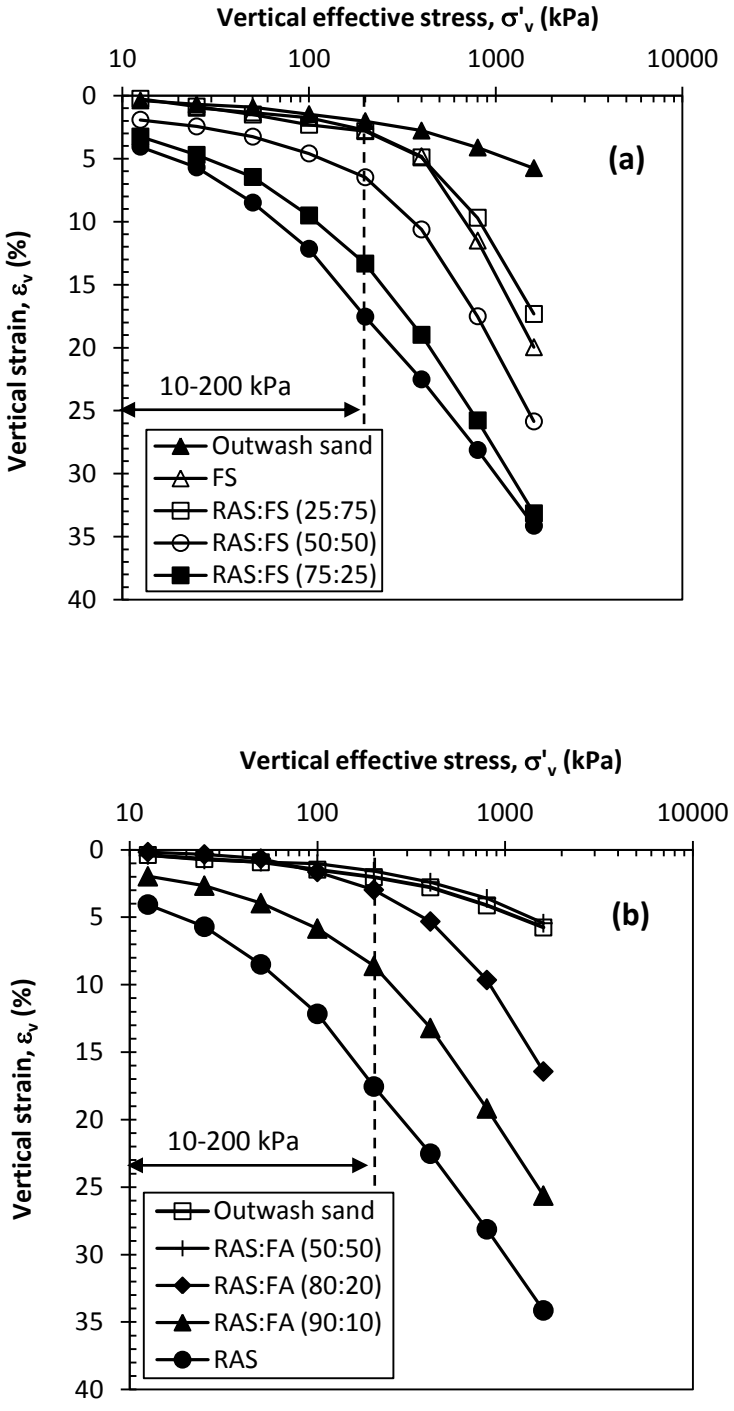

Fig. A.5. One-dimensional compression curves of (a) compacted RAS:FS mixtures and (b) stabilized RAS

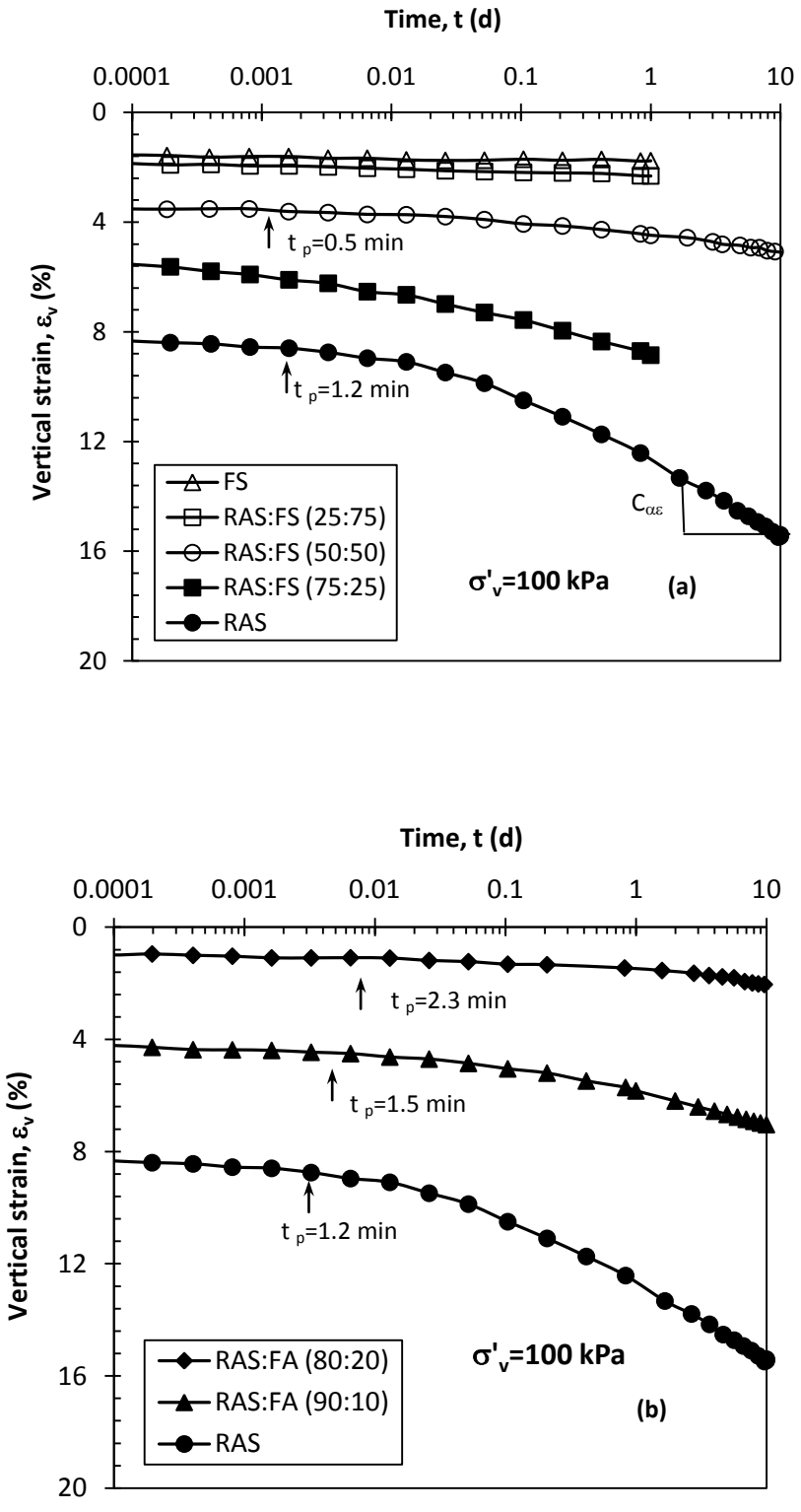

Fig. A.6. Variation of ε_v with time for (a) compacted RAS:FS mixtures and (b) stabilized RAS

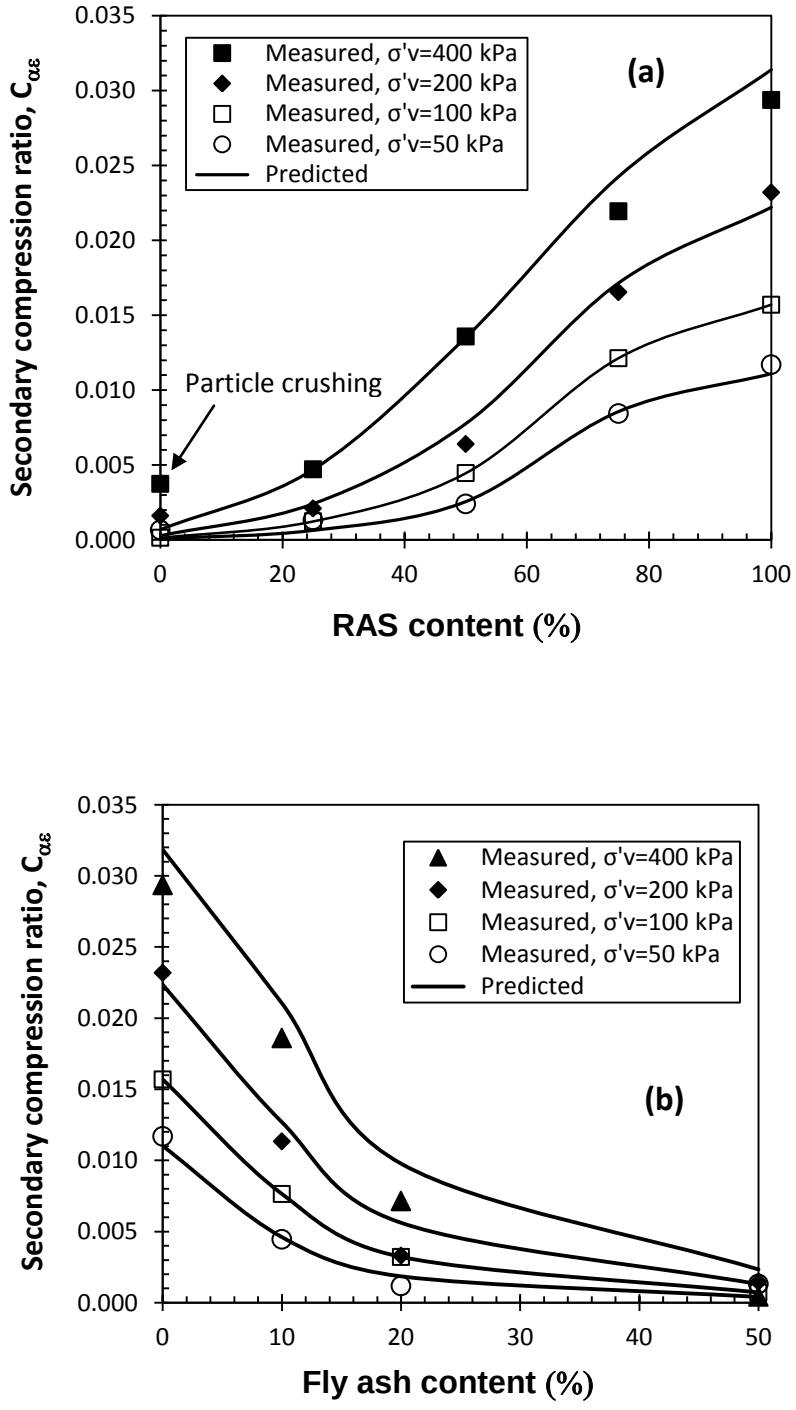

Fig. A.7. Comparison between predicted and measured $C_{\alpha\varepsilon}$ of (a) compacted RAS:FS mixtures at different RAS content and stress levels (b) stabilized RAS with fly ash content and stress levels

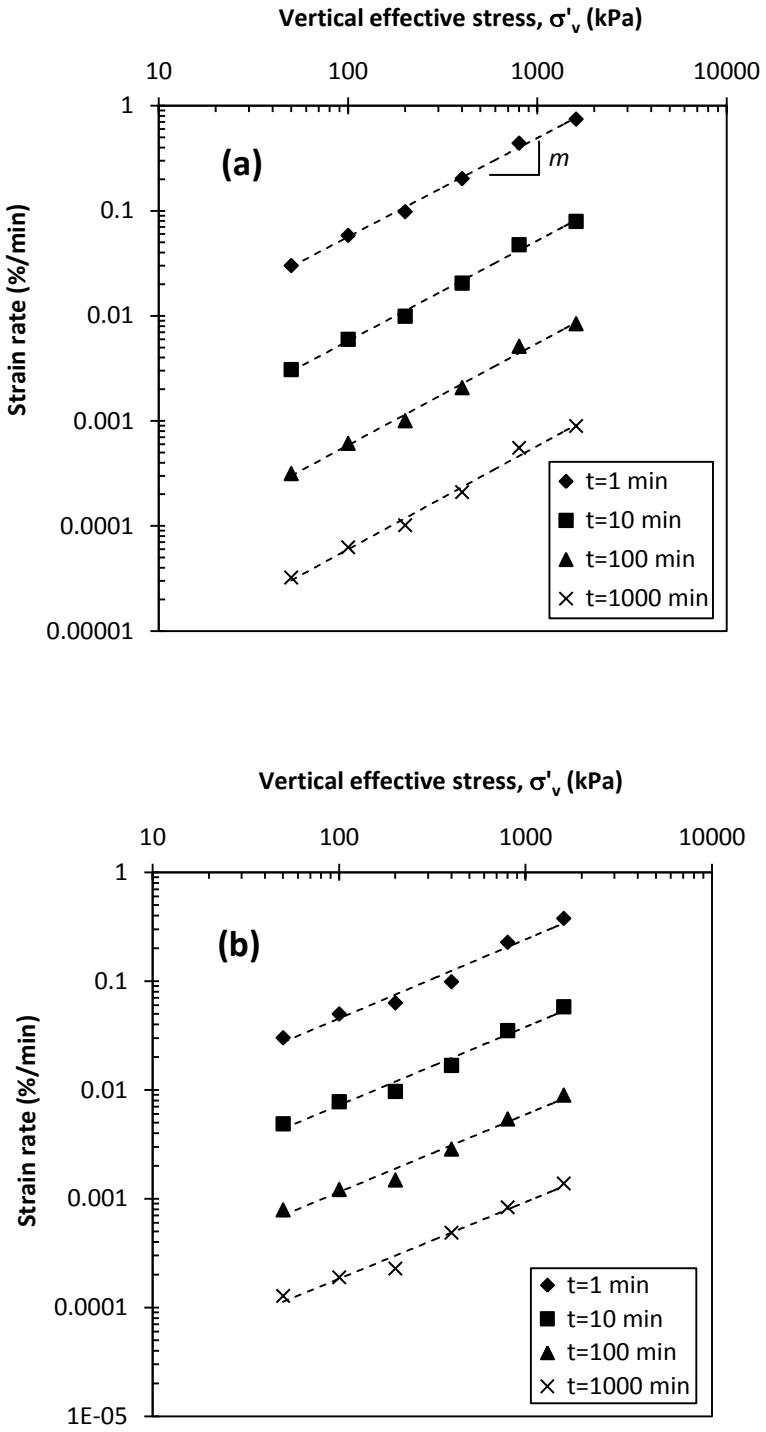

Fig. A.8. Variation of strain rate with vertical stress for (a) compacted RAS:FS (25:75) mixture and (b) stabilized RAS with 20% fly ash

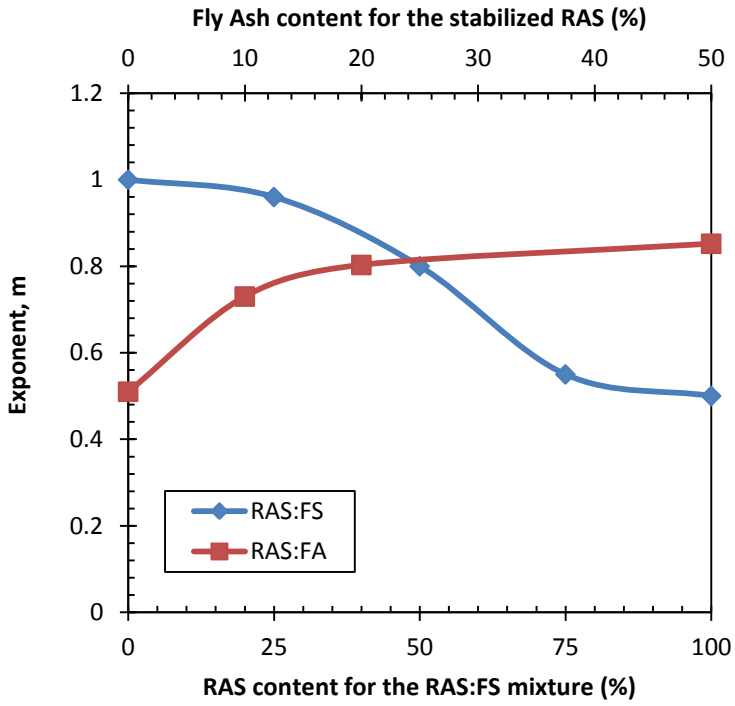

Fig. A.9. Variation of exponent *m* with RAS content in RAS:FS mixture and fly ash content in stabilized RAS

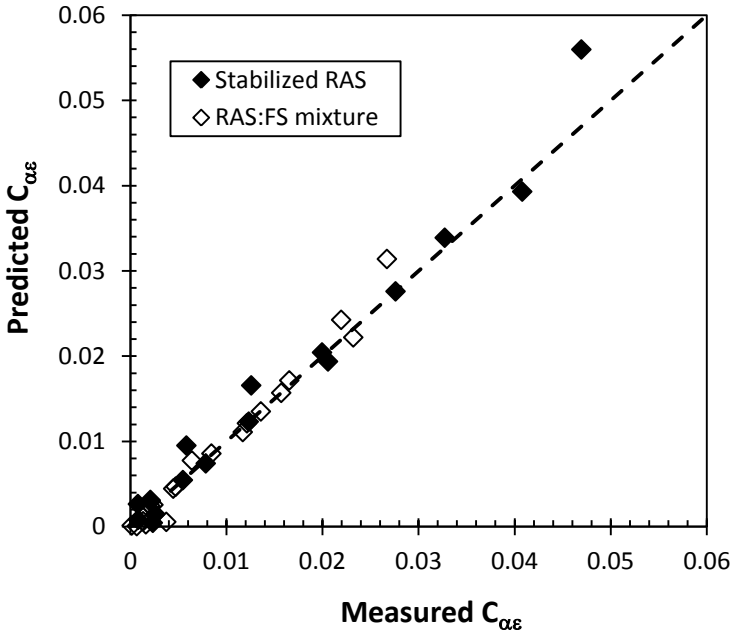

Fig. A.10. Comparison between predicted and measured $C_{\alpha\varepsilon}$

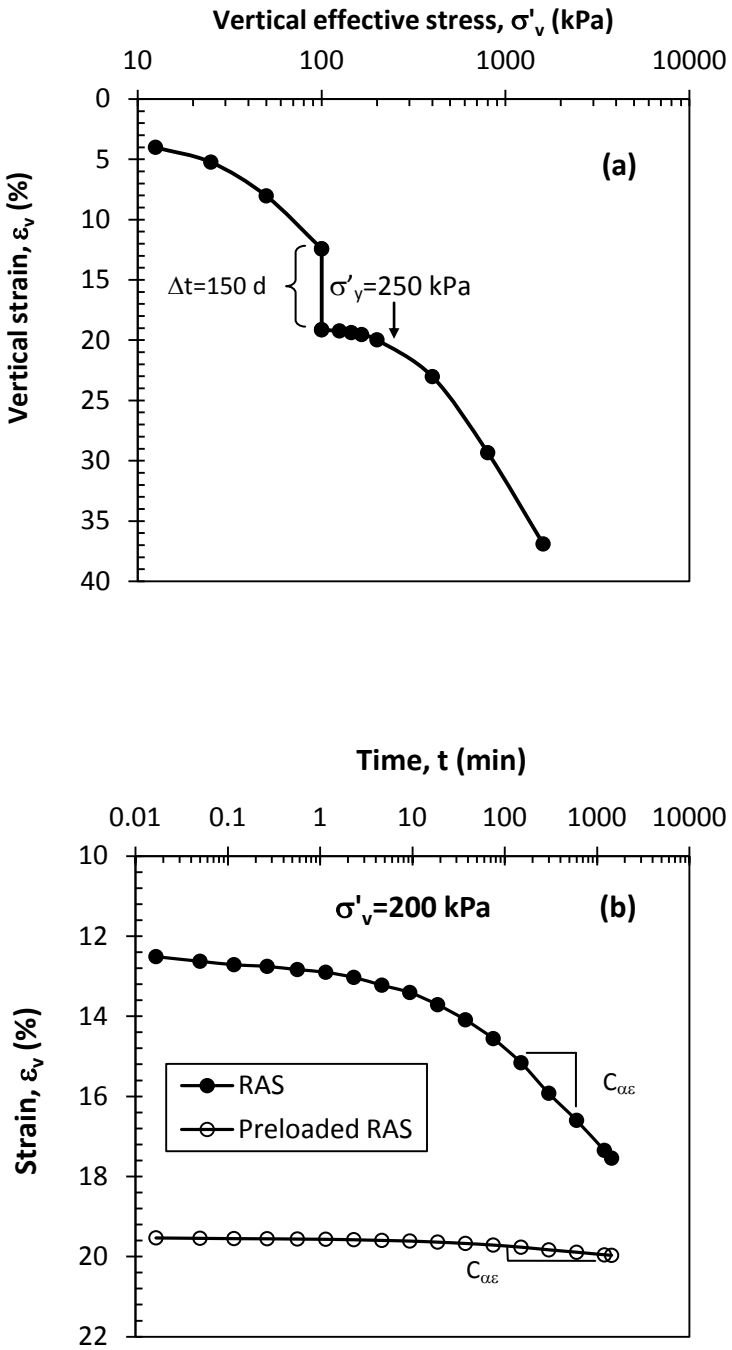

Fig. A.11. Effect of preloading on compressibility of RAS

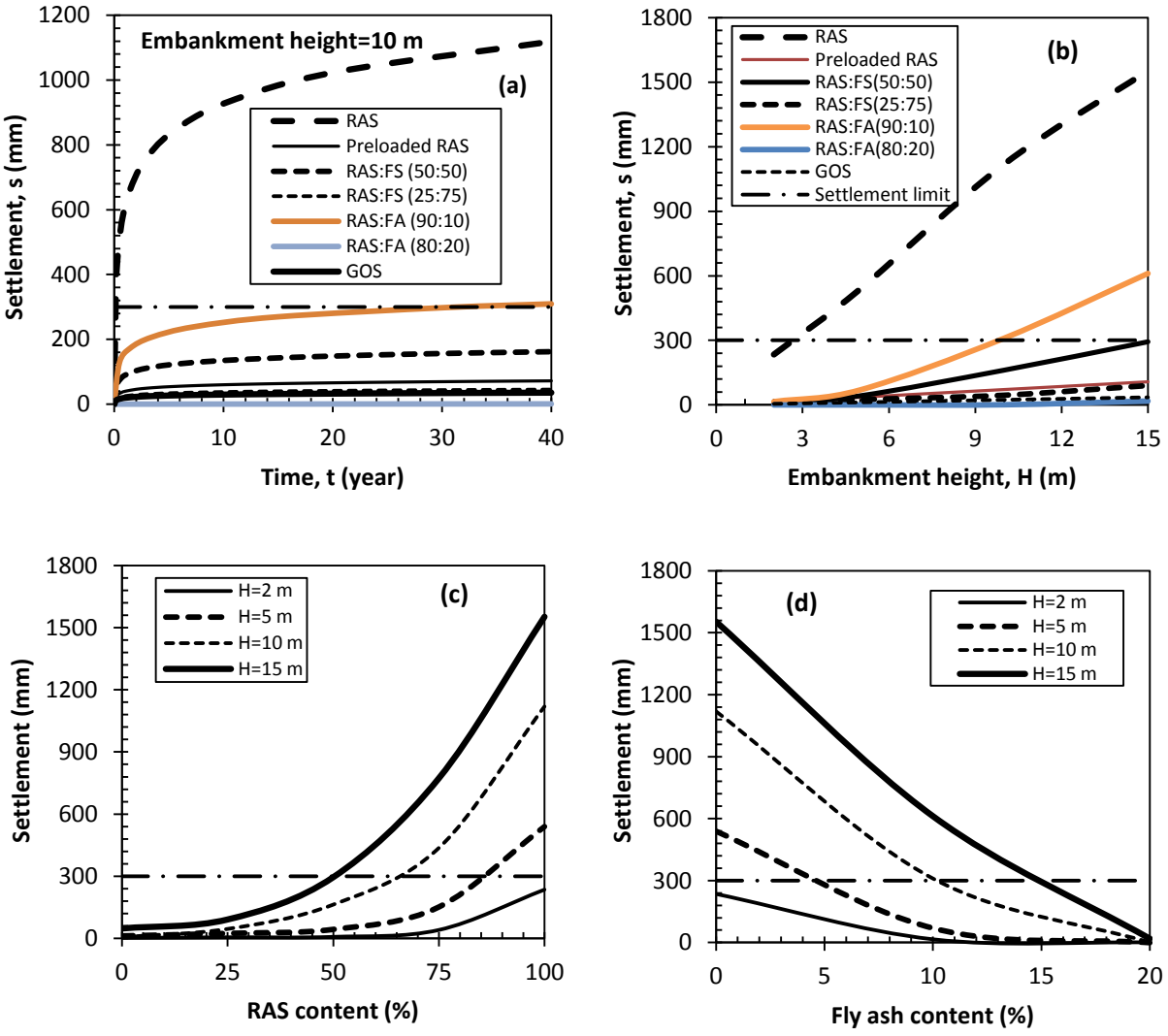

Fig. A.12. Variation of embankment settlement with (a) time, (b) embankment height, (c) RAS content, and (d) fly ash content